Axisymmetric Theory and the Interactive, Asymmetric Monsoon

by

Nikki C. Privé

B.S. Mechanical Engineering
University of Maryland, College Park (1999)

M.S. Atmospheric Science
Massachusetts Institute of Technology (2002)

Submitted to the Department of Earth, Atmospheric, and Planetary Science
in partial fulfillment of the requirements for the degree of

Doctor of Science in Atmospheric Science

at the

MASSACHUSETTS INSTITUTE OF TECHNOLOGY

June 2005

Author .....
Department of Earth, Atmospheric, and Planetary Science
April 28, 2005

Certified by .....
R. Alan Plumb
Director, Program in Atmospheres, Oceans, and Climate
Professor of Meteorology
Thesis Supervisor

Accepted by .....
Maria Zuber
Head of Department
E.A. Griswold Professor of Geophysics and Planetary Science

Axisymmetric Theory and the Interactive, Asymmetric Monsoon

by

Nikki C. Privé

Submitted to the Department of Earth, Atmospheric, and Planetary Science
on April 28, 2005, in partial fulfillment of the
requirements for the degree of
Doctor of Science in Atmospheric Science

Abstract

The applicability of axisymmetric theory of angular momentum conserving circulations to the large-scale steady monsoon is studied in a general circulation model with idealized representations of continental geometry and simple physics. The axisymmetric theory is expanded to explain the the location of the monsoon; assuming quasi-equilibrium, the poleward boundary of the monsoon circulation will be colocated with the maximum in subcloud moist entropy, with the monsoon rains occurring slightly equatorward of this maximum. Starting from an axisymmetric aquaplanet framework, the model complexity is incrementally increased to include first a subtropical continent, then eddies and zonal variation in the flow, and finally asymmetry of the large-scale forcing. It is found that the meridional circulation which develops over a zonally symmetric continent is in good agreement with the axisymmetric theory, but a cross-equatorial meridional circulation does not form over a continent of limited longitudinal width, where the flow is highly asymmetric. The equator proves to be a substantial barrier to boundary layer meridional flow; flow into the summer hemisphere from the winter hemisphere tends to occur in the free troposphere rather than in the boundary layer. The monsoon location is found to be strongly correlated with the maximum subcloud moist entropy, both in the modeled cases and in observed monsoons around the globe. The net effect of eddies is a slight weakening of the monsoon due to redistribution of the moist entropy field. Advection is found to strongly shape the overall distribution of subcloud moist entropy, and to limit the range of the monsoon circulation and precipitation.

Thesis Supervisor: R. Alan Plumb
Title: Director, Program in Atmospheres, Oceans, and Climate
Professor of Meteorology

Acknowledgments

Where could I possibly begin, save for at the beginning? To my parents, for cake via postal service, for letting me use various power tools, and for not asking too many questions. To six years of housemates, especially Geoff, Josh, and Lenny, for putting up with the fish sauce, and fabric in the shower. To my friends from Blair, for cards at 5 a.m. and a reminder that there is life after school. To my friends from MoW and Grey's, for amusing emails, for encouraging my pyromania, and for Tanc's impressions of Henreitta Pussycat and Stephen Hawking. To Deepika, for helping me with a new hobby, plus all the wonderful people at PR. To Elaine - you still need to cut my hair!

To my advisor, Alan Plumb, for many helpful discussions and for finding my spelling mistakes. To my committee: Elfatih Eltahir, Kerry Emanuel, and John Marshall, for useful suggestions and different viewpoints. To Will Heres, for computer assistance with a sense of humor. To Olivier Pauluis, for holding my hand through the setup of the MITGCM. To Chris Hill, for fixing lots of esoteric computer problems and for scrounging access to better machines. To Ed Hill and Jean-Michel Campin, for debugging my hare-brained programming mistakes. To Prof. Gadgil, for asking a question that lead to a large portion of the final thesis.

Many people have helped to make my stay here more tolerable, even enjoyable at times. To Mary Elliff, for enthusiasm and for understanding the importance of tea. To my year-mates, Rob Korty, Peter Huybers, and Arnico Panday, for Thursday night sessions at the chalkboard. To my lab-mates, Jessica Neu, Alan Kuo, Kirill Semeniuk, Mike Ring, and Ivana Cerovecki, for arguments about the weather and for putting up with open-air headphones. To my officemates, Tieh-Yong Koh, Fabio Dalan, Irene Lee, Yang Zhang, and Roberto Rondanelli, for letting me hog the best corner of the office for my plants and a barely-used desk. To Greg Lawson, Jeff Scott, Bill Boos, Cegeon Chan, and David Flagg, for afternoon and late-night chats. To the bridge-players, who never call the director on me.

To the soft, gentle darkness of the lab at night, and the little things that make life easier. To my car, I promise to buy you a new battery and some tires this year. To the CT2, for four years of speedy, if not timely, service. To the 80, for timely, if not frequent service. To rec.arts.sf.written, for new additions to my library. To *Death By Chocolate*, so tasty!

This document is quite long, and somewhat tedious to read. Actually, quite tedious, especially chapters 3 and 4. To ease your way through, I have some musical recommendations, as follows: Chapter 1, **76-14**, Global Communications; Chapter 2, **6 and 12 String Guitar**, Leo Kottke; Chapter 3, **Stalker**, Robert Rich and B. Lustmord; Chapter 4, **Courier**, Richard Shindell; Chapter 5, **garbagemx36**, Autechre; Chapter 6, **Little Peppermints**,

Antje Duvekot, just put track 5 on repeat.

NCEP reanalysis data provided by the NOAA-CIRES Climate Diagnostics Center, Boulder, Colorado, USA, from their web site at http://www.cdc.noaa.gov/. ERA-40 reanalysis data provided by the European Centre for Medium-range Weather Forecasting, from their web site at http://www.ecmwf.int/research/era/.

This material is based upon work supported under a National Science Foundation Graduate Research Fellowship. Any opinions, findings, conclusions or recommendations expressed in this publication are those of the author and do not necessarily reflect the views of the National Science Foundation.

...I must confess, that in this latter occurs a difficulty, not well to be accounted for, which is, why this Change of the Monsoons should be any more in this [Indian] Ocean, than in the same Latitudes in the Æthiopick, where there is no thing more certain than a S.E. Wind all the Year.

These are particulars that merit to be considered more at Large, and furnish a sufficient Subject for a just Volume; which will be a very commendable Task for such, who being used to Philosophick Contemplation, shall have leasure to apply their serious thoughts about it.

- Edmond Halley, 1686

Contents

Chapter 1

Introduction

In the summer of 2004, flooding from heavy monsoon rains in southeast Asia resulted in the deaths of more than two thousand people. Millions were displaced from their homes, three quarters of the country of Bangladesh was submerged in flood waters, and billions of dollars of crops were lost (DER Subgroup[1], 2004). Rainfall during the monsoon season accounts for a large percentage of the annual precipitation in west Africa, southeast Asia, and northern Australia, and these regions rely heavily on monsoon rains to support agriculture. During the 1970s and 1980s, the west African monsoon was particularly weak over the Sahel region, resulting in widespread drought and famine; the causes of this failure of the monsoon are still not fully understood. Nearly one quarter of the globe can be considered to have a monsoonal climate, although the Asian monsoon is the largest and most prominent of the worldwide monsoons.

Although monsoons strongly impact society, agriculture, and economics around the globe, there has been relatively little advance in our understanding of mechanisms which drive monsoons since Halley's 1686 depiction of flow in the tropics. Accurate predictive capabilities for future monsoon seasons do not currently exist, but would be invaluable for saving lives and property and for agricultural planning. Reliable forecasting requires a thorough understanding of the basic dynamics of the monsoon; this will be the focus of this thesis.

1.1 Observed Features of the Worldwide Monsoon

The monsoon is fundamentally a seasonal reversal of wind direction, with the term monsoon derived from the Arabic *mausim,* or season. During the summer, the monsoon is generally accompanied by heavy rains, with dry conditions during the winter months. Areas close

[1]Bangladesh Disaster and Emergency Response Subgroup

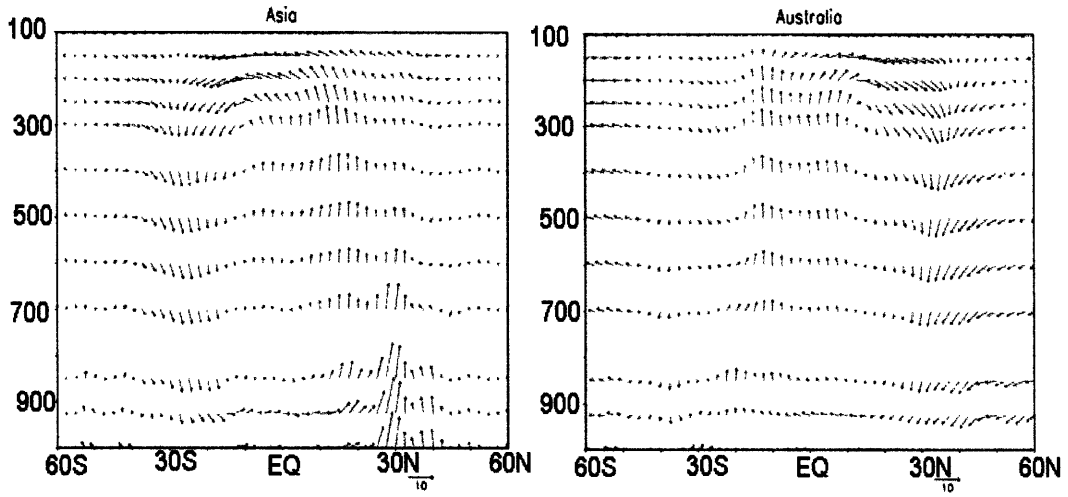

Figure 1-1: Summer zonal mean flow on the latitude-height plane from long term monthly mean NCEP reanalysis data. Vertical velocity in units of 1E2 Pa/s, meridional flow in m/s. Left, mean July flow over Asia averaged between 60E and 120E. Right, mean February flow over Australia averaged between 120E and 160E.

to the equator are not monsoonal because there is no seasonal reversal in wind direction, although they may experience intense precipitation from the intertropical convergence zone (ITCZ). Monsoon regions are located in the tropics and subtropics, far enough from the equator that seasonality exists, but where tropical convection remains a strong player in local climate. Observed monsoons exist over Australia, southeast Asia and India, Amazonia, West Africa, and the North American southwest.

Continents feel seasons more strongly than oceans due to the much smaller heat capacity of soil in comparison to water. During summer, land surfaces tend to heat quickly, strongly forcing the atmosphere above, while the ocean stores much of the incoming radiative energy internally and shows a slower and weaker seasonal response. Since the monsoon is a response to seasonal forcing, it is closely associated with continental areas; however, it has been proposed that a localized, positive, subtropical SST anomaly could also result in a monsoon (Yano and McBride, 1998), were there some mechanism for producing such an anomaly.

The zonal mean flow in the monsoon area shows strong, deep ascent over the monsoon region as part of a cross-equatorial circulation with subsidence in the opposite hemisphere (Figure 1-1). This circulation has the character of a broad Hadley circulation, and has been interpreted as the relocation of the ITCZ into the monsoon area (eg. Gadgil (2003)). The zonal wind field features upper level easterlies over the tropics, flanked by a strong upper level westerly jet in the winter hemisphere subtropics and a weaker upper level westerly jet in the summer hemisphere midlatitudes (Figure 1-2). The easterlies extend down to the

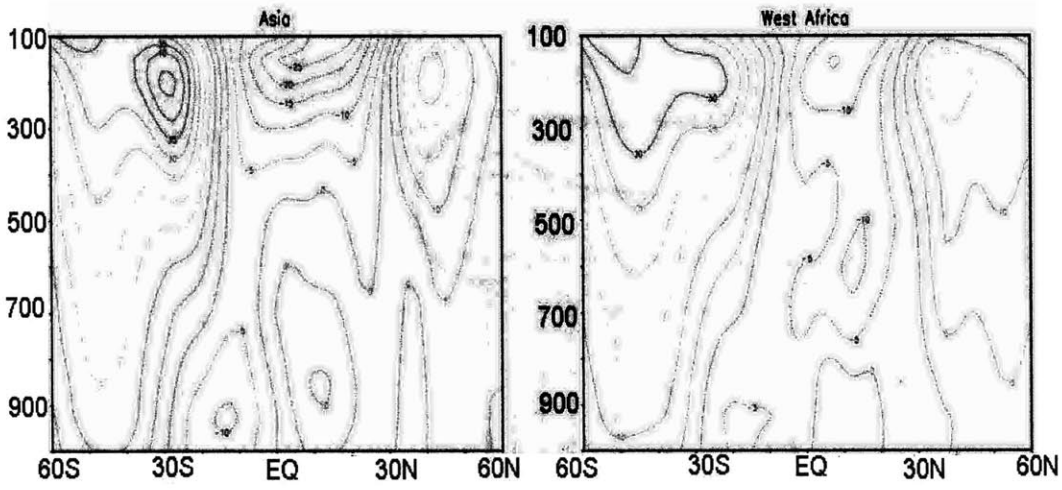

Figure 1-2: Summer zonal mean zonal wind on the latitude-height plane from long term monthly mean NCEP reanalysis data, units m/s. Left, mean July flow over Asia averaged between 60E and 120E. Right, mean July flow over west Africa averaged between 10W and 10E.

surface in the winter hemisphere tropics, with weak easterlies or near zero winds at the surface on the poleward edge of the monsoon. Westerly winds exist at low levels between the equator and the monsoon where air is carried poleward, retaining relatively high angular momentum from the equator.

The horizontal flow associated with the monsoon is complex. A large cyclonic circulation develops over the monsoon region in the lower troposphere in response to the heated land surface. Equatorward of this cyclone, significant cross-equatorial flow carries moisture from the tropical ocean into the monsoon area (Figure 1-3). Aloft, a divergent anticyclone develops with outflow from the monsoonal ascent. The anticyclone associated with the Asian monsoon is particularly large, spanning much of Asia and northern Africa, as shown in Figure 1-4. Precipitation associated with the monsoon can be very intense and occurs over a large area, primarily along the coastline. As the summer progresses, the rain spreads further inland; in Asia and Australia, the precipitation maximum remains near the coast, whereas the precipitation maximum in the African monsoon moves inland while the coastal precipitation wanes.

The monsoon has strong intraseasonal variability over a range of time scales. On time scales of a few days exist monsoon depressions, synoptic scale low pressure systems which are responsible for the majority of monsoon precipitation. On a monthly timescale, the monsoon experiences an active/break cycle which strongly impacts agricultural interests. During the active phase, the strongest precipitation occurs over the landmass, while during

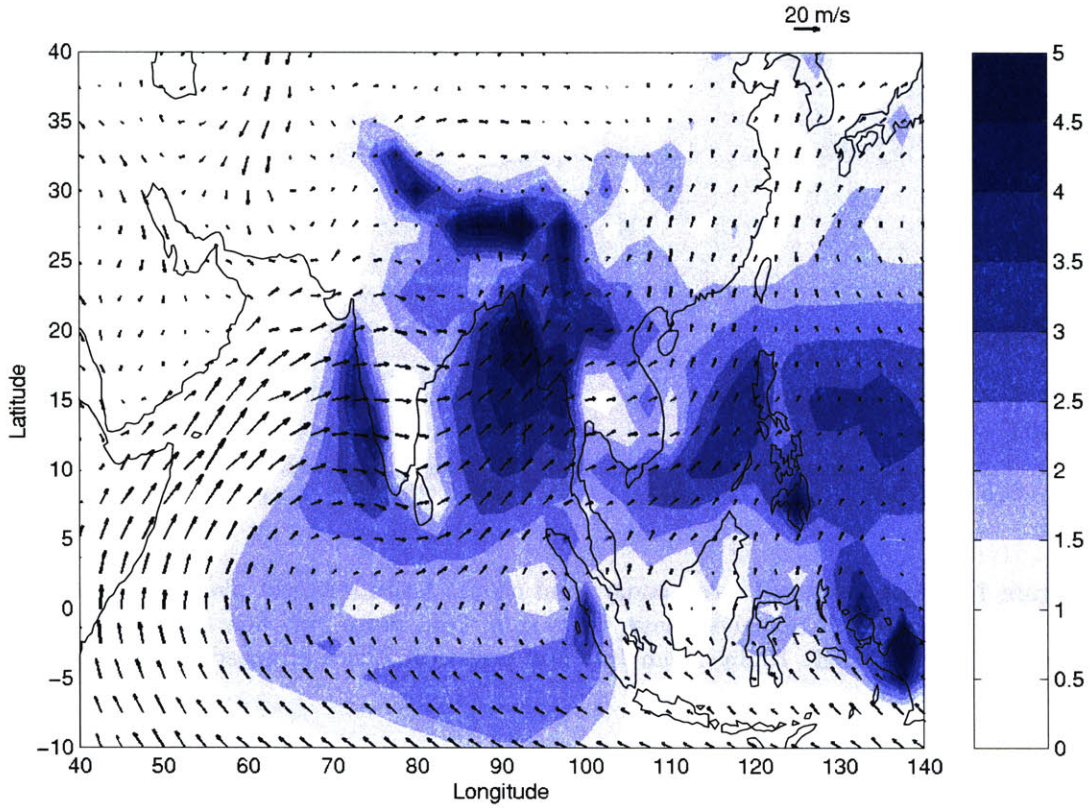

Figure 1-3: Long term mean July flow in the Asian monsoon region, from ECMWF reanalysis data. Contours are precipitation, contour interval 0.5 mm/day; vectors are boundary layer horizontal winds.

the break period the rainfall maximum shifts equatorward and occurs over the ocean just off of the coast; each phase may last several weeks. The causes of this variation between active and break regimes are not well understood, and are beyond current forecasting capabilities. On the seasonal timescale, the Asian monsoon experiences delayed onset: the wind reversal and initiation of continental precipitation occur approximately one month after the landmass reaches high surface temperatures (Xie and Saiki, 1999). This phenomenon is poorly modeled in most general circulation models, and is again not well understood.

1.2 Axisymmetric Theory

Angular momentum has long been known to have a strong impact on the steady zonal mean circulation in the atmosphere. An early depiction of meridional circulation in the tropics was made by Hadley (1735), who reasoned that differential heating by the sun leads to a direct overturning cell with ascent in the tropics where heating is strongest, and with

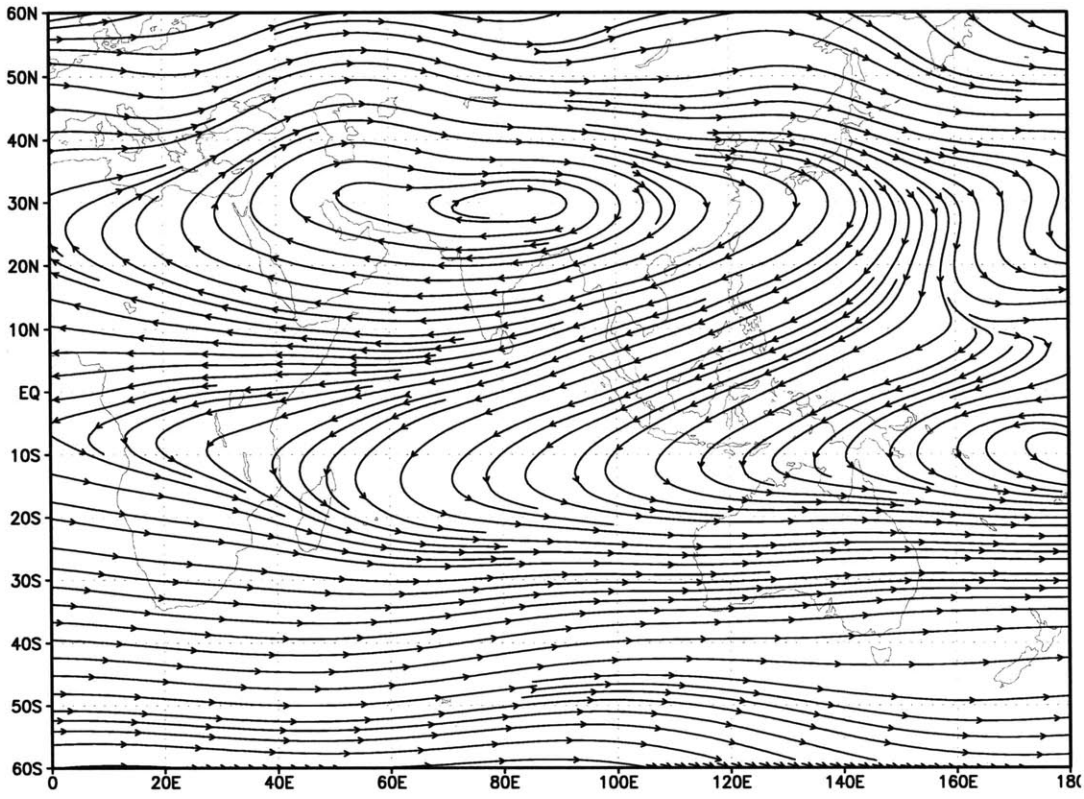

Figure 1-4: Long term mean July streamlines at 150 mb in the Asian monsoon region, from NCEP reanalysis data.

subsidence at higher latitudes. Hadley hypothesized that conservation of absolute angular momentum of the low-level equatorward flow would yield the observed easterly flow in the tropics.

Conservation of angular momentum acts to constrain the steady state zonal wind field. Hide (1969) noted that superrotation at the equator in the absence of sinking motions requires local longitudinal pressure gradients, as this is the only force which can increase the angular momentum of the atmosphere to a value greater than that of the solid earth at the equator. This was generalized by Schneider (1977) to show that in a viscous, axisymmetric framework, extrema of absolute angular momentum must occur in a region of a source or sink of momentum, so that such extrema are confined to the lower boundary of the atmosphere in the absence of sources or sinks aloft. The net advective flux of momentum across a contour of constant angular momentum must be zero: advection cannot compensate for a diffusive friction which has a downgradient flux of momentum across contours of constant momentum. Any extremum of angular momentum which exists away from the bottom surface would be destroyed by viscous processes and cannot be maintained in a steady

state.

Schneider noted that under axisymmetry, the tropical temperature field is controlled by the requirement there exist no extrema of angular momentum, so that meridional gradients of temperature must be small. The assumption of a particular temperature field with no meridional flow and with zonal wind in thermal wind balance with temperatures may be invalid if an extremum of angular momentum would result. Instead, a meridional circulation of sufficient strength to homogenize temperatures in the tropics is needed.

Held and Hou (1980) used the concepts developed by Schneider (1977) to focus on the annual-mean meridional circulation by assuming a radiative-convective equilibrium (RCE) state with maximum temperatures at the equator. A wind field with flow in thermal wind balance with the radiative convective equilibrium temperatures cannot develop for this case, as upper level westerlies would result at the equator, which are not allowed. Instead, an angular-momentum conserving (AMC) meridional circulation develops with two cells, each with ascent near the equator and subsidence in the subtropics, with equatorward flow in the boundary layer and poleward flow aloft. The flow carries high angular momentum air from the equatorial region into the subtropics in the upper troposphere, where westerly jets form along the boundaries of the circulation cells. Poleward of these boundaries, the thermal equilibrium solution is in balance with the RCE temperatures.

Lindzen and Hou (1988) extended this theory to the case where there is a nonzero gradient in RCE temperature at the equator - in thermal equilibrium, this would result in infinite zonal wind speeds near the equator and a discontinuity with westerlies on one side and easterlies on the other. As this thermal wind distribution is not allowed on several counts, an AMC meridional circulation develops instead. Two circulation cells form, one large 'winter' cell featuring ascent poleward of the latitude of the RCE temperature maximum and cross-equatorial flow with subsidence in the winter hemisphere, and a second, much weaker circulation cell in the summer hemisphere, poleward of the ascent region. The zonal wind field again features strong westerly jets at the subtropical edge of the circulation, but in this case there is an equatorial easterly jet resulting from conservation of angular momentum as off-equatorial air is transported to the equator. As the RCE temperature maximum is shifted poleward off of the equator, the cross-equatorial circulation broadens and strengthens considerably; this cell is considerably stronger than the symmetric cells found by Held and Hou (1980). Observations show that the real atmosphere features a circulation similar to that descibed by Lindzen and Hou (1988), with a dominant winter cell, during most of the year; the annual-mean circulation with two cells of equal size and with equatorial ascent occurs only briefly after equinox.

Plumb and Hou (1992) examined the circulation induced by a localized subtropical forcing with zero gradient in RCE temperature across the equator. For weak forcing, the

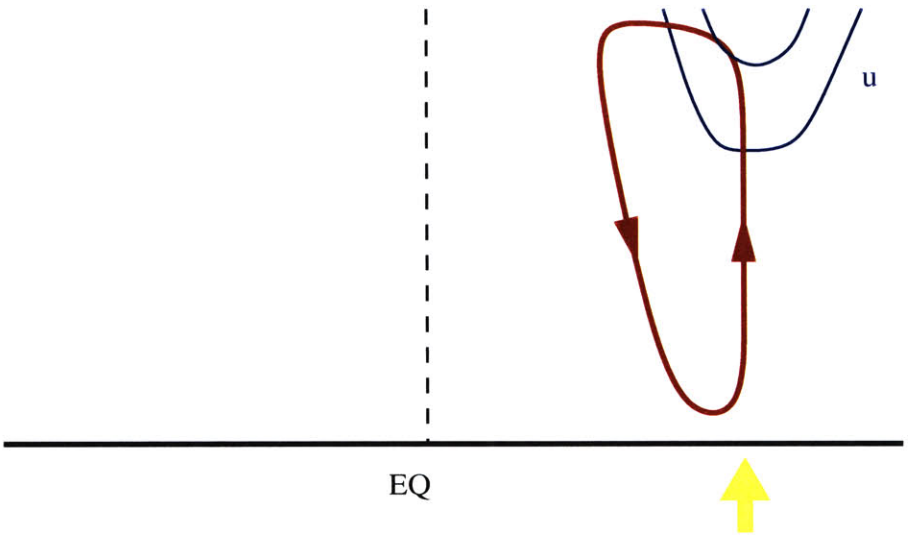

Figure 1-5: Diagram of zonal winds (blue) and meridional circulation (red) for subthreshold forcing.

thermal equilibrium solution is permissible, with RCE temperature distribution throughout the globe. In this regime, the meridional flow is weak and viscously driven, and the zonal wind is in thermal wind balance with the temperature (Figure 1-5). For strong forcing, zonal wind in the thermal equilibrium solution would result in an extremum of angular momentum in the upper troposphere; instead, a meridional circulation develops which redistributes the temperatures in the tropics. This strong circulation cell is cross-equatorial in extent, and conserves angular momentum, forming an upper level easterly jet near the equator (Figure 1-6). The critical condition for the development of a meridional circulation is the existence of an extremum of angular momentum in the thermal equilibrium solution, which can be rewritten as the vanishing of absolute vorticity in the thermal equilibrium solutions. The forcing strength needed to reach this threshold is dependent on the latitudinal distribution of the equilibrium temperatures through

$$-\frac{1}{2}\frac{gD}{T_0}\frac{1}{cos\phi}\frac{\partial}{\partial\phi}\left[\frac{cos^3\phi}{sin\phi}\frac{\partial\hat{T}_e}{\partial\phi}\right] < 2\Omega^2 a^2 sin\phi\, cos^2\phi \tag{1.1}$$

where g is the acceleration of gravity, ϕ is the latitude, D is the height of the tropopause, T_0 is a reference temperature, $\hat{T}_e$ is the depth-averaged radiative-convective equilibrium temperature, and a is the radius of the earth. Plumb and Hou hypothesized that the abrupt onset of the monsoon might be related to this threshold behavior, with the thermal equilibrium solution during the pre-onset period switching to the AMC regime as the surface forcing reaches the threshold strength.

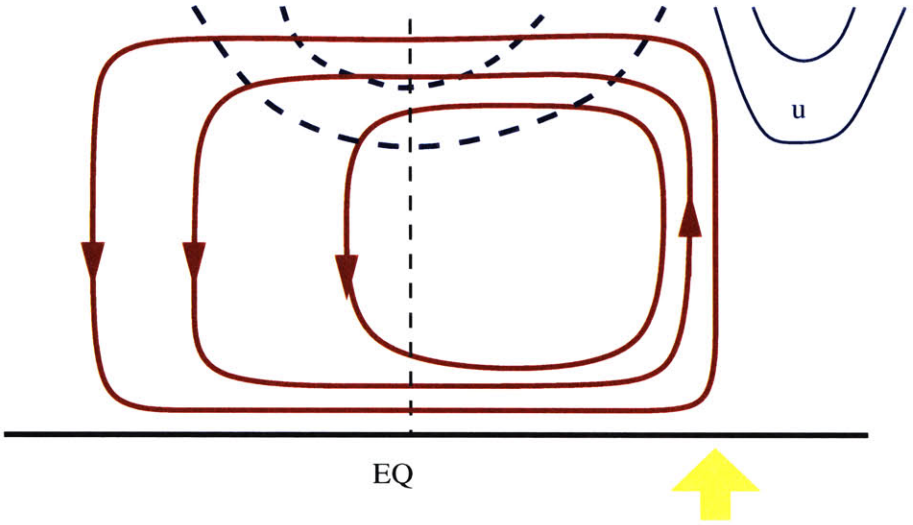

Figure 1-6: Diagram of zonal winds and meridional circulation for supercritical forcing as in Figure 1-5.

Emanuel (1995) showed that the threshold conditions can be written in terms of the subcloud moist static entropy for a moist convecting atmosphere. Assuming a moist adiabatic lapse rate, and making use of the Maxwell relations, the threshold may be written as

$$\left[\frac{\partial}{\partial\phi}\left(\frac{cos^3\phi}{sin\phi}(T_s - T_t)\frac{\partial s_b}{\partial\phi}\right)\right] = -4\Omega^2 a^2 cos^3\phi\, sin\phi \tag{1.2}$$

where s_b is the subcloud moist entropy, T_s is the surface temperature, and T_t is the temperature at the tropopause. Zheng (1998) verified the behavior in a moist axisymmetric aquaplanet model.

Schneider (1983) also examined the atmospheric response to a localized (δ-function) forcing, and found that two different regimes of AMC circulation are possible, depending on the strength and location of the forcing: a 'local' circulation which is confined to one hemisphere, and a 'global' circulation which is nearly symmetric about the equator. There are two thresholds for the behavior of the circulation. For weak forcing below the first threshold, only the local circulation is possible, although this circulation is AMC unlike the local viscously driven circulations found by Plumb and Hou. Both local and global circulations are possible for forcing above the first threshold and below the second; above the second threshold, only the global circulation can attain. The magnitude of forcing at the two thresholds is dependent upon the location of the forcing region; the forcing magnitude increases as the forcing is shifted poleward.

The impact of moist convection on the meridional circulation was explored by Fang and

Tung (1996) and Fang and Tung (1997). Deep moist convection acts to rapidly communicate subcloud conditions throughout the depth of the troposphere so that the vertical profile of temperature and humidity approaches a moist adiabat. The effects of moist convection can be represented as very short Newtonian cooling timescale in local areas of deep convection, with a longer 'dry' timescale elsewhere. The strength of the circulation is dependent upon the longer cooling timescale in subsiding regions, while the temperature in the tropics is determined by the local temperature in the area of ascent and deep convection. In a moist atmosphere, the ascent branch of the circulation narrows and the vertical velocity increases in comparison to a dry circulation.

1.3 Simple models of the monsoon

The first published depiction and explanation of the monsoon was written by Halley (1686), who put forth the hypothesis of the monsoon as a giant sea-breeze circulation. In the winter, the land is cooler than the nearby ocean, causing equatorward flow from the continent toward the ocean; while in the summer the land is warmer than the ocean, inducing the opposite flow pattern with rising air over the land leading to precipitation. This simple theory remained uncontested for several hundred years, and the sea-breeze paradigm is still seen in textbooks and popular science articles today. However, the sea-breeze theory fails to account for the abrupt onset of the Asian monsoon and the active/break cycle. The sea-breeze paradigm also neglects the rotational effects which are significant at the large horizontal scales of the monsoon.

Gill (1980) explored the response of a linear shallow water model on the β-plane to localized forcings centered both on and off of the equator. When the forcing is centered north of the equator, a region of ascent is colocated with the applied forcing, and pressure minimum is offset to the northwest of the forcing (Figure 1-7). To the east of the forcing, a tropical Kelvin wave signature is seen, with easterly flow but no meridional flow. A Rossby-wave regime exists to the west of the forcing, strongly biased to the northwest of the forcing, with cyclonic flow around the low-pressure region and westerlies near the latitude of the forcing. There is also a significant signal in the southern hemisphere, with cross-equatorial flow to the south and west of the forcing. This flow pattern is quite similar to the lower tropospheric flow in the vicinity of the Asian monsoon during summer.

1.4 Cross-equatorial flow

The equator, where the Coriolis parameter f changes sign, is a strong dynamical barrier in the atmospheric mixed layer. In the free troposphere, the atmosphere may be considered

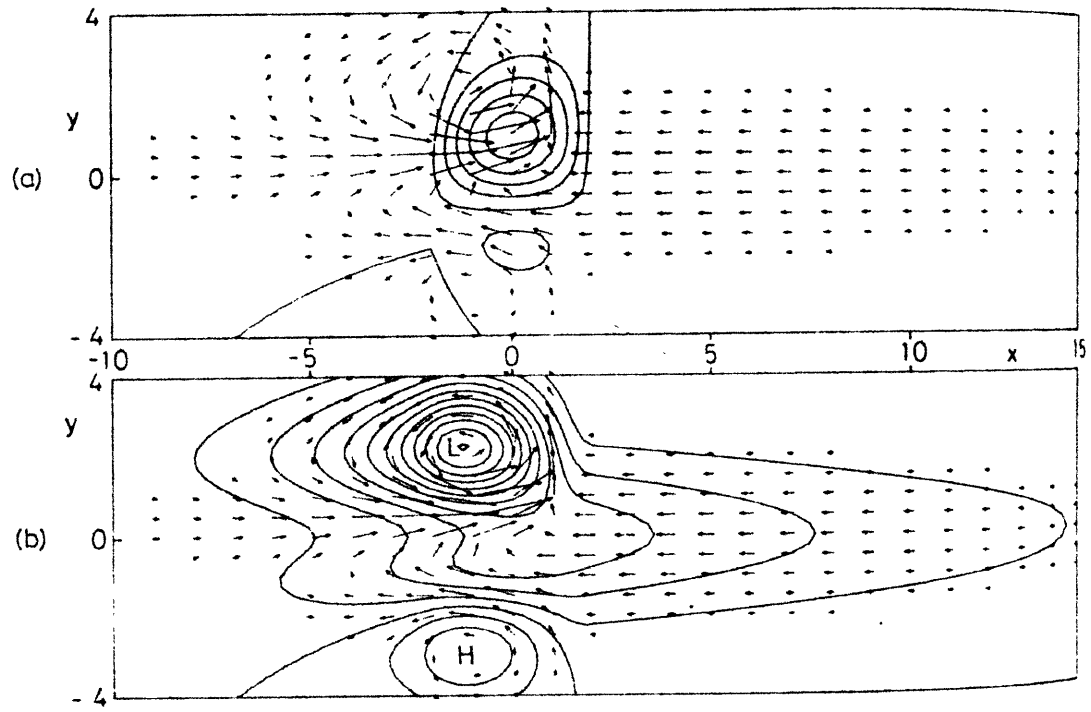

Figure 1-7: Flow induced in a linear model with localized off-equatorial heat source (from Gill (1980), Figure 3). Top, contours of vertical velocity, arrows show low-level horizontal flow. Bottom, contours show perturbation pressure.

to be almost angular momentum conserving, so that the flow follows contours of angular momentum. The flow may act to homogenize angular momentum in the free troposphere, allowing cross-equatorial flow. However, in the mixed layer, viscous effects are strong and can discourage cross-equatorial flow: the meridional momentum budget is a balance between viscous effects, flow induced by mixed-layer temperature gradients, and flow induced by geopotential gradients just aloft of the mixed layer. Because of angular momentum conservation in the free troposphere, the mixed-layer meridional flow induced by the free tropospheric geopotential gradient has a latitude-dependent upper bound, which approaches zero at the equator. Therefore, a temperature gradient in the mixed layer is needed in order to induce a cross-equatorial flow.

Pauluis (2001) has addressed the difficulties in achieving low-level cross-equatorial flow in an axisymmetric framework. For a given mixed layer depth and pressure gradient, there is a maximum possible mass flux that can cross the equator in the mixed layer; this mass flux decreases with shrinking mixed layer depth and with weakening pressure gradient. Thus, if the pressure gradient across the equator is weak, or if the mixed layer is too shallow, the low-level return flow of the Hadley circulation may not be able to cross the equator entirely

in the mixed layer, and some portion of the flow must rise and cross the equator in the free troposphere. The resulting Hadley cell is horseshoe-shaped, with a 'jump' in the lower branch of the flow at the equator. While the jumping behavior is only weak in dry models, the presence of moist convection and associated precipitation weakens the moist stability of the flow near the equator, and the jumping behavior reaches deep into the troposphere.

The dynamical barrier to cross-equatorial flow may also be described in terms of potential vorticity. A parcel of air which crosses the equator will have potential vorticity which is opposite in sign to the background potential vorticity; the potential vorticity of the parcel must be modified for the parcel to make its equatorial crossing permanent. Rodwell and Hoskins (1995) investigated the effects of surface drag and diabatic heating over the Indian Ocean on low-level cross-equatorial flow. These processes act to modify the potential vorticity of the flow, changing the sign of the PV from negative to positive as the flow crosses the equator. If the diabatic processes are not able to change the sign of PV of the flow, the air recirculates into the originating hemisphere in the eastern Indian Ocean.

Investigations into the dynamical mechanisms which allow low-level cross-equatorial flow frequently focus on the response of the tropical atmosphere to a localized, off-equatorial heating. As previously discussed, Gill (1980) achieved significant cross-equatorial flow in a linear, viscous shallow-water model with off-equatorial forcing. Sashegyi and Geisler (1987) examined the response of a linear model of a stratified fluid on a rotating sphere to a prescribed idealized off-equatorial heating. They found a response similar to that of Gill (1980), with two major circulation cells: a zonally-oriented cell with ascent near the heating region and descent to the west, and a meridional overturning cell with cross-equatorial flow and descent in the opposite hemisphere.

Low-level cross-equatorial flow is associated with monsoons across the globe, although the influence of this flow is not well understood. Near West Africa, the flow crosses the equator over the ocean and turns southwesterly as it approaches the coastline during the monsoon season. Over the western Pacific and Indian oceans, the flow is much more complex (Figure 1-3). Numerous studies (eg. Anderson (1976), Rodwell and Hoskins (1995)) have shown that the presence of Africa and the East African mountain range straddling the equator help to form the Findlater jet. In boreal winter, cross-equatorial flow to the Australian monsoon is impacted by the Maritime continent with its volcanic islands. Cross-equatorial flow also occurs over central South America during boreal winter, with northeasterly flow near the equator turning northerly near 10S and then northwesterly over southern Brazil, perhaps deflected by the Andes mountains. Qian et al. (2002) have shown that the presence of cross-equatorial flow, along with seasonal variation in precipitation, can be used to identify monsoonal regions around the globe. One exception is the North American summer monsoon, for which there is no clear area of associated cross-equatorial flow; instead,

southeasterly flow over the warm Caribbean Sea and western Atlantic ocean converges over the North American monsoon region.

The presence of the East African jet, first discovered by Findlater (1969), has focused attention on the role of orography in inducing cross-equatorial flow. During boreal summer, cross-equatorial flow is found in the western Pacific and in a narrow jet along the western Indian Ocean, but there is little cross-equatorial flow in the central and eastern Indian Ocean. Easterly winds crossing the Indian Ocean encounter the East African Highlands, forcing the wind into an intense but narrow low-level cross-equatorial jet along the eastern coast of Africa. This jet accounts for a significant percent of the global total cross-equatorial flow, and is thought to strongly impact the monsoon in the Indian subcontinent. Hoskins and Rodwell (1995) found that the removal of the East African orography in their model lead to a large decrease in the strength of the East African jet. Sashegyi and Geisler (1987) have shown that orography can concentrate the cross-equatorial flow induced by a tropical heat source into a western boundary current, but the net cross-equatorial mass flux is not substantially increased by inclusion of topography.

Moisture budgets taken over the Indian peninsula have shown that cross-equatorial flow supplies a substantial fraction of the moisture needed for monsoon precipitation (Ninomiya and Kobayashi (1999), Kishtawal et al. (1994)), although evaporation from the Arabian Sea is also a significant source of moisture for the monsoon. Findlater (1969) found a positive correlation between the strength of the jet and the intensity of rainfall over western India during the monsoon, with the rainfall peaking about 2 days after the peak in jet strength. Cross-equatorial flows are also associated with the southeast Asian monsoon, where local cross-equatorial flow converges over China with flow crossing from the Bay of Bengal (Ninomiya and Kobayashi, 1999).

1.5 Location of the monsoon

The Asian monsoon shows a strong east-west tilt, with the monsoon extending furthest poleward along the east coast of Asia. To the west of the monsoon region, the Saharan desert exists at roughly the same latitude as the Asian monsoon. The Australian monsoon also shows an east-west tilt, but the West African monsoon does not show such a tilt and sometimes has strongest precipitation at the western coast. Numerical studies have suggested various dynamical mechanisms which contribute to asymmetry of the monsoon.

Rodwell and Hoskins (1996) hypothesized that Rossby waves induced to the west of the monsoon (as in Gill (1980)) are associated with subsidence, which in turn discourages moist convection. Using a simple model with prescribed, idealized forcing, they found a broad area of subsidence to the northwest of a subtropical heat source. This effect was examined in

a model of intermediate complexity with interactive forcing by Chou et al. (2001) and Chou and Neelin (2003). By comparing two cases, one with full spherical geometry, and the other on an f-plane, Chou et al. (2001) found that the Rodwell-Hoskins effect does substantially contribute to the east-west asymmetry of the monsoon. Chou and Neelin (2003) conducted a similar experiment using more realistic continental geometries, and found that the Rodwell-Hoskins effect significantly affected the asymmetry of the monsoon in North America and Asia, but not in Africa.

The strong influence of the large-scale circulation on the geometry of the monsoon has been demonstrated in several studies. Xie and Saiki (1999) found that the low-level cyclonic circulation over the summer continent carries dry continental air into the subtropics along the western edge of the landmass, while moist oceanic air is carried inland along the eastern edge. This suppresses moist convection to the west, while encouraging rainfall in the east. In their model, the feedback between precipitation and soil moisture accentuated this asymmetry, slowing the inland progression of moist convection over the western continent. In a perpetual summer case, the east-west asymmetry of the monsoon was eliminated when sufficient time was allowed to overcome the resistance to precipitation along the western half of the continent.

Chou et al. (2001) considered the effects of advection of moisture and temperature into the monsoon region, which they termed 'ventilation'. When these advection terms were artificially removed while retaining the moisture convergence associated with divergence, monsoon precipitation spread further poleward over the continent. Chou et al. suggested that the advection of low moist static energy air from the cool midlatitude oceans acts to suppress moist convection over the western continent and to limit the poleward extent of the monsoon. In a separate experiment, the ocean heat transport from the tropics into the midlatitudes was increased, raising the subcloud moist static energy in the subtropics and midlatitudes; the resulting precipitation over the continent was greatly increased overall with reduced asymmetry.

1.6 Continental geometry

Relatively few studies have been made using simple continental geometries; most GCM studies use realistic representations of continents, while idealized rectangular continents are only favored for less sophisticated numerical models. Two exceptions to this are the work of Cook and Gnanadesikan (1991) and Dirmeyer (1998), both of which used a simplified continental geometry with a full GCM.

Dirmeyer (1998) experimented with the latitudinal positioning of a single rectangular continent, and found three different dynamical regimes of the monsoon. When the coastline

was located in the tropics, year-round continental precipitation was observed; when the coastline was located in the subtropics, a seasonal monsoon was observed with summer precipitation in the southeast corner of the continent; when the coastline was located in the midlatitudes, a "Mediterranean" climate was seen, with dry summers and wet winters over the landmass. For the subtropical continent cases, the monsoon was primarily supplied with moisture by the tropical easterlies, with little moisture transport across the southern coastline. The longitudinal width of the continent did not strongly affect the monsoon for the subtropical case; the monsoon was weakest when a continent of 360° width was used, in which case the moisture supply by easterlies from the ocean was lost. However, in the subtropical cases the ITCZ never shifted onto the continent and instead remained in the southern hemisphere year-round; the summer monsoon precipitation was relatively weak.

Cook and Gnanadesikan (1991) used a rectangular continent centered on the equator with simplified hydrology in a perpetual summer experiment. They found that moisture availability over the continent restricted the extent of subtropical precipitation: in a case with a swamp continent, summer subtropical precipitation extended fully across the width of the landmass. But in a case with interactive bucket hydrology, the continent rapidly became arid, and subtropical precipitation was limited to the eastern side of the continent, where easterlies carried moist oceanic air inland. Chou et al. (2001) used a similar continental geometry in an experiment with seasonal cycle, and found that when ocean heat transport was neglected, monsoon precipitation over the interior of the continent was very weak for cases with interactive surface hydrology.

The weakness of monsoon precipitation in many of the modeling experiments with an equatorially centered continent raises a question: is an east-west coastline necessary to produce a robust monsoon? Xie and Saiki (1999) found that onset of the monsoon was caused by baroclinic waves of a low-level easterly jet along the coastline - without the coastline and subsequent meridional temperature contrast, these waves might not exist. The warm tropical ocean along the coastline also acts as an important moisture source for the monsoon; the minimal precipitation seen in the continental interior in experiments with an equatorially-centered continent supports the importance of a nearby moisture source. This has implications for paleoclimate; for instance, the equatorially-centered continent of Pangea existed during the Permian.

1.7 Goals of this Work

There are two different dynamical models of the steady monsoon: the Gill (1980) model of the response to a localized off-equatorial heat source as an additive function of linear Kelvin and Rossby wave regimes; and the axisymmetric, nonlinear model of Plumb and Hou (1992)

which considers the monsoon as a Hadley circulation with subtropical ITCZ. This study focuses on the nonlinear, axisymmetric theory, to determine how well this framework can describe the dynamics of the three dimensional monsoon.

There is a wide gap in modeling the monsoon between the highly idealized axisymmetric theory and full GCM studies with realistic physics. While the axisymmetric theory is useful for developing an understanding of the basic physical mechanisms which drive and affect the monsoon, it is unclear how the simplifications which are involved limit the applicability to the fully three dimensional monsoon. On the other hand, the wealth of feedbacks present in the full GCM studies make diagnosis of the monsoon behavior extremely difficult. The goal of this work is to bridge the gap between the idealized axisymmetric theory and the more complex three dimensional monsoon.

The major questions which we wish to address are:

1) How well does axisymmetric theory represent the fully three dimensional monsoon?

2) What determines the strength and location of the monsoon?

A general circulation model with simplified representations of some physical processes and with idealized continental geometry is chosen to achieve intermediate complexity. This allows for a reasonably more realistic portrayal of processes which are suspected to be intrinsic to the monsoon, while at the same time reducing the feedbacks to make analysis more tractable. The complexity of the model geometry is gradually increased from an axisymmetric to an asymmetric framework. By comparing the changes which result from each incremental increase in complexity, the various interacting mechanisms which comprise the monsoon can be separated and examined.

We begin by expanding upon the work of Plumb and Hou (1992) and Emanuel (1995). A major limitation of the axisymmetric theory is the use of a prescribed, non-interactive forcing. While Plumb and Hou (1992) assigned a local subtropical anomaly of thermal equilibrium temperature in a dry model, Emanuel (1995) and Zheng (1998) assumed a saturated surface with constant, prescribed temperature and surface wind speeds. How well does the theory apply when a continent with interactive surface forcing is introduced? The theory hinges on the distribution of RCE temperatures at the tropopause; in order to achieve a temperature maximum over the landmass, the surface forcing must be communicated into the upper troposphere. Deep moist convection is very effective at such communication, but dry convection is not. Given an initially arid landmass with little moist convection, how is threshold behavior affected? Axisymmetric theory predicts that the threshold for a global meridional circulation requires increased forcing as the forcing region is shifted poleward. How, then, does the continental location impact the monsoon?

Axisymmetric studies are limited by the exclusion of zonally asymmetric forcing and of horizontal eddies; they cannot explain asymmetry of the monsoon. The Rodwell-Hoskins

effect is completely neglected in an axisymmetric framework, as Rossby waves do not exist; similarly, the baroclinic eddies which Xie and Saiki found to initiate the monsoon are not included. The model is expanded to a three-dimensional setup, but the surface conditions and continental geometry are kept zonally symmetric; comparison of these results with the two dimensional case will reveal the role of eddies in formation of the monsoon.

Finally, a continent of limited longitudinal extent is introduced to explore the effects of zonally asymmetric forcing. Chou et al. (2001) and Xie and Saiki (1999) found that advection of relatively cool, dry air by the asymmetric circulation contributes to east-west asymmetry of the monsoon by suppressing convection along the western edge of the continent. Why is asymmetry seen in the Asian and Australian monsoons, but not in West Africa?

The model is described in Chapter 2; model results from the two dimensional cases are discussed in Chapter 3. Three dimensional model results are presented in Chapter 4, a discussion of the correspondence of the model results to observations is found in Chapter 5, and conclusions are given in Chapter 6.

Chapter 2

Model

The model used is the MIT General Circulation Model (MITGCM), release 1.0. The GCM consists of a dynamical core coupled to an atmospheric physics package. This chapter will give an overview of the model dynamics and will describe in greater detail the components of the physics package. Some general characteristics of the behavior of the MITGCM will also be discussed.

2.1 Model Dynamics

The dynamical kernel of the model is described by Marshall et al. (2004). The atmospheric MITGCM has been tested extensively against the Held and Suarez (1994) results, although a different physics package was used than that implemented in this thesis.

The model gridspace used in this thesis is a partial sphere between 64S and 64N, with 40 pressure levels in the vertical at 25 mb intervals. A staggered spherical polar grid is used with 4° latitudinal resolution and 6° longitudinal resolution. There is no orography, and the surface is assigned to the 1012.5 mb pressure level. The top of the atmosphere is located at 0 mb; there is no sponge layer at the upper boundary. Lindzen et al. (1968) found that the imposition of a rigid lid results in spurious reflection of vertically propagating waves, and conjectured that this results would also occur with the lid positioned at $p = 0$. However, Kirkwood and Derome (1977) found that the wave reflection off of a rigid lid at $p = 0$ does not result in large errors except for in cases of extremely crude vertical resolution. The vertical resolution used in the MITGCM here is relatively high, and the impact of wave reflection off is not expected to be significant. Physical and thermodynamic calculations are made with a 5 minute timestepping interval. The Eulerian flux form of the momentum equations is used, with the quasi-second order Adams-Bashforth method for advection of both momentum and tracers.

2.2 Atmospheric Physics

The atmospheric physics package acts on a single column. Radiation and cloud physics are not included; instead, the atmosphere undergoes Newtonian cooling with a cooling timescale of $\tau_{NC} = 60$ days.

$$Q_{NC} = \tau_{NC}^{-1}(T_{NC} - T) \tag{2.1}$$

where T is the temperature at a gridpoint, and Q_{NC} is the cooling rate. $T_{NC} = 200$ K for all gridpoints; this profile for T_{NC} is chosen for its simplicity. There is no representation of stratospheric chemistry, and the stratosphere is cooled toward 200 K by (2.1).

The moist convective scheme of Emanuel (1991) is used, including the modifications of Emanuel and Živković Rothman (1999). This scheme employs a buoyancy-sorting approach and was designed with the goal of accurately depicting the convective tendency of moisture. The parameters used as part of this scheme have been optimized against observed data from the Tropical Ocean Global Atmosphere Coupled Ocean-Atmosphere Response Experiment (Emanuel and Živković Rothman, 1999). The convection scheme also acts to transport momentum through convective updraughts and downdraughts. The convective momentum tendency of horizontal winds is treated as a vertical eddy-flux of velocity which incorporates entrainment and detrainment of the convective drafts (after Gregory et al. (1997)).

The convection scheme includes dry adiabatic adjustment, which is performed over regions which are unstable to unsaturated ascent. Instability of this nature is most common near the surface where strong heating occurs. The horizontal velocities and moisture are considered to mix rapidly in the unstable layer, and are assigned the mean values within the layer. The temperature is redistributed to stabilize the layer while holding the mean enthalpy constant.

A mixed layer of momentum only (not thermodynamic quantities) is included at the lower boundary of the model. The depth of the momentum mixed layer is assigned to be 200 mb for all locations and times; this relatively deep mixed layer is chosen to allow greater cross-equatorial flow than with a shallow mixed layer. There is also a momentum tendency term due to turbulent surface fluxes, of the form

$$\vec{F}_s = \frac{-g\rho_s c_D \vec{u}_s v_s^* L}{dp_s} \tag{2.2}$$

where $\vec{F}_s$ is the momentum tendency, ρ_s is the density of the surface air, c_D is the surface drag coefficient, $\vec{u}_s$ is the surface velocity, L is a vertical wind profile coefficient, and dp_s is the pressure difference between the surface and the first model layer. v_s^* is a modified surface velocity, defined as

$$v_s^* = \sqrt{w_D^2 + w_{s0}^2 + v_s^2 + u_s^2} \tag{2.3}$$

where w_{s0} is a minimum surface wind speed, w_D is a convective downdraft velocity scale, and v_s and u_s are the surface meridional and zonal velocities.

Very simple representations of ocean and land surfaces are implemented. A slab ocean is used, with SST profile fixed in time. The standard atmospheric physics package with this version of the MITGCM does not include representations of land surface, so a set of simple land parameterizations was developed. Over land, a bucket hydrology following Manabe (1969) is used. Surface evaporation is modified by a factor $\mathcal{B}$

$$\mathcal{B} = \begin{cases} 1 & B \geq 0.75B_0 \\ \frac{B}{0.75B_0} & B < 0.75B_0 \end{cases} \qquad \frac{\partial B}{\partial t} = P - E \tag{2.4}$$

where B_0 is an assigned bucket depth indicating the amount of moisture that can be stored per unit surface area, B is the current moisture in the bucket per unit area, E is the evaporation rate, and P is the precipitation rate. Any excess moisture gained by precipitation is considered to be runoff, so that the maximum value for B is B_0, and likewise the bucket moisture content is constrained to a minimum value of 0 cm. For all runs, the land is assigned a uniform bucket depth of 20 cm.

Because a Newtonian cooling scheme is used, the flux balance at the surface cannot be calculated using radiative fluxes. Instead, the net downward flux into the surface (THF) is prescribed as a function of latitude:

$$THF(\phi) = LHF(T_s) + SHF(T_s) \tag{2.5}$$

where ϕ is the latitude, LHF is the latent heat flux into the atmosphere, SHF is the sensible heat flux into the atmosphere, and T_s is the surface temperature. The surface temperature and heat fluxes are interdependent and calculated iteratively. There is no diurnal cycle.

The latent and sensible heat fluxes are calculated from bulk parameterizations:

$$SHF(T_s) = 100\rho_s C_d c_{pp}(v_s^*(T_s - T_{Sa}) - v_s' T') \tag{2.6}$$

$$LHF(T_s) = 100 L_v \rho_s C_d \mathcal{B} e(v_s^*(q_s(T_s) - q) - v_s' q') \tag{2.7}$$

$$v_s' = \sqrt{w_D^2 + v_s^2 + u_s^2}$$

where SHF and LHF are the sensible and latent heat fluxes from the surface to the atmosphere, C_d is the surface drag, e is an efficiency factor, v_s' is the perturbation surface wind speed, ρ_s is the air density at the surface, L_v is the latent heat of vaporization at the surface, q_s is the saturated specific humidity at the surface, q is the specific humidity of the

air just above the surface, e_s is the saturation vapor pressure, $q^{'}$ is the turbulent specific humidity perturbation scale, c_{pp} is the heat capacity of moist air at constant pressure, T_{Sa} is the temperature of air at the surface, and $T^{'}$ is the turbulent temperature perturbation scale. For all model runs, the ocean surface drag coefficient were set to be 1.2×10^{-3}, and the land surface drag coefficients were set to 3.6×10^{-3}.

Using a prescribed net radiative flux has the benefits of allowing direct control over the land surface forcing, and of reducing the number of feedbacks between the forcing and the circulation in comparison to a situation with interactive radiation. Fewer feedbacks permit easier diagnosis of the underlying dynamical mechanisms; this helps to avoid one of the main pitfalls of GCMs wherein the dynamics of the flow can be too complex be readily unraveled and understood. However, the loss of these feedbacks makes the resulting flow less realistic; for example, surface temperatures may become very hot over a desert-like land area as there no increase in the outgoing longwave radiation with increased surface temperatures. Radiative feedbacks due to the presence of clouds and the greenhouse effect are similarly neglected. However, direct control of the land surface forcing allows the behavior of the monsoon to be explored in parameter space by testing a range of different forcing strengths.

A Shapiro filter is used to remove numerical noise, similar to hyperdiffusion. The form of the filter used is given by the function S, where

$$S = \left[1 - \frac{\Delta t}{\tau_{shap}} \left(\frac{1}{4}\delta_{ii}\right)^n\right] \left[1 - \frac{\Delta t}{\tau_{shap}} \left(\frac{1}{4}\delta_{jj}\right)^n\right] \tag{2.8}$$

where τ_{shap} is a damping time scale, Δt is the timestep, δ_{ii} is the grid spacing in the x-direction, and δ_{jj} is the grid spacing in the y-direction. This filter is applied to the horizontal velocity fields, temperature, and specific humidity at the end of each time step. An order of $n = 8$ is chosen for the Shapiro filter with $\tau_{shap} = \Delta t$; this filter is strong enough to remove numerical instabilities while allowing the existence of desirable synoptic scale waves. A quadratic vertical viscosity term is included in the GCM, with the coefficient ν constant with height and position.

The radiative convective equilibrium calculations are made by neglecting the pressure forcing terms in the horizontal momentum equations and removing the Shapiro filter - no horizontal flow develops and there is no thermodynamic communication between vertical columns.

All model runs are initialized with zero winds and empty buckets over the land surface. The initial fields of temperature and specific humidity were assigned to a standard vertical profile, shown in Figure 2-1. In most cases, a perpetual summer setup is used with no seasonal variation in SST or in land surface forcing. The model is run until an equilibrium state is reached.

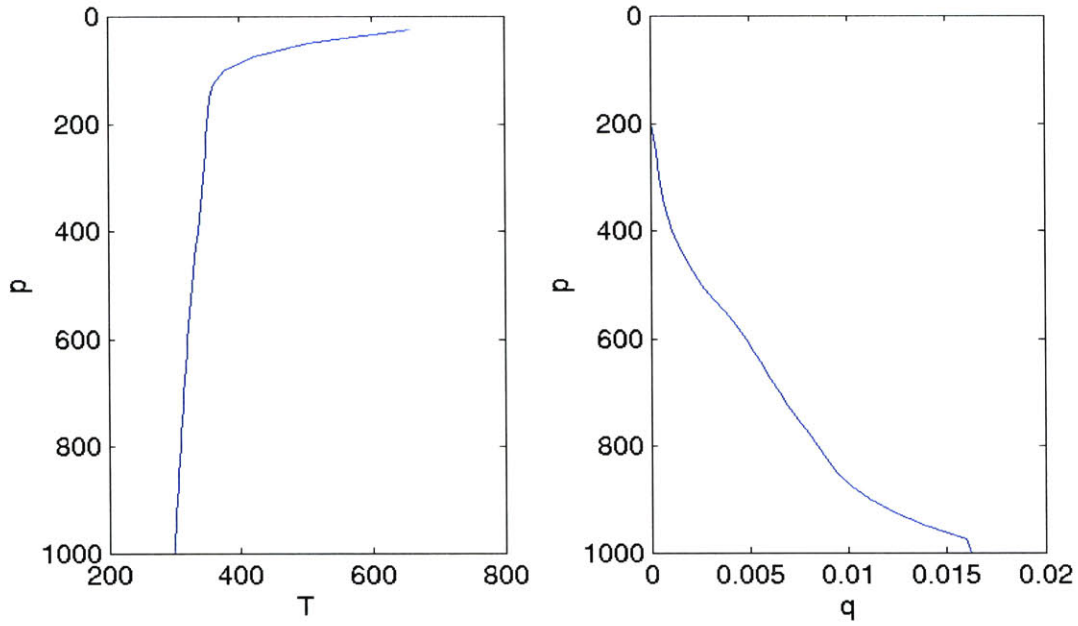

Figure 2-1: Initial vertical profiles of temperature (left, K) and specific humidity (right, kg/kg).

2.3 Characterizing the MITGCM

As the atmospheric version of the MITGCM used here has not been extensively described in existing literature, the general characteristics of the model behavior will be discussed.

2.3.1 Comparison with Axisymmetric Theory

As the focus of this thesis is on the axisymmetric theory of Hadley circulations, a comparison with the analytic theory is helpful in characterizing the model behavior. First, the work of Held and Hou (1980) is reproduced in a dry version of the MITGCM. The moist convection scheme is omitted, a stratosphere is added at a height of 12 km, and the equatorially-centered equilibrium temperature profile from Held and Hou (1980) is applied (their equation (2)). The model is spun up from rest until a steady state circulation is attained. Three different levels of viscous forcing are tested: $\nu = 5$, 10, and 20 Pa^2/s. The MITGCM differs from the Held and Hou model in that the atmosphere is not Boussinesq, there is no rigid lid, and there is a momentum mixed layer.

Figure 2-2 shows an example of the resulting meridional circulation. The circulations which occur with stronger or weaker viscosity are similar in extent and strength, although the lower viscosity cases are prone to inertial instability. This instability manifests as stacked inertial rolls, similar to that found by Held and Hou (1980) in their lowest viscosity case.

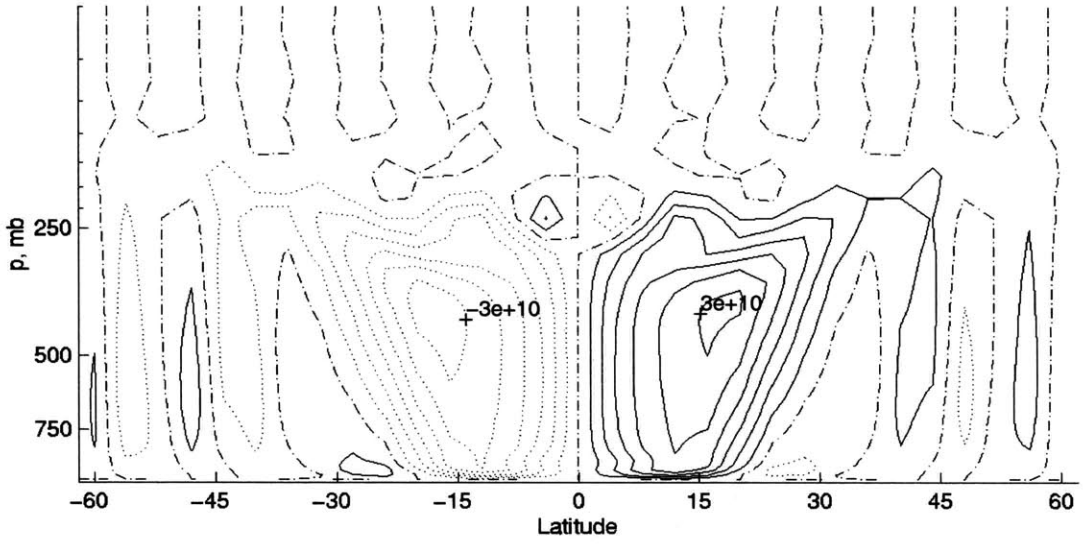

Figure 2-2: 250 day time mean streamfunction, $\nu = 10Pa^2/s$, solid lines indicate clockwise flow, dashed lines indicate counter-clockwise flow, contour interval kg/s, dash-dot is zero line.

The analytic theory predicts that the poleward limit of the circulation at the tropopause should occur at 28.6°, coincident with the maximum westerly zonal wind. The maximum zonal wind and boundary of the meridional circulation occurs at 30° in the MITGCM, which is in good agreement with the theory. The strength of the circulation is similar to that found by Held and Hou in the numerical cases with viscosity near $\nu = 5m^2/s$.

The circulations are close to angular momentum conserving, especially with low viscosity. Figure 2-3 shows the upper tropospheric absolute vorticity for all three cases. Angular momentum is uniform in regions with zero absolute viscosity; the viscosity is near zero from the equator to the poleward edge of the circulation in all cases, with a sudden increase beyond the limit of the meridional cell.

The upper tropospheric zonal wind may be predicted by the analytic theory. The surface drag used in the MITGCM is quadratic, unlike the drag used by Held and Hou (1980); the drag is linearized using a mean value of the surface wind speed in order to calculate the theoretical zonal wind field. The predicted surface winds are stronger than the modeled surface winds by a factor of two. The upper tropospheric winds, shown in Figure 2-4, are quite reasonably close to the predicted winds both in the Hadley region and in the midlatitudes. The modeled temperature field (not shown) is also very close to the predicted temperatures.

For comparison, the model is run with the full dynamics, including moist processes, in

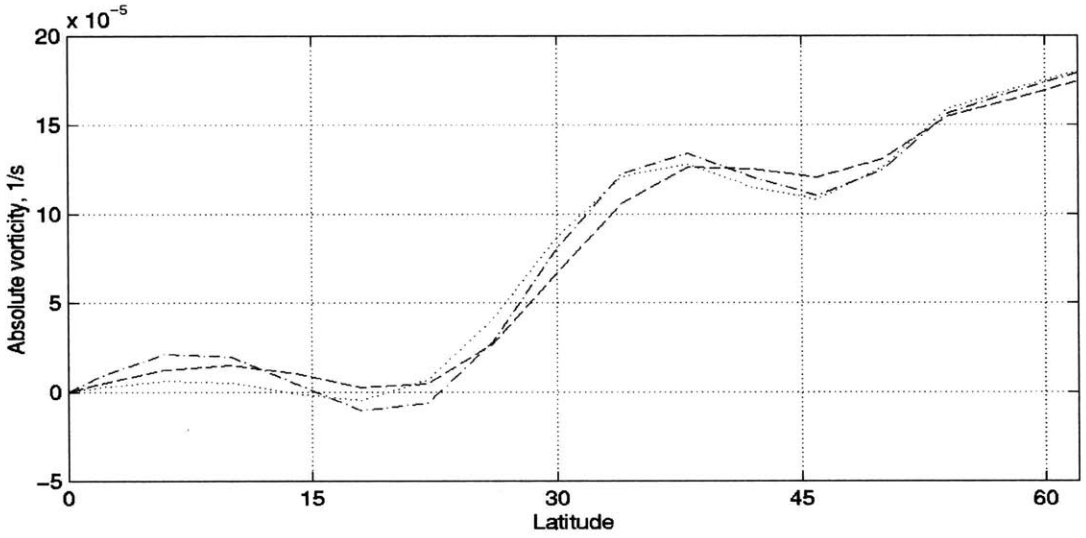

Figure 2-3: 250 day time mean absolute vorticity at 200 mb. $\nu = 5Pa^2/s$, dotted line; $\nu = 10Pa^2/s$, dash-dot line; $\nu = 20Pa^2/s$, dashed line.

an axisymmetric aquaplanet setting with SST maximum at the equator.

$$SST(\phi) = SST_0 - \Delta T sin(\phi)^2 \tag{2.9}$$

where $SST_0 = 302$K, and $\Delta T = 28$K. The viscosity is set to $\nu = 10Pa^2/s$. Two Hadley cells form with ascent at the equator and subsidence in the subtropics, as shown in Figure 2-5; a broad precipitation maximum forms at the equator. The size and form of the Hadley cells are very similar to that found by Held and Hou (1980) and in the dry results, although the circulation is stronger by a factor of three in the aquaplanet case. However, the forcing in the aquaplanet case is meant to correspond to the observed annual mean SST forcing, rather than to correspond to the forcing used in Held and Hou (1980), so that a difference in circulation strength is not unexpected.

2.3.2 General Model Behavior

A test case is performed in 2D on the latitude-height plane, using an aquaplanet setup with SST uniformly warm at all latitudes,

$$SST(\phi) = 302K \tag{2.10}$$

The model is run for 200 days with an initial zero wind field. The circulation which results is extremely weak in comparison to the observed Hadley circulation, as seen in Figure 2-6. Precipitation (not shown) is nearly uniform at 3.79 mm/day at all latitudes. Clearly, the

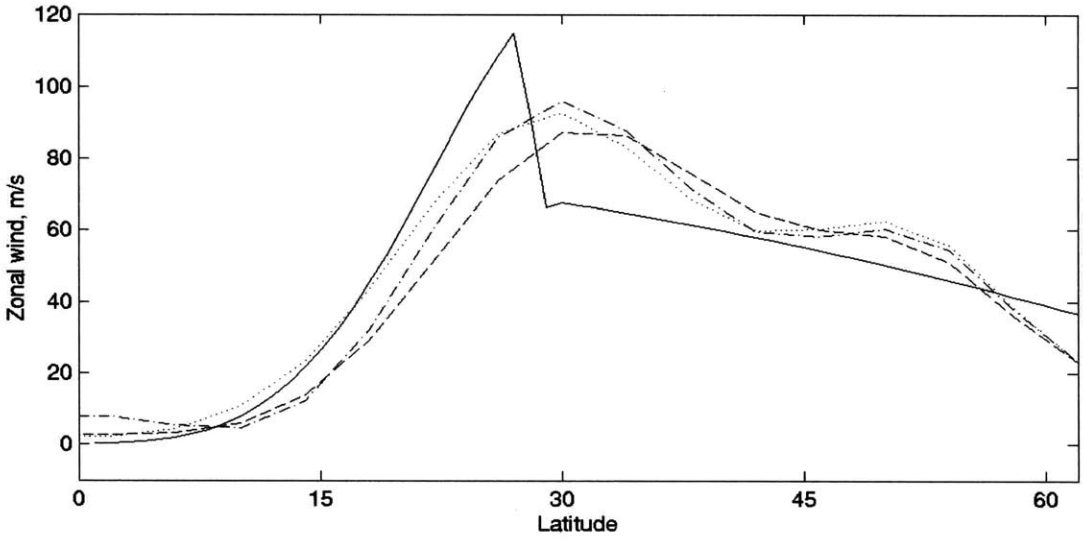

Figure 2-4: 250 day time mean zonal wind at 200 mb. Theory, solid line; $\nu = 5Pa^2/s$, dotted line; $\nu = 10Pa^2/s$, dash-dot line; $\nu = 20Pa^2/s$, dashed line.

model does not self-organize to form a robust meridional circulation or localized deep moist convection.

To explore the model behavior in three dimensions, an aquaplanet case is run with summer-like SST distribution:

$$SST(\phi) = 302\,K - 28sin(\phi - 8N)^2 \tag{2.11}$$

The zonal mean meridional circulation features a cross-equatorial Hadley cell (Figure 2-7) with a smaller local summer Hadley circulation. Eddy-driven Ferrel cells are present in the midlatitudes. The upper tropospheric zonal wind field includes an easterly jet over the tropics flanked by westerly jets on either side. In the lower troposphere, the easterly jets near 10S and 20N result from equatorward flow of the meridional circulation. In the tropics, there is a broad peak in rainfall, with greatest precipitation near the equator and a secondary maximum in the subtropics near 18N. This subtropical precipitation maximum is related to the strong low level winds associated with the local summer Hadley circulation, which increase surface latent heat fluxes and causes a local maximum in boundary layer moist static energy at 14N.

Approximately 30 days after initializing the model, the westerly subtropical jets develop large eddies. After the initial perturbation of the jets, the dominant wave signals are of wavenumber 5-7 in the subtropics. The Eliassen-Palm flux signature (Figure 2-8) shows baroclinic wave structure in the midlatitudes, with the wave energy becoming barotropic in

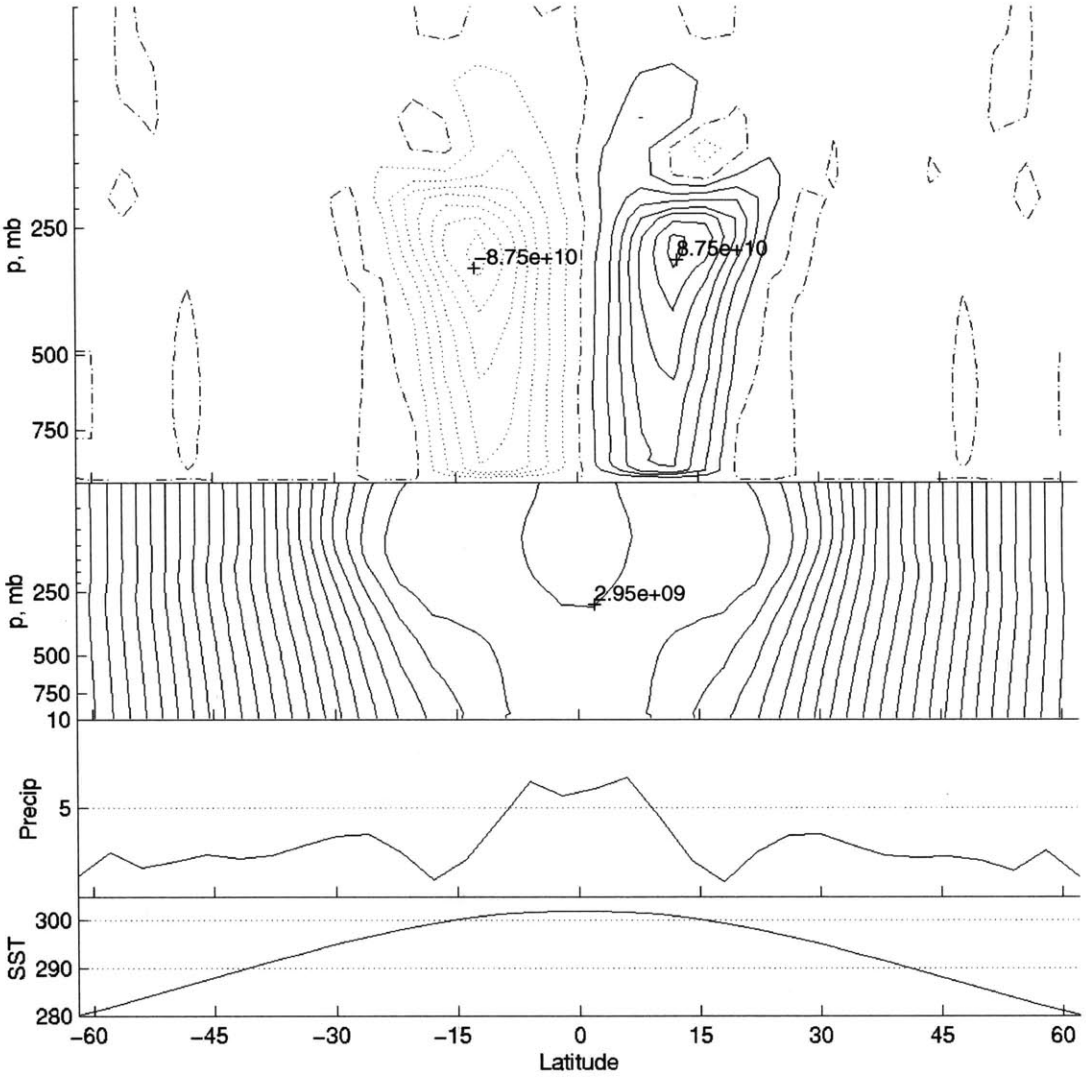

Figure 2-5: Aquaplanet case with SST maximum at the equator, 100 day time mean fields. Top, streamfunction, contour interval 1.25e10 kg/s, dotted lines indicate counter-clockwise flow, solid lines indicate clockwise flow, dash-dot is zero contour. Upper center, absolute angular momentum, contour interval 1E8 m^2/s. Lower center, precipitation, mm/day. Bottom, SST, K.

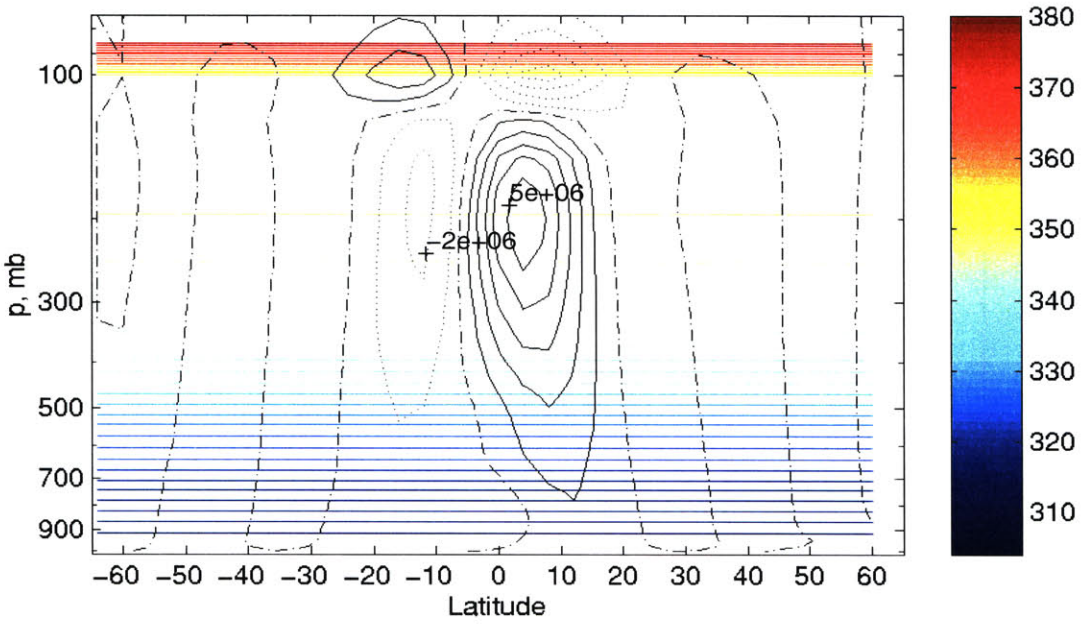

Figure 2-6: Streamfunction, kg/s, and θ_v (color), K, aquaplanet case with uniform SST. Time mean, days 150-200. Zero circulation line, dash-dots.

the upper troposphere, with dissipation in the subtropics.

Wavenumber-phase speed spectra are shown in Figure 2-9 for the 250 mb meridional wind at various latitudes, calculated using the method of Randel and Held (1991) and Hayashi (1971). There is a strong westward propagating wavenumber five signal in both the southern and northern hemisphere midlatitudes, as well as eastward propagating waves ranging from wavenumber three to eight. The tropics have very weak upper level waves in the meridional wind near the equator, with mainly eastward propagating waves of wavenumber 3-4. A fast wavenumber four signal is especially prominent near 10S. There is no equivalent of the Madden-Julian oscillation observed in the tropics with this setup.

The wavenumber-phase speed spectra for the precipitation field is much noisier than that of the meridional wind, as seen in Figure 2-10. Eastward propagating waves of wavenumber six and higher show the greatest precipitation in the midlatitudes. In the tropics, slower moving westward propagating waves are dominant in the precipitation field, in contrast to the meridional velocity field.

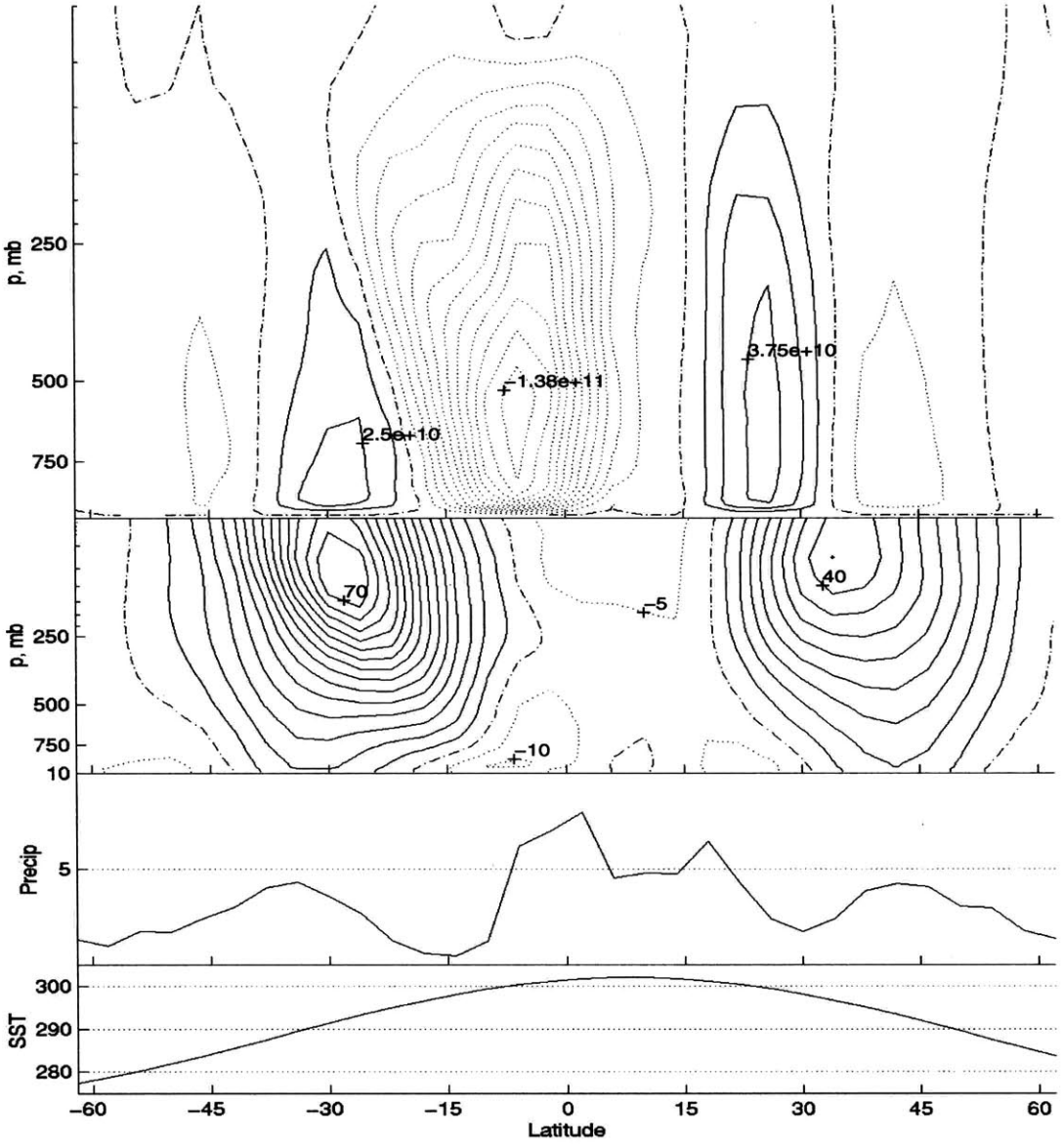

Figure 2-7: Aquaplanet case in three dimensions with SST maximum at 8N, zonal mean fields, 100 day time mean. Top, streamfunction, contour interval 1.25e10 kg/s, dotted lines indicate counter-clockwise flow, solid lines indicate clockwise flow, dash-dot is zero contour. Upper center, zonal wind, contour interval 5 m/s, dotted line indicates easterlies, solid lines indicate westerlies. Lower center, precipitation, mm/day. Bottom, SST, K.

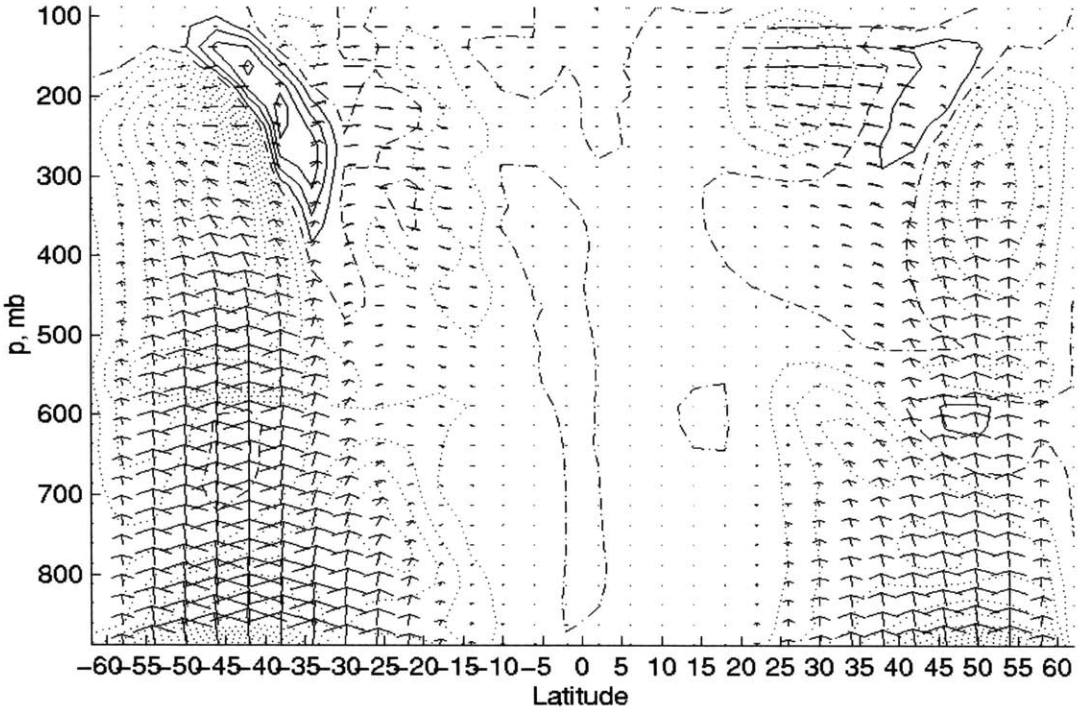

Figure 2-8: Aquaplanet case in three dimensions with SST maximum at 8N, Eliassen-Palm fluxes and divergence over 100 days, contour interval 30 m/s^2, solid contours indicate divergence, dotted contours indicate convergence.

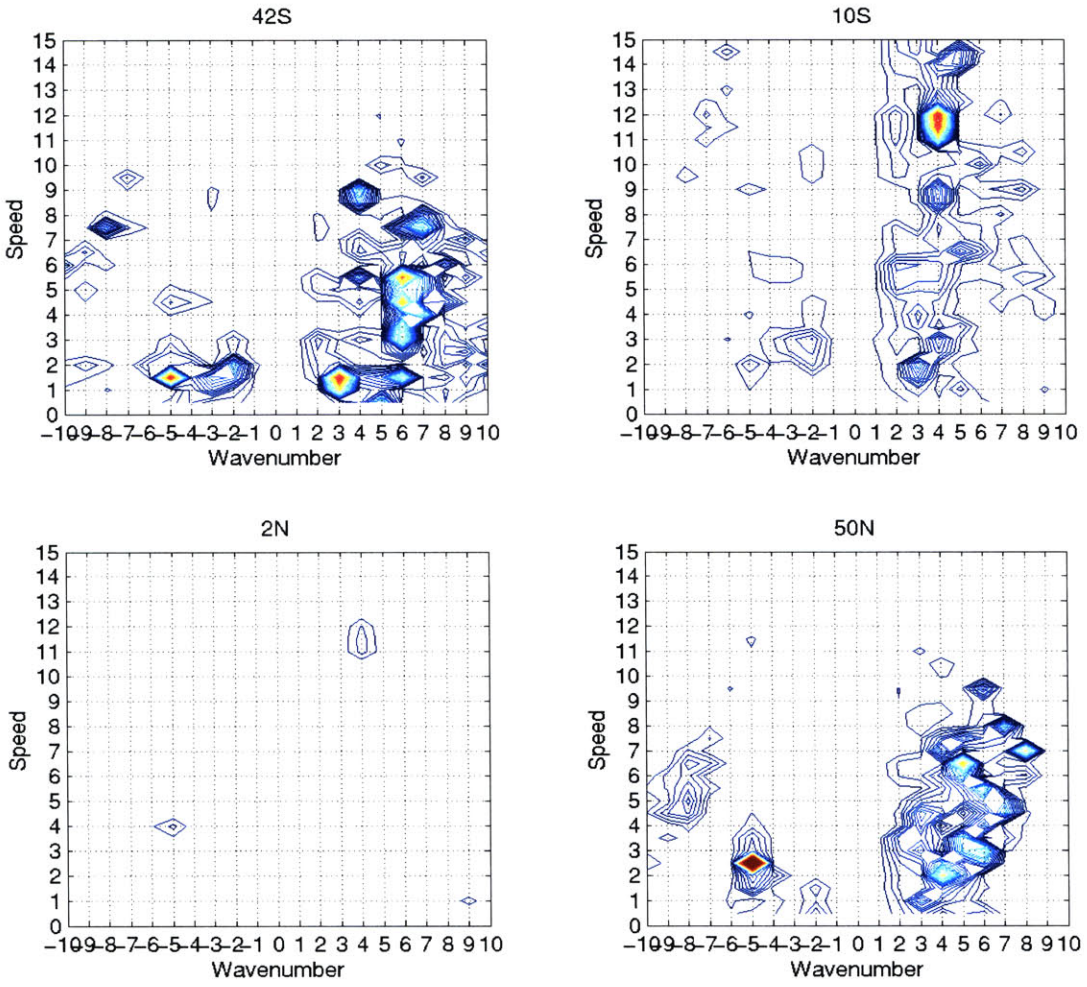

Figure 2-9: Aquaplanet case in three dimensions with SST maximum at 8N, zonal wavenumber-phase speed spectra of 250 mb v-wind at different latitudes, negative wavenumber indicates westward propagating waves, positive wavenumber indicates eastward propagating waves, speed in m/s. Contour interval 2E-8 $ms^{-1} * \Delta c^{-1}$, with Δc the unit phase speed interval of 1.0 ms^{-1}. a) 42S; b) 10S; c) 2N; d) 50N.

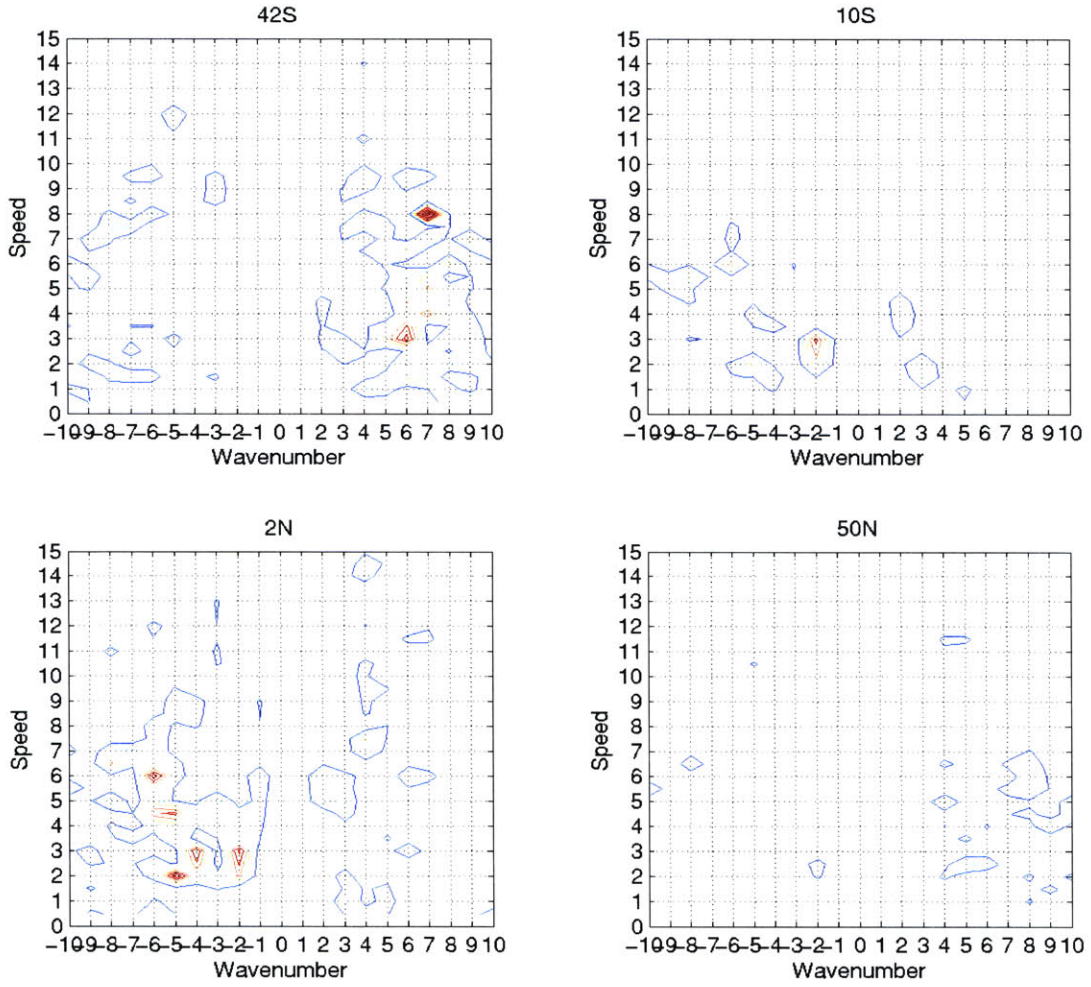

Figure 2-10: Aquaplanet case in three dimensions with SST maximum at 8N, Zonal wavenumber-phase speed spectra of precipitation at different latitudes, negative wavenumber indicates westward propagating waves, positive wavenumber indicates eastward propagating waves, speed in m/s. Contour interval 2E-9 $mm/day * \Delta c^{-1}$, with Δc the unit phase speed interval of 1.0 ms^{-1}. a) 42S; b) 10S; c) 2N; d) 50N.

Chapter 3

Two Dimensional Cases

An axisymmetric framework on the height-latitude plane is implemented in the model in order to explore the applicability of the axisymmetric theory with more realistic interactive forcing. All fields are invariant in longitude in this setup, but zonal flow is allowed. The behavior of the model is first characterized with a series of aquaplanet experiments; the steady state results of Held and Hou (1980), Lindzen and Hou (1988), and Plumb and Hou (1992) are tested by varying the distribution of SST. A simple continent is then introduced in the subtropics, and the surface forcing over the landmass is varied in strength to determine the role of threshold-type behavior of the meridional circulation. The location of the continental coastline is also varied to explore the dynamics of the circulation.

3.1 Aquaplanet

An aquaplanet surface is employed to characterize the atmospheric response to different forcing distributions. A time-invariant distribution of SST is used to study the steady response of the circulation; the model is spun up from rest until an equilibrium state is reached. First, a simple Lindzen and Hou (1988) type forcing is used with off-equatorial SST maximum located at a range of latitudes throughout the tropics and subtropics. Then the response to a Plumb and Hou (1992) type localized off-equatorial forcing is tested, and the importance of viscous effects and convective momentum transfer on the momentum budget are explored. The impact of the latitudinal position of the localized forcing is also investigated.

3.1.1 Summer SST Cases

The dynamical atmospheric response to an off-equatorial SST maximum is examined in a series of model experiments with varied SST profile. In these cases, the model is ini-

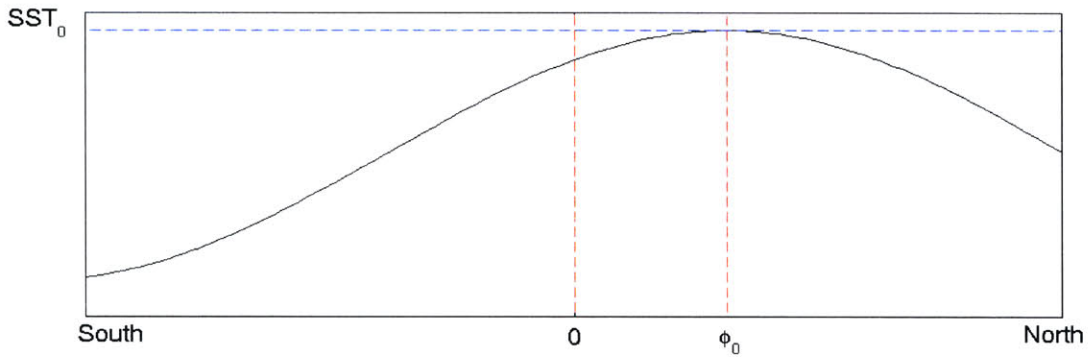

Figure 3-1: Diagram of summer-like SST distribution.

tialized from a resting state and run with a prescribed, time-invariant SST profile until a near-equilibrium state is reached. The SST distribution, shown in Figure 3-1, is assigned according to

$$SST(\phi) = SST_0 - \Delta T sin(\phi - \phi_0)^2 \tag{3.1}$$

where ϕ is the latitude, ϕ_0 is the latitude of maximum SST (SST_0), and ΔT is the magnitude of the meridional variation in SST. ΔT of 28K is used for these cases, SST_0 is 302K and ϕ_0 is varied from 0N to 25N. This setup is similar to that used by Lindzen and Hou (1988), although the radiative-convective equilibrium temperature is determined by the surface forcing and physical processes, rather than being directly assumed. Given the moist convective physics of the model, the radiative convective equilibrium temperature is expected to approximate a moist adiabat in the vertical at all latitudes; thus the meridional distribution of the RCE temperature in the upper troposphere will follow that of the SST.

The resulting steady-state circulations are in good agreement with the axisymmetric theory. When the SST maximum is moved off the equator (eg., Figure 3-2), the cross-equatorial 'winter' Hadley cell dominates with a much weaker 'summer' cell confined to the warmer hemisphere poleward of the SST maximum. The ascent region and the precipitation maximum are located slightly equatorward of the SST maximum, which differs from the result found by Lindzen and Hou (1988); this is a consequence of the moist convective dynamics, and will be discussed further in section 3.3. The maximum strength of the winter cell and the latitudinal breadth of this cell increase as the SST maximum is moved poleward; the summer cell weakens, and does not exist for ϕ_0 poleward of 8N (eg. Figure 3-3). As seen in Figures 2-5, 3-2, and 3-3, the Hadley cells nearly conserve angular momentum.

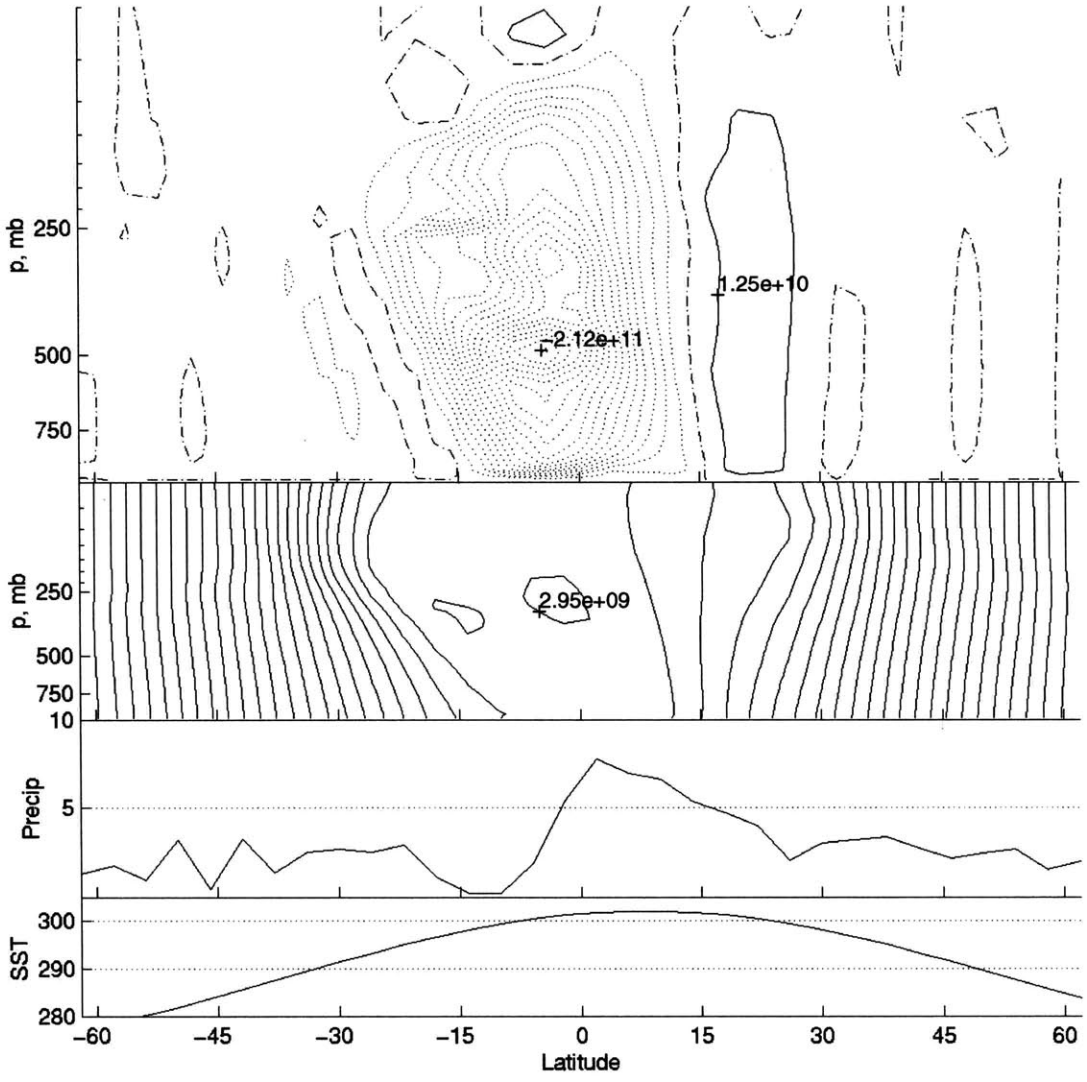

Figure 3-2: Aquaplanet case with SST maximum at 8N; as in Figure 2-5

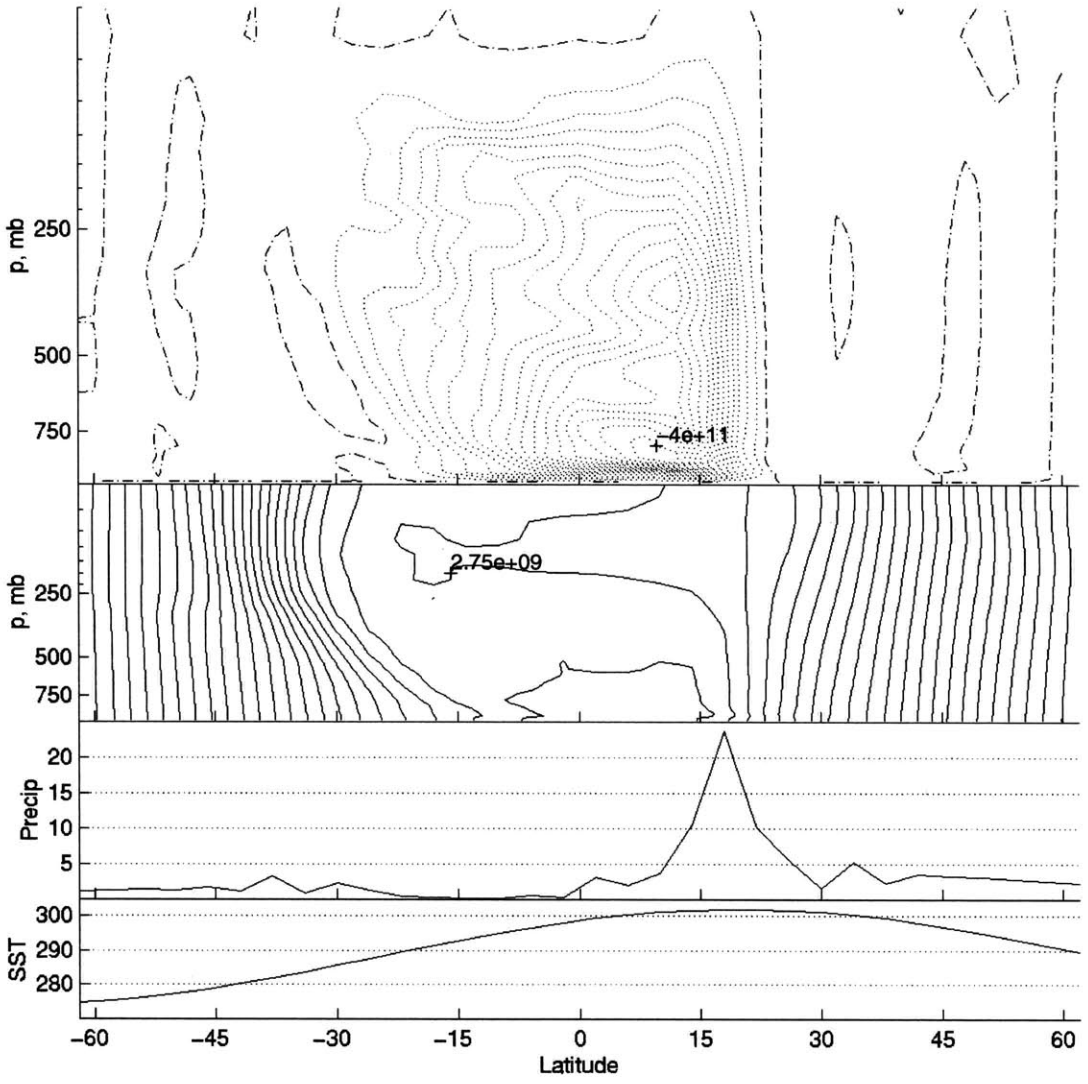

Figure 3-3: Aquaplanet case with SST maximum at 20N, 100 day time mean fields. Top, streamfunction, contour interval 2.5e10 kg/s, dotted lines indicate counter-clockwise flow, solid lines indicate clockwise flow, dash-dot is zero contour. Upper center, absolute angular momentum, contour interval 1e8 m^2/s. Lower center, precipitation, mm/day. Bottom, SST, K.

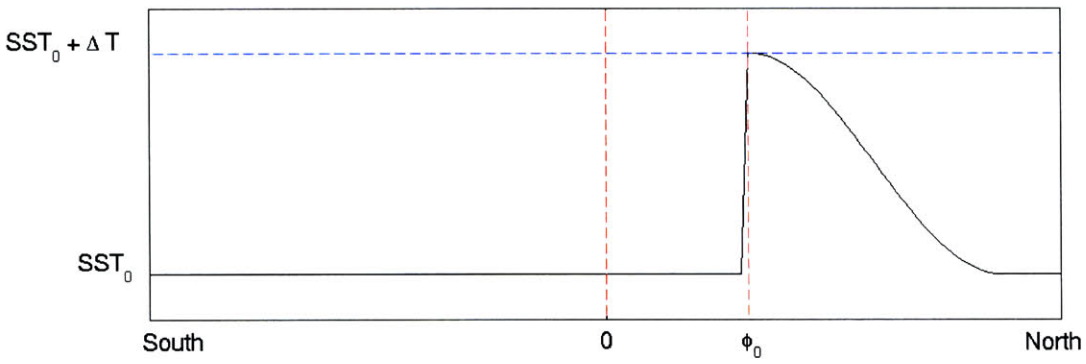

Figure 3-4: Diagram of SST distribution for case with localized perturbation.

3.1.2 Localized Forcing Cases

The response of the atmosphere to a localized subtropical forcing is examined in the aqua-planet setup. The model is spun up from rest with SST of 302K at all latitudes for 200 days, then an SST perturbation of the form

$$SST(\phi) = 302K + \Delta T cos^2((\phi - \phi_0)\frac{5\pi}{4}),\ \phi_0 < \phi < (\phi_0 + 42°) \qquad (3.2)$$
$$SST((\phi) = 302K\ \phi \leq \phi_0,\ (\phi_0 + 42°) \leq \phi$$

is introduced, where ΔT is the strength of the SST perturbation. The model is then integrated until an equilibrium state is reached. This form of the local SST perturbation is chosen to emulate the presence of a continent, with an abrupt interface between land and ocean in the subtropics. A range of ΔT are tested to characterize any threshold behavior.

Subtropical Threshold Behavior

The threshold behavior of Plumb and Hou (1992) and Emanuel (1995) is investigated in a series of cases with $\phi_0 = 16N$ in (3.2); this latitude is chosen as representative of a subtropical monsoon. The strength of the applied SST perturbation (ΔT in (3.2) is varied from $0.5\,K$ to $2.5\,K$. Three different cases are compared: a nearly inviscid case with vertical viscosity $\nu = 10\,Pa^2/s$ and no convective momentum transport (CMT); a low viscosity case with $\nu = 10Pa^2/s$ but with convective momentum transport included; and a high viscosity case with $\nu = 100\,Pa^2/s$ including convective momentum transport. Comparison of the results of these three different cases highlights the relative effects of viscosity and convection on conservation of angular momentum in the upper troposphere.

Low Viscosity Cases The low viscosity cases show clear threshold behavior of the circulation both with and without the inclusion of convective momentum transfer (Figure 3-5).

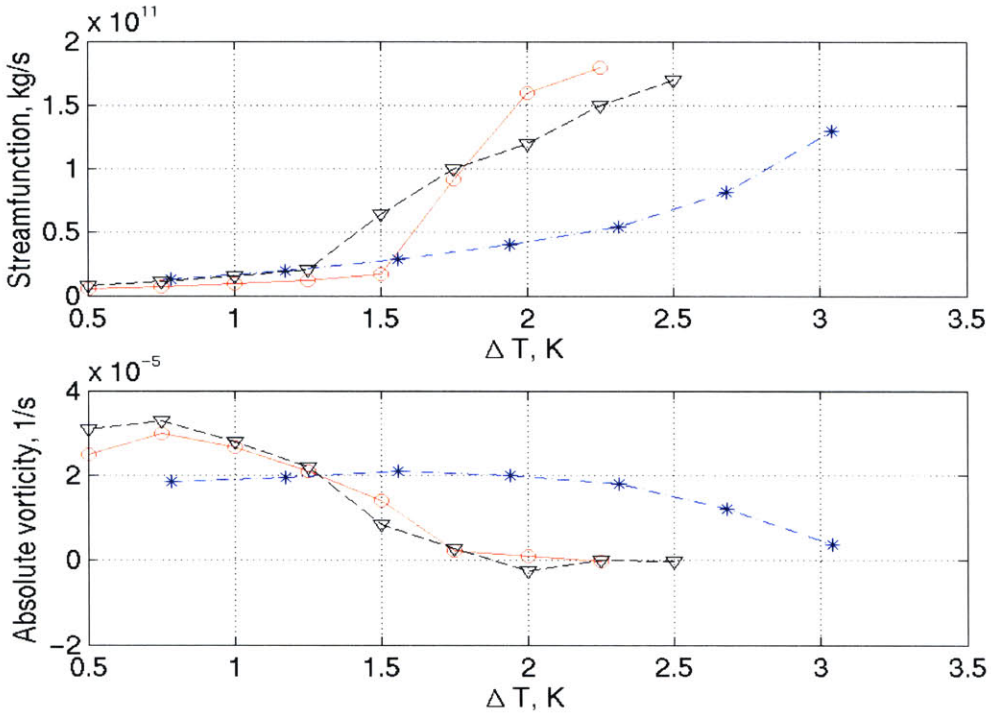

Figure 3-5: Steady-state results as a function of subtropical forcing, aquaplanet surface with subtropical SST perturbation. Low viscosity case without CMT, solid lines with circles; low viscosity case with CMT, dashed line with triangles; high viscosity case with CMT, dot-dash line with asterisks. Top, absolute global minimum circulation streamfunction strength, kg/s, as a function of ΔT. Bottom, minimum 150 mb absolute vorticity between 6N and 64N, s^{-1}, as a function of ΔT.

When the SST perturbation is small, the resulting circulation is weak, and the upper tropospheric absolute vorticity (Figure 3-6) does not approach the critical value at zero. Above a threshold forcing level, the circulation intensifies much more rapidly with increased ΔT, and the upper level absolute vorticity drops to near zero. This threshold is near $\Delta T = 1.25\,K$ for the case which includes CMT, and near $\Delta T = 1.5\,K$ for the case without CMT. When forcing levels are below the threshold, the circulation is confined to one hemisphere and does not cross the equator, an example is shown in Figure 3-7. Above the threshold forcing, the circulation becomes cross-equatorial and considerably stronger, as illustrated in Figure 3-8. In these cases, the upper tropospheric absolute vorticity is close to zero in the circulation cell (Figure 3-6), which is closely angular momentum conserving. Large-scale ascent occurs near the SST maximum, and is accompanied by precipitation. The northern limit of the circulation moves gradually poleward with increased surface forcing, shifting from near 22N for $\Delta T < 1.0K$ to near 28N for $\Delta T \geq 2.5K$.

Because the ocean temperature is uniform away from the applied local perturbation, the

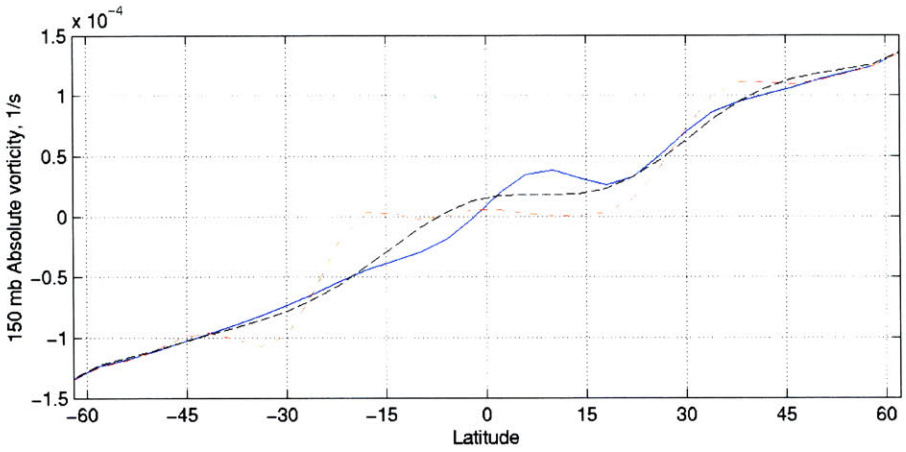

Figure 3-6: 150 mb absolute vorticity, aquaplanet cases. Solid blue line, low viscosity case with $\Delta T = 1.0K$; red dash-dot line, low viscosity case with $\Delta T = 2.0K$; black dashed line, high viscosity case with $\Delta T = 2.0K$..

zonal wind (not shown) is near zero everywhere except for in the vicinity of the meridional circulation. For subthreshold forcing, the zonal wind field features a weak upper level westerly jet just poleward of the large-scale circulation. The weak meridional circulation (Figure 3-7) is not strongly angular momentum conserving. When a strong cross-equatorial circulation is present (Figure 3-8), angular momentum is nearly constant across the equatorial region, with a strong easterly jet at the equator. In these cases, the cross-equatorial circulation carries warm air from the region of the forcing into the opposite hemisphere, resulting in an upper level meridional gradient in temperature even though the surface temperature is uniform.

In the aquaplanet setup, there are strong feedbacks between the circulation and the surface fluxes, especially the latent heat flux. As the circulation intensifies, the surface winds increase, which enhances the surface heat fluxes and in turn strengthens the circulation; this type of interaction has been coined the 'wind-induced surface heat exchange' (WISHE) feedback (Emanuel, 1986). Threshold behavior is exaggerated by WISHE, which strengthens already strong circulations but has less impact on weak circulations.

After introduction of the subtropical SST perturbation, the circulation rapidly develops and strengthens over the course of approximately 100 days before it begins to weaken; the circulation then gradually approaches a steady state after an additional 100 days (Figure 3-9). The initial peak in strength is at least twice (if not much greater) the strength of the final steady circulation. This peak strength is seen in other axisymmetric studies, such as Plumb and Hou (1992), and is intensified in this model by the WISHE feedback. The timescale for the circulation to reach the initial peak strength is related to the length of

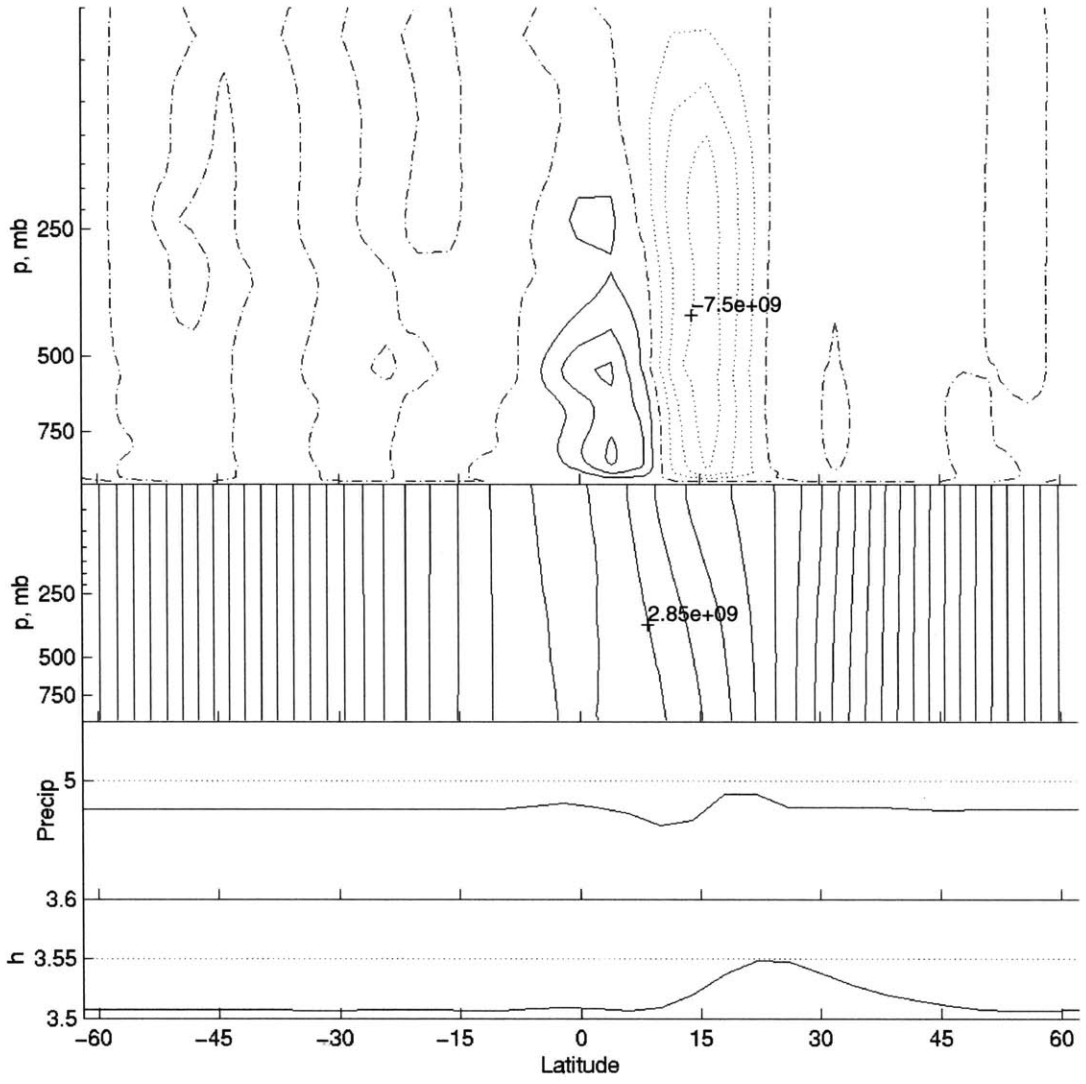

Figure 3-7: Aquaplanet case with localized perturbation at 16N, low viscosity with no CMT, $\Delta T = 1.0$K; 100 day time mean fields. Top, streamfunction, contour interval 2.5e9 kg/s, dotted lines indicate counter-clockwise flow, solid lines indicate clockwise flow, dash-dot is zero contour. Upper center, absolute angular momentum, contour interval 1E8 m^2/s. Lower center, precipitation, mm/day. Bottom, 1000 mb moist static energy, 10^5 J.

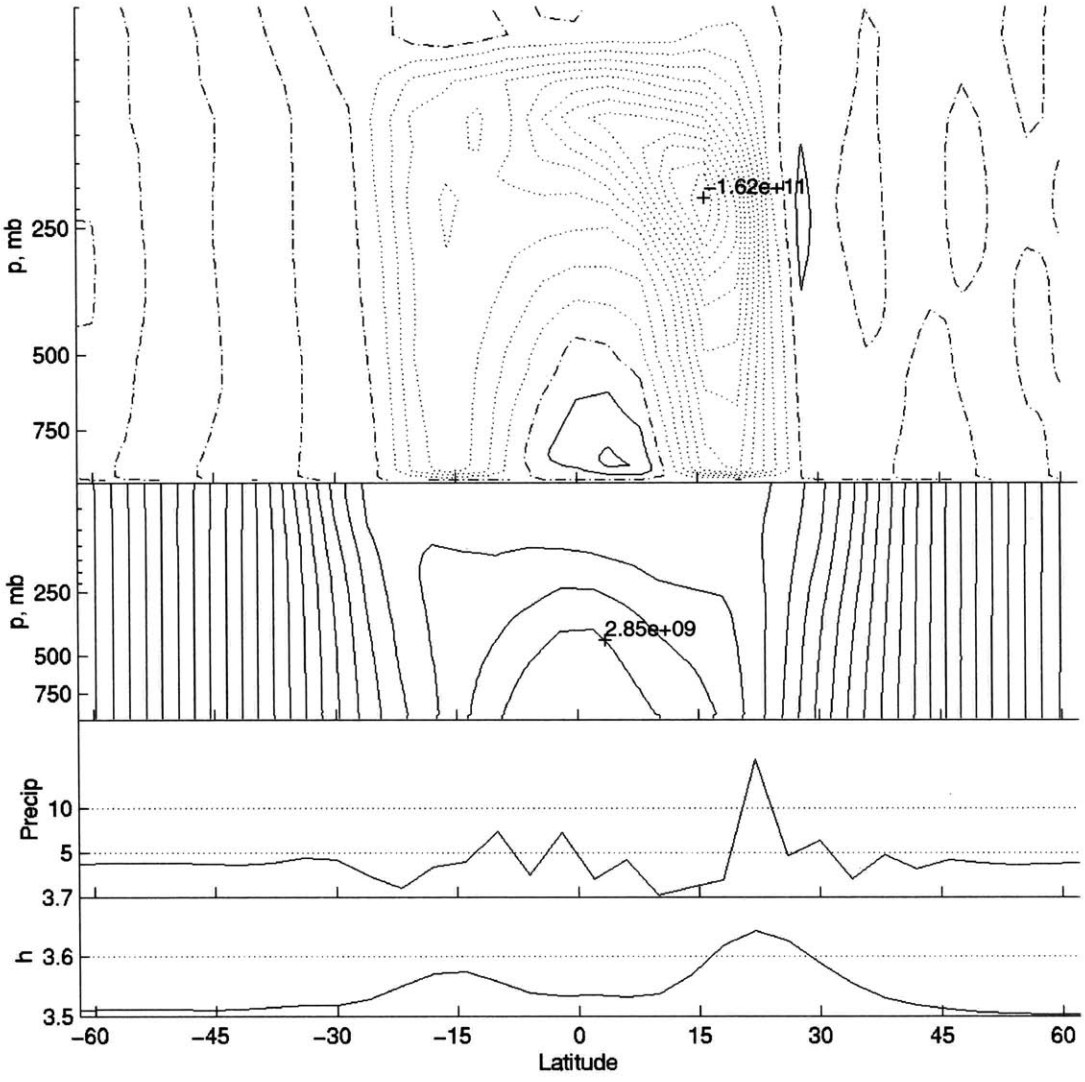

Figure 3-8: Aquaplanet case with localized perturbation at 16N, low viscosity with no CMT, $\Delta T = 2.0$K, 75 day time mean fields. Top, streamfunction, contour interval 1.25e10 kg/s, dotted lines indicate counter-clockwise flow, solid lines indicate clockwise flow, dash-dot is zero contour. Upper center, absolute angular momentum, contour interval 1E8 m^2/s. Lower center, precipitation, mm/day. Bottom, 1000 mb moist static energy, 10^5 J.

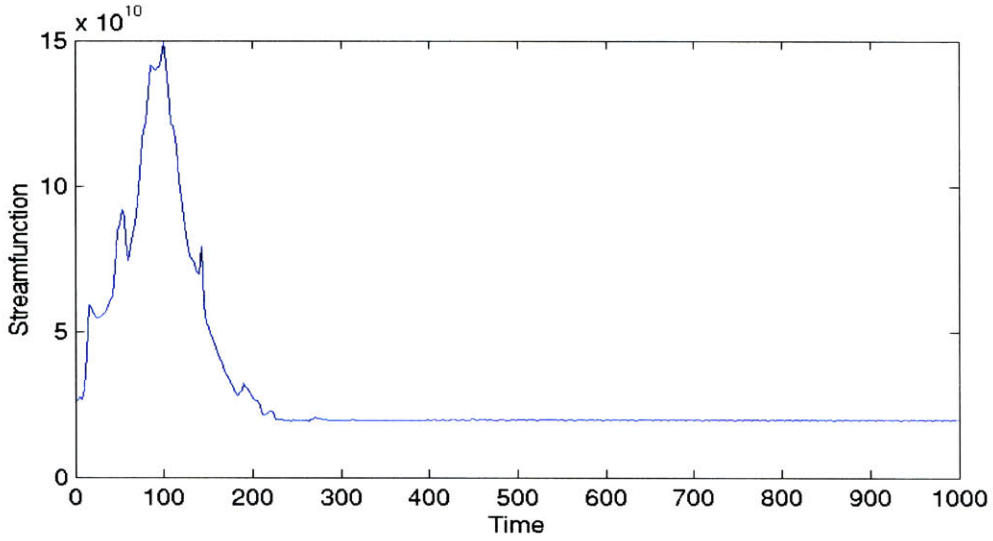

Figure 3-9: Absolute minimum streamfunction (kg/s) as a function of time after introduction of subtropical SST perturbation, aquaplanet case with low viscosity and CMT included, $\Delta T = 1.25$ K.

time needed for the upper tropospheric flow to traverse the upper leg of the circulation from the region of ascent to the region of subsidence. In an angular momentum conserving flow, this is the time needed for the flow to fold over the contours of absolute angular momentum in the upper troposphere to produce nearly uniform angular momentum across the tropics. A series of model runs were made with varied Newtonian cooling timescale, which affects the overturning timescale for the circulation, to examine the effects on the adjustment time for spin-up. When the Newtonian cooling timescale was doubled, the initial adjustment timescale increased to 300 days; when the Newtonian cooling timescale was halved, the initial adjustment timescale decreased to approximately 50 days. The change in initial adjustment time was commensurate with the change in overturning timescale for both of these cases.

For forcing just above the threshold ($\Delta T = 1.5$ to $1.75\,K$), the circulation and precipitation show oscillatory behavior in the low viscosity cases. The entire circulation strengthens and weakens with a timescale of 100 to 300 days, with strongest precipitation coincident with strongest circulation, an example is seen in Figure 3-10. The upper level absolute vorticity also shows periodic behavior, approaching the critical value of zero when the circulation is weak, but becoming positive and subcritical when the circulation is strong. This oscillation is due to the WISHE feedback between circulation strength and surface fluxes. For the $\Delta T = 1.75K$ case (with CMT), a second experiment is run where the surface fluxes are calculated using the wind speeds from day 300 after day 300. The oscillatory behavior

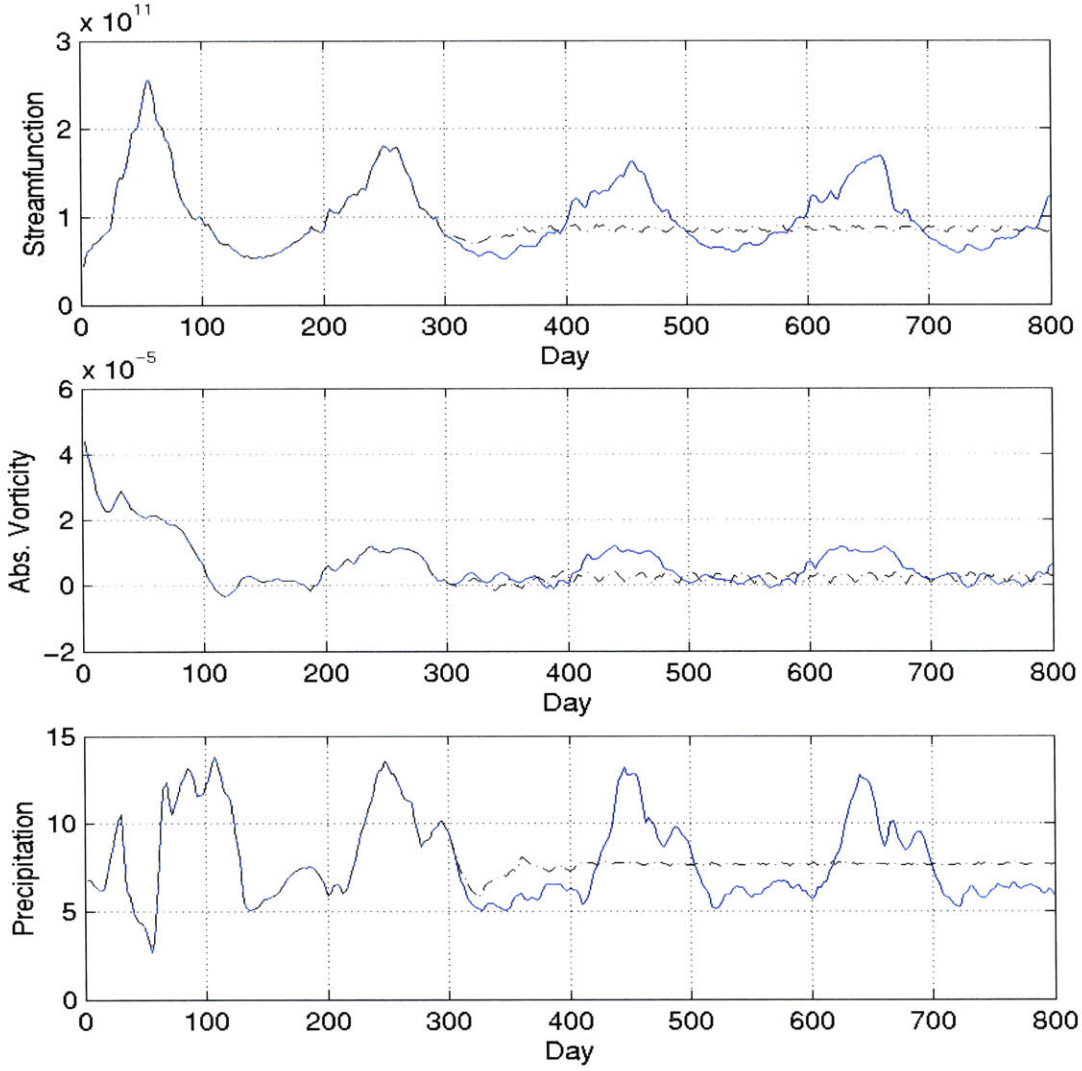

Figure 3-10: Aquaplanet case with low viscosity and CMT included, $\Delta T = 1.75$K. Solid line, case with time-varying wind speeds used in surface flux calculation' dot-dash line for case where surface fluxes are fixed after day 300 at the day 300 values. Top, absolute maximum negative streamfunction (kg/s) as a function of time after introduction of subtropical SST perturbation. Center, 150 minimum absolute vorticity from 18N to 64N, s^{-1}. Bottom, precipitation at 22N, mm/day.

immediately ceases and the circulation approaches a steady state with maximum stream-function strength at an intermediate value (dot-dash line in Figure 3-10). The precipitation maximum slides in latitude, beginning near 18N when the circulation is weak and moving poleward to 26N as the circulation strengthens. As the circulation begins to weaken, a new precipitation maximum forms at 18N while the previous precipitation maximum at 26N dies out.

High Viscosity Case The vertical viscosity strongly impacts the momentum budget and the subsequent behavior of the meridional circulation. For weak forcing ($\Delta T < 1.5\,K$, not shown), the meridional circulation is local with a modest increase in precipitation near the SST maximum, similar to the $\nu = 10\,Pa/s$ case (shown in Figure 3-7). In this regime, the circulation strength is close to that of the $\nu = 10Pa/s$ cases, and the subtropical upper level absolute vorticity does not approach the critical value at zero. For forcing of $\Delta T \geq 1.5\,K$, a larger, cross-equatorial meridional circulation results, with more significant precipitation maximum in the subtropics (Figure 3-11); however, the circulation strength is much less than in the corresponding $\nu = 10\,Pa/s$ cases (Figure 3-5; Figure 3-8). Threshold behavior is much less clear, with a gradual strengthening of the circulation occurring as the forcing is increased, seen in Figure 3-5. The subtropical upper tropospheric absolute vorticity (Figure 3-6) remains far from critical, although the circulation becomes global in extent. In the case with strongest forcing, the upper tropospheric absolute vorticity is nearly constant across the upper branch of the circulation, but is not close to zero. The circulation crosses contours of constant angular momentum more easily than in the low viscosity cases. There is no oscillatory behavior such as observed for some of the low-viscosity cases.

These results clearly indicate that viscous effects are more influential than convective momentum transfer in allowing non-conservation of angular momentum. While vertical viscosity acts throughout the troposphere in the vicinity of the upper level jets, convective momentum transport acts only in localized regions near deep moist convection. The local magnitude of the momentum tendency due to convective momentum transport in regions of deep convection is of the same order as the tendency due to viscosity in regions of moderate wind shear.

Jumping Behavior

One feature common to all of the aquaplanet cases with localized SST forcing is the tendency of cross-equatorial circulations to 'jump' in the lower troposphere when approaching the equator. As the lower tropospheric flow moves northward in the southern hemisphere, it is initially confined to the mixed layer, below 800 mb (Figure 3-8). After passing 10S, the circulation abruptly ascends and crosses the equator in mid-troposphere; once past

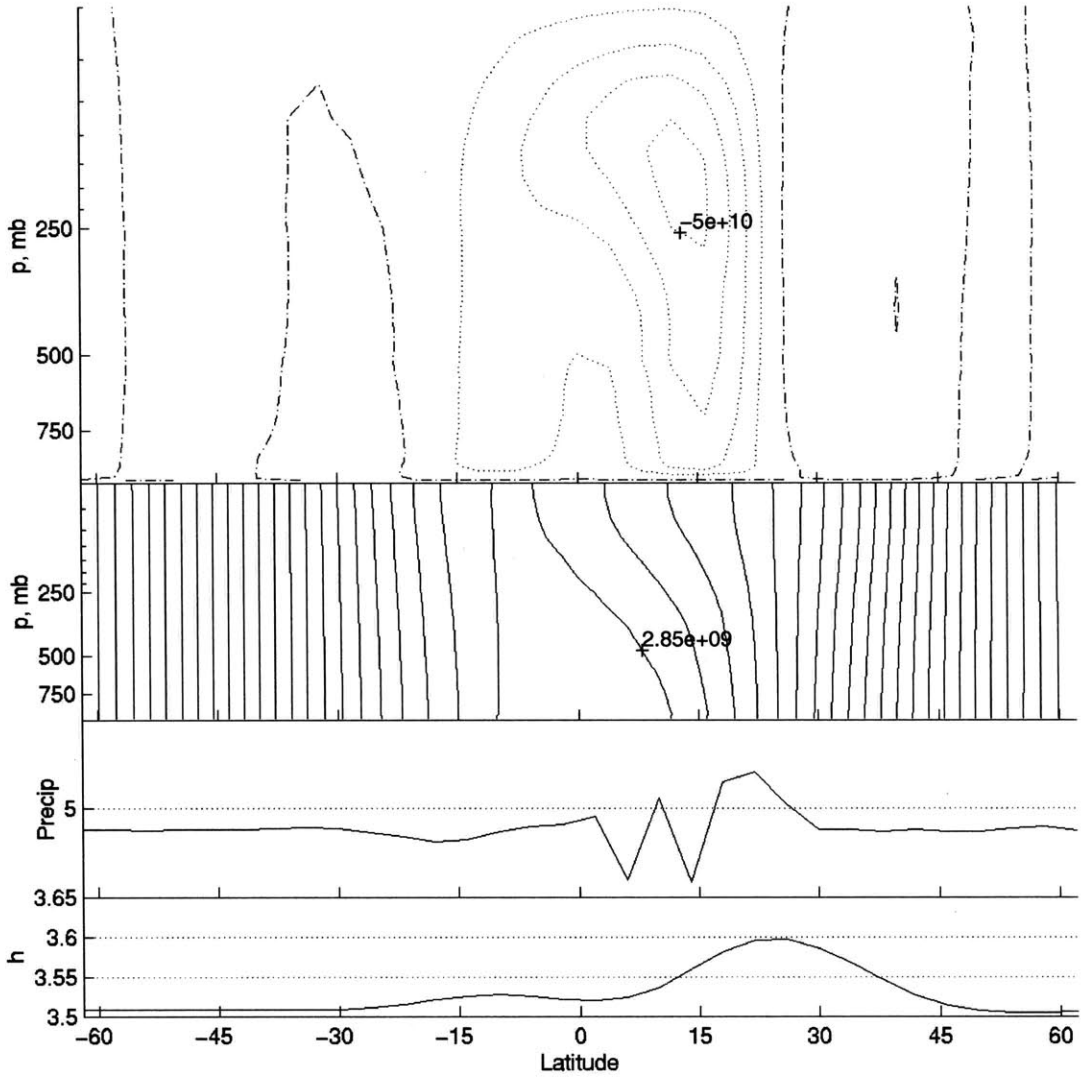

Figure 3-11: Aquaplanet case with localized perturbation at 16N, high viscosity with CMT, $\Delta T = 1.94$K, 100 day time mean fields. Top, streamfunction, contour interval 1.25e10 kg/s, dotted lines indicate counter-clockwise flow, solid lines indicate clockwise flow, dash-dot is zero contour. Upper center, absolute angular momentum, contour interval 1e8 m^2/s. Lower center, precipitation, mm/day. Bottom, 1000 mb moist static energy, 10^5 J.

the equator, the flow descends once again to the mixed layer over the tropical ocean and continues northward. This flow pattern results in a secondary precipitation maximum in the southern hemisphere tropics between the equator and 6S.

Jumping of the circulation has several effects on the large-scale flow. The moisture content of the low-level flow is depleted during the jump as the air rises to the mid-troposphere, but is replenished through large latent heat fluxes at the surface in the northern hemisphere after the flow has returned to the mixed layer. Jumping also alters the streamfunction intensity. When jumping does not occur, the maximum streamfunction of the cross-equatorial circulation is located in the lower troposphere near the equator; there is a weaker local streamfunction maximum in the upper troposphere just equatorward of the ascent region. The initiation of jumping eliminates the lower tropospheric streamfunction maximum, so that the upper tropospheric maximum becomes the new global maximum.

Jumping of the meridional circulation has been addressed extensively by Pauluis (2001); a brief summary will be given here. The meridional wind in the mixed layer is driven by forcing both by the geopotential gradient within the mixed layer, which is influenced both by the geopotential gradient in the free troposphere just above the mixed layer and by forcing in the mixed layer itself. The free tropospheric geopotential is tied to the zonal wind through thermal wind balance, and is thus restricted by conservation of angular momentum. An easterly wind in the free troposphere will drive equatorward flow, while westerlies force poleward flow; the maximum mixed layer flow induced by the free tropospheric zonal wind is a function of latitude, and decreases to zero at the equator. By itself, zonal wind in the free troposphere is thus unable to cause cross-equatorial flow. Additionally, a free tropospheric zonal wind distribution with easterlies on one side of the equator and westerlies on the other is desired in order to encourage cross-equatorial flow in the near-equatorial region; this flow structure requires ascent at or near the equator due to conservation of angular momentum.

A pressure gradient across the equator is needed in the mixed layer in order to allow cross-equatorial flow. It is difficult to maintain significant horizontal pressure gradients in the tropics; one way to do so is through the temperature field. The existence of a cross-equatorial gradient in the surface temperature is a likely source of pressure gradient in the mixed layer. For a given pressure gradient across the equator, the possible mass transport in the mixed layer is proportional to the thickness of the mixed layer. When the mixed layer is thin or the pressure gradient is weak, only a limited mass flux is possible in the mixed layer, so flow attempting to cross the equator must rise into the free troposphere in order to cross. This jump into the free troposphere produces westerlies on the summer side of the equator (as high momentum air travels poleward), allowing poleward flow within the mixed layer. Thus, after crossing the equator in the free troposphere, the flow may return to the mixed layer. In a moist atmosphere, the vertical moist stability near the equator is

weak, and the resulting jump is quite deep. Large-scale ascent encourages moist convection near the equator, which affects the stability and reinforces the deep jumping behavior after onset of precipitation.

In the modeled case with uniform ocean SSTs, the pressure gradient across the equator is very weak, sometimes even increasing northward, so that cross-equatorial flow is strongly inhibited even though the mixed layer is 200 mb deep.

In order to explore the effect of equatorial SST gradient on jumping behavior, a summer-type SST gradient is once again used, with ϕ_0 at 20N in (3-1). In the previous summer-type cases, there was no sign of jumping of the flow (Figure 3-3). For this case, the SST gradient at the equator is reduced by flattening the SST profile:

$$SST(\phi) = SST_0 - \Delta T sin(0.64(\phi - \phi_0))^2 \tag{3.3}$$

The results of this experiment (Figure 3-12) show clear jumping of the flow; with this model setup, fairly strong SST gradients across the equator are needed to prevent jumping.

Latitudinal Influence on Circulation

Lindzen and Hou (1988) found that displacing the thermal equilibrium temperature maximum off of the equator results in a much larger and stronger Hadley circulation than when the temperature maximum is located exactly on the equator. As the temperature maximum is moved poleward within the tropics, the size and strength of the circulation also increases. However, the maximum displacement investigated by Lindzen and Hou was 8° from the equator, and subtropical temperature maxima were not examined. In their setup, the entire thermal equilibrium temperature profile was shifted, so that as the temperature maximum is moved poleward in the summer hemisphere, the winter hemisphere becomes colder, and the temperature gradient at the equator increases.

The net mass flux of the overturning circulation is controlled by the rate of subsidence in the winter hemisphere (Fang and Tung, 1997). In the tropics, vertical motions are generally balanced by diabatic heating,

$$\omega S = Q \tag{3.4}$$

where ω is the vertical velocity, S is the static stability, and Q is the net diabatic heating. The net diabatic heating in the model is the sum of the Newtonian cooling (Q_{NC}) and the convective heating (Q_{CNV}), with

$$Q_{NC} = \tau_{NC}^{-1}(T_{NC} - T) \tag{3.5}$$

where τ_{NC} is the timescale for Newtonian cooling. Although T_{NC} and τ_{NC} are independent

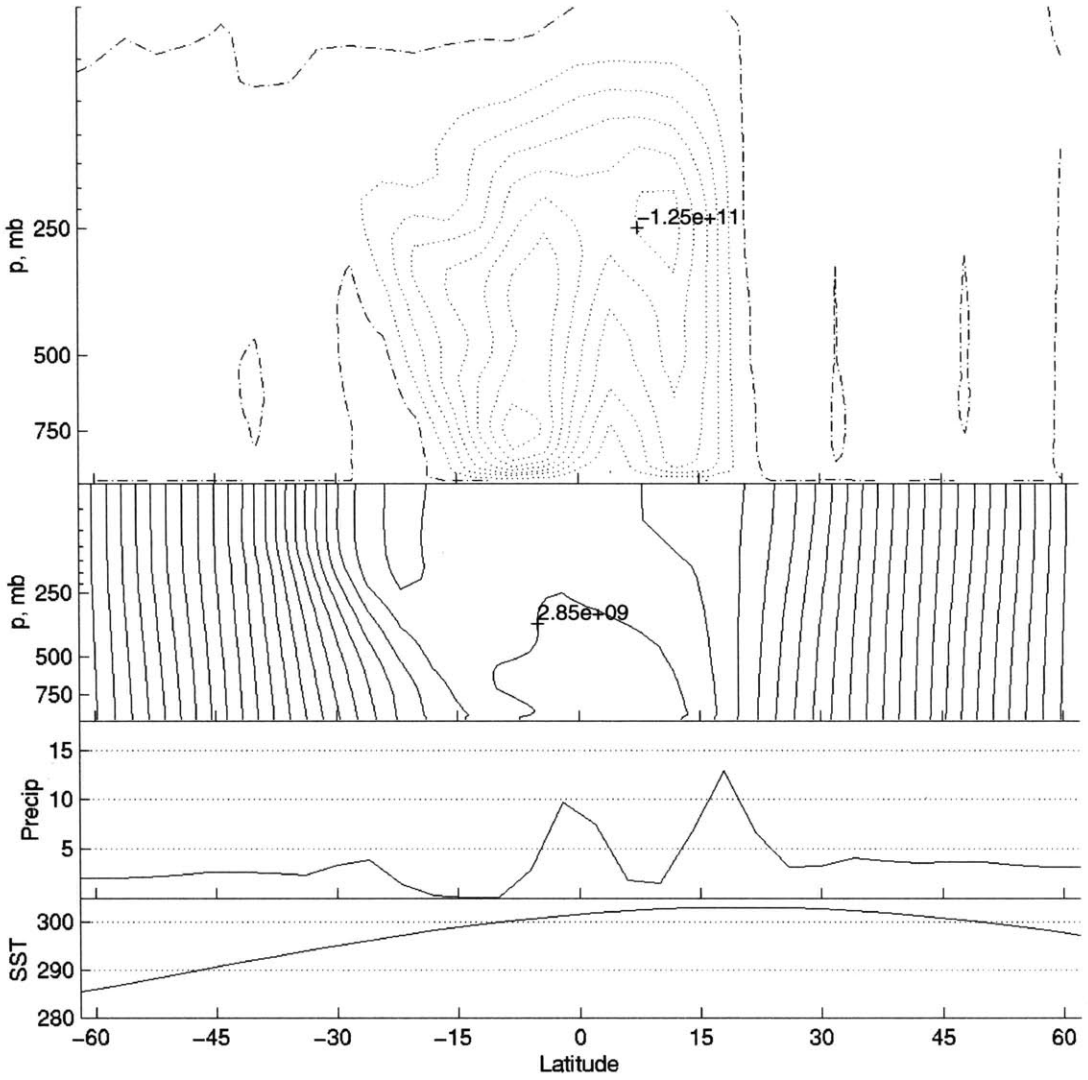

Figure 3-12: Aquaplanet case with SST maximum at $\phi_0 = 20$N and distribution given by (3.3), 100 day time mean fields. Top, streamfunction, contour interval 1.5e10 kg/s, dotted lines indicate counter-clockwise flow, solid lines indicate clockwise flow, dash-dot is zero contour. Upper center, absolute angular momentum, contour interval 1E8 m^2/s. Lower center, precipitation, mm/day. Bottom, SST, K.

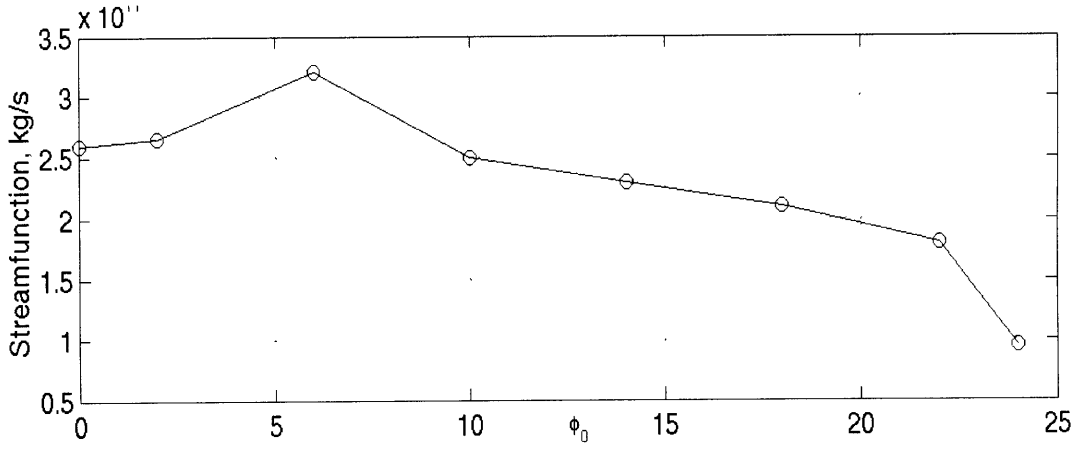

Figure 3-13: Aquaplanet case with localized SST perturbation at varied latitudes (ϕ_0) in the northern hemisphere, absolute maximum negative streamfunction, kg/s.

of latitude in the model setup used here, the convective heating does vary meridionally, and is influenced by sea surface temperatures. Altering the SST in the winter hemisphere may affect the strength of the overturning circulation.

In order to explore the dependency of the circulation upon the latitude of the forcing without altering the winter hemisphere state, a series of aquaplanet runs are made with uniform SST and a localized boreal hemisphere SST perturbation, which is varied in location:

$$SST(\phi) = 302K + \Delta T cos^2((\phi - \phi_0)\frac{5\pi}{4}),\ \phi_0 < \phi < (\phi_0 + 42°) \tag{3.6}$$
$$SST(\phi) = 302K\ \phi \leq \phi_0,\ elsewhere$$

ϕ_0 is varied from 0N to 26N, and ΔT is chosen to be 4.25 K. This ΔT was chosen to yield cross-equatorial circulations for the entire range of ϕ_0 tested. A vertical viscosity of $\nu = 10\,Pa^2/s$ is used, and CMT is included.

The maximum streamfunction increases as ϕ_0 is moved poleward from 0N to 6N (Figure 3-13), although the circulation width only broadens slightly, with no sign of jumping behavior. As ϕ_0 moves from 6N to 10N, the circulation nearly doubles in width but decreases sharply in strength as jumping initiates and the lower tropospheric streamfunction maximum is destroyed. As ϕ_0 is moved poleward from 10N to 22N, the circulation slowly decreases in strength and gradually broadens, with deepening jumps at the equator. As the circulation broadens, the easterly jet rapidly intensifies, resulting in greater viscous effects with weakening angular momentum conservation in the upper branch of the circulation. The streamfunction drops in strength again as ϕ_0 is moved from 22N to 24N. The $\phi_0 = 24N$

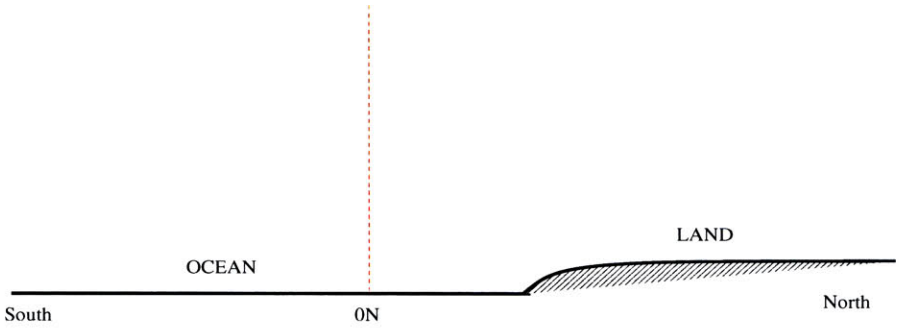

Figure 3-14: Diagram of continental case setup in axisymmetric cases.

case is tested with $\Delta T = 4.0K$, which results in a weak, local AMC circulation with upper tropospheric absolute vorticity near zero. The $\phi_0 = 24N$ at $\Delta T = 4.25K$ case is close to the local-to-global AMC transition as described by Schneider (1983), but far above the critical threshold for the existence of an AMC circulation (Plumb and Hou, 1992); the proximity to this transition is the likely cause of the sharp reduction in streamfunction from $\phi_0 = 22N$ to $24N$.

3.2 Continental Cases

A subtropical continent with interactive surface temperatures and heat fluxes is implemented in the model. The strength of the land surface forcing may be directly manipulated through the total surface heat flux field (2.5), which is prescribed as a function of latitude, and a range of forcings is tested. The total heat flux profile is given by

$$THF(\phi) = THF_0 - \Delta THF sin((\phi - \phi_T))^2 \tag{3.7}$$

where ΔTHF is $50\,W/m^2$, and THF_0 ranges from 120 to $150\,W/m^2$. For all of these cases, the continent extends from the southern coastline northward to the model boundary at 64N; the coastline is located at latitude ϕ_L. Convective momentum transport is included with a vertical viscosity of $\nu = 10\,Pa^2/m$. First, a subtropical continent is used with $\phi_L = 16$N; for comparison with the aquaplanet results, the ocean is assigned a uniform temperature profile. In a second configuration, the subtropical continent is accompanied by a more realistic summer-type ocean SST distribution. The role of the meridional position of the continent is then explored by shifting the coastline to 8N in one case and to 24N in another case. Finally, the transient behavior of the circulation is explored in a set of experiments with seasonally varying land forcing.

For each run, the model is first spun up from rest with a relatively cold continent

($THF_0 = 80W/m^2$) for 200 days. The land surface forcing is then increased to the summer value over a timescale of 100 days, and the model is run for at least 700 additional days until a steady state is reached. The continent is initially dry, with no water in the surface buckets.

3.2.1 Radiative Convective Equilibrium

The viability of the absolute angular momentum field in thermal wind balance with the radiative convective equilibrium temperature distribution is the determining factor for the existence of a strong meridional circulation; thus, the radiative convective equilibrium state is of interest. Unlike over the ocean, a saturated moist adiabat cannot be assumed over the land. The MITGCM may be run with horizontal filtering removed and with the pressure tendency terms neglected in the horizontal momentum equations, which results in a radiative convective equilibrium state with zero winds. The RCE states are calculated in this fashion with a subtropical continent with coastline at $\phi_L = 16$N and $\phi_T = 8N$, and land surface forcing ranging from $THF_0 = 120$ to $160\,W/m^2$. In each case, the model is integrated for 100 days to reach an equilibrium state. Because the moisture content of the atmosphere strongly affects the radiative convective equilibrium state, two different continental hydrology states are tested: in the first, an arid continent with completely dry land surface buckets is used, while in the second, a swamp-type continent is implemented.

Arid Continent

In these cases, the continent is initialized to have a completely dry surface, but the land hydrology is interactive. Moisture which is initially present in a continental air column may precipitate out and become stored in the surface buckets, but the column total moisture content is not enough to saturate the buckets.

Due to the relatively arid land surface, the surface heat flux is dominated by the sensible heat flux; since the total surface heat flux over the continent is prescribed, relatively large sensible heat fluxes result. The lower troposphere over the landmass is then considerably warmer than over the ocean. The low moisture content of the continental atmosphere results in a vertical temperature profile which is far from saturated; over the ocean, however, the atmosphere is closer to a saturated adiabat in the vertical. Even though the lower troposphere is much warmer over the land than over the ocean, the upper troposphere may have the opposite temperature gradient, with cooler air over the continent. This is seen in Figure 3-15 for the weaker land surface forcing cases ($THF_0 \leq 130\,W/m^2$). However, very strong land surface forcing ($THF_0 \geq 150\,W/m^2$) results in an upper troposphere temperature maximum over the subtropical continent, although the temperature gradient

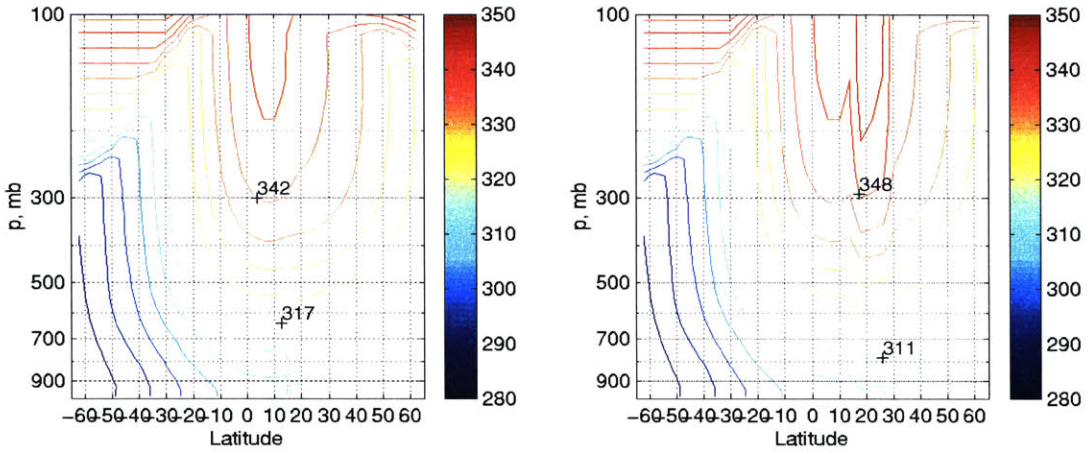

Figure 3-15: Radiative convective equilibrium θ_v, $THF_0 = 130 W/m^2$. Left, case with arid continent; right, case with swamp continent.

is much stronger in the lower troposphere. For the $THF_0 = 140\, W/m^2$ case, there is a very weak upper tropospheric temperature maximum over the continental coastline.

Swamp Continent

When a swamp-like continent with saturated surface is implemented, the upper tropospheric response to the land surface forcing is stronger than with an arid continent. In these cases, the atmosphere over the landmass follows close to a moist adiabat in the vertical, as over the ocean. The surface fluxes over the continent are dominated by the latent heat flux, especially near the coastline where the forcing is greatest, with sensible heating playing a more significant role in the midlatitudes. In the subtropics, the sensible heat flux may even be negative over the continent. For the weakest forcing, $THF_0 = 120 W/m^2$ (not shown), the upper tropospheric temperature features a weak local maximum at 18N. For land forcing of $THF_0 \geq 130 W/m^2$, there is a significant upper tropospheric temperature maximum at 18N with strong gradient across the coastline, as illustrated in Figure 3-15. The differences between the RCE states of the arid and swamp continents highlight the importance of moisture availability over the landmass.

3.2.2 Uniform SST

In order to allow comparison to the aquaplanet case with localized subtropical SST perturbation, a continent with coastline at ϕ_L = 16N, ϕ_T of 8N, and uniform SST of 302 K at all ocean latitudes is implemented. The only difference between this case and the previous aquaplanet case with localized SST perturbation at 16N (§3.1.2) is the replacement of the prescribed SST perturbation with an interactive continent in the boreal hemisphere.

For the weakest continental forcing tested, $THF_0 = 120\,W/m^2$, no monsoon occurs, as shown in Figure 3-16. The subcloud moist static energy is greater over the ocean than over the land, and there is little precipitation over the continent. The meridional circulation is limited to a very weak, shallow circulation just along the coastline, with subsidence in the mid and upper troposphere over the continental subtropics. The wind field (not shown) features a westerly upper level jet over the boreal midlatitudes, due to the chosen distribution of THF; winds are very weak in the tropics and southern hemisphere.

When the land forcing is increased to $THF_0 = 125\,W/m^2$, deep moist convection onsets over the subtropical continent with maximum rainfall at 18N; a second precipitation maximum of similar intensity occurs over the ocean near 6N (Figure 3-17). The subcloud moist static energy is slightly greater over the subtropical continent than over the ocean, with maximum at 18N. Large scale ascent occurs along the coastline, with a latitudinally narrow meridional circulation with subsidence near 10N. There is a weaker, shallow circulation inland between 20N and 35N, capped at 700 mb, which is similar to the cell seen in the $THF_0 = 120\,W/m^2$ case.

The $THF_0 = 130\,W/m^2$ case is very similar to the $THF_0 = 125\,W/m^2$ case, although the deep circulation is slightly stronger and large-scale ascent has shifted poleward to 22N (Figure 3-18). The upper level easterly jet (not shown) is also strengthened by a factor of four. The precipitation field shows a strong maximum at 22N, with only weak local maxima over the ocean. The subcloud moist static energy is significantly greater over the continent than over the ocean, with maximum near 22N. The upper tropospheric absolute vorticity (Figure 3-19) is not close to the critical value at zero, and the deep circulation is not strongly angular momentum conserving.

For land forcing of $THF_0 \geq 135W/m^2$, the meridional circulation is more global in extent, with ascent over the subtropical continent and subsidence over the southern hemisphere ocean (Figure 3-20). Jumping of the circulation at the equator occurs for all cases with cross-equatorial flow, and becomes more pronounced as the land surface forcing increases. The upper level tropical easterly jet (not shown) is very strong, which is a common feature in axisymmetric models. The angular momentum field is significantly distorted by the circulation, although the flow is able to cross some contours of angular momentum in the tropics, where there is strong easterly shear. The precipitation field features a strong local precipitation maximum over the continent, which shifts poleward with increasing THF_0 (Figure 3-21). The precipitation maximum is located near or slightly equatorward of the subcloud moist static energy maximum. There are multiple secondary maxima of precipitation located over the tropical ocean; the number and position of these maxima vary between cases.

Although the strength of the meridional circulation increases with increased land surface

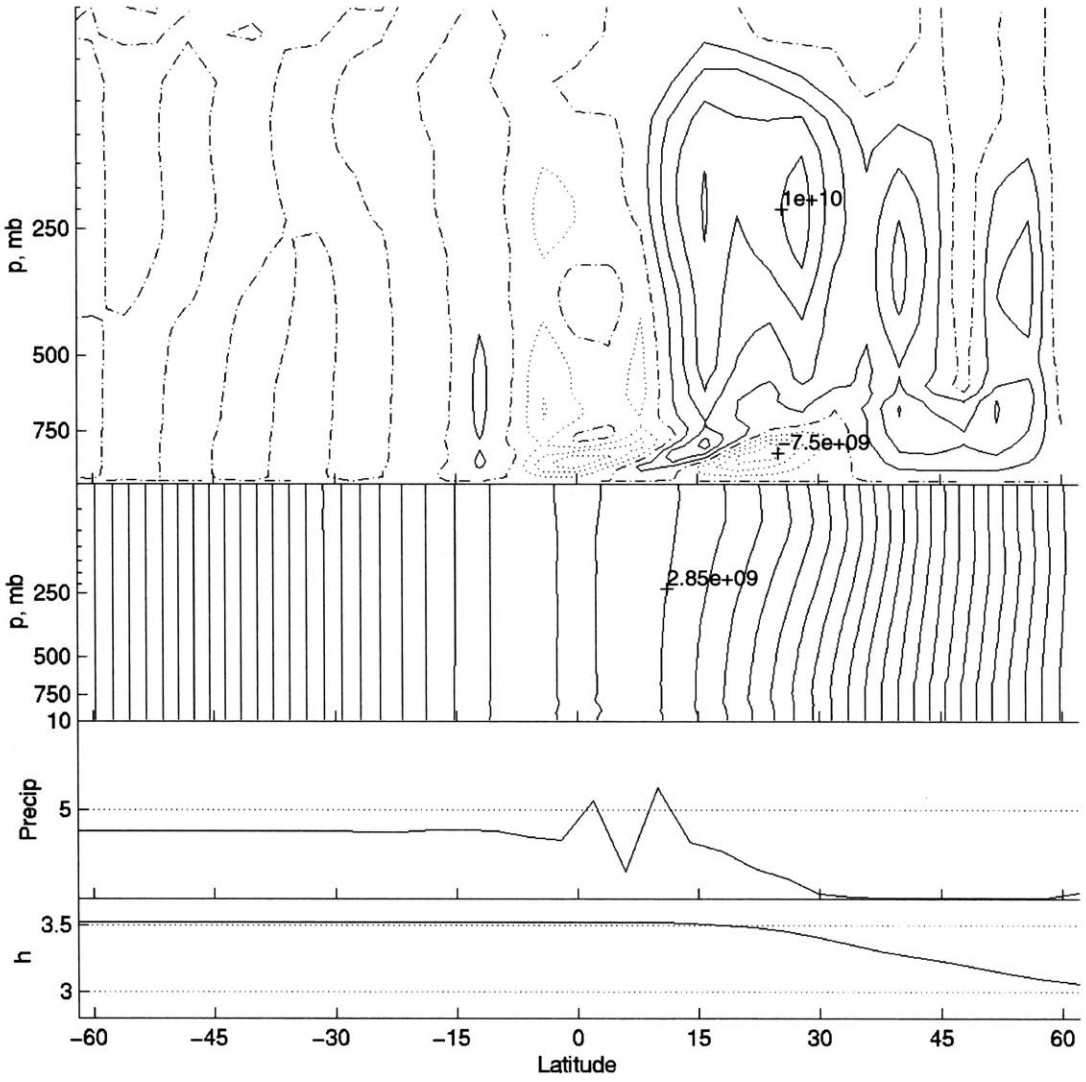

Figure 3-16: Continental case with uniform SST and $THF_0 = 120\,W/m^2$, 100 day time mean fields. Top, streamfunction, contour interval 2.5e9 kg/s, dotted lines indicate counter-clockwise flow, solid lines indicate clockwise flow, dash-dot is zero contour. Upper center, absolute angular momentum, contour interval 1E8 m^2/s. Lower center, precipitation, mm/day. Bottom, 1000 mb moist static energy, 10^5 J.

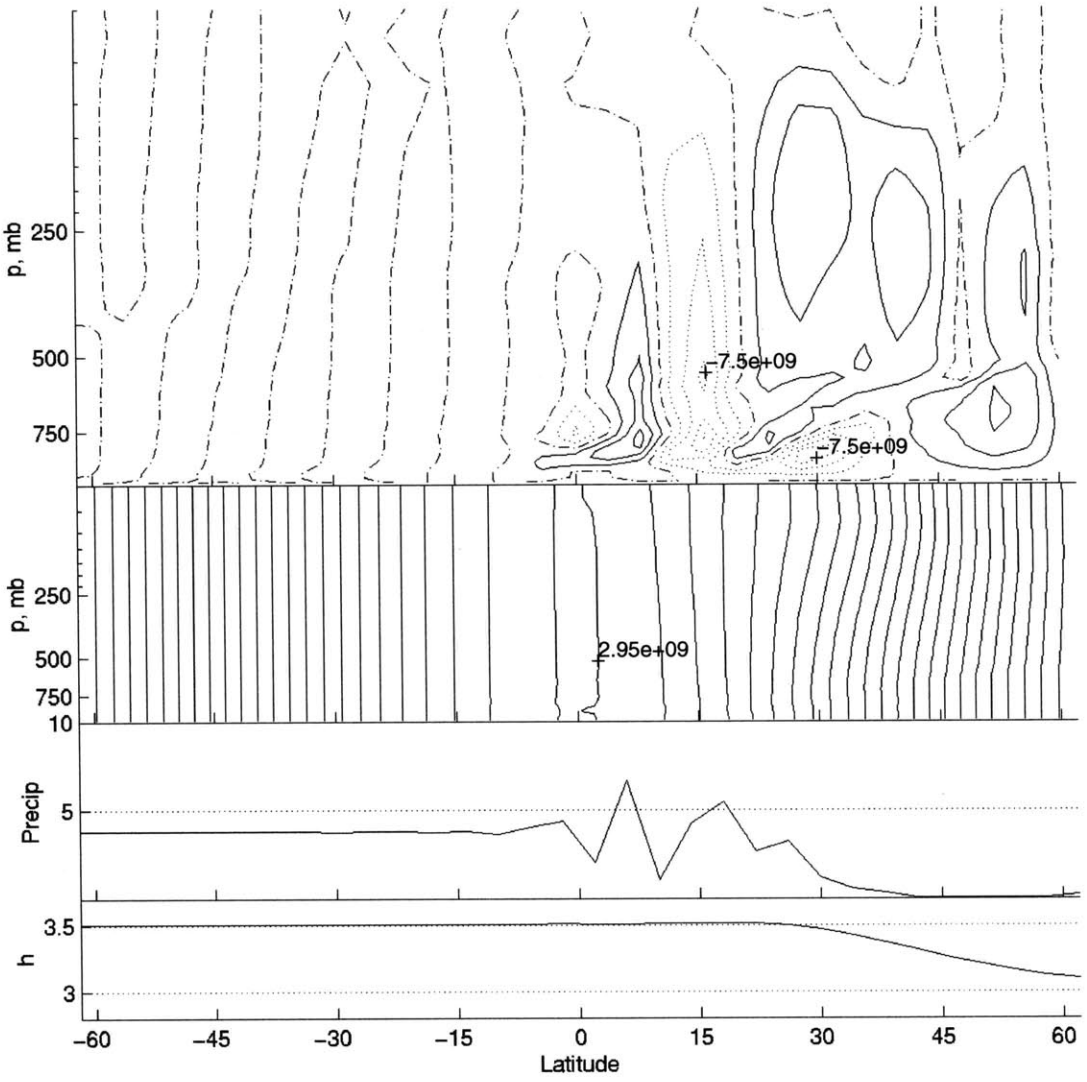

Figure 3-17: Continental case with uniform SST and $THF_0 = 125W/m^2$, 100 day time mean fields. Top, streamfunction, contour interval 2.5e9 kg/s, dotted lines indicate counter-clockwise flow, solid lines indicate clockwise flow, dash-dot is zero contour. Upper center, absolute angular momentum, contour interval 1E8 m^2/s. Lower center, precipitation, mm/day. Bottom, 1000 mb moist static energy, 10^5 J.

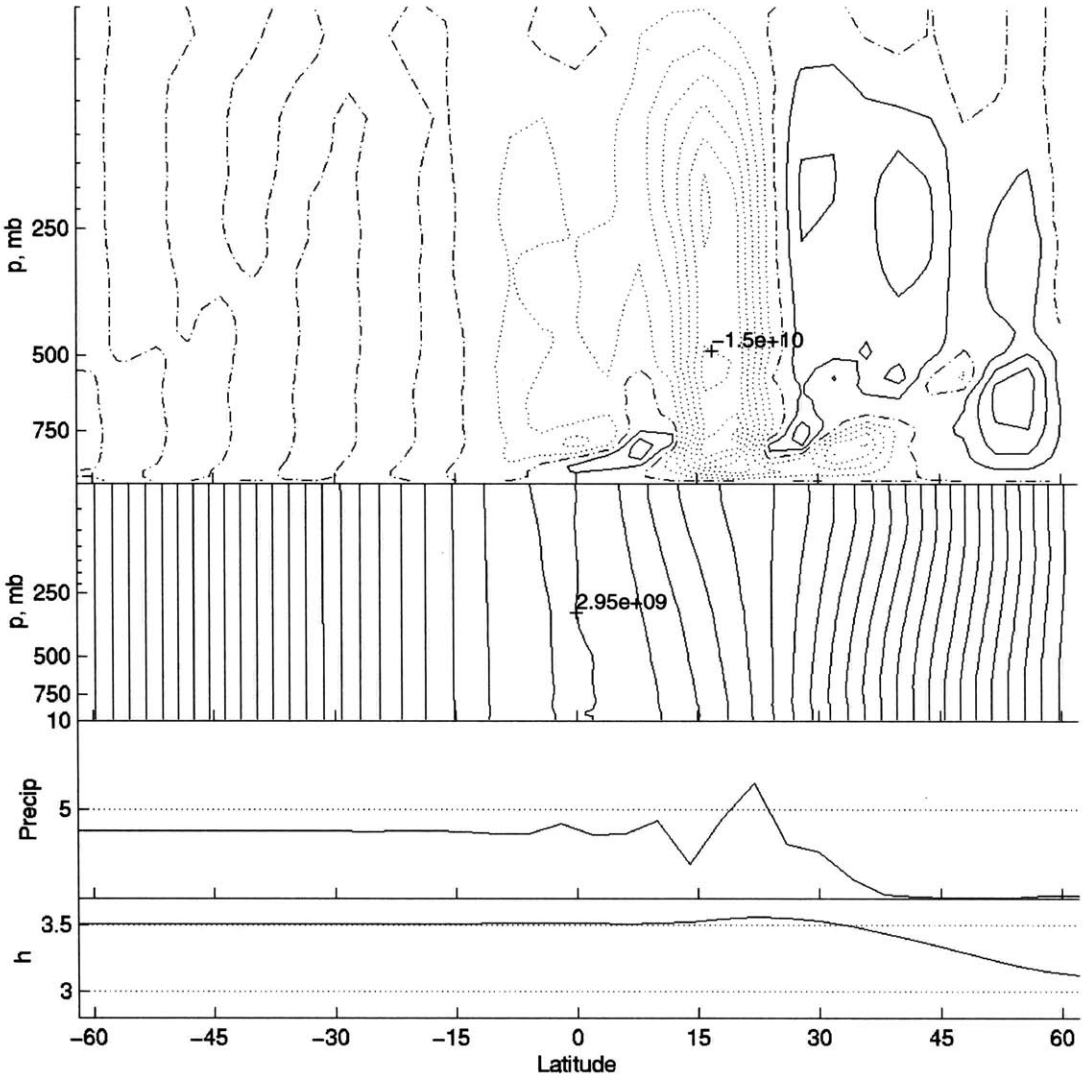

Figure 3-18: Continental case with uniform SST and $THF_0 = 130W/m^2$, 100 day time mean fields. Top, streamfunction, contour interval 2.5e9 kg/s, dotted lines indicate counter-clockwise flow, solid lines indicate clockwise flow, dash-dot is zero contour. Upper center, absolute angular momentum, contour interval 1E8 m^2/s. Lower center, precipitation, mm/day. Bottom, 1000 mb moist static energy 10^5 J.

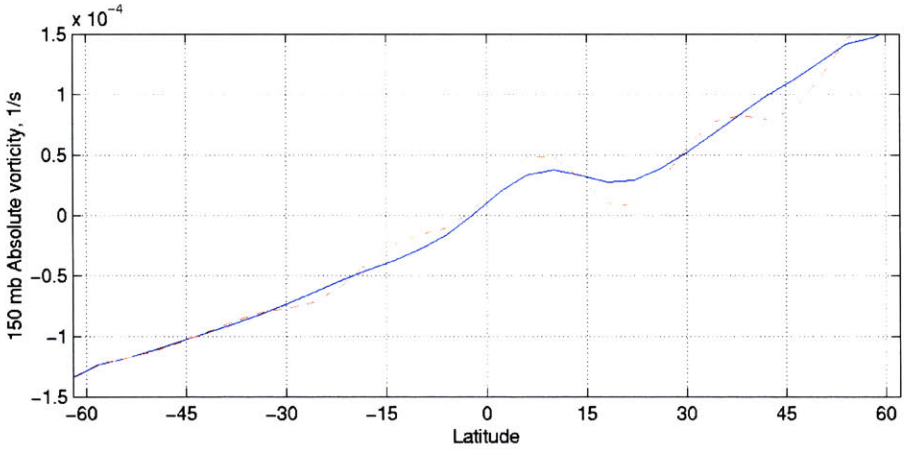

Figure 3-19: 150 mb absolute vorticity, continental cases with uniform SSTs and coastline at ϕ_L = 16N.. Solid blue line, case with $THF_0 = 130W/m^2$; red dash-dot line, case with $THF_0 = 140W/m^2$.

forcing, there is little indication of threshold behavior (Figure 3-22). The upper level absolute vorticity gradually approaches the critical value at zero for $THF_0 \geq 140W/m^2$ (Figure 3-19), but a cross-equatorial circulation develops when the vorticity is still sub-critical. The threshold behavior may be compared with that of the aquaplanet case with low viscosity and included convective momentum transport (Figure 3-5).

Why does the aquaplanet case show clear threshold behavior while the continental case does not? There are two factors which contribute to this difference in behavior. First, the threshold behavior in the aquaplanet case is accentuated by WISHE-type feedbacks, as already discussed; however, these feedbacks do not occur over the continent given the constrained surface forcing. Second, the location of large scale ascent moves poleward with increased surface forcing (Figure 3-21) in the continental case, but is nearly stationary in the aquaplanet case. As shown previously (§3.1.2), the circulation tends to weaken as the ascent region moves poleward through the subtropics; this would act to obscure threshold behavior in the continental case.

The precipitation over the continent does not show threshold behavior, with both the local maximum precipitation and the area integrated continental precipitation showing a slow, steady increase with strengthening surface forcing. The extent and strength of the meridional circulation does not strongly impact the monsoon precipitation. When the circulation switches from a localized cell to a cross-equatorial cell, there is no sudden increase in the quantity of precipitation over the continent. The flow associated with a local circulation is capable of supporting fairly intense rainfall over the continent. Jumping behavior of the cross-equatorial circulation prevents transport of moisture from the southern hemi-

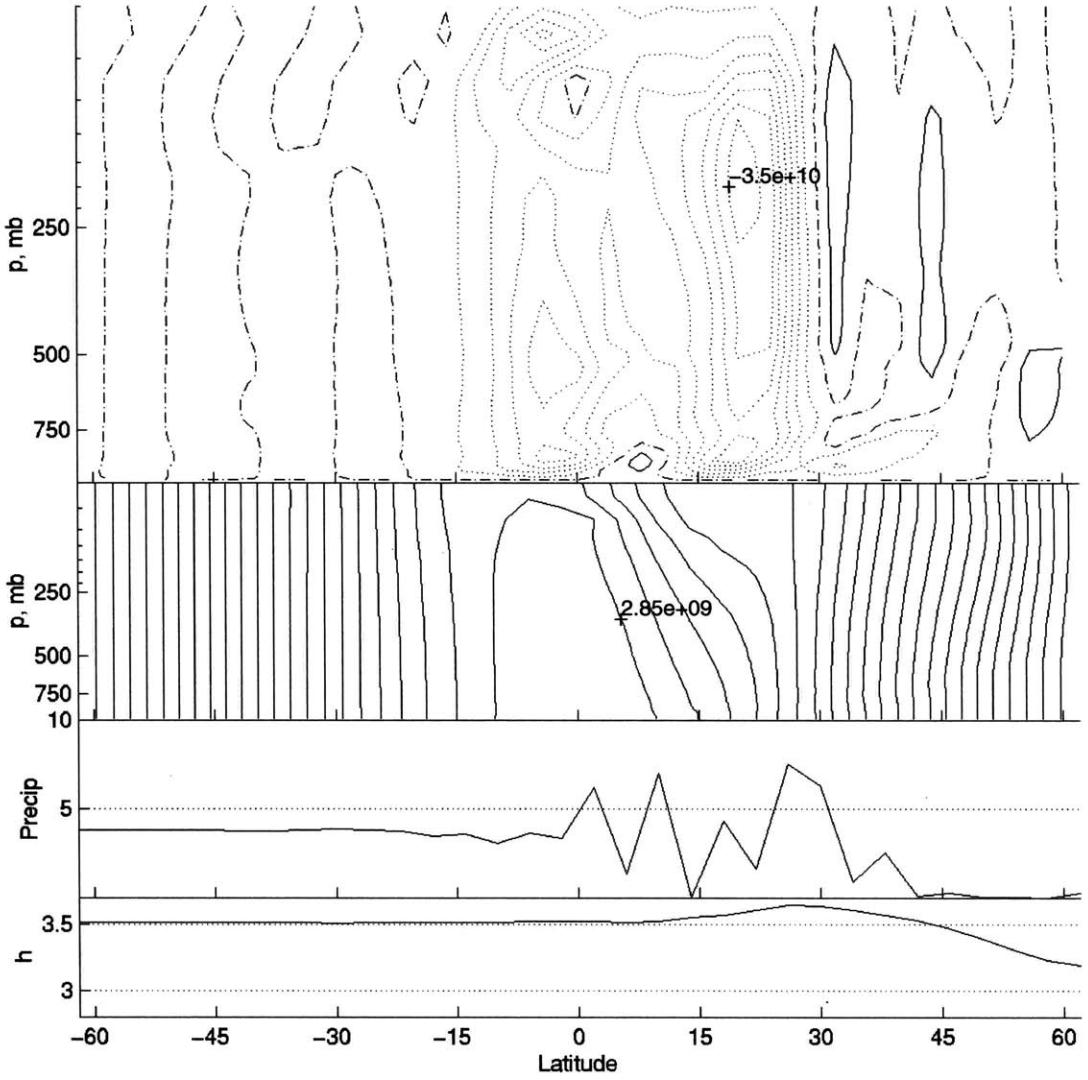

Figure 3-20: Continental case with uniform SST and $THF_0 = 140W/m^2$, 100 day time mean fields. Top, streamfunction, contour interval 5e9 kg/s, dotted lines indicate counter-clockwise flow, solid lines indicate clockwise flow, dash-dot is zero contour. Upper center, absolute angular momentum, contour interval 1E8 m^2/s. Lower center, precipitation, mm/day. Bottom, 1000 mb moist static energy, 10^5 J.

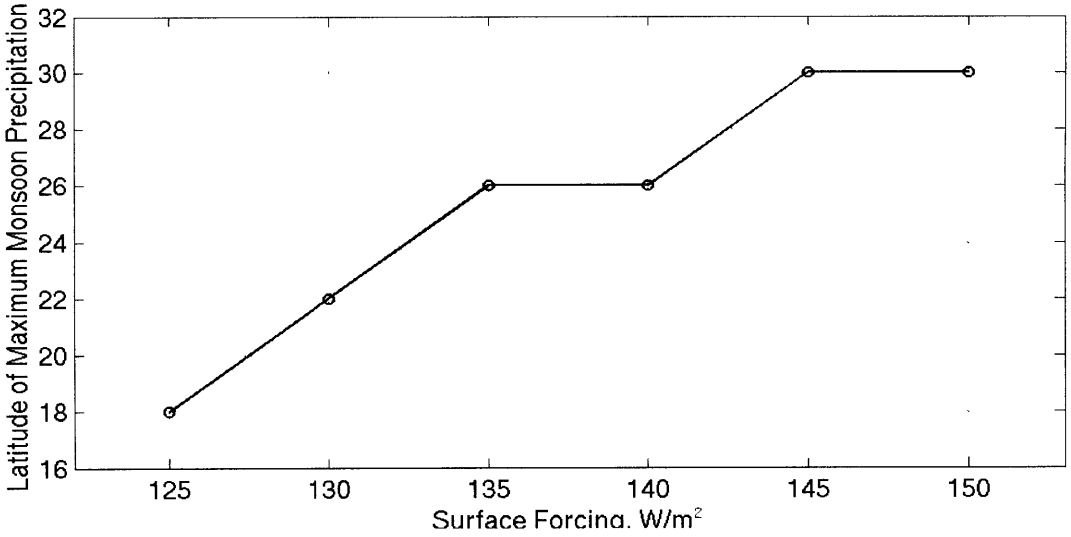

Figure 3-21: Continental case with uniform SST, coastline at 16N. Location of monsoon as a function of surface forcing strength.

sphere into the northern hemisphere, so that the moisture supply for the monsoon must be garnered from the boreal tropical ocean. Thus, the moisture supply for the monsoon is nearly blind to the extent of the circulation.

As in the aquaplanet cases, there is a transitional period while a steady circulation is established which ranges in duration from 200 to 250 days; this period shortens with increasing land forcing. The initial state after the application of summer-type land forcing features precipitation near the coast, with a strong meridional circulation cell which shows no tendency to jump. During the transitional period, the circulation cell broadens and the precipitation maximum over the landmass shifts slowly poleward. After 50-100 days, the lower tropospheric leg of the meridional cell begins to show jumping behavior, which then becomes more severe as time progresses. The faster adjustment period and lack of oscillating behavior of the circulation in the continental cases are due to the lack of WISHE feedback over the continental surface.

3.2.3 Summer SST

A summer-like SST profile is implemented with subtropical continent in an effort to achieve more realistic flow in the equatorial region. The SST distribution is fixed and does not vary with time:

$$SST(\phi) = SST_0 - \Delta T sin(\phi - 8N)^2 \tag{3.8}$$

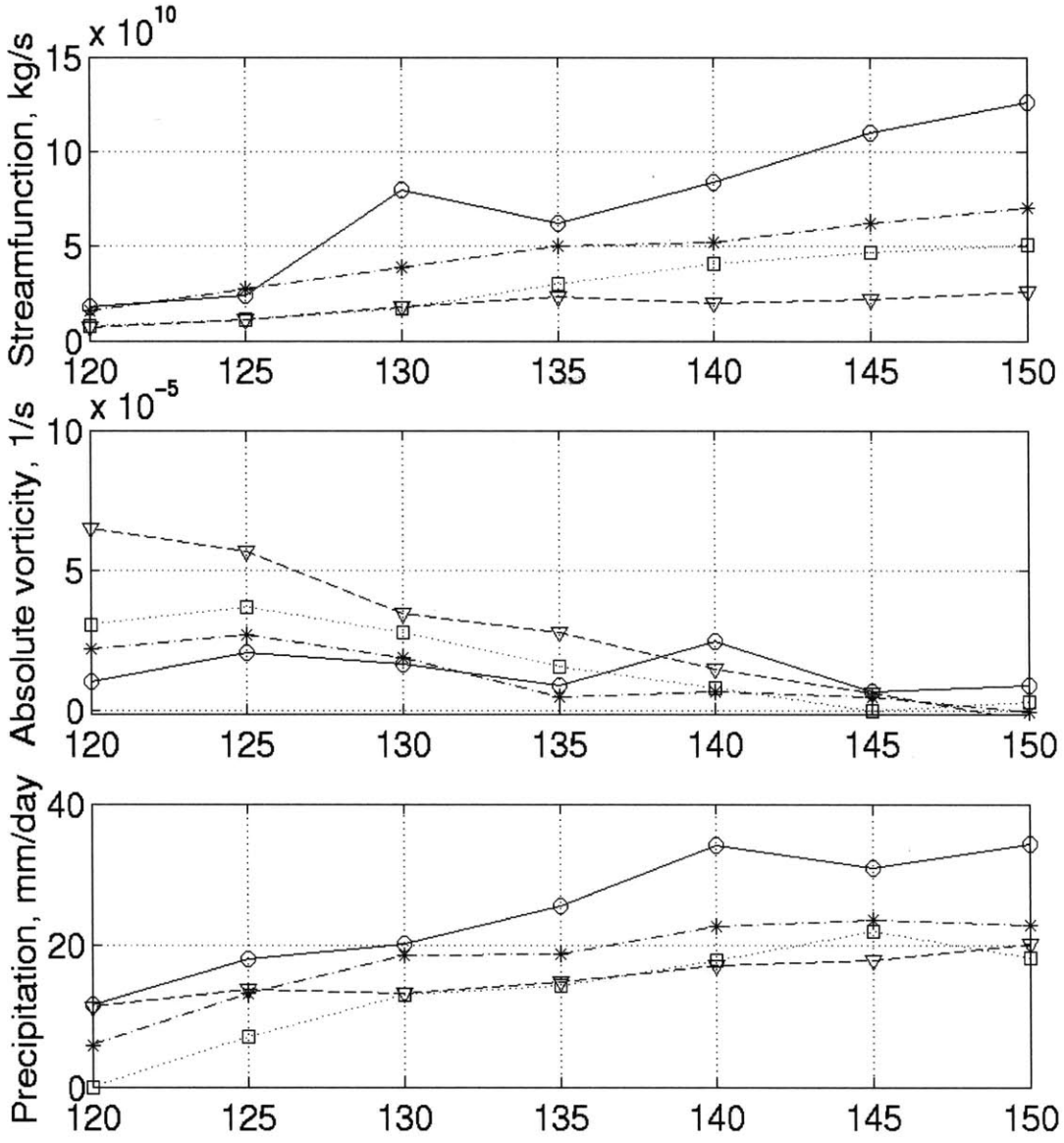

Figure 3-22: Steady-state results for continental cases in 2D as a function of THF_0 (W/m^2). Uniform SST with coastline at 16N, dotted line with squares; "summer" SST with coastline at 8N, solid line with circles; "summer" SST with coastline at 16N, dot-dash line with asterisks; "summer" SST with coastline at 24N, dotted line with triangles. a) absolute maximum negative circulation streamfunction strength, kg/s. b) minimum 150 mb absolute vorticity (s^{-1}), 6N to 64N; c) net continental precipitation in equivalent units of rainfall at the equator, mm/day

where $SST_0 = 302\,K$ and $\Delta T = 28\,K$. As before, the coastline is located at $\phi_l = 16$N with the same land surface forcing profile as in (3.7).

The overall meridional circulation is visually similar in appearance to a simple superposition of the flow from the aquaplanet case with the $\phi_0 = 8N$ summer SST profile (Figure 3-2) and the previous continental cases with uniform SST. Over the tropical ocean, a strong meridional cell forms as a result of the SST distribution: ascent occurs in the boreal hemisphere near the SST maximum at 8N, with subsidence in the southern hemisphere tropics.

For the $THF_0 = 120\,W/m^2$ case, a shallow, weak continental circulation is peripherally joined to the large, vigorous oceanic circulation cell (Figure 3-23). The precipitation field features a double ITCZ with maxima at 2N and near 10N; rainfall over the continent is very weak. The Hadley circulation is close to angular momentum conserving. There is a weak easterly jet (not shown) located near 20N at 750 mb in thermal wind balance with the temperature field. In the upper troposphere, the temperature maximum (not shown) occurs over the tropical ocean and decreases poleward over the continent. Although the land forcing is sufficient to cause a low-level temperature maximum over the subtropical continent, the region is dry, so that the subcloud moist static energy maximum occurs over the ocean near 16N.

When the land forcing is increased to $THF_0 = 125\,W/m^2$, deep moist convection onsets over the subtropical continent, with broad maximum at 18N (Figure 3-24). A larger and more intense precipitation band remains near the equator with double peaks at 2S and 6N. The meridional circulation reflects the precipitation distribution: there is a strong tropical cell in the southern hemisphere with ascent near the equator, and a weaker extension of this cell in the northern hemisphere with ascent near 18N. Unlike the $THF_0 = 120W/m^2$ case (Figure 3-23), ascent over the continent is deep. The subcloud moist static energy has a global maximum near 22N, with positive northward gradient throughout the boreal tropics. The local low-level easterly jet along the coastline seen in the $THF_0 = 120\,W/m^2$ case is no longer present, but there is easterly shear throughout the entire troposphere over the subtropical continent. The $THF_0 = 130\,W/m^2$ case is very similar to the $THF_0 = 125\,W/m^2$ case in terms of the large-scale flow (not shown).

For surface forcing of $THF_0 \geq 135\,W/m^2$, the meridional circulation develops a double-celled form; the $THF_0 = 140\,W/m^2$ case is shown in Figure 3-25. The region of ascent and strong precipitation over the continent shifts poleward as the land surface forcing is increased, while the strong ascent over the equator remains stationary. Weak subsidence exists between these two ascent regions over the northern hemisphere tropical ocean, resulting in a strong tropical circulation cell with an attached weaker narrow cell in the subtropics. The dip in the circulation strength (Figure 3-22) at $THF_0 = 135W/m^2$ is related to the formation of two circulation cells instead of the single cell seen for $THF_0 = 125, 130\,W/m^2$.

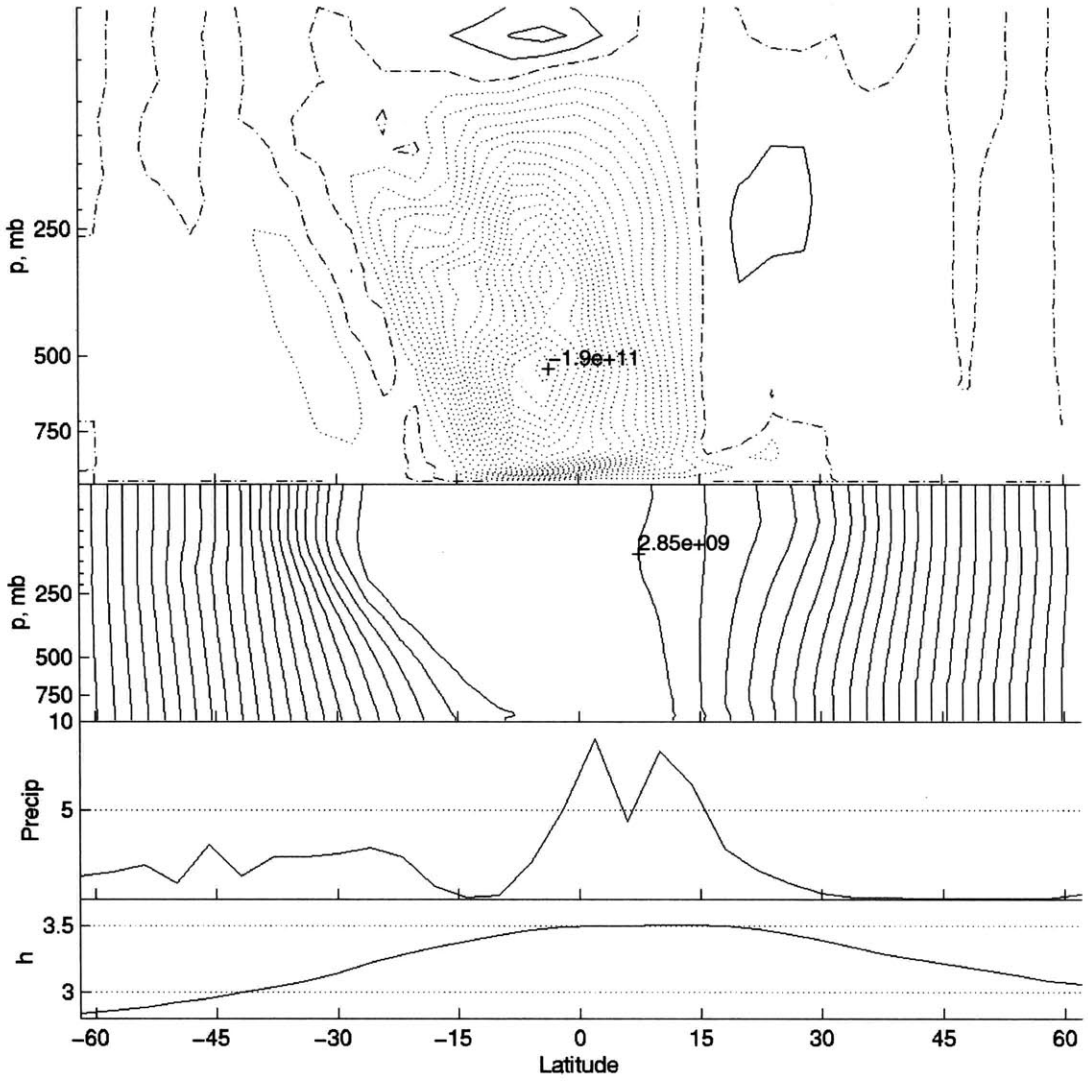

Figure 3-23: Continental case with summer SST and $THF_0 = 120\,W/m^2$, 100 day time mean fields. Top, streamfunction, contour interval 1e10 kg/s, dotted lines indicate counter-clockwise flow, solid lines indicate clockwise flow, dash-dot is zero contour. Upper center, absolute angular momentum, contour interval 1E8 m^2/s. Lower center, precipitation, mm/day. Bottom, 1000 mb moist static energy, 10^5 J.

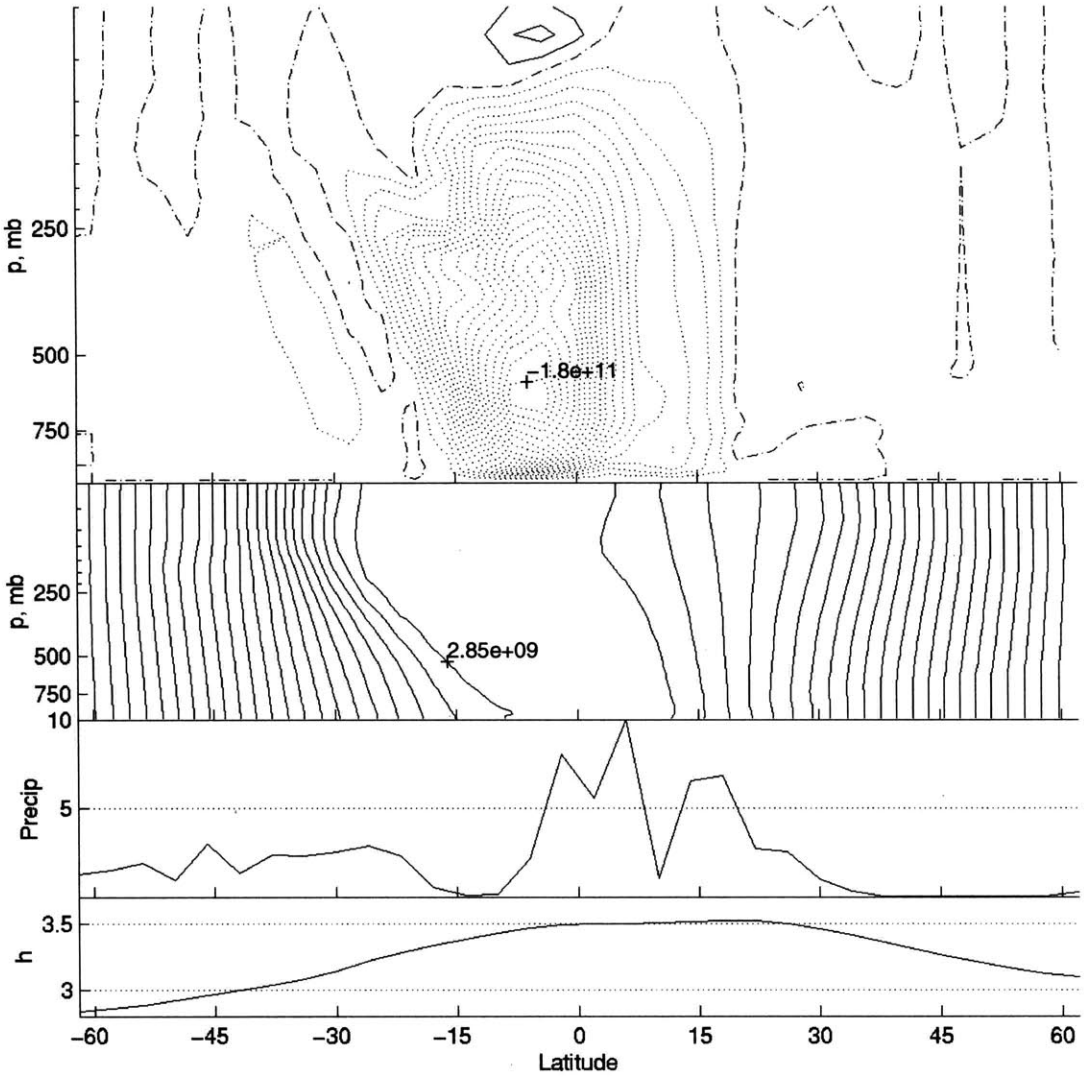

Figure 3-24: Continental case with summer SST and $THF_0 = 125\,W/m^2$, 100 day time mean fields. Top, streamfunction, contour interval 1e10 kg/s, dotted lines indicate counter-clockwise flow, solid lines indicate clockwise flow, dash-dot is zero contour. Upper center, absolute angular momentum, contour interval 1E8 m^2/s. Lower center, precipitation, mm/day. Bottom, 1000 mb moist static energy, 10^5 J.

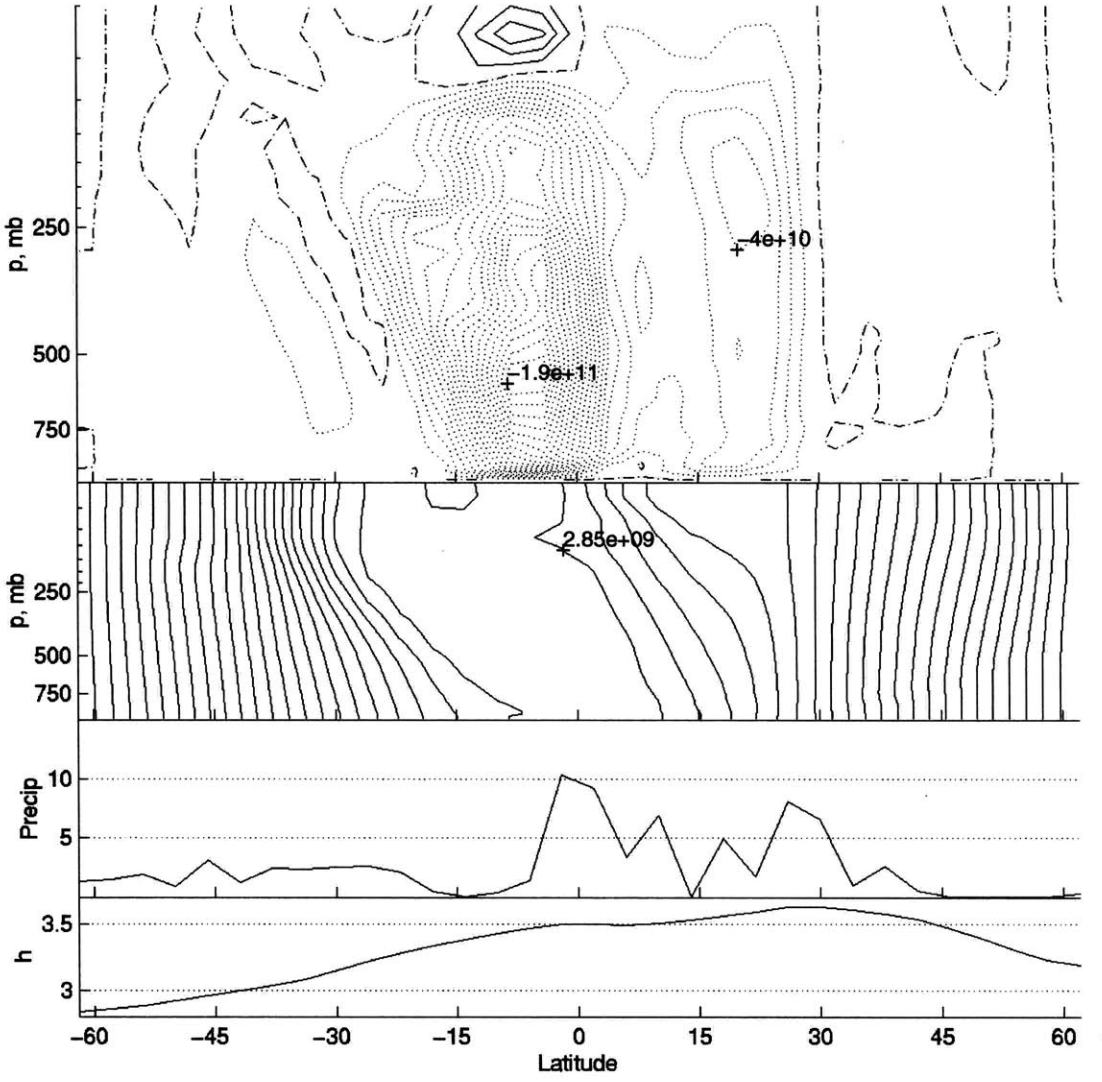

Figure 3-25: Continental case with summer SST and $THF_0 = 140\,W/m^2$, 100 day time mean fields. Top, streamfunction, contour interval 1e10 kg/s, dotted lines indicate counter-clockwise flow, solid lines indicate clockwise flow, dash-dot is zero contour. Upper center, absolute angular momentum, contour interval 1E8 m^2/s. Lower center, precipitation, mm/day. Bottom, 1000 mb moist static energy, 10^5 J.

The continental precipitation maximum shifts from 26N in the $THF_0 = 135W/m^2$ case to 30N in the $THF_0 = 150\,W/m^2$ case. The subcloud moist static energy maximum over the continent also increases with increased land surface forcing, and shifts poleward as well, moving from 26N in the $THF_0 = 135W/m^2$ case to 34N in the $THF_0 = 150W/m^2$ case. The upper level tropical easterly jet (not shown) is very strong in these cases, with maximum wind speeds of greater than $60\,m/s$ at the core of the jet. A low-level easterly jet forms over the subtropical continent near 700 mb in thermal balance with the temperature gradient, intensifying with increased surface forcing, although the core wind speeds remain less than $10m/s$. The jet center shifts slightly poleward from 34N for $THF_0 = 135W/m^2$ to 38N for $THF_0 = 150W/m^2$.

Over the subtropics and landmass, the circulation is similar in form to that of the uniform SST case (§3.2.2), but stronger. For weak land forcing ($THF_0 \leq 135\,W/m^2$), the streamfunction over the continent is almost twice as strong in the summer SST case as in the uniform SST case (Figure 3-22), but for $THF_0 \geq 140\,W/m^2$, the circulation is similar in intensity. The precipitation over the continent is greater in the summer SST case than in the uniform SST case, and the upper level absolute vorticity (not shown) is slightly closer to zero. The 150 mb absolute vorticity over the continent is near the critical value of zero for $THF_0 \geq 135\,W/m^2$; however, there is no sign of threshold behavior of the circulation strength. As the continental forcing is increased from $THF_0 = 120\,W/m^2$ to $THF_0 = 140\,W/m^2$, the net rainfall over the landmass increases steadily (Figure 3-22). For forcing of $THF_0 \geq 140W/m^2$, the net precipitation reaches a plateau. The double-celled circulation structure is reminiscent of the jumping behavior seen in the case with uniform SST, and has a similar impact of the northward moisture flux.

Continental Location

The aquaplanet cases with varied latitudinal position of the SST perturbation have shown that the strength and extent of the meridional circulation are strongly dependent upon the location of the forcing (Figure 3-13). When the forcing is sufficiently close to the pole, a local AMC circulation results, while a strong cross-equatorial circulation obtains when the forcing is close to the equator. The size and strength of the meridional circulation affects the moisture supply for the monsoon; thus, the effect of the continental location on the strength of the monsoon is of interest. Monsoons are observed to occur in regions with different coastal position: in West Africa, the coastline is located near 8N, while the monsoon in southwestern North America is located near 30N. The impact of coastal location is also valuable in paleoclimate studies. Two different experiments are performed, one with continental coastline at $\phi_L = 8$N, and a second with coastline at $\phi_L = 24$N. The ocean SST

distribution is given by (3.8) for both cases, with SST maximum at 8N.

8N coastline For the case with coastline at ϕ_L = 8N, the land surface heat flux profile is given by (3.7) with $\phi_T = 0N$, so that the forcing over the continent is shifted 8° equatorward from the previous cases with ϕ_L = 16N. In this manner, the forcing profile relative to the coastline is the same as in the ϕ_L = 16N case.

With weak applied land surface forcing ($THF_0 \leq 125\,W/m^2$), the circulation of the ϕ_L = 8N case is very similar to that of the ϕ_L = 16N coastline case (Figure 3-23, 3-24). In these cases, there is only weak precipitation over the land, and the precipitation maxima remain over the tropical equatorial ocean. In the $THF_0 = 120\,W/m^2$ case (not shown), the meridional circulation over the continent is shallow, and capped by subsidence above 700 mb. In the $THF_0 = 125\,W/m^2$ case (Figure 3-26), the circulation over the landmass close to the coastline is deep, with a local maximum of precipitation near the coast which is not as strong as the equatorial precipitation band. The streamfunction strength over the continent is quantitatively very similar between the ϕ_L = 8N and ϕ_L = 16N coastline cases for $THF_0 \leq 125\,W/m^2$ (Figure 3-22). The upper level easterly jet in the tropics (not shown) is much weaker with the ϕ_L = 8N coastline, as expected since the ascent branch of the circulation occurs closer to the equator than in the ϕ_L = 16N coastline case. The subcloud moist static energy field is greater in the ϕ_L = 16N coastline case than in the ϕ_L = 8N case both over the tropical northern hemisphere ocean and over the subtropical continent.

As the land forcing is increased further ($THF_0 \geq 130\,W/m^2$), the continental circulation strength and precipitation become more intense in the ϕ_L = 8N case compared to the ϕ_L =16N case (Figure 3-22). For the $THF_0 = 130\,W/m^2$ case (Figure 3-27), the circulation features a broad region of strong large scale ascent, ranging from approximately 4S to 20N, with little sign of the jumping behavior seen in the ϕ_L = 16N case. Although the circulation over the continent is much stronger for the ϕ_L = 8N case, the precipitation is only slightly greater than the ϕ_L = 16N case, and occurs 4° closer to the equator. The subcloud moist static energy in the ϕ_L = 8N case is nearly the same as in the $\phi_L = 16N$ case over the tropical ocean, but the maxima over the continental region is not as strong. Correspondingly, the upper level temperature maximum over the landmass is greater in the ϕ_L = 16N case than in the ϕ_L = 8N case.

For $THF_0 \geq 135\,W/m^2$, the meridional circulation begins to show signs of equatorial ascent in addition to the continental ascent region (eg. Figure 3-28). However, the flow does not show the strong jumping tendency seen in the ϕ_L = 16N case, and there is significant mass transport in the boundary layer at the equator. As a result, the flow features increased meridional moisture flux in the ϕ_L = 8N case, with net moisture transport across the

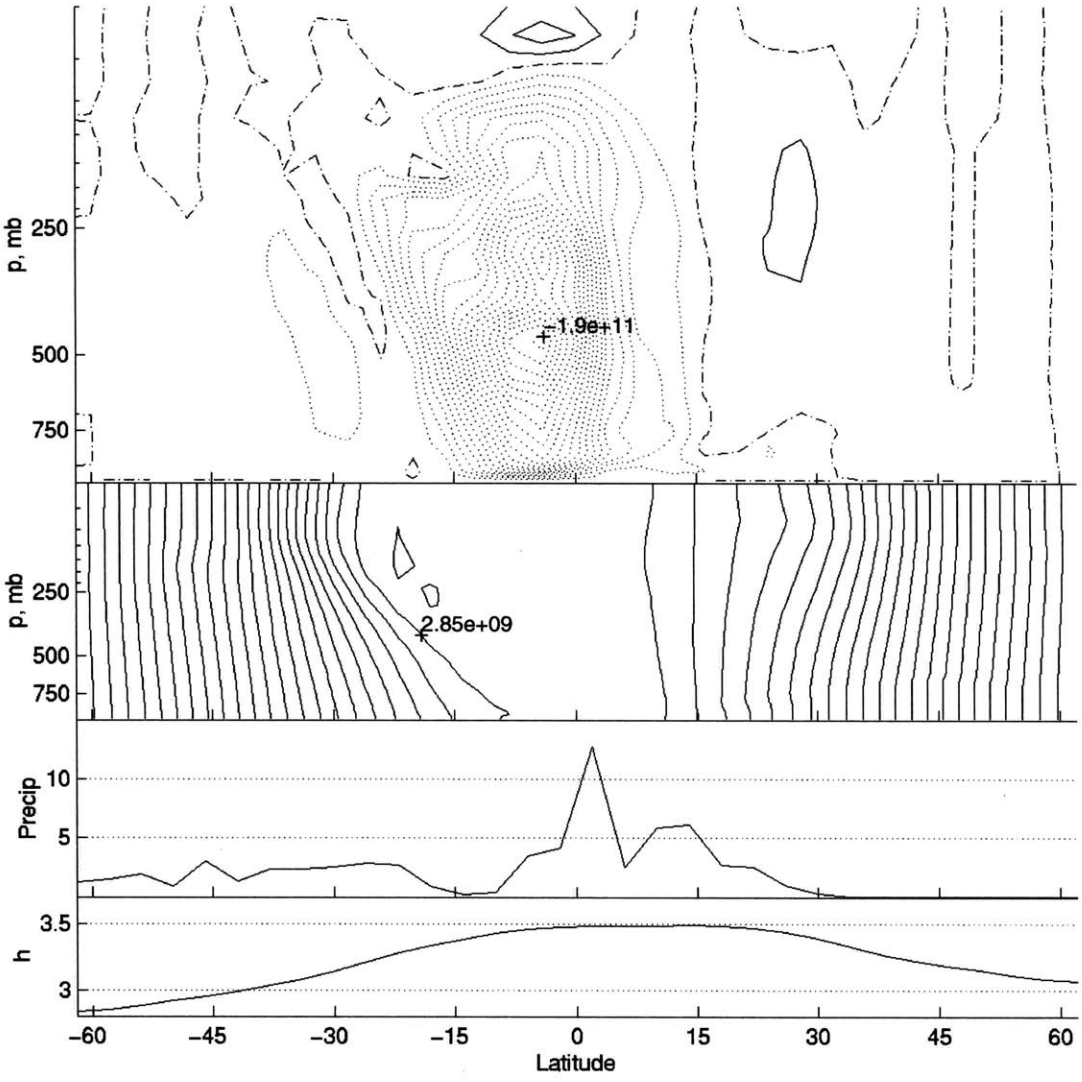

Figure 3-26: Continental case with summer SST, coastline at 8N and $THF_0 = 125\,W/m^2$, 100 day time mean fields. Top, streamfunction, contour interval 1e10 kg/s, dotted lines indicate counter-clockwise flow, solid lines indicate clockwise flow, dash-dot is zero contour. Upper center, absolute angular momentum, contour interval 1e8 m^2/s. Lower center, precipitation, mm/day. Bottom, 1000 mb moist static energy, 10^5 J.

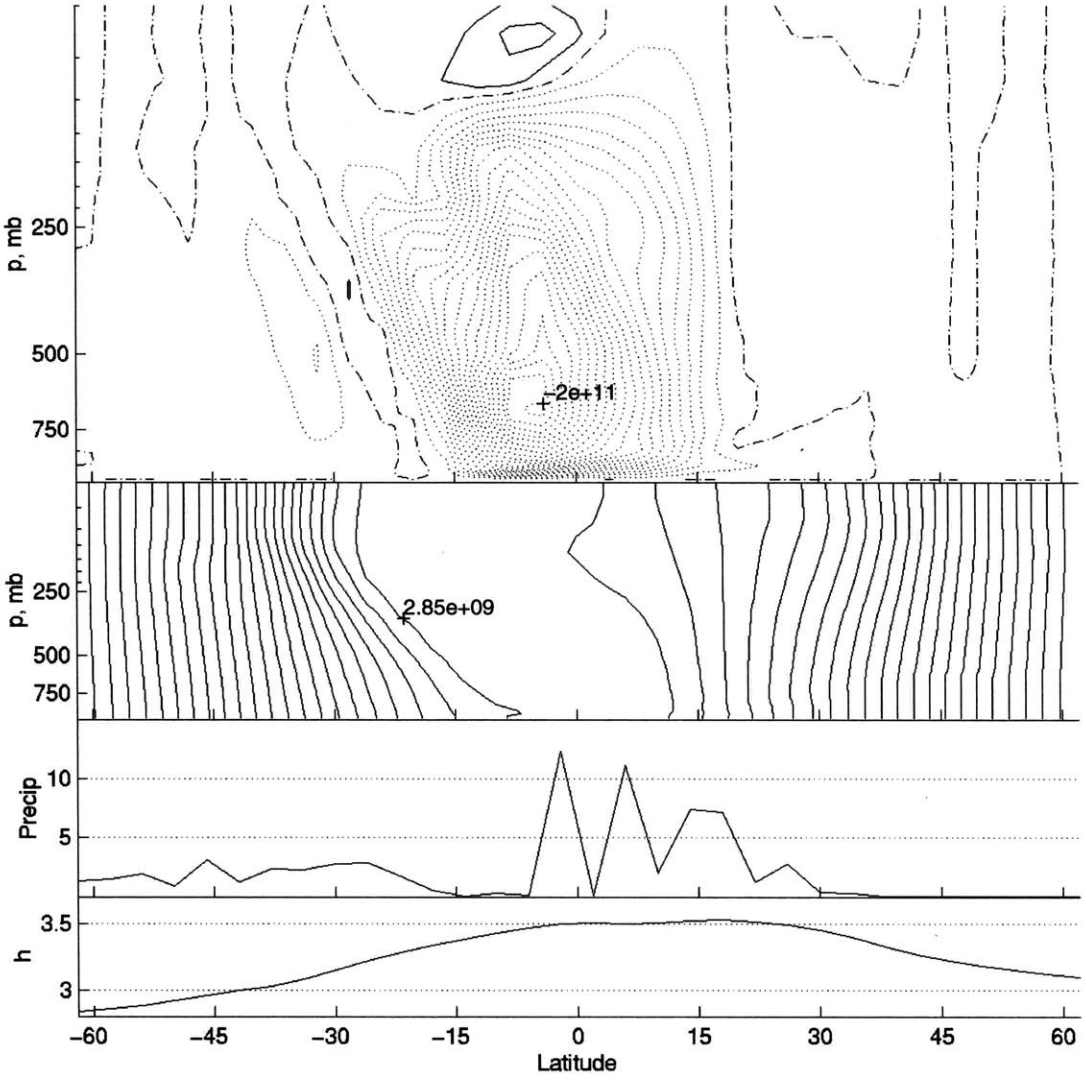

Figure 3-27: Continental case with summer SST, coastline at ϕ_L = 8N and THF_0 = 130 W/m^2, time mean fields days 500-600. Top, streamfunction, contour interval 1e10 kg/s, dotted lines indicate counter-clockwise flow, solid lines indicate clockwise flow, dash-dot is zero contour. Upper center, absolute angular momentum, contour interval 1e8 m^2/s. Lower center, precipitation, mm/day. Bottom, moist static energy.

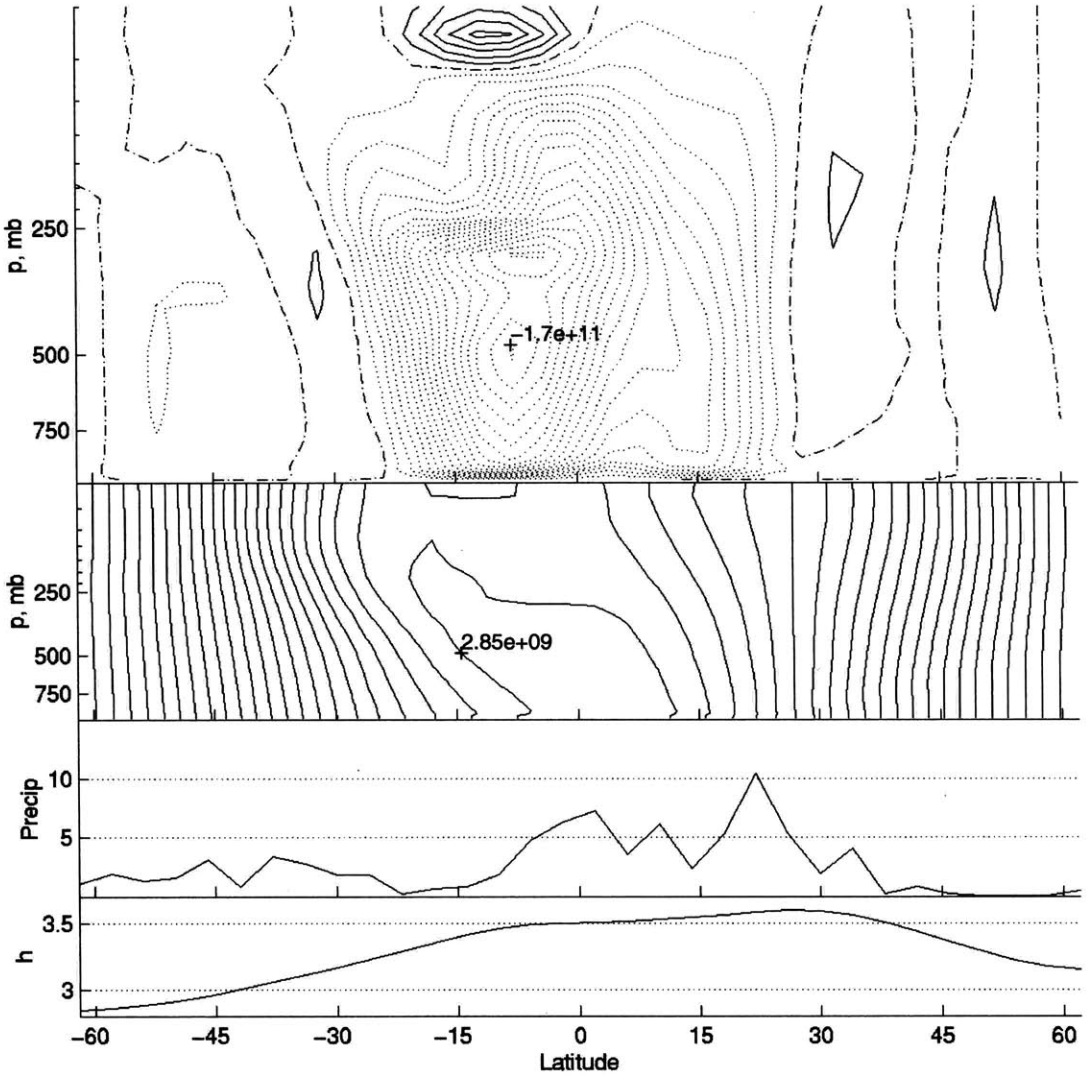

Figure 3-28: Continental case with summer SST, coastline at 8N and $THF_0 = 140\,W/m^2$, 100 day time mean fields. Top, streamfunction, contour interval 1e10 kg/s, dotted lines indicate counter-clockwise flow, solid lines indicate clockwise flow, dash-dot is zero contour. Upper center, absolute angular momentum, contour interval 1e8 m^2/s. Lower center, precipitation, mm/day. Bottom, 1000 mb moist static energy, 10^5 J.

coastline nearly twice as great as in the $\phi_L = 16$N case. Because the coastline and the heated continent are close to the equator, the large-scale pressure gradient across the equator in the mixed layer has a stronger negative-northward gradient. The difference in net continental precipitation between the $\phi_L = 8$N and $\phi_L = 16N$ cases increases, with much stronger total continental rainfall in the $\phi_L = 8$N case (Figure 3-22). The continental precipitation maximum remains shifted 4° equatorward relative to the $\phi_L = 16$N case. The boundary layer moist static energy maximum is also shifted 4° equatorward in comparison to the 16N case, and the continental peak in h_b is not as strong.

Several factors may contribute to the strengthening of the continental streamfunction for $\phi_L = 8N$ in comparison to the $\phi_L = 16$N case. First, the region of large scale ascent is located closer to the equator, which has been shown in the aquaplanet case to yield more intense circulations (§3.1.2). Second, jumping behavior significantly weakens the circulation in the $\phi_L = 16$N case. As the jumping tendency is not as strong in the $\phi_L = 8$N case, the circulation is not as severely affected. The decrease in circulation strength from the $THF_0 = 130\,W/m^2$ case to the $THF_0 = 135\,W/m^2$ case (Figure 3-22) is a result of the initiation of jumping in the $THF_0 = 135\,W/m^2$ case. There is again little sign of threshold behavior of the circulation strength or the precipitation field.

24N coastline The coastline is now shifted poleward to $\phi_L = 24$N, with the land surface heat flux profile given by (3.7) with $\phi_T = 16N$. The ocean temperature profile is kept at the summer-type distribution given by (3.8), with maximum at 8N.

Over the tropical region, a large cross-equatorial Hadley cell induced by the SST gradient occurs, with a weak Hadley cell of opposite sense in the boreal hemisphere. For $THF_0 = 120W/m^2$ (not shown), the circulation over the continent is extremely weak. Although there is a local precipitation maximum over the coastal continent, the majority of the precipitation remains over the tropical ocean in the ascent region of the cross-equatorial Hadley cell.

As the surface forcing is increased, the meridional circulation over the land becomes deep, but remains narrow in latitudinal extent and weak in comparison to the cross-equatorial Hadley cell (Figure 3-29). The continental circulation cell is completely separate from the cross-equatorial cell for all land surface forcing levels. Although the strength of the continental cell is much less than that seen in the $\phi_L = 16$N cases, the net precipitation over the landmass is comparable (Figure 3-22).

At low surface forcing levels, the upper tropospheric absolute vorticity (Figure 3-22) is much higher over the continent than that seen in the 16N and 8N cases, which is expected due to the greater latitude of the continent. As the land surface forcing is increased, the upper level absolute vorticity decreases rapidly, and approaches the critical value at zero for $THF_0 \geq 140\,W/m^2$ (Figure 3-22). Examination of the absolute angular momentum

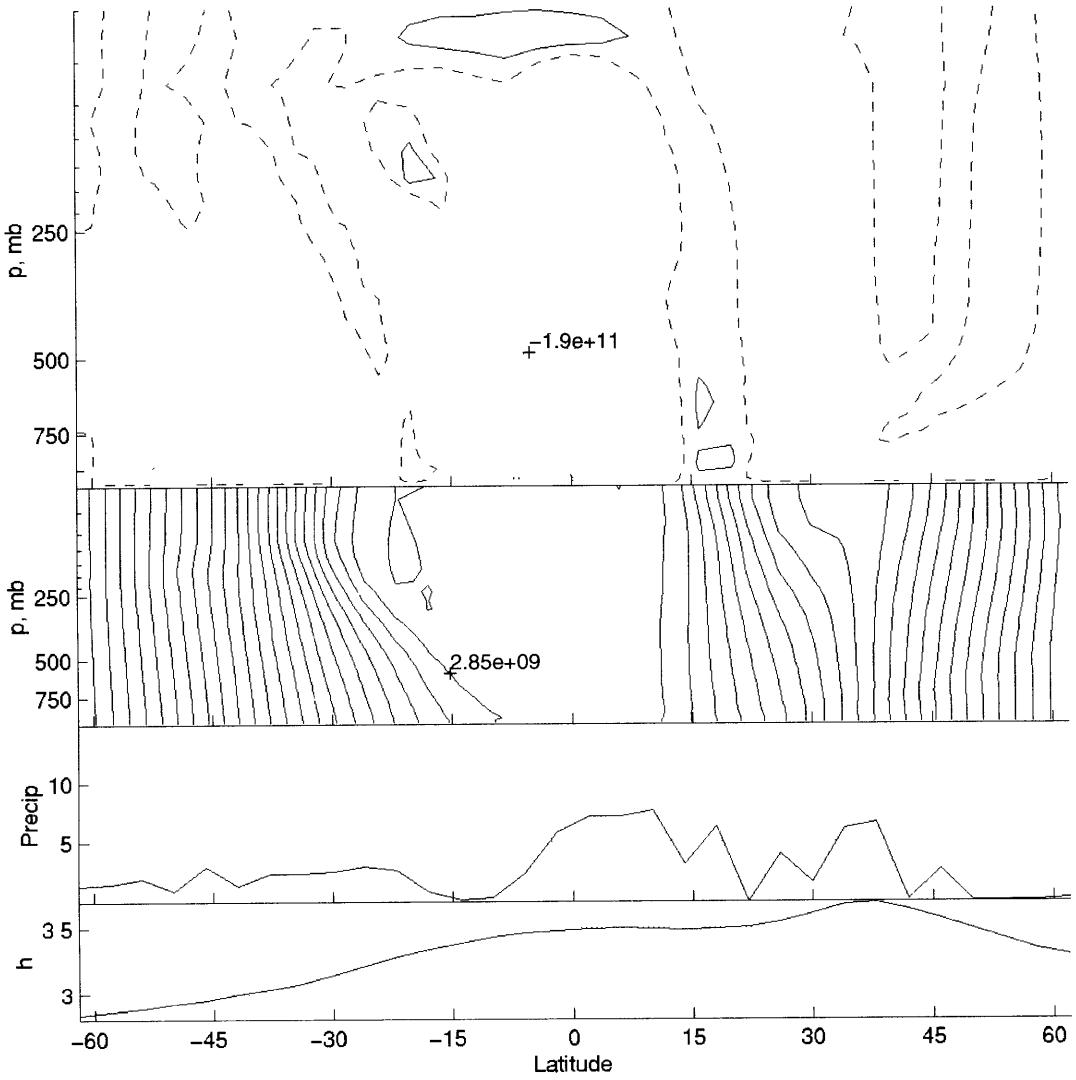

Figure 3-29: Continental case with summer SST, coastline at 24N and $THF_0 = 140\,W/m^2$, 100 day time mean fields. Top, streamfunction, contour interval 1e10 kg/s, dotted lines indicate counter-clockwise flow, solid lines indicate clockwise flow, dash-dot is zero contour. Upper center, absolute angular momentum, contour interval 1e8 m^2/s. Lower center, precipitation, mm/day. Bottom, 1000 mb moist static energy, 10^4 J.

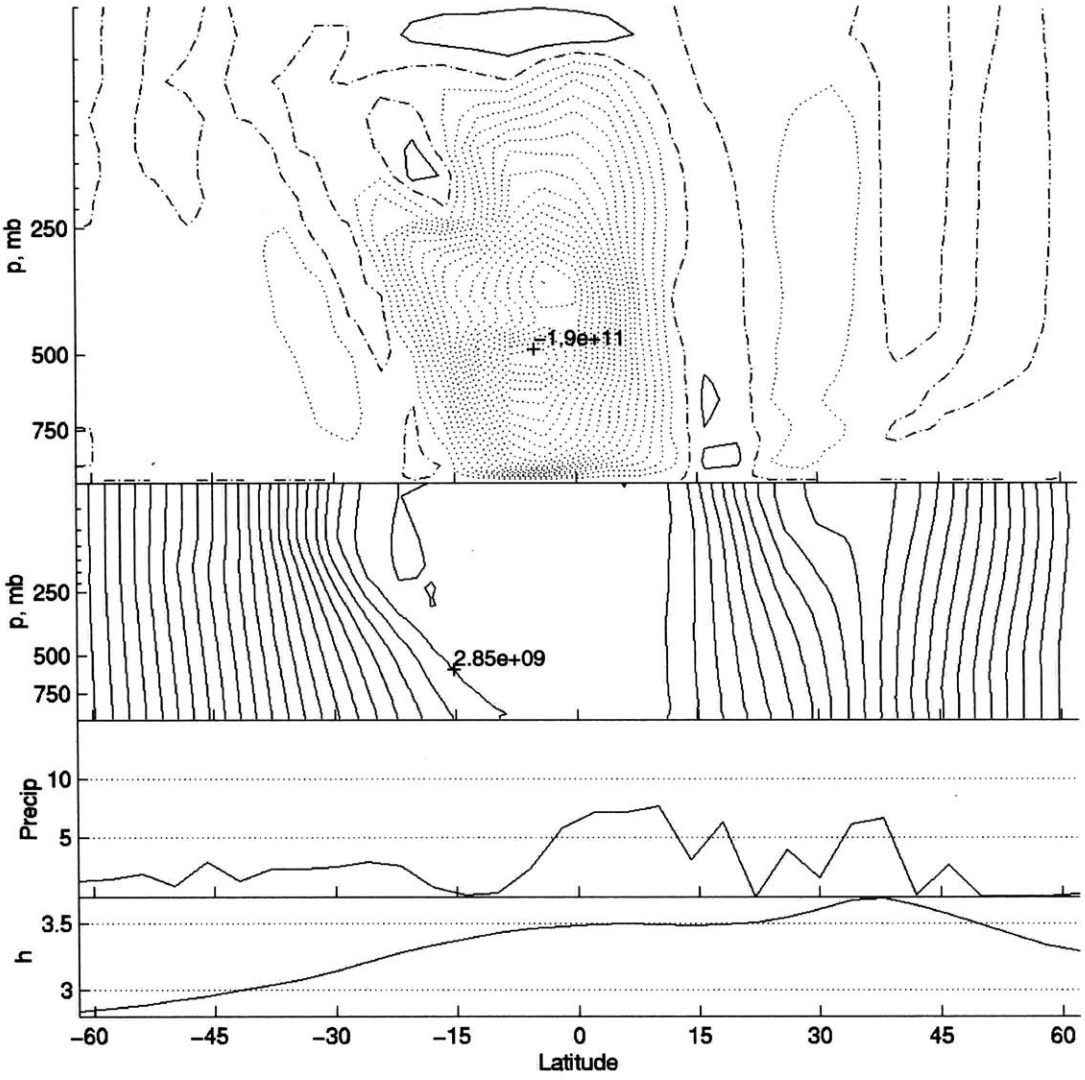

Figure 3-29: Continental case with summer SST, coastline at 24N and $THF_0 = 140\,W/m^2$, 100 day time mean fields. Top, streamfunction, contour interval 1e10 kg/s, dotted lines indicate counter-clockwise flow, solid lines indicate clockwise flow, dash-dot is zero contour. Upper center, absolute angular momentum, contour interval 1e8 m^2/s. Lower center, precipitation, mm/day. Bottom, 1000 mb moist static energy, 10^4 J.

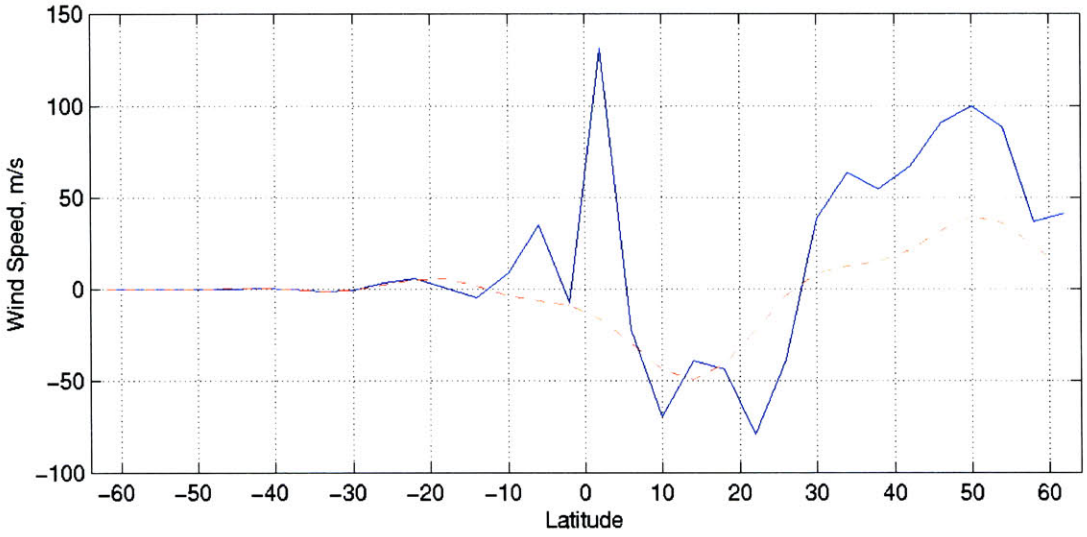

Figure 3-30: Comparison of tropopause zonal winds from theory (solid blue line) with modeled winds (dash-dot red line). Modeled winds are taken from the axisymmetric case with continent at $\phi_L = 16$N with $THF_0 = 140W/m^2$, shown in Figure 3-20.

where u_T and T_T are respectively the zonal wind and temperature at some chosen pressure surface in the upper troposphere, T_0 is the temperature at the surface, and s_b is the subcloud moist entropy. These relations have been used by Emanuel (1995) to express the threshold criteria for formation of a Hadley circulation in response to subtropical forcing in terms of the subcloud moist entropy distribution.

The validity of the assumptions and approximations is tested by comparing the estimated tropospheric zonal wind to the modeled zonal wind. An example is show in Figure 3-30 for the modeled case with $THF_0 = 140W/m^2$ with uniform ocean and coastline at $\phi_L = 16$N. The estimated wind is expected to be close to the modeled wind only in regions of deep moist ascent, but not in regions of subsidence or over the dry inland continent. The modeled wind is close to the estimated wind over the tropical ocean, although the estimated winds are excessively large near the equator where f is small. Near the monsoon, the estimated winds are stronger than the modeled winds, which is not surprising, as the analytic theory does not account for viscosity. However, the estimated and modeled winds in the monsoon region have the same sign, and cross zero at the same latitude. The surface winds are very weak in the modeled case, so that the position of zero wind shear is close to the position of zero upper tropospheric winds - thus, the model and the estimated winds agree relatively well as to the location of zero shear of zonal wind.

Assuming a meridional circulation which conserves absolute angular momentum in the free troposphere, the ascent branch of the circulation may have no vertical shear of zonal

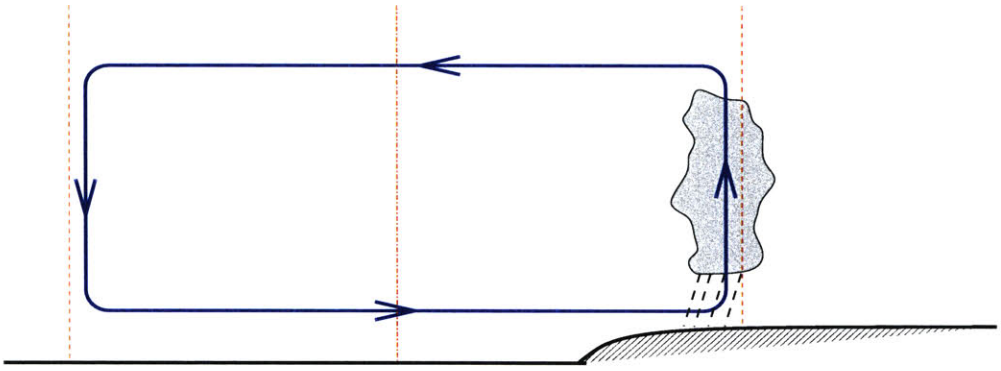

Figure 3-31: Schematic diagram of circulation and deep convection.

wind (Figure 3-31). The maximum AAM that the circulation may have in the free troposphere is the AAM near the surface in the region of large-scale ascent. For example, in the case with zero surface winds, the equatorward branch of the circulation may support easterly flow, but not westerly flow (Figure 3-32). The boundary of the cross-equatorial meridional circulation in the summer hemisphere must be located in a region of zero vertical wind shear. Poleward of the monsoon, over the arid continent, there is little circulation, and the atmosphere approaches a radiative convective equilibrium state (Figure 3-31). The assumption of conservation of angular momentum in the rising branch of of the circulation is reasonable: with zero wind shear, there should be little viscous momentum tendency, and the convective momentum transport redistributes momentum only in a vertical column and will not affect the momentum in a region of zero shear.

The statistical equilibrium theory may be applied to this framework in order to tie the monsoon location to the subcloud moist static energy. Let us assume a forcing region in the subtropics which results in a localized area of high subcloud moist static energy, h_b, where

$$h = L_v q + (c_{pd} + r_t c_l)T + (1 + r_t)gz \tag{3.13}$$

with L_v the latent heat of vaporization, specific humidity q, specific heat of dry air c_{pd} and of liquid water c_l, mixing ratio of water vapor r and of total water content r_t, and geopotential height z. For the sake of this argument, the forcing region is considered to be sufficiently strong to meet the threshold criteria for creation of an angular momentum conserving meridional circulation (Plumb and Hou (1992), Emanuel (1995)). The subcloud moist static energy is closely related to the moist entropy through

$$\delta h_b = T \delta s_b \tag{3.14}$$

The boundary of the meridional circulation is coincident with the zero line of zonal wind

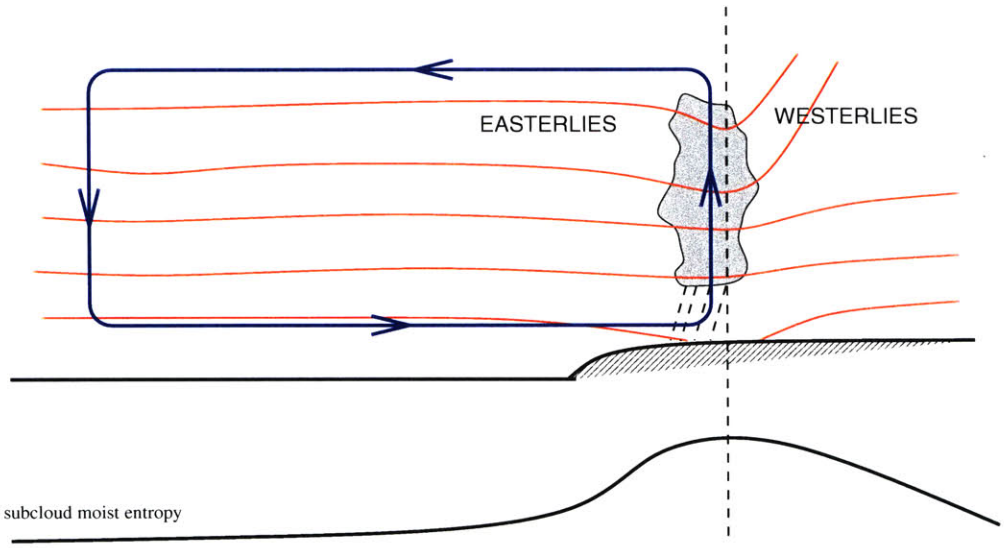

Figure 3-32: Schematic diagram of boundary layer moist static energy (bottom) and relation to virtual potential temperature (red lines, top) and large-scale circulation (blue, top).

shear in the troposphere (Figure 3-32). From (3.11), $\frac{\partial u}{\partial p} = 0$ when either $\frac{\partial T}{\partial p}$ or $\frac{\partial s^*}{\partial y}$ are zero; as it is highly unlikely that the vertical temperature gradient is zero, the zero wind shear line will occur at the latitude at which s^* is maximum ($\frac{\partial s_b}{\partial y} = 0$) since $s^* = s_b$ following a moist adiabat. The maximum s_b is colocated with the maximum h_b, through (3.14). Large scale ascent will occur near and equatorward of this maximum in h_b, with the boundary of the circulation coincident with the h_b maximum. The precipitation is colocated with the large scale ascent, so that the subcloud moist static energy distribution determines the location of the monsoon circulation and precipitation.

What, then, determines the subcloud moist static energy distribution? In RCE with this model setup, the subcloud moist static energy profile follows that of the prescribed continental net surface heat flux ($THF(\phi)$), although the actual value of h_b is constrained by moisture availability. In radiative convective equilibrium, the greatest subcloud h_b over the continent will be located at the southernmost region of the continent, where the net surface heat flux is greatest. When a large-scale circulation is present, advection of subcloud moist static energy becomes important; along the coastline, the cross-equatorial circulation carries relatively low moist static energy air from the tropical ocean onto the heated continent, reducing the moist static energy at the coastline from the RCE value. As the flow continues poleward over the landmass, the surface heat flux increases the moist static energy, until it reaches the same value that would occur in RCE. The latitude at which this occurs is the location of the maximum subcloud moist static energy, given the prescribed distribution of land surface flux used here. As the land surface forcing is increased, the circulation

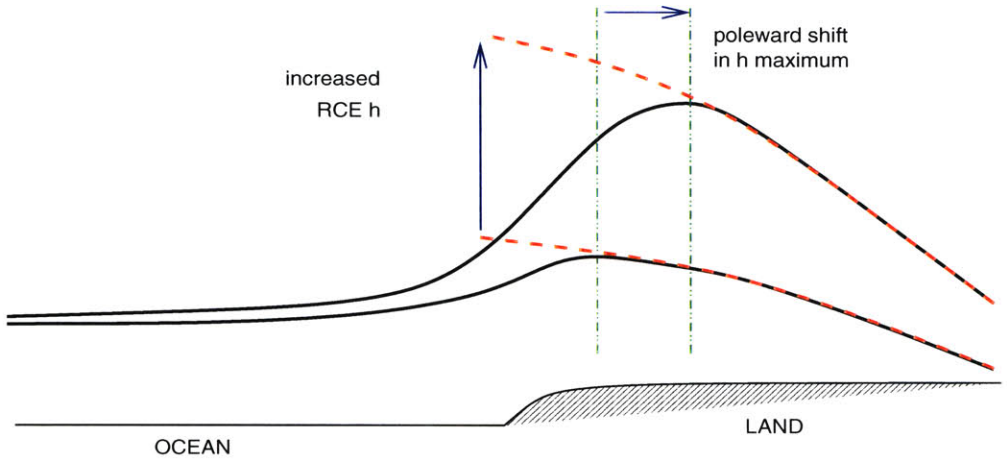

Figure 3-33: Schematic diagram of subcloud moist static energy. Dashed red line shows RCE h_b, solid black line shows h_b in the presence of a large-scale circulation.

intensifies, advecting more of the relatively cool ocean air over the continent. The greater land surface fluxes heat the poleward flowing air faster, but there is a greater mass flux to be heated and the RCE moist static energy also increases, so that the flow takes longer to reach the RCE h_b, and the location shifts poleward (Figure 3-33).

This theory can be tested with the model. First, the radiative convective equilibrium state can be calculated as in §3.2.1. Because the moist static energy is strongly affected by the humidity, two different regimes are used to test the range of possibility: first, a case with a swamp-like continent is used, and second, a desert-like continent is investigated. The profiles of subcloud moist static energy for these cases can then be compared to that seen in the case with full dynamics. In the swamp case with full dynamics, the subcloud moist static energy is very close to the swamp-RCE profile poleward of the circulation (Figure 3-34), as expected. The full-dynamics case has h_b which lies between the swamp and desert-RCE curves poleward of the monsoon (Figure 3-34); this is sensible since the circulation in the full dynamics case does carry some moisture inland, where it is further diffused by the horizontal filter. The location of the poleward boundary of the monsoonal circulation cell is found to be coincident with the latitude of maximum subcloud moist static energy for all previously described continental cases, with the precipitation peak occurring at or equatorward of this point. In some of the aquaplanet cases with localized SST perturbation, the ascent branch of the circulation is not closely AMC, due to numerical filtering of the zonal wind by the Shapiro filter (eg. Figure 3-8). In these cases, the flow increases in AAM as it ascends, so that positive vertical wind shear is allowed; the maximum subcloud h_b is located slightly equatorward of the boundary of the meridional circulation, where $\frac{\partial s_b}{\partial y} < 0$.

The theory also helps to explain the flow seen in the case with coastline at $\phi_L = 8\text{N}$;

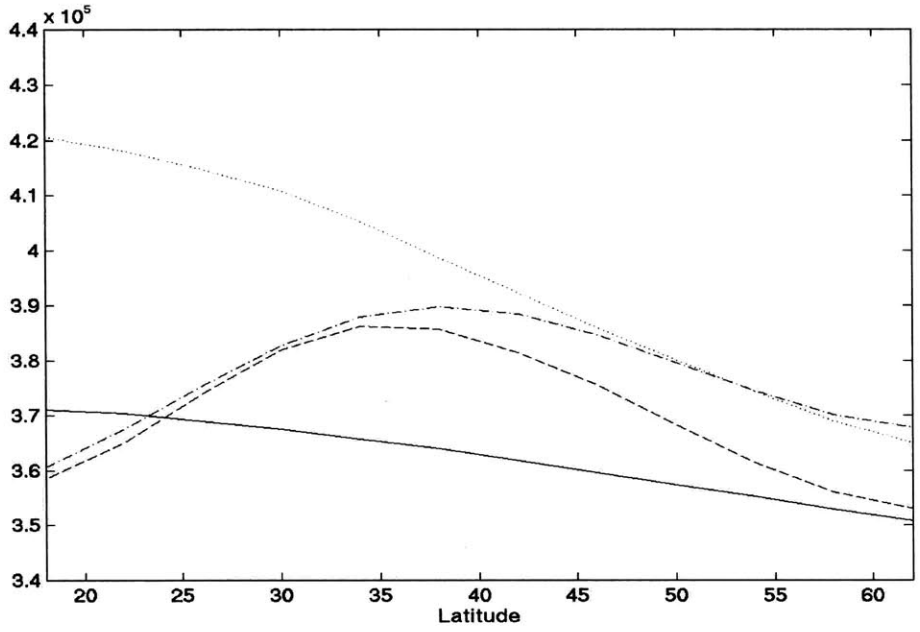

Figure 3-34: 1000 mb field of moist static energy, h_b, of steady state, land surface forcing $THF_0 = 160\,W/m^2$. Solid line, radiative-convective equilibrium (RCE) state with dry land surface; dotted line, RCE state with "swamp" continent; dashed line, full dynamics case with dry surface; dash-dot line, full dynamics case with "swamp" continent.

although the continent is shifted 8° equatorward from the ϕ_L = 16N case, the monsoon location only shifts 4° equatorward. The subcloud moist static energy profiles reveal that in the 16N case, strong latent heat fluxes over the ocean at 10N increase the subcloud moist static energy which is advected onto the land. In the 8N coastline case, the air which is advected across the coastline has lower moist static energy, and must travel further across the heated continent in order to reach the RCE h_b.

3.4 Seasonal

A series of experiments with seasonally varying land forcing are performed in order to investigate the pertinence of the steady state, perpetual summer results to the seasonal monsoon. The transient period prior to establishment of a steady circulation is nearly 200 days long for the continental cases - this is considerably greater than a seasonal timescale. The delay in onset of jumping of the circulation questions the importance of the jumping behavior to the seasonal, transient monsoon. In order to retain simplicity, the ocean SST does not vary in time and is uniformly 302K at all latitudes. The coastline is located at ϕ_l = 16N, and the land forcing is given by (3.7), with $\phi_T = 8N$. To represent seasonal variation in radiative forcing, THF_0 is varied sinusoidally in time from $80\,W/m^2$ at winter solstice to

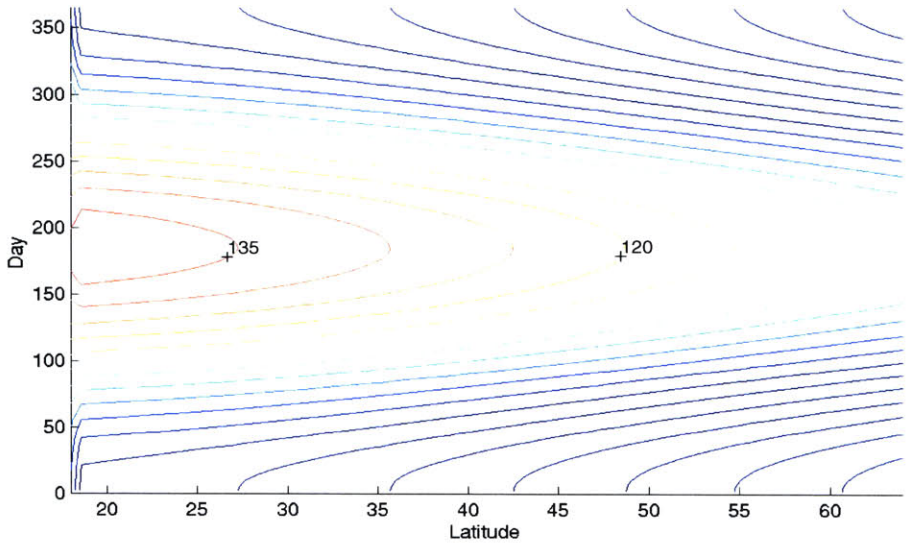

Figure 3-35: Prescribed THF over land, annual cycle from winter solstice (Day 0) to winter solstice.

the maximum summer value, with period of 365 days (Figure 3-35). The summer solstice magnitude of THF_0 is varied from $125 W/m^2$ to $150 W/m^2$, as in the perpetual summer cases. Due to the unrealistic choice of ocean surface temperatures, the results are not expected to be suitable for study of the dynamics of monsoon onset. The model is first spun up in a winter solstice regime for 200 days, then the seasonal cycle is initiated, and the model is run for 5 annual periods. For all cases tested, the circulation and precipitation fields quickly adjusted to the seasonal cycle, and there was very strong interannual consistency. The last four years of the model run were averaged to create a mean annual progression.

During the winter season, the cold landmass yields a direct meridional circulation cell with ascent over the northern hemisphere tropical ocean and subsidence over the cold continent (Figure 3-36). The strong equatorward flow in the lower troposphere associated with this circulation increases surface fluxes over the warm tropical ocean and results in a strong precipitation maximum near 10N. A twin circulation cell with opposite flow develops between the equator and the precipitation maximum in the northern hemisphere.

For land forcing of $THF_0 \leq 130\, W/m^2$, the summer monsoon is weak, with a shallow capped meridional circulation over the subtropical continent (not shown). The precipitation maximum remains over the tropical ocean, with a peak at 10N, and although the continental subtropical precipitation is greatest during the summer months, the actual rainfall is slight (Figure 3-37). As the summer progresses, the boreal hemisphere upper level westerly jet (not shown) weakens, and a low-level easterly jet develops in balance with the poleward-increasing temperature gradient. Although the perpetual summer cases at these forcing

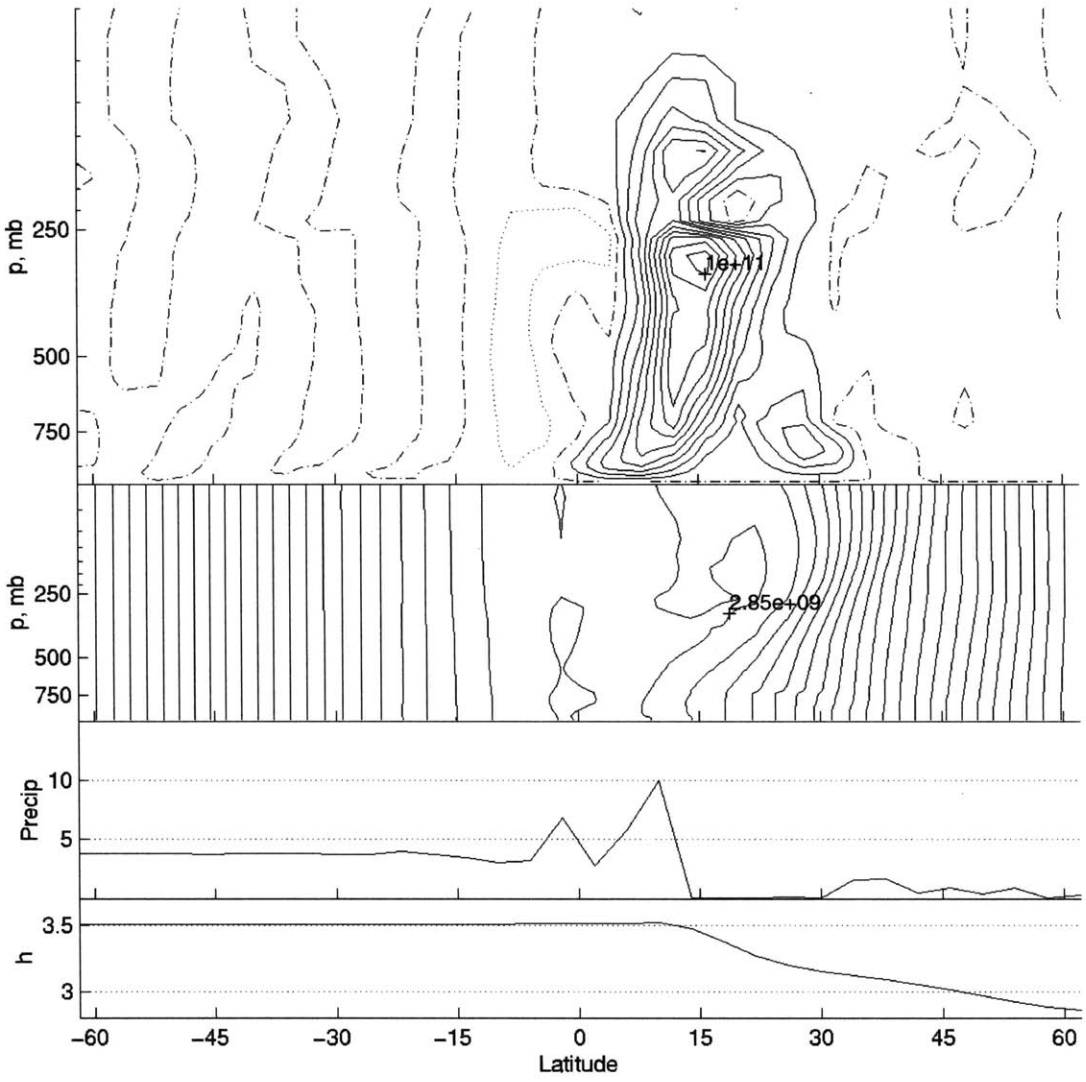

Figure 3-36: Seasonal case annual mean winter solstice state. Top, streamfunction, contour interval 1e10 kg/s, dotted lines indicate counter-clockwise flow, solid lines indicate clockwise flow, dash-dot is zero contour. Upper center, absolute angular momentum, contour interval 1E8 m^2/s. Lower center, precipitation, mm/day. Bottom, 1000 mb moist static energy, 10^5 J.

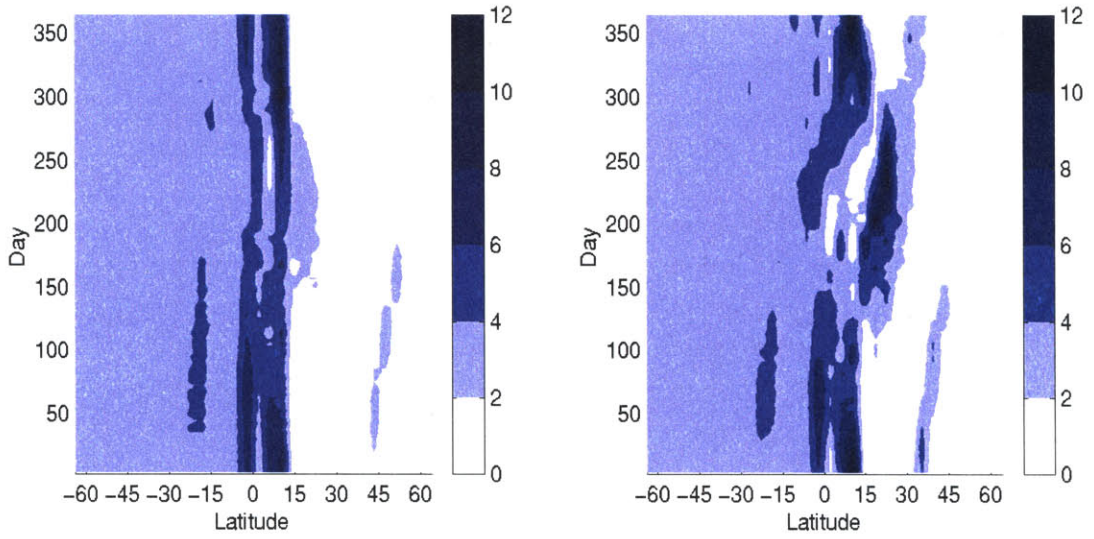

Figure 3-37: Seasonal case annual mean precipitation, contour interval 2mm/day. Left, $THF_0 = 130W/m^2$, right, $THF_0 = 150W/m^2$.

levels show deep convection and large scale ascent over the continent, such flow does not develop in the seasonal case.

For stronger land forcing ($THF_0 \geq 140W/m^2$), large-scale ascent and deep convection form over the subtropical continent during the summer. The precipitation maximum over the boreal tropical ocean at first weakens during spring, then shifts poleward onto the continent and intensifies during the course of the summer (Figure 3-37). At the beginning of fall, the continental precipitation maximum weakens abruptly, the rainfall peak then continues to migrate poleward during the winter until it dies out the following spring. During early summer (Figure 3-38), the meridional circulation features ascent over the subtropical continent and subsidence over the northern hemisphere tropical ocean, but has little cross-equatorial flow. As the summer progresses, the circulation strengthens and broadens, with increased cross-equatorial flow. By the late summer, the circulation is quite broad, and jumping behavior occurs, as seen in Figure 3-39. A new precipitation maximum develops just south of the equator in response to the ascent branch of the jump around day 200, then migrates slowly into the northern hemisphere and intensifies as the continental maximum diminishes at the end of summer (Figure 3-37).

The upper level easterly tropical jet strengthens over the course of the summer (not shown), in correspondence with the broadening and strengthening of the meridional circulation. A separate low-level easterly jet in thermal balance with the temperature gradient forms over the continental coastline, then strengthens and shifts poleward during the summer. The tendency of the monsoon to shift poleward with increased land surface forcing is

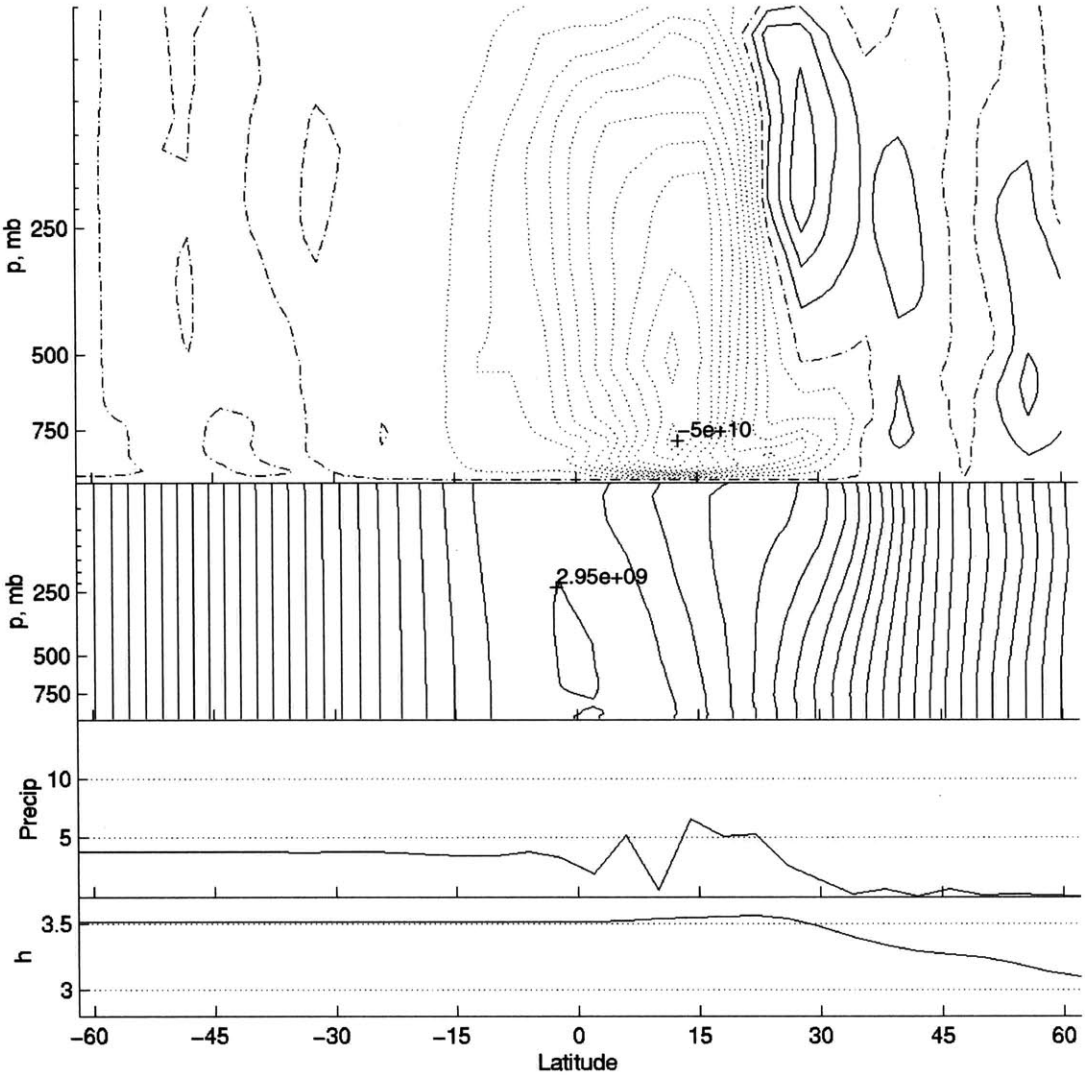

Figure 3-38: Seasonal case annual mean early summer state (one week before summer solstice), $THF_0 = 150W/m^2$. Top, streamfunction, contour interval 5e9 kg/s, dotted lines indicate counter-clockwise flow, solid lines indicate clockwise flow, dash-dot is zero contour. Upper center, absolute angular momentum, contour interval 1E8 m^2/s. Lower center, precipitation, mm/day. Bottom, 1000 moist static energy, 10^5 J.

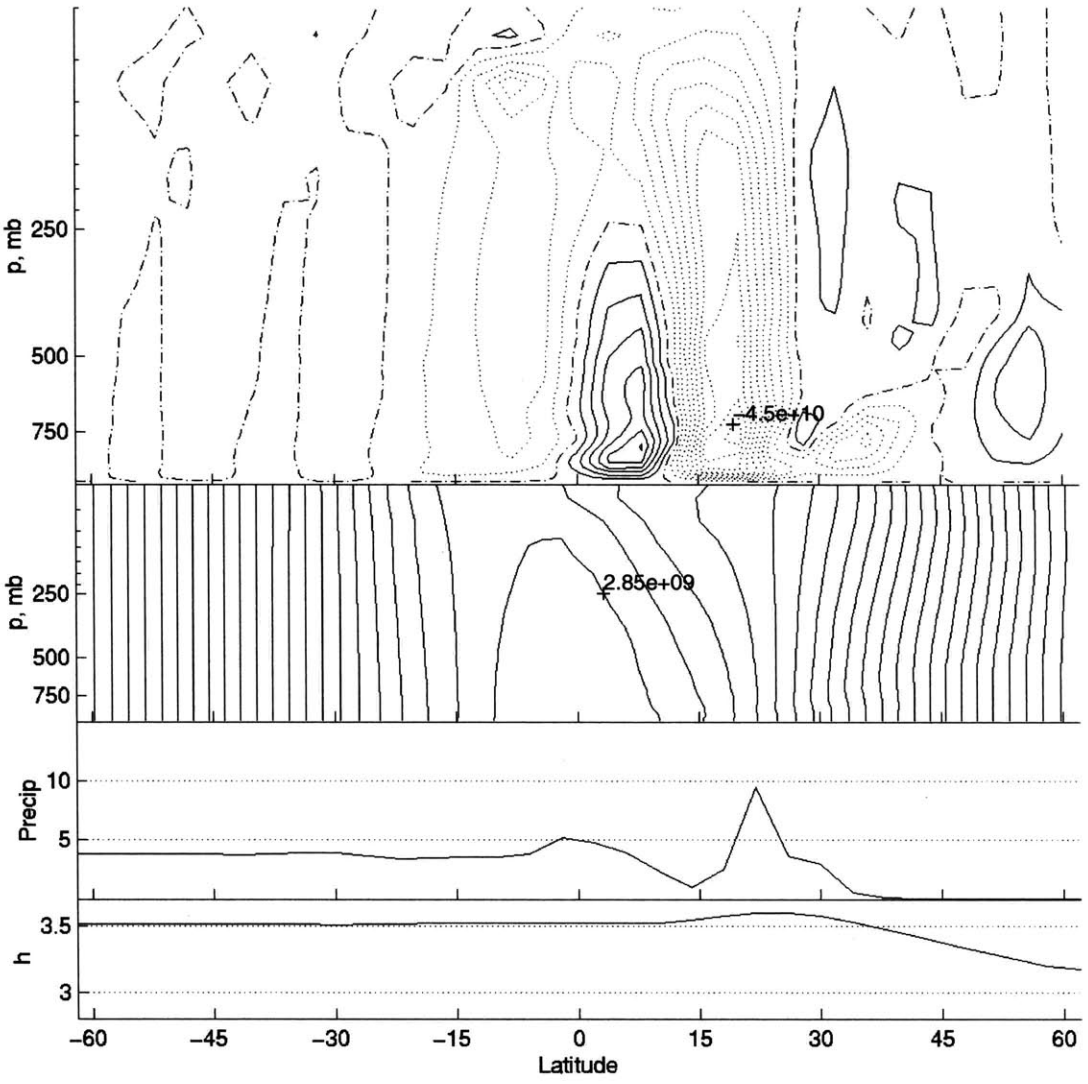

Figure 3-39: Seasonal case annual mean late August state, $THF_0 = 150W/m^2$. Top, streamfunction, contour interval 5e9 kg/s, dotted lines indicate counter-clockwise flow, solid lines indicate clockwise flow, dash-dot is zero contour. Upper center, absolute angular momentum, contour interval 1E8 m^2/s. Lower center, precipitation, mm/day. Bottom, 1000 moist static energy, 10^5 J.

seen in the seasonal cases as well as in the perpetual summer cases.

The seasonal cases show that the steady state solutions are pertinent to the seasonal monsoon during late summer only. Of course, the summer monsoon in each seasonal case is weaker than the monsoon seen in the perpetual summer case with the same solstice THF_0, as the average land forcing in the seasonal case is less than that in the perpetual summer case. The mean summer net surface flux between June 1 and August 31 in the seasonal case is approximately $10W/m^2$ less than the solstice THF_0. In the seasonal experiment, the $THF_0 \leq 130W/m^2$ cases have a mean summer $THF_0 < 125W/m^2$ and do not result in a monsoon, which is similar to the perpetual summer results for $THF_0 < 125W/m^2$.

In the early and mid-summer, the steady state solution differs considerably from the seasonal monsoon. The meridional circulation associated with the monsoon during early summer is localized in extent, confined to the boreal hemisphere. In mid June, the circulation becomes cross-equatorial and begins to fold over the contours of AAM in the upper troposphere (Figure 3-38). The jumping behavior which is a major feature of the steady state solutions is not observed until mid July in the seasonal cases.

Chapter 4

Three Dimensional Cases

A fully three-dimensional model framework is used to explore the applicability of the axisymmetric theory when eddies and longitudinal variations in forcing are introduced. Initially, a zonally symmetric continental geometry is used, with SSTs and land surface forcing applied uniformly in longitude. Eddies and longitudinal variation of the flow field and thermodynamic properties are permitted; the role of these eddies in the large-scale monsoon flow can be explored by comparing these model results to the results from the axisymmetric case. The zonal symmetry is then broken with a simple rectangular continent which is only 180° in longitude to examine the impact of asymmetrical forcing. The importance of continental geometry is further investigated with an Africa-Asia conglomerate landmass, and with an equatorially-centered continent. The roles of cross-equatorial flow and advection of moist entropy by the large-scale circulation are explored by the addition of a thin, impermeable wall to redirect the low-level flow.

The spinup procedure for these cases is the same as that used with the two dimensional cases: the model is run with weak land surface forcing for 200 days, then the forcing is increased to the 'summer' forcing maximum over a timescale of 100 days. As the three dimensional cases equilibrate faster than the two dimensional cases, shorter length runs may be used to capture the steady state solution. The model is run for a total of three hundred days after the maximum summer land forcing levels are applied, with longer runs used for individual cases if warranted.

4.1 Zonally Symmetric Continent

Geometric symmetry of the landmass and of the surface forcing is retained while allowing longitudinal variations in the state of the atmosphere in order to isolate the effects of horizontal eddies. For example, Xie and Saiki (1999) found that baroclinic eddies played a strong role in onset of the monsoon in their model by initiating precipitation over the

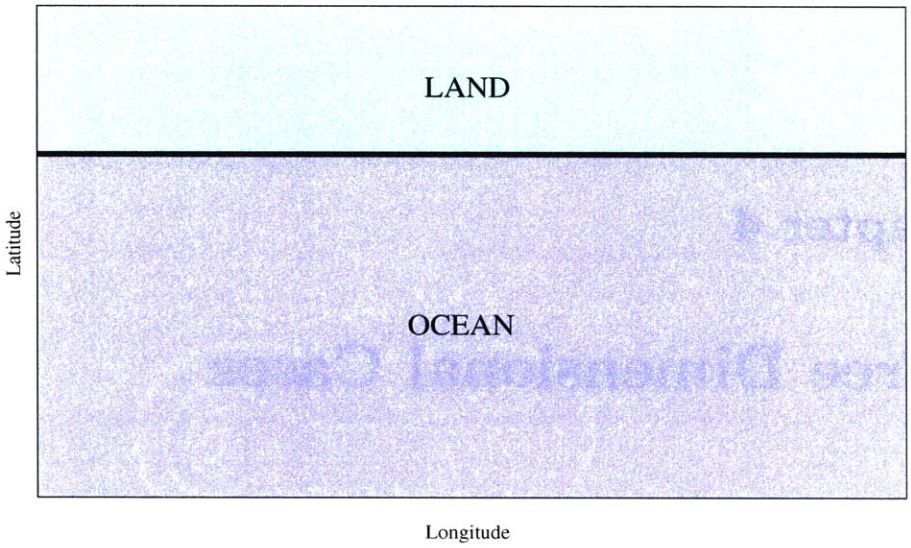

Figure 4-1: Diagram illustrating the model setup with zonally symmetric continent.

previously arid landmass. The purpose of these experiments is to explore how eddies affect the monsoon circulation by altering fluxes of momentum, moisture, and other properties, and also to determine whether the monsoon is self-organizing into longitudinally localized structures.

The continent is 360° in longitudinal width, extending from the coastline at ϕ_L northward to the model boundary at 64N (Figure 4-1). South of the coastline, the ocean SST is function of latitude only. The land surface forcing is given by

$$THF(\phi) = LHF(T_s(\lambda, \phi)) + SHF(T_s(\lambda, \phi)) \tag{4.1}$$

where λ is the longitude, and $THF(\phi)$ is assigned according to (3.7). The surface temperature on land and the sensible and latent heat fluxes are allowed to vary with longitude, but the continental total surface heat flux is a function only of latitude.

4.1.1 Uniform Ocean SSTs

For comparison with the two dimensional cases (§3.2.2), a uniformly warm ocean is implemented with SST of 302K at all ocean latitudes. The continental coastline is located at $\phi_L = 16$N. A range of land surface forcing strength is tested, as in the two dimensional cases.

Three different dynamical regimes occur, depending upon the strength of the land forcing: non-monsoonal flow for very weak forcing, a local, weak monsoon for intermediate forcing, and a vigorous global monsoon for strong forcing. The transition from non-monsoonal

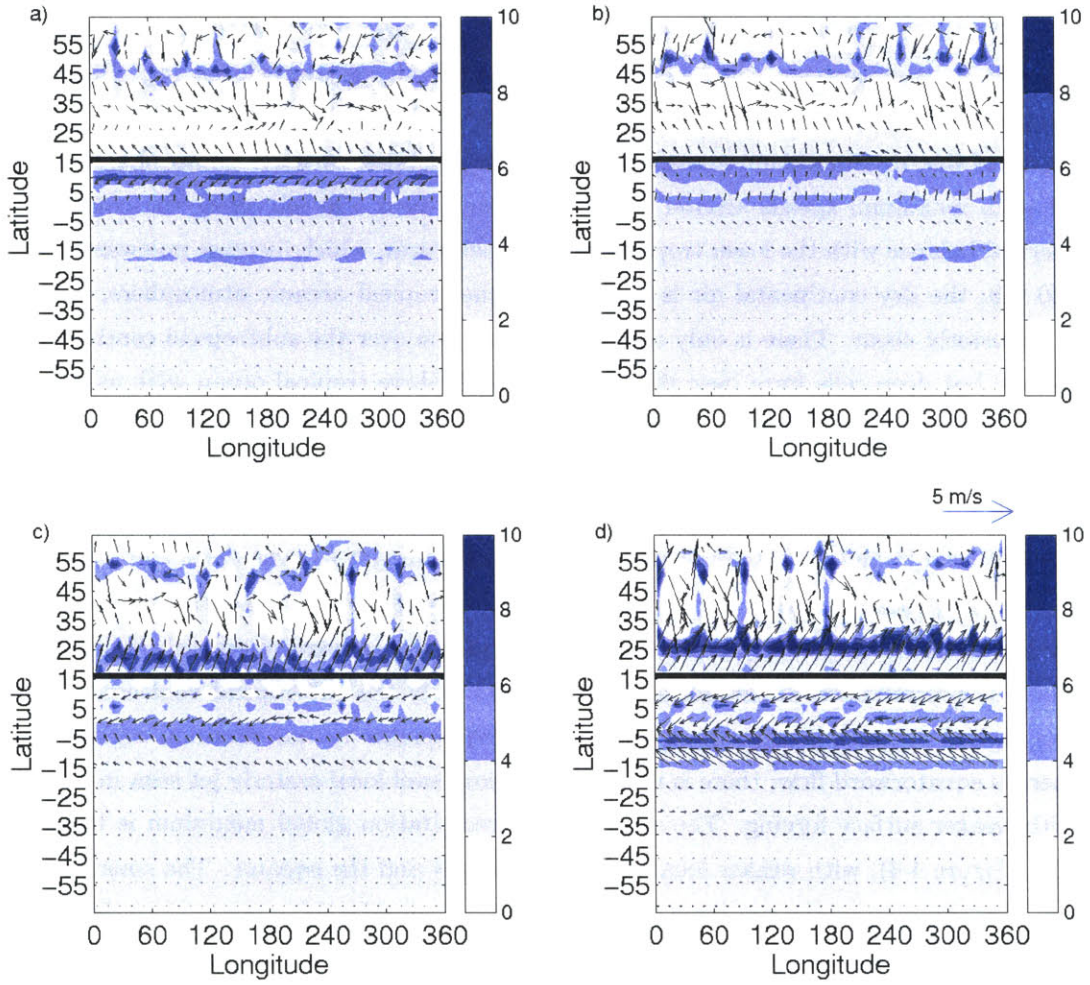

Figure 4-2: 1000 mb wind and precipitation, 360° continent and uniform SST distribution. 100 day time mean. Contour interval 2 mm/day. a) $THF_0 = 125\,W/m^2$; b) $THF_0 = 130\,W/m^2$; c) $THF_0 = 140\,W/m^2$; d) $THF_0 = 150\,W/m^2$.

to weak monsoon occurs for land forcing of $THF_0 = 135\,W/m^2$; in comparison, the axisymmetric case developed a weak monsoon for forcing of $THF_0 = 125\,W/m^2$. The transition to global monsoon occurs for forcing of $THF_0 = 140W/m^2$ in the three dimensional case, but at $THF_0 = 135W/m^2$ in the axisymmetric case.

In the three dimensional non-monsoonal cases, the maximum precipitation remains over the tropical ocean, with only light precipitation along the immediate coastline (Figures 4-2, 4-3). A local precipitation peak is located over the midlatitude continent, associated with baroclinic disturbances of the westerly jet. The midlatitude westerly jet (eg. Figure 4-3) is considerably weaker in the three dimensional cases than in the two dimensional cases, as expected due to momentum transport by horizontal eddies. A lower tropospheric easterly jet with maximum speeds around $5\,m/s$ is centered near 700 mb along the coastline, in thermal balance with the lower tropospheric temperatures, which increase poleward. Above 700 mb, the dry continental air is cooler than the tropical oceanic atmosphere, resulting in a westerly shear. There is only a shallow circulation over the subtropical continent; two narrow but deep cells form over the northern hemisphere tropical ocean with ascent near 10N. These deep cells form in response to the local maximum in oceanic surface fluxes, the fluxes in turn are affected by the presence of relatively strong local surface winds. In the $THF_0 = 125, 130W/m^2$ cases, the zonal mean subcloud moist static energy decreases precipitously inland from the coastline, with nearly constant h_b over the warm ocean.

A weak, local monsoon occurs for land forcing of $THF_0 = 135\,W/m^2$, with a weak, narrow meridional circulation cell confined to the summer hemisphere only (Figure 4-4). There is precipitation maximum and deep ascent over the subtropical continent. Upper tropospheric easterlies (not shown) exist from the equator to the monsoon region, where there is equatorward flow; there is no sign of the low level local easterly jet seen in the cases with weaker surface forcing. The zonal mean precipitation global maximum is located at 18N (Figure 4-4), with weaker local maxima near 50N and the equator. The zonal mean h_b has a maximum over the continent near 26N which is considerably greater than the tropical oceanic h_b. A corresponding upper tropospheric maximum in θ_v (not shown) is located in this region; in the lower troposphere, the maximum absolute temperatures occur poleward of the monsoon near 32N, where an arid land surface results in strong sensible heat fluxes.

Precipitation is widespread along the coastline (Figure 4-5), with some local regions of heavier rainfall which are generally stationary but also show eastward propagation. A contrasting set of model experiments are performed (not shown) one in which the bucket hydrology is set to be completely arid, and one in which the buckets are saturated. In these two cases with prescribed bucket moisture content, long-lived, stationary precipitation maxima are not observed. Feedbacks between the surface hydrology and the precipitation with interactive bucket moisture content act to reinforce precipitation in region of intense

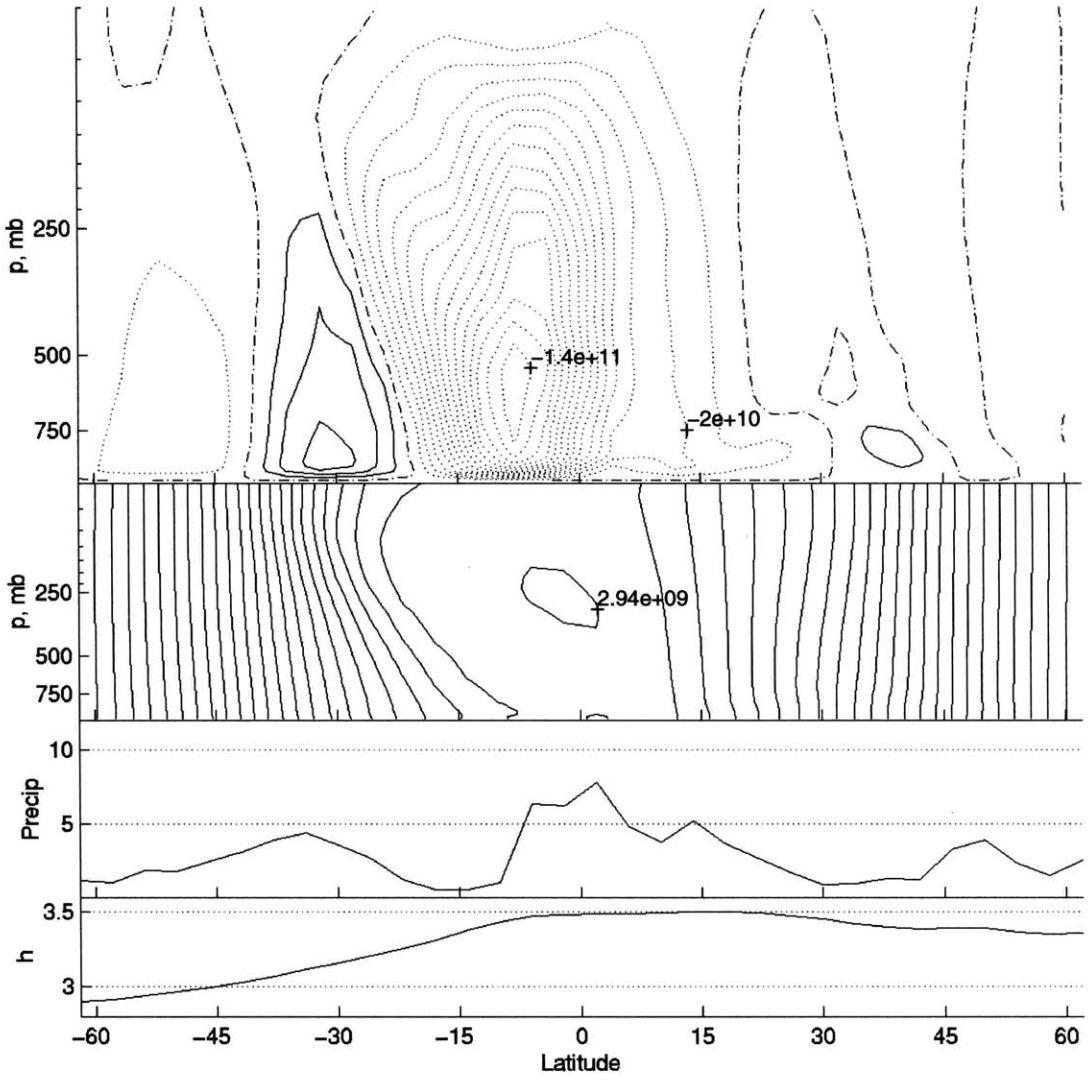

Figure 4-3: Zonally symmetric continent, coastline at 16N, $THF_0 = 130\,W/m^2$, zonal mean fields, 100 day time mean. Top, streamfunction, contour interval 5e9 kg/s, dotted lines indicate counter-clockwise flow, solid lines indicate clockwise flow, dash-dot is zero contour. Upper center, zonal wind, contour interval 5 m/s, dotted line indicates easterlies, solid lines indicate westerlies. Lower center, precipitation, mm/day. Bottom, 1000 mb moist static energy, $10^5\,J$.

precipitation, so that strong rainfall may persist in a local region for an extended period. The eastward propagating signals seen in Figure 4-5, which are particularly noticeable during the onset of the monsoon, are associated with the instability of the midlatitude westerly jet. This jet is strongest during ramp-up of the land forcing (the first 100 days of Figure 4-5), but weakens after monsoon onset.

A strong, global monsoon occurs for $THF_0 \geq 140\,W/m^2$, with intense precipitation over the subtropical continent; an example is seen in Figure 4-7. With increasing surface forcing the strength of the cross-equatorial circulation cell increases and the monsoon region moves poleward, as in the two dimensional cases (Figure 4-6). The meridional circulation shows the same tendency to jump at the equator (eg. Figure 4-7) as in the two dimensional cases, with a double or triple peaked precipitation region near the equator. A strong upper tropospheric easterly jet (not shown) is centered at the equator, with easterlies ranging from the monsoon region to the southern hemisphere subtropics. The upper branch of the circulation crosses more contours of angular momentum than in the axisymmetric cases, but there is still considerable distortion of the angular momentum field by the flow. The zonal mean subcloud h has a strong maximum over the subtropical continent, which increases in magnitude and shifts poleward with increased surface forcing.

The net effect of eddies appears to be a weakening of the monsoon in comparison to the two dimensional cases: stronger land surface forcing is needed to induce a global mean monsoon in the three dimensional cases. Although there is significant wave generation over the midlatitude continent, in the subtropics the waves are very weak, with little signature in the Eliassen-Palm (EP) flux (not shown). The precipitation field over land is nearly zonally uniform in a long term time mean, and although there are localized regions of strong and weak precipitation at any specific time, there is no tendency toward organization into large scale structures. A low-level easterly jet is present in the weaker land forcing cases and meets the necessary criterion for baroclinic instability, but this jet does not generate waves. The tropical waves which are present in the equatorial region do not appear to strongly influence flow over the continent.

The circulation strength as a function of the land forcing is illustrated by the dotted line in Figure 4-8. There is little indication of threshold behavior of the circulation, which is not unexpected given the results of the axisymmetric cases (Figure 3-22). However, the meridional circulation is not as conservative of angular momentum when eddies are included, as indicated by the upper tropospheric absolute vorticity which does not closely approach zero even in the for a global circulation (Figure 4-8).

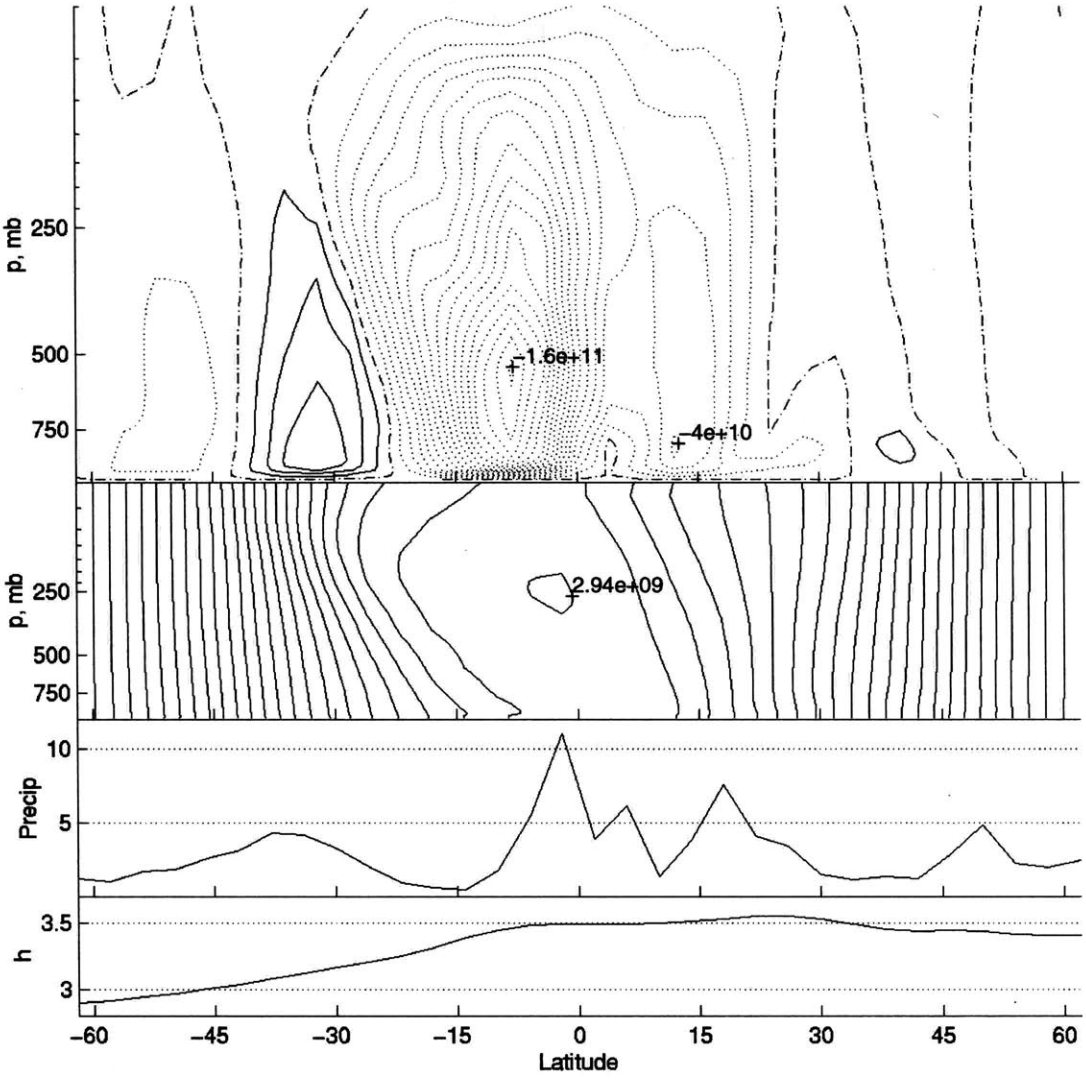

Figure 4-4: Zonally symmetric continent, coastline at 16N, $THF_0 = 135W/m^2$, zonal mean fields, 100 day time mean. Top, streamfunction, contour interval 5e9 kg/s, dotted lines indicate counter-clockwise flow, solid lines indicate clockwise flow, dash-dot is zero contour. Upper center, absolute angular momentum, 1E8 m^2/s. Lower center, precipitation, mm/day. Bottom, 1000 mb moist static energy, $10^5 J$.

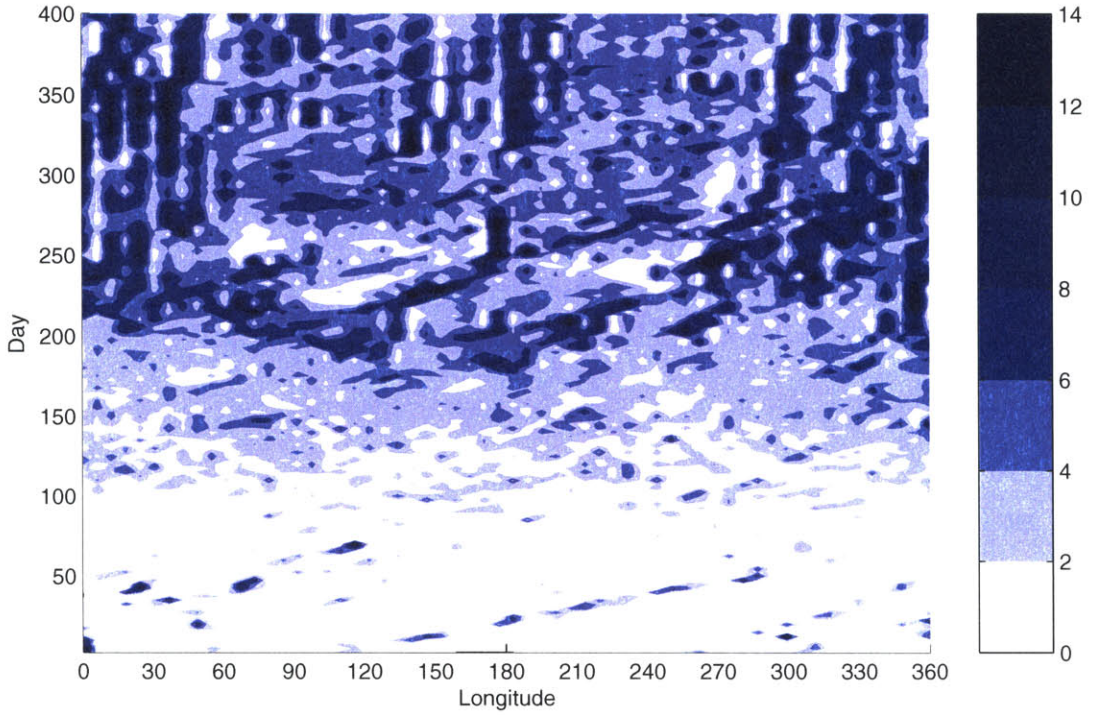

Figure 4-5: Zonally symmetric continent with uniform SST, coastline at 16N, $THF_0 = 135 W/m^2$, Hovmoeller diagram of precipitation at 18N, beginning at time of initial ramp-up of land forcing. Maximum land forcing reached at day 100.

4.1.2 'Summer' SSTs

A more realistic ocean SST distribution is added, with temperature given by (3.8), while retaining zonal symmetry of the land surface. These cases may be compared to the axisymmetric cases of §3.2.3. In general, the zonal mean circulation of the continental cases with this summer-like SST profile has the visual appearance of a superposition of the aquaplanet circulation from Figure 2-7 and the circulation attained in the cases with uniform ocean temperature, §3.2.2. However, there are several interesting differences between these summer cases and the uniform ocean results. Unlike the cases from §4.1.1, a cross-equatorial meridional circulation will occur in response to the ocean SST distribution, regardless of the applied land forcing; this prevents the weak and global monsoon regimes from being distinct.

The zonal mean circulation is non-monsoonal for $THF_0 \leq 125\, W/m^2$, with little precipitation over the subtropical continent. The ITCZ is located over the tropical ocean with multiple precipitation peaks near the equator and 10N (Figure 4-9). A strong, cross equatorial circulation (Figure 4-10) associated with the ocean SST gradient is completely disconnected from the shallow local circulation over the subtropical continent. Although

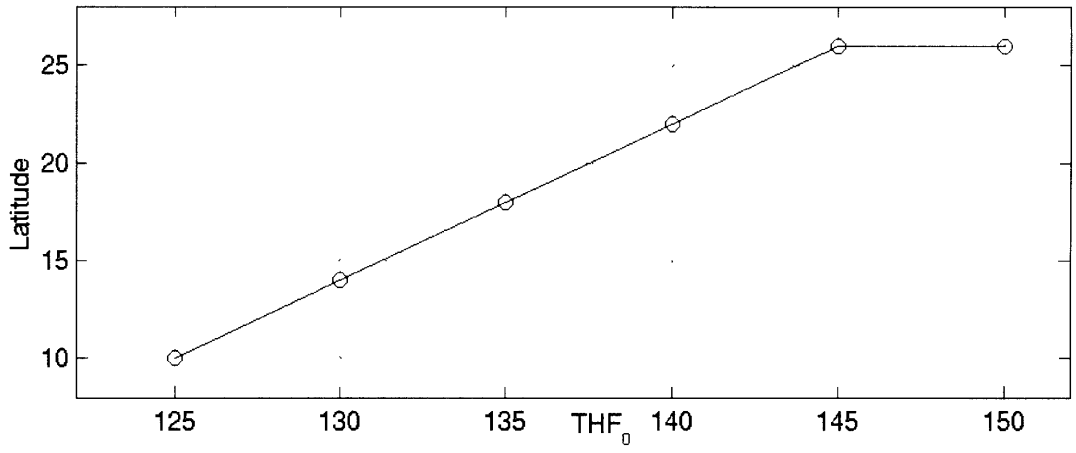

Figure 4-6: Location of maximum monsoon precipitation in 3D cases with uniform ocean SST as a function of continental surface forcing THF_0, W/m^2.

there is a low-level easterly jet along the coastline near 700 mb, this jet does not generate waves.

The case with $THF_0 = 130W/m^2$ differs from the corresponding case in §4.1.1 in two important ways. First, the zonal mean circulation shows weak but deep ascent over the coastal continent, with this ascending branch connected to the cross-equatorial circulation cell over the ocean (Figure 4-11). The zonal mean precipitation field has maxima near the equator and at 14N, with considerable rainfall over the continent at the immediate coastline. In comparison, the uniform ocean case did not feature deep zonal mean ascent over the coastal region. The results are closer to the two dimensional circulation with summer SST (§3.2.2) for this case. The zonal mean subcloud moist static energy is nearly flat across the entire tropical region, from the equator to the coastline; poleward of the coastline, h_b decreases inland. According to the theory of §3.3, the boundary of the meridional circulation may occur anywhere in the region of flat h_b. In fact, the circulation boundary occurs at the poleward-most edge of the flat h_b region, slightly inland of the coastline, while the maximum precipitation occurs equatorward of the coastline, in agreement with the theory.

The second difference is the development of a strong and persistent westward propagating wave disturbance over the subtropical continent in the case with summer-like ocean (Figure 4-12). After an initial period of weak, sporadic rainfall following ramp-up of the surface forcing, a strong localized disturbance emerges along the coastline approximately 150 days after full strength summer land forcing has been established. The anomaly shows strong cyclonic flow in the lower troposphere around a surface low with enhanced precipitation in the region of southwesterlies on the east side of the anomaly, and arid conditions on the west side (Figure 4-13). The disturbance is approximately 60° in longitudinal extent

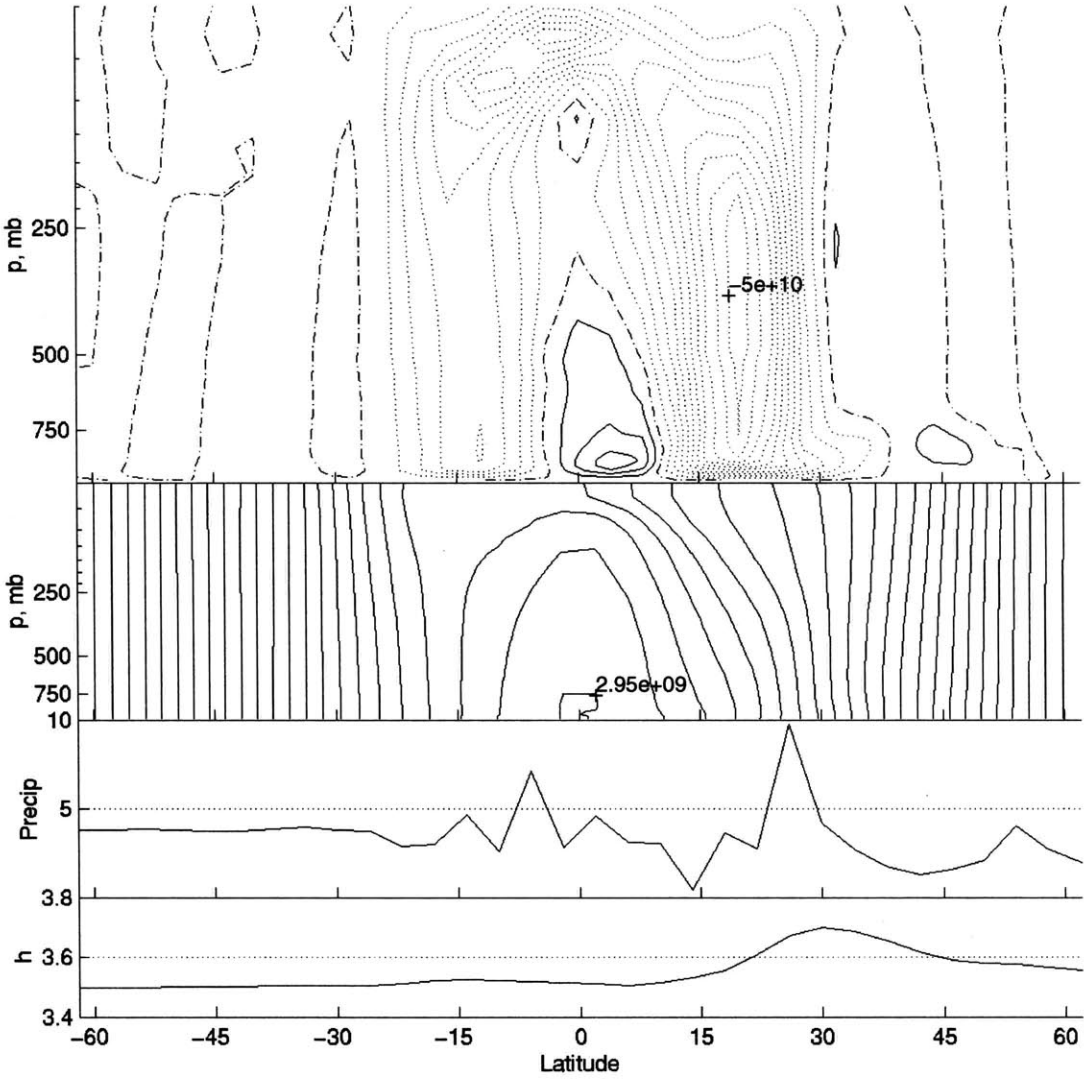

Figure 4-7: Zonally symmetric continent with uniform SST, coastline at 16N, $THF_0 = 150\,W/m^2$, zonal mean fields, 100 day time mean. Top, streamfunction, contour interval 5e9 kg/s, dotted lines indicate counter-clockwise flow, solid lines indicate clockwise flow, dash-dot is zero contour. Upper center, absolute angular momentum, contour interval 1e8 m^2/s. Lower center, precipitation, mm/day. Bottom, 1000 mb moist static energy, $10^5 J$.

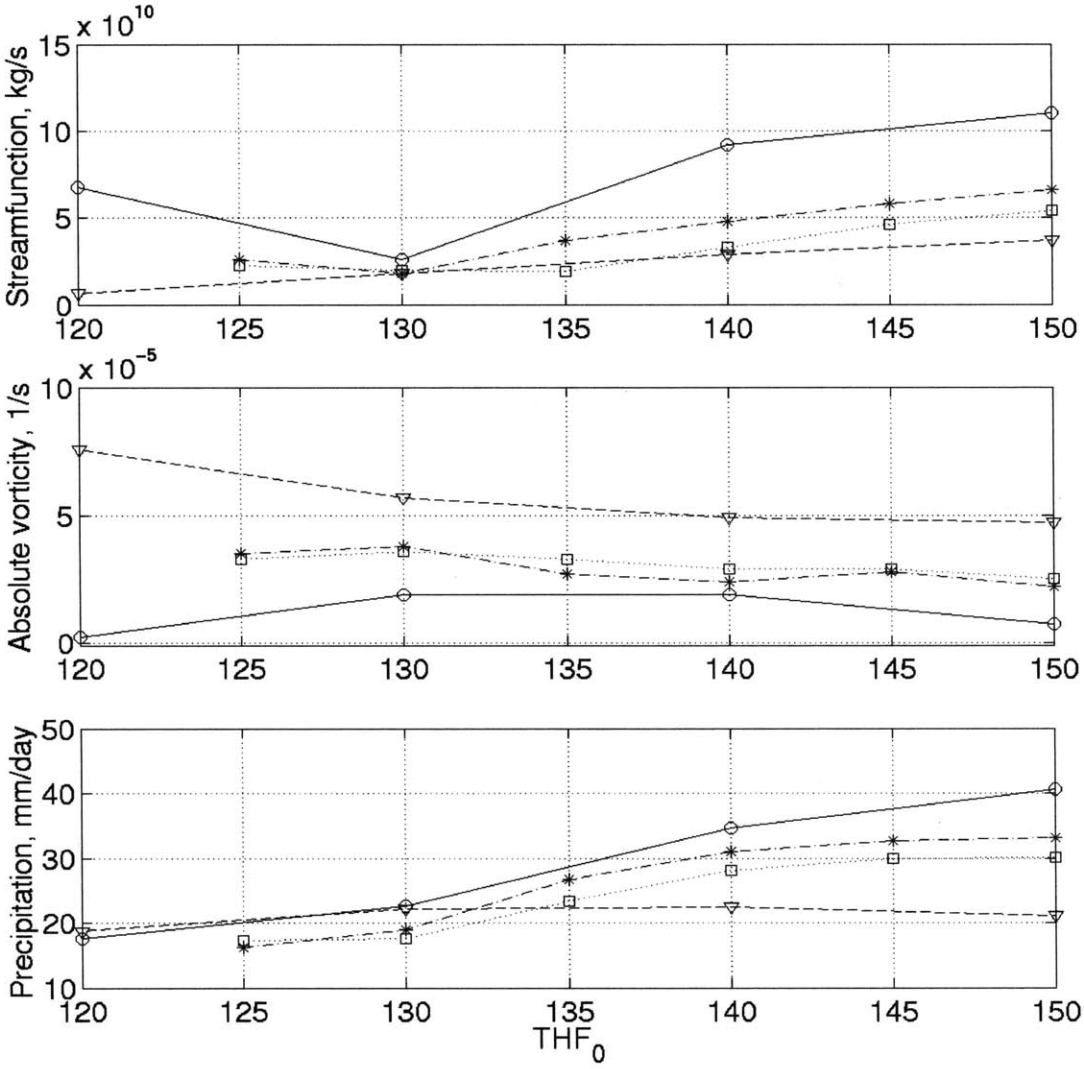

Figure 4-8: Steady-state zonal mean results for continental cases in 3D as a function of THF_0 (W/m^2). Uniform SST with ϕ_L = 16N, dotted line with squares; "summer" SST with ϕ_L = 8N, solid line with circles; "summer" SST with ϕ_L = 16N, dot-dash line with asterisks; "summer" SST with ϕ_L = 24N, dotted line with triangles. a) maximum "winter" circulation streamfunction strength, kg/s. b) minimum 150 mb absolute vorticity (s^{-1}) over continent c) net continental precipitation in equivalent units of rainfall at the equator, mm/day

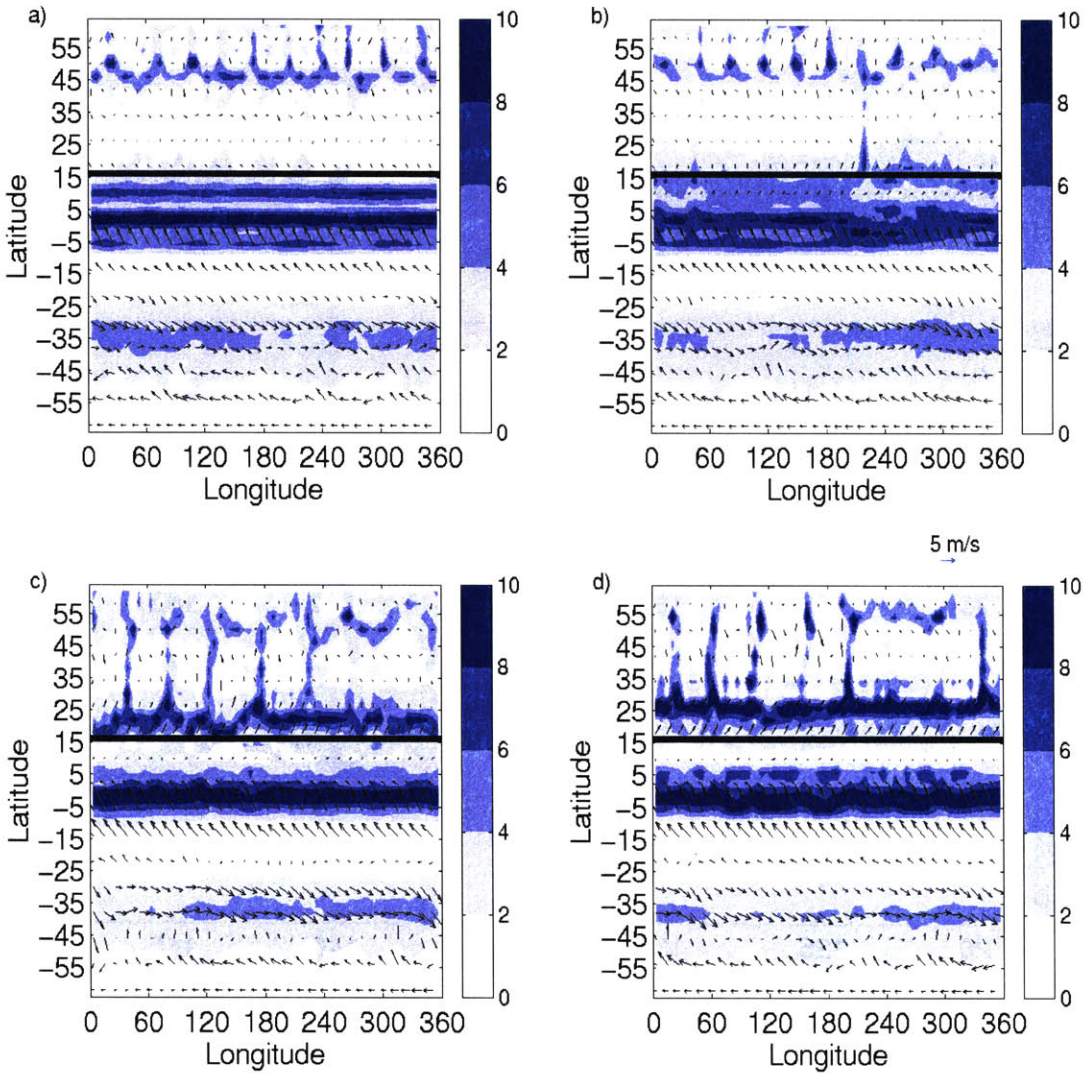

Figure 4-9: 1000 mb wind and precipitation, 360° continent and summer SST distribution. Contour interval 2 mm/day. a) $THF_0 = 125\,W/m^2$; b) $THF_0 = 130\,W/m^2$; c) $THF_0 = 140\,W/m^2$; d) $THF_0 = 150\,W/m^2$.

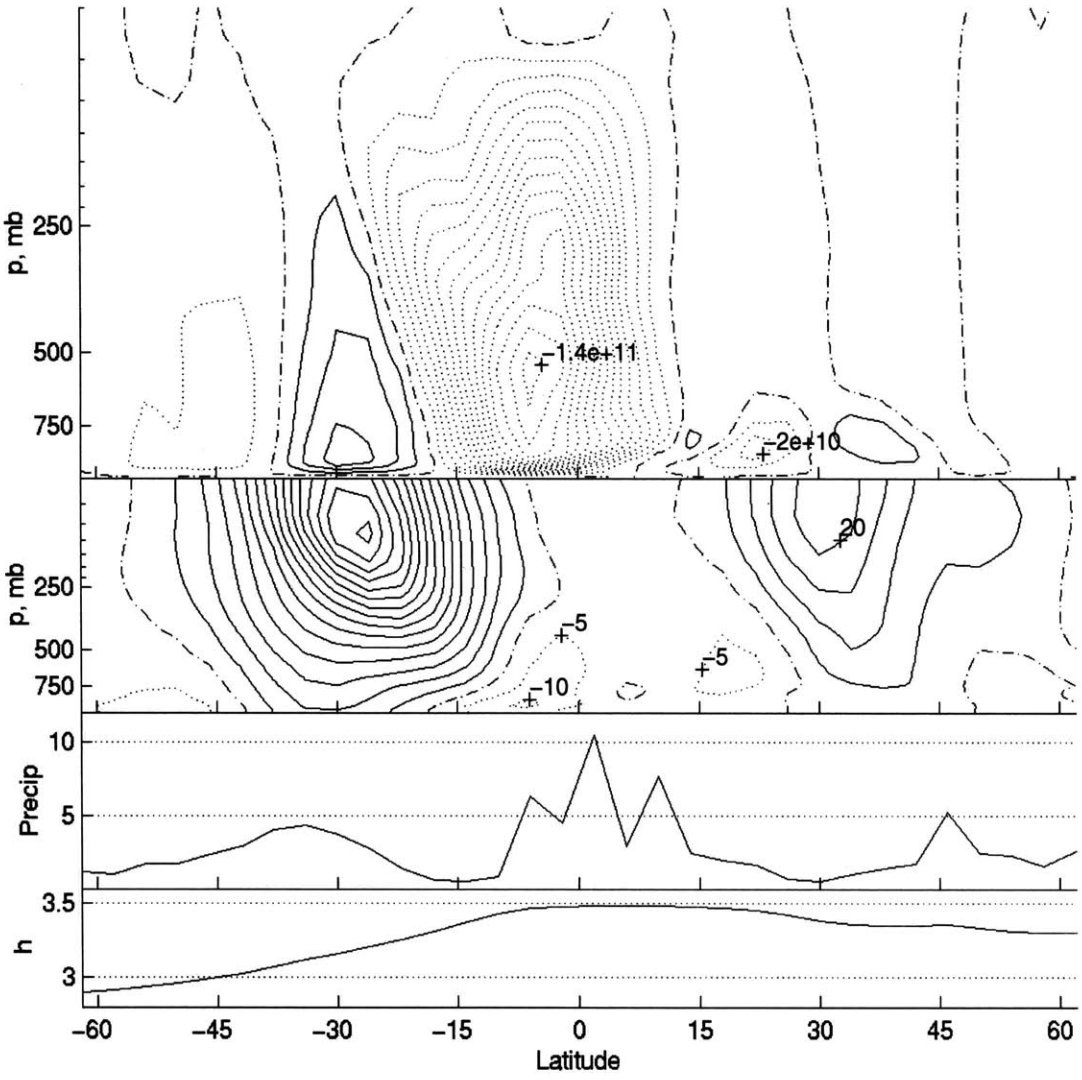

Figure 4-10: Zonally symmetric continent, coastline at 16N, $THF_0 = 125W/m^2$, summer-like SSTs; zonal mean fields, 100 day time mean. Top, streamfunction, contour interval 1e10 kg/s, dotted lines indicate counter-clockwise flow, solid lines indicate clockwise flow, dash-dot is zero contour. Upper center, zonal wind, contour interval 5 m/s, dotted line indicates easterlies, solid lines indicate westerlies. Lower center, precipitation, mm/day. Bottom, 1000 mb moist static energy, $10^5 J$.

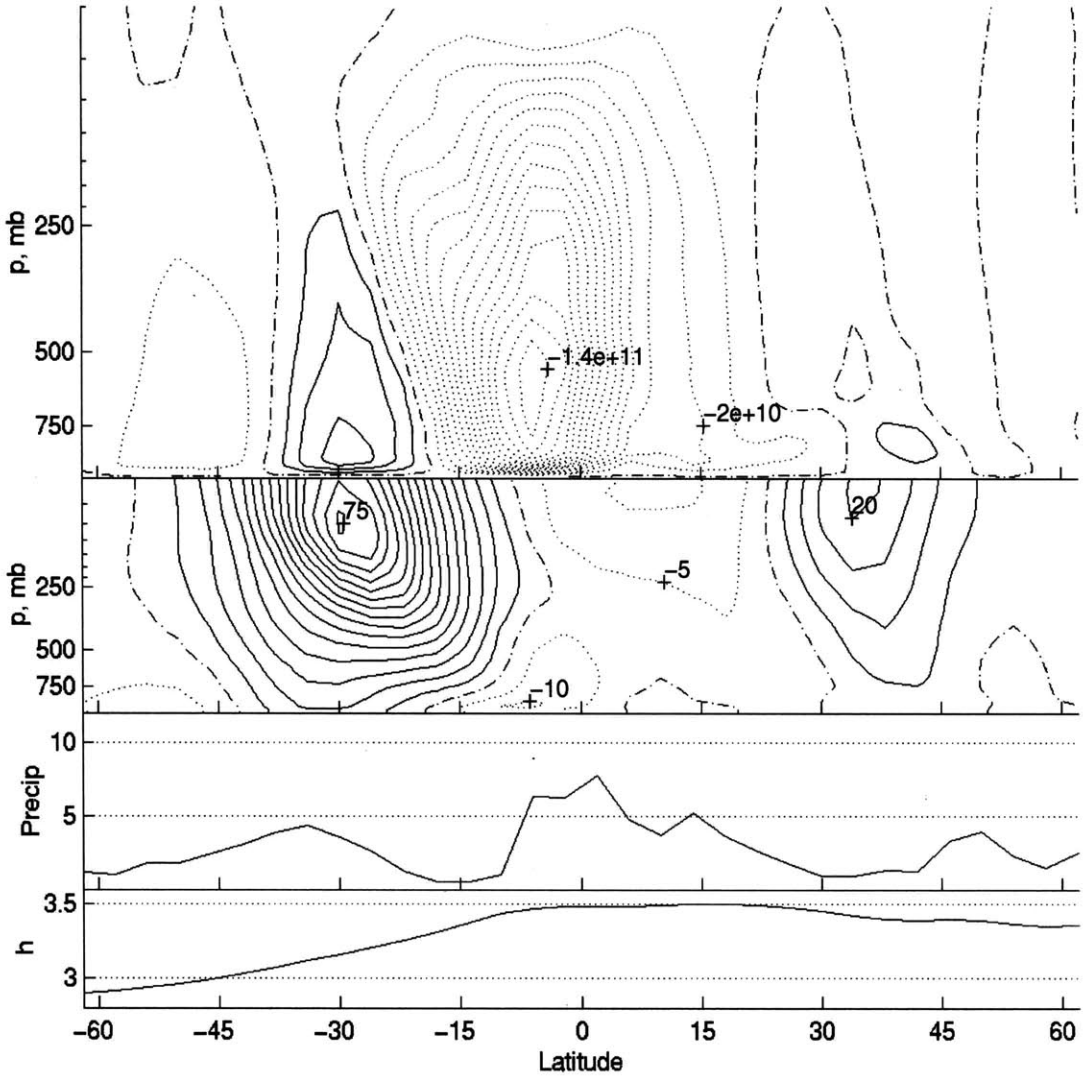

Figure 4-11: Zonally symmetric continent, coastline at 16N, $THF_0 = 130W/m^2$, summer-like SSTs; zonal mean fields, 100 day time mean. Top, streamfunction, contour interval 1e10 kg/s, dotted lines indicate counter-clockwise flow, solid lines indicate clockwise flow, dash-dot is zero contour. Upper center, absolute angular momentum, contour interval 1E8 m^2/s. Lower center, precipitation, mm/day. Bottom, 1000 mb moist static energy, $10^5 J$.

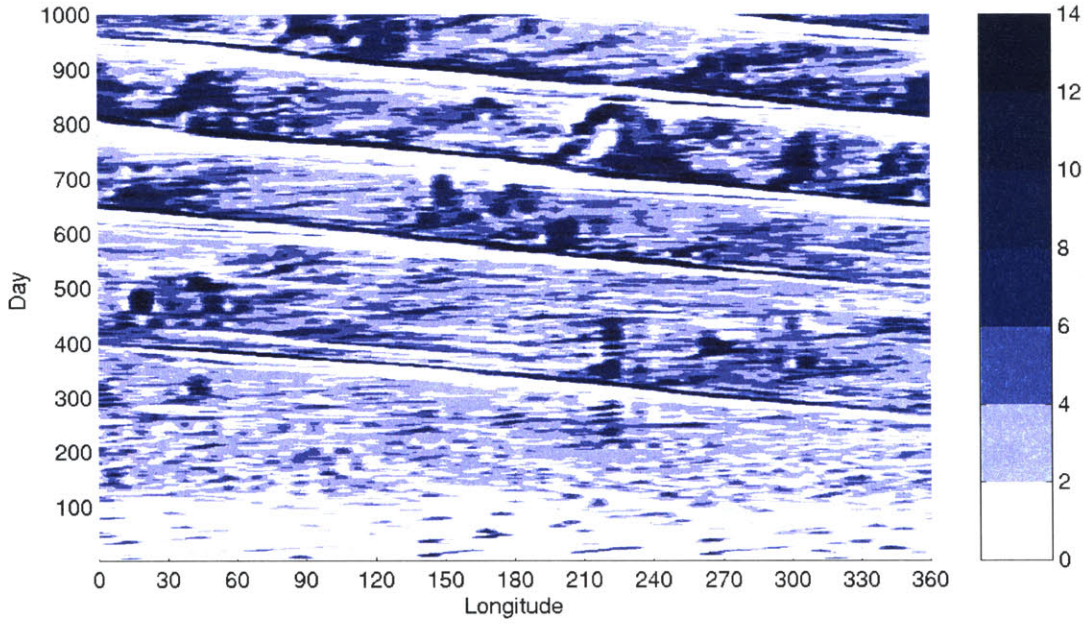

Figure 4-12: Zonally symmetric continent, coastline at 16N, $THF_0 = 130\,W/m^2$, Hovmoeller diagram of precipitation at 18N, beginning at time of initial ramp-up of land forcing. Maximum land forcing reached at day 100.

and 30° in meridional extent, and moves westward with a speed of 3.25 m/s, persisting for at least 450 days. The anomaly is warm-core at all levels (Figure 4-14), with ascent in the lower troposphere colocated with the positive eddy temperature and poleward flow. There is ascent on the eastern side of the disturbance, with subsidence to the west; the ω field tilts eastward with height from the surface to 750 mb, with little tilt above 750 mb. The meridional wind field also tilts eastward with height from the surface to 750 mb; this direction of tilt is seen in baroclinic waves in a region of easterly shear (Thorncroft and Hoskins, 1994), such a region is seen along the coastline below 750 mb. The change in tilt of the meridional wind and ω at 750 mb occurs where the vertical shear changes from easterly below to weakly westerly above. The Eliassen-Palm flux signature is also indicative of a baroclinic wave structure, with downward flux originating near the cores of the easterly jet (not shown).

For stronger surface forcing ($THF_0 \geq 135\,W/m^2$), there is a strong precipitation peak over the continent (Figure 4-16); this peak shifts poleward with increased forcing. Over the ocean, there is another precipitation maximum near 2S, with moderate, widespread precipitation throughout the tropics (Figure 4-9). Deep ascent is located over the subtropical continent and just south of the equator, with a global cross-equatorial meridional circulation (Figure 4-16). Jumping of the circulation occurs for all cases, and becomes more

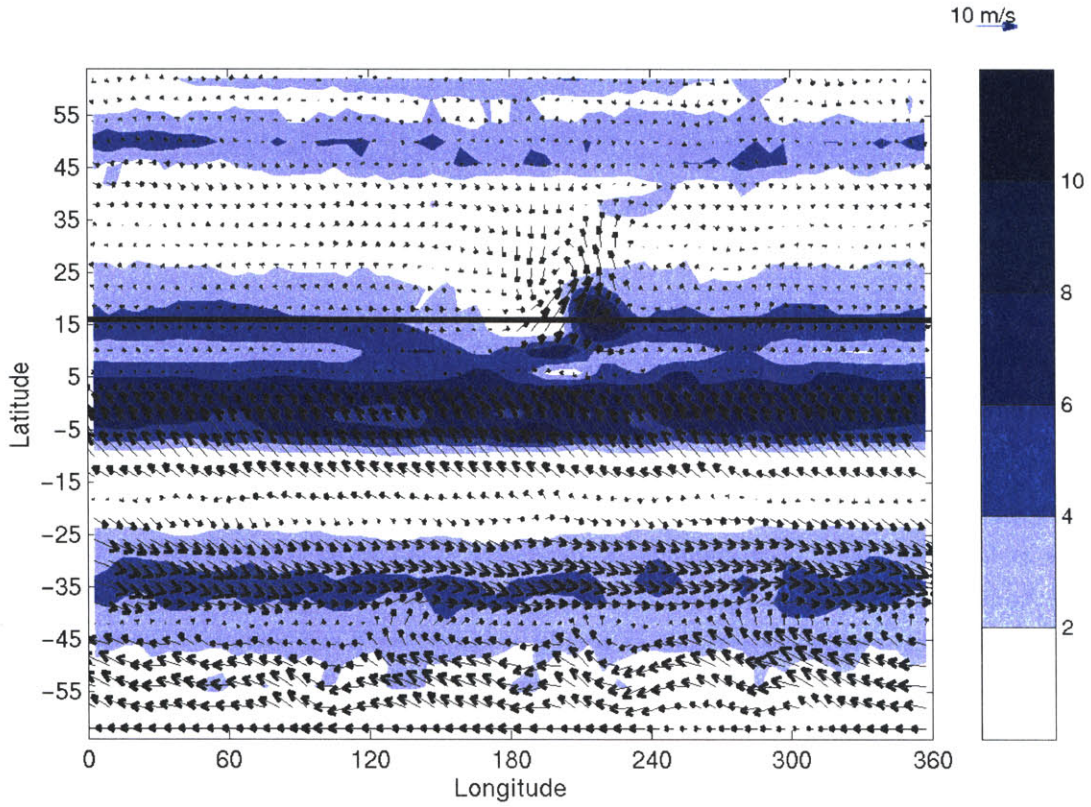

Figure 4-13: Zonally symmetric continent, coastline at 16N, $THF_0 = 130\,W/m^2$, Composite of 1000 mb winds and precipitation, 3.25 m/s westward, mean days 327.5 to 387.5. Precipitation in mm/day.

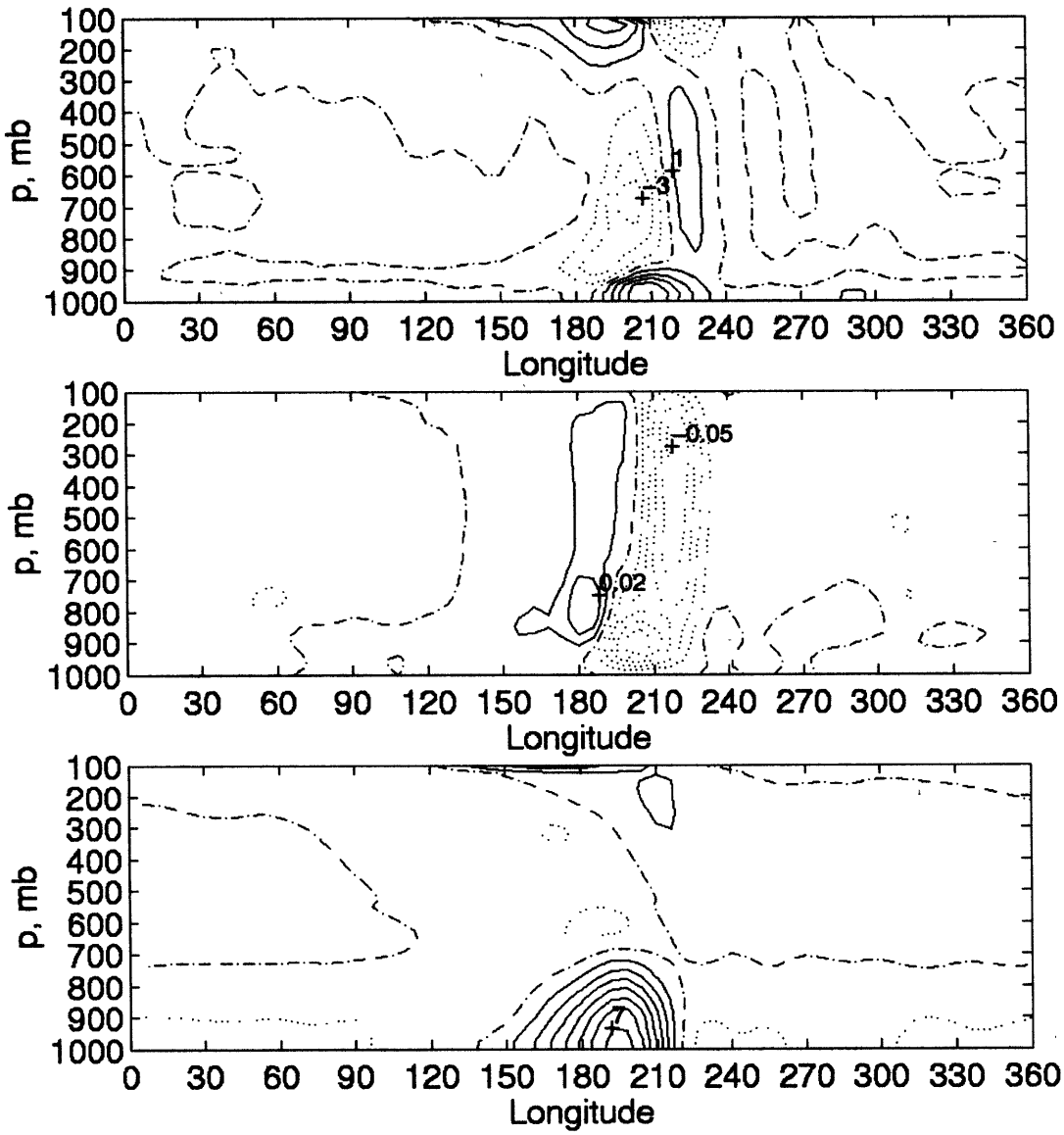

Figure 4-14: Zonally symmetric continent, coastline at 16N, $THF_0 = 130\,W/m^2$, Composite of fields on slice at 18N, 3.25 m/s westward, mean days 327.5 to 387.5. Top, meridional wind, contour interval 1.0 m/s; center, ω, contour interval 0.1 Pa/s; bottom, eddy temperature, contour interval 1K. Dotted contours indicate negative values.

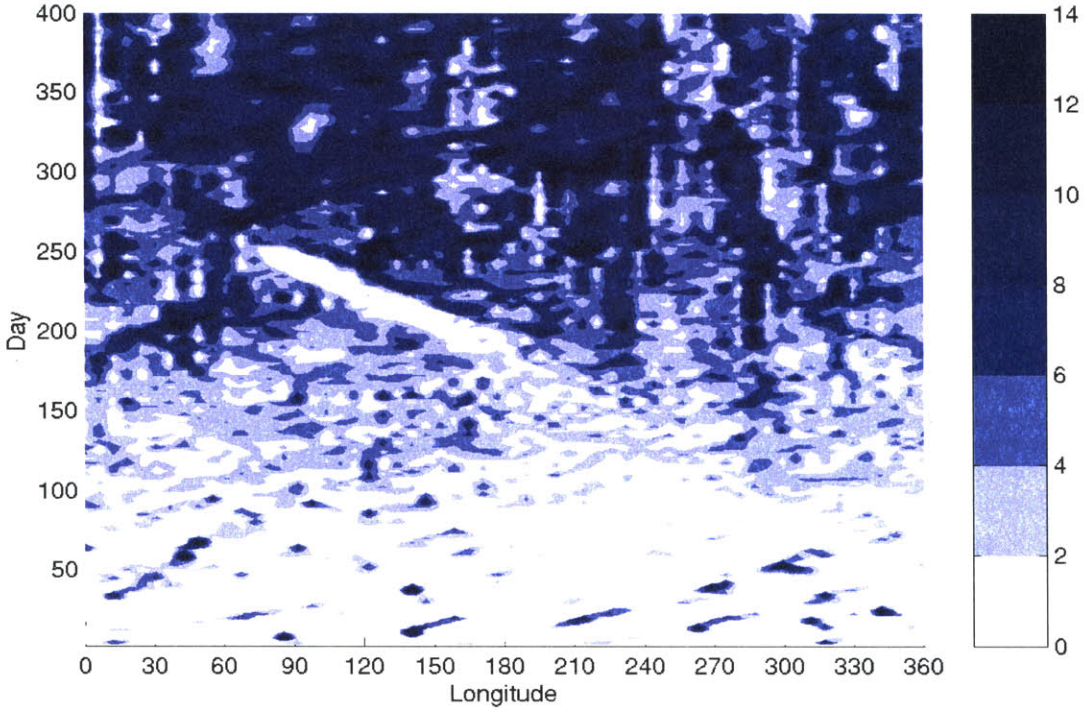

Figure 4-15: Zonally symmetric continent, coastline at 16N, $THF_0 = 135\,W/m^2$, Hovmoeller diagram of precipitation at 18N, beginning at time of initial ramp-up of land forcing. Maximum land forcing reached at day 100.

exaggerated as the land forcing is increased. There are some regions of localized intense precipitation over the continent (Figure 4-15), some of these features remain stationary, while other propagate westward; however, the westward propagating waves are much shorter lived than in the $THF_0 = 130\,W/m^2$ case (Figure 4-12).

4.1.3 8N coastline

As in the two dimensional setup, a series of cases with coastline $\phi_L = 8N$ are performed. The surface forcing is also shifted, and is given by (3.7) with $\phi_T = 0N$; the ocean SST maximum remains at $\phi_0 = 8N$. This relocation of the coastline impacts the large-scale circulation in several ways: first, the close proximity of the heated continent to the equator increases the large-scale boundary layer pressure gradient across the equator; second, the low-level easterly jet along the coastline increases in strength as the Coriolis parameter f decreases due to thermal wind balance; third, a weaker forcing is needed to induce a global circulation near the equator according to the axisymmetric theory of Plumb and Hou (1992); and fourth, the maximum ocean SST is adjacent to the coastline.

For the non-monsoonal cases, $THF_0 \leq 125\,W/m^2$, the meridional circulation over the subtropical continent is shallow, with subsidence aloft. The case with $THF_0 = 120\,W/m^2$ has very little precipitation over the subtropical continent (Figure 4-17), with ITCZ near 2N. Strong sensible heat fluxes over the coastal continent result in a low level easterly jet with winds of more than $10\,m/s$, centered near 800 mb along the coastline. This easterly jet is much stronger than the easterly jet in the 2D case with coastline at 8N; the 2D case has more rainfall over the coastal continent, which decreases the sensible heat flux in favor of latent heat flux, so that the low level temperature gradient is weakened. The 750 mb meridional wind and precipitation fields at 10N (not shown) show sporadic wave-like disturbances which move rapidly westward at approximately 6.5 m/s and survive for at most a few tens of days.

The $THF_0 = 130\,W/m^2$ case (Figure 4-18) is quite similar to that with coastline at $\phi_L = 16N$ The zonal mean subcloud moist static energy is nearly flat in the northern hemisphere tropics, with h_b decreasing poleward of 16N. There is deep ascent over the coastal continent, although the greatest precipitation remains offshore near the equator. The easterly low level jet along the coastline is weaker than in the $THF_0 = 120\,W/m^2$ case, with core speeds less than $7.5\,m/s$, as sensible heat fluxes are weakened in the presence of weak precipitation. The precipitation (and wind) at 10N features wave like disturbances which propagate westward at $4 - 5\,m/s$, and which may diminish quickly or which may persist for tens of days. As in the $THF_0 = 130\,W/m^2$ case from §4.1.2, these waves are warm-core systems, with an eastward tilt of the meridional wind and ω (not shown) with

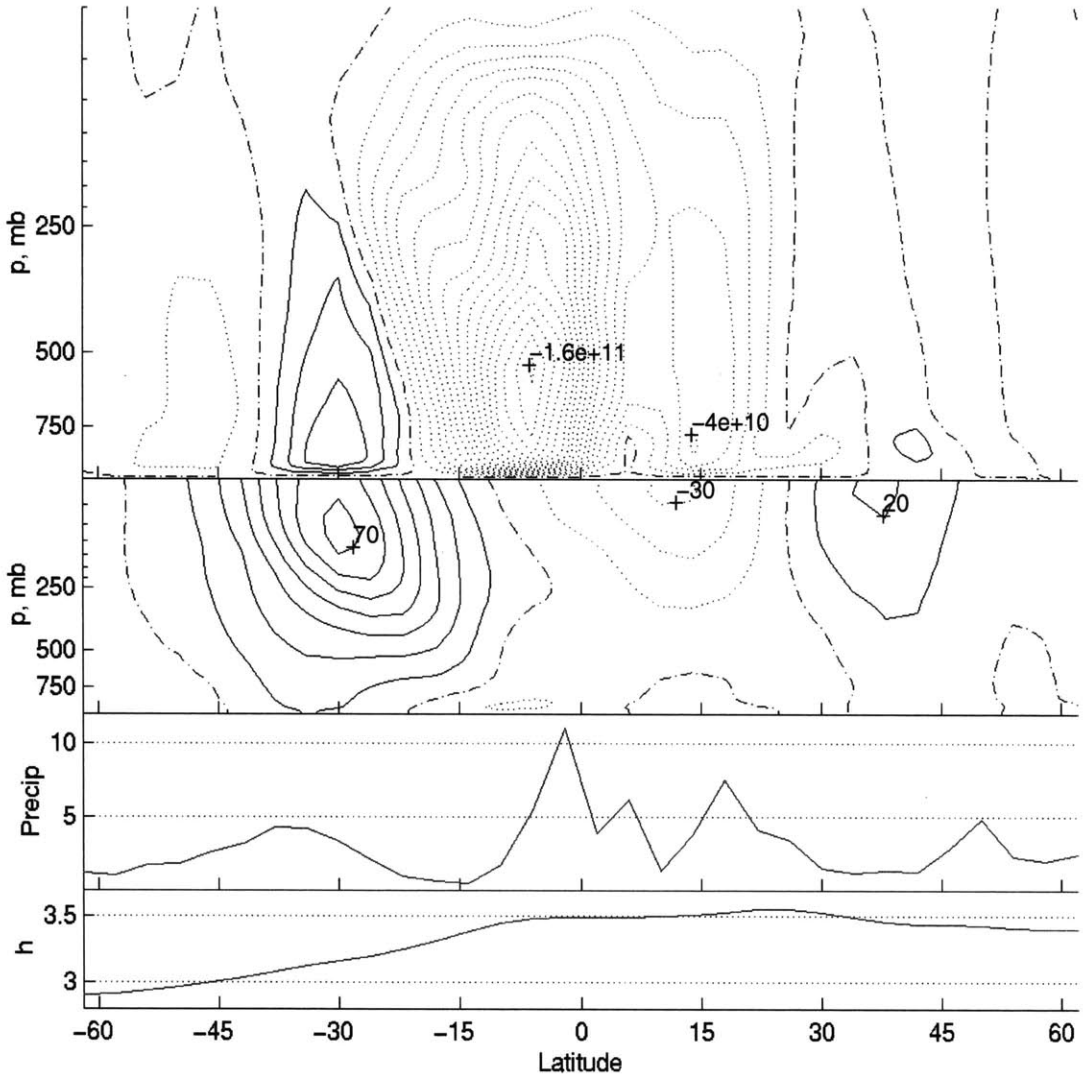

Figure 4-16: Zonally symmetric continent, coastline at 16N, $THF_0 = 135W/m^2$, summer-like SSTs; zonal mean fields, 100 day time mean. Top, streamfunction, contour interval 1e10 kg/s, dotted lines indicate counter-clockwise flow, solid lines indicate clockwise flow, dash-dot is zero contour. Upper center, absolute angular momentum, contour interval 1E8 m^2/s. Lower center, precipitation, mm/day. Bottom, 1000 mb moist static energy, $10^5 J$.

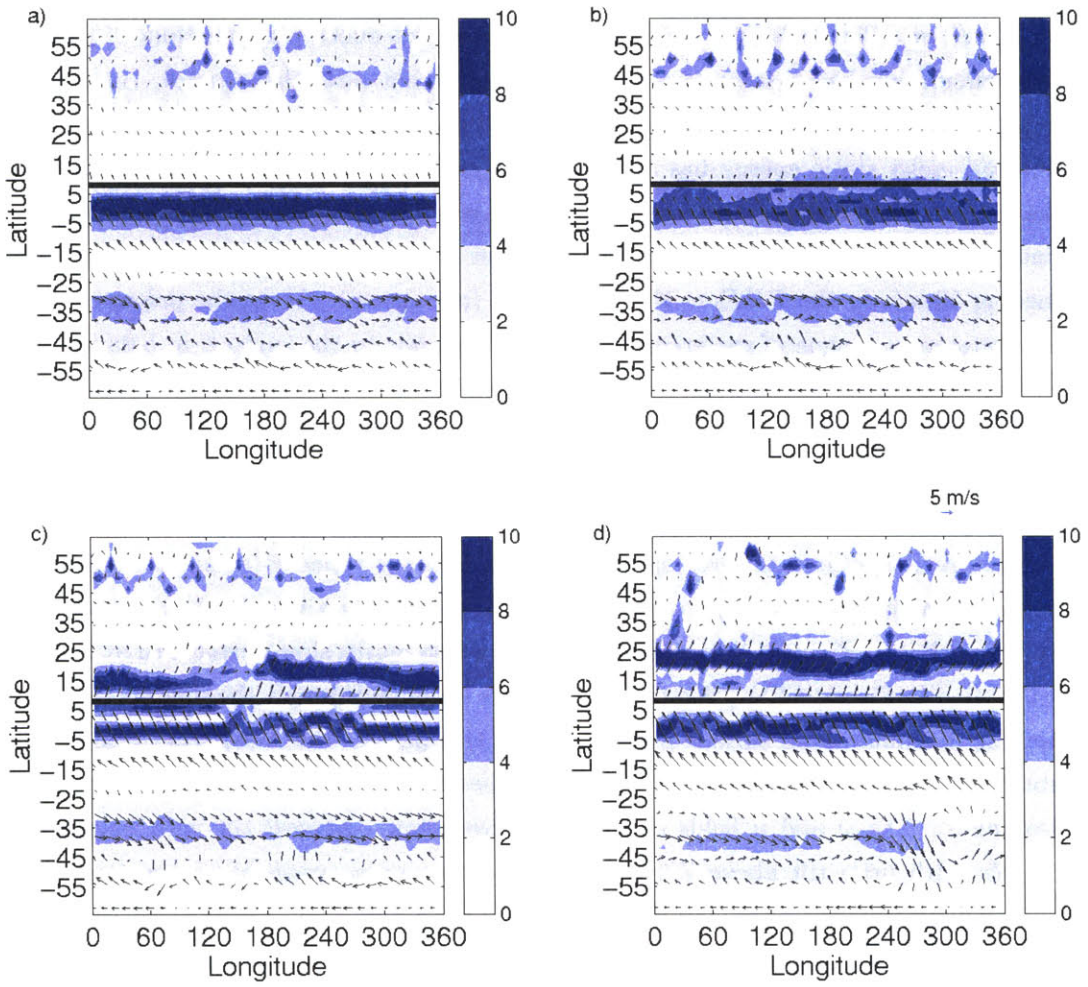

Figure 4-17: 1000 mb wind and precipitation, 360° continent, ϕ_L =8N, 100 day time mean. Contour interval 2 mm/day. a) $THF_0 = 125\,W/m^2$; b) $THF_0 = 130\,W/m^2$; c) $THF_0 = 140\,W/m^2$; d) $THF_0 = 150\,W/m^2$.

height from the surface to approximately 750 mb, above which there is little tilt. The vertical shear is easterly from the surface to roughly 700 mb, with very weak westerly shear aloft. The Eliassen-Palm flux has a baroclinic wave signature with source near 700 mb between 10N and 30N (Figure 4-19).

A zonal mean monsoon occurs in response to stronger land surface forcing ($THF_0 \geq 140\,W/m^2$, eg. Figure 4-20)), with deep ascent over the subtropical continent. The zonal mean circulation has a secondary region of deep ascent near the equator, but does not show jumping behavior and has strong flow across the equator in the mixed layer. The subcloud moist static energy has a pronounced global maximum over the continent; this maximum is located slightly poleward of the precipitation maximum. The zonal mean zonal wind field has a strong easterly jet in the upper tropospheric tropics, with wind speeds reaching $50\,m/s$ in the $THF_0 = 150\,W/m^2$ case (not shown). Along the poleward edge of the monsoon, a tongue of easterlies (not shown) extends to the surface, in balance with a poleward-increasing temperature gradient between the cooler monsoon region and the arid interior of the continent. The Eliassen Palm flux (not shown) again shows a baroclinic signature associated with this jet, although the wind speeds are much weaker than in the cases with weaker land forcing, with maximum winds of less than $5\,m/s$. Precipitation in the monsoon region is generally widespread, but two different types of localized anomalies are observed: one fast-moving type which is short-lived and moves westward at approximately $3\,m/s$ (red line in Figure 4-21); and second type which moves slowly westward at $1-2\,m/s$ (yellow line in Figure 4-21). The faster waves are dominant during the first 100 days after reaching maximum land surface forcing; during this period, the zonal wind field over the subtropical continent has easterly shear from the surface to 750 mb, with weak westerly shear aloft. The ω and v fields of the fast waves show eastward tilt with height below 750 mb, with little tilt above 750 mb. The slower moving wave has a greater lifespan, persisting for approximately 150 days in the $THF_0 = 140W/m^2$ case and 75 days in the $THF_0 = 150W/m^2$ case; the faster moving waves dissipate after a few tens of days in both cases. The Eliassen-Palm flux signature (not shown) for the fast waves show baroclinic wave generation centered near 18N at 700 mb. The slow wave is dominant after day 300, when the monsoon has become well established inland, and there is easterly shear from the surface into the upper troposphere. The ω and v fields tilt eastward with height throughout the depth of the troposphere, although the Eliassen-Palm flux shows the greatest divergence near 700 mb at 30N. Both the fast and slow waves are warm-core, with large-scale ascent and precipitation on the eastern side, with subsidence and suppression of convection to the west. The slow waves are centered considerably inland from the coast, near 18N, where the low-level easterlies are strongest.

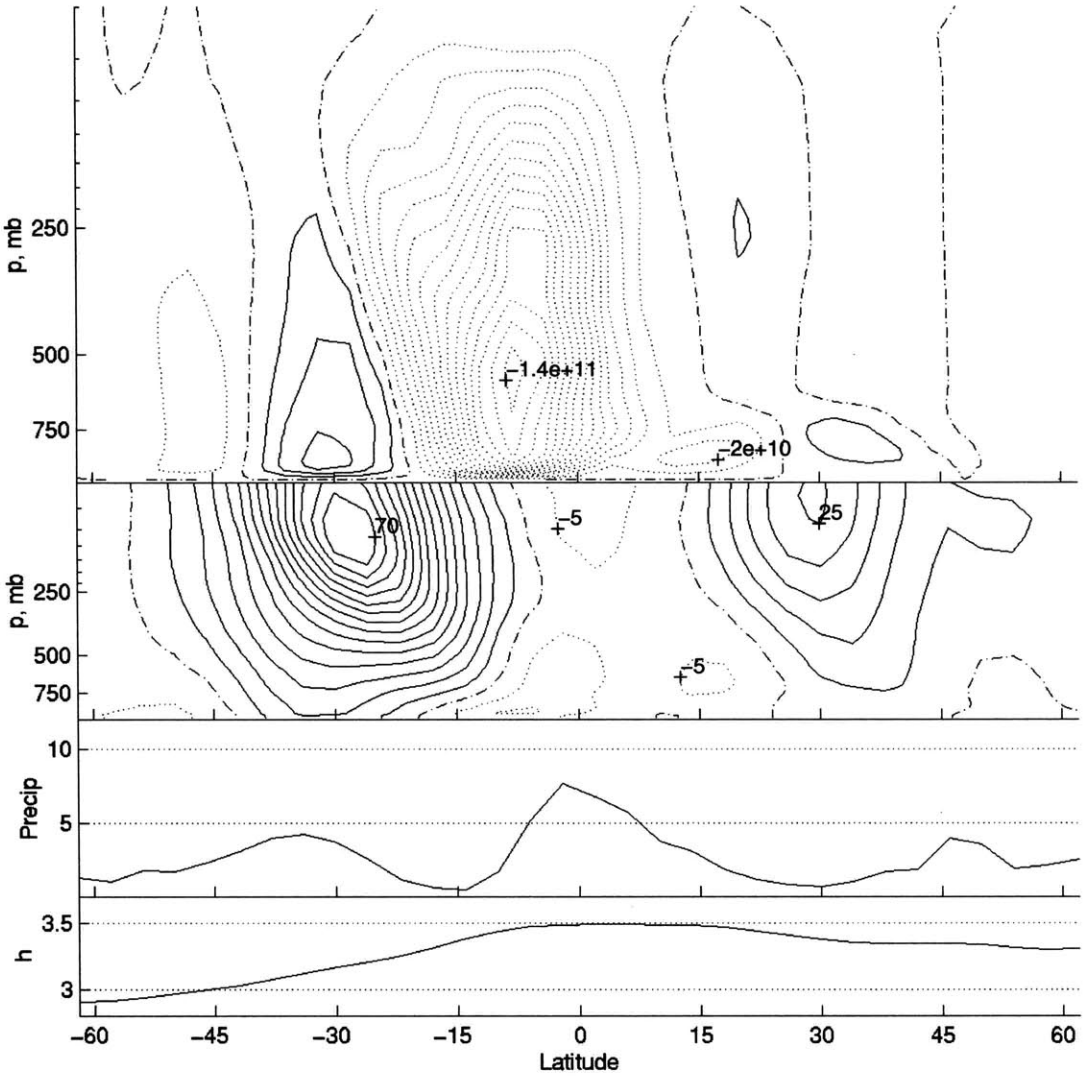

Figure 4-18: Zonally symmetric continent, coastline at 8N, $THF_0 = 130\,W/m^2$, summer-like SSTs; zonal mean fields, 100 day time mean. Top, streamfunction, contour interval 1e10 kg/s, dotted lines indicate counter-clockwise flow, solid lines indicate clockwise flow, dash-dot is zero contour. Upper center, zonal wind, contour interval 5 m/s, dotted line indicates easterlies, solid lines indicate westerlies. Lower center, precipitation, mm/day. Bottom, 1000 mb moist static energy, $10^5 J$.

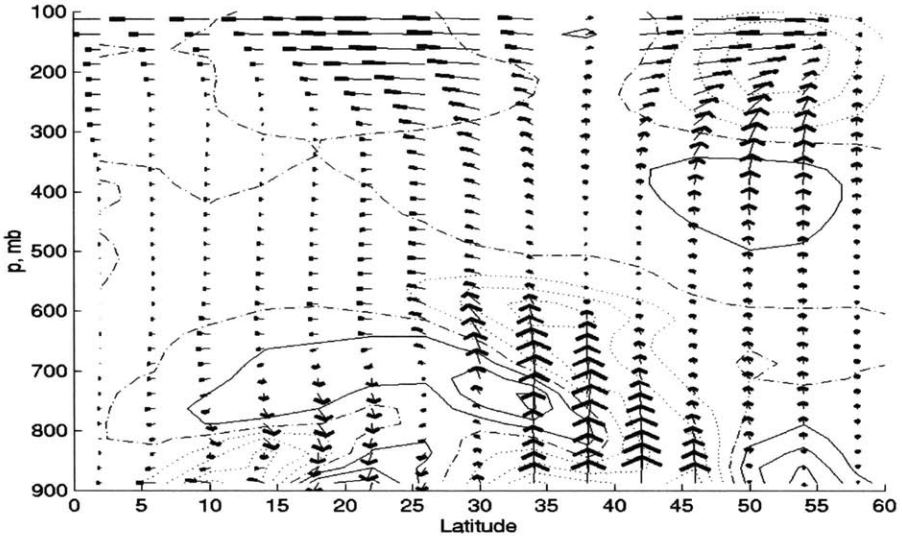

Figure 4-19: Eliassen-Palm flux and divergence for case with zonally symmetric continent, coastline at 8N, $THF_0 = 130\,W/m^2$, summer-like SSTs; zonal mean fields, 100 day time interval.

4.1.4 24N coastline

The coastline is shifted poleward to $\phi_L = 24N$ while retaining the summer-type SST profile (3.8). As in the $\phi_L = 8$N coastline case, the surface forcing profile is also shifted poleward, so that $\phi_T = 16N$ in (3.7). The resulting circulation is very similar to that seen in the two dimensional case with coastline at $\phi_L = 24$N: the monsoon circulation is narrow and localized, completely separate from the cross-equatorial circulation associated with the SST distribution.

The flow is non-monsoonal in character for $THF_0 = 120\,W/m^2$ (not shown), with no zonal mean deep ascent over the subtropical continent. There is weak, sporadic precipitation over the continental interior, which is associated with baroclinic disturbances of the upper level westerly jet. The ITCZ is located near the equator at 2N, with a broad swath of moderate precipitation across the tropical ocean. The subcloud moist static energy is greatest near the SST maximum at 8N, and decreases steadily northward.

For surface forcing of $THF_0 \geq 130W/m^2$, the flow is arguably monsoonal, with deep ascent and strong precipitation over the continent (Figure 4-23). The associated meridional circulation remains local, only 10° in meridional extent, and is completely separate from the cross-equatorial Hadley cell. This behavior was seen previously in the two dimensional cases §3.2.3, although the narrow circulation does not show the strong conservation of angular momentum seen in the two dimensional case (Figure 4-23, may be compared with Figure 3-29). A strong easterly jet forms in the upper troposphere where this narrow cell has

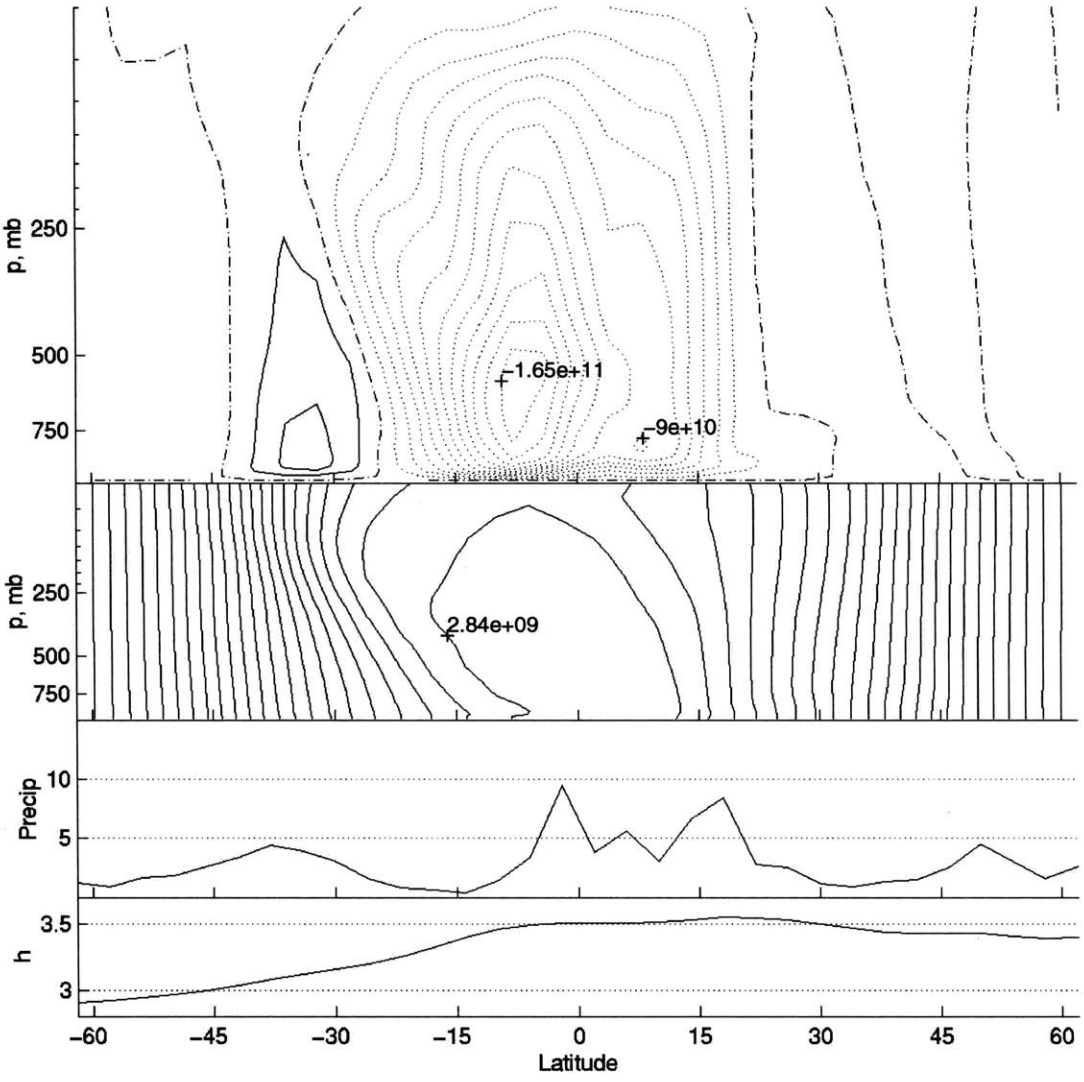

Figure 4-20: Zonally symmetric continent, coastline at ϕ_L =8N, $THF_0 = 140\,W/m^2$, summer-like SSTs; zonal mean fields, 100 day time mean. Top, streamfunction, contour interval 1.5e10 kg/s, dotted lines indicate counter-clockwise flow, solid lines indicate clockwise flow, dash-dot is zero contour. Upper center, absolute angular momentum, contour interval 1E8 m^2/s. Lower center, precipitation, mm/day. Bottom, 1000 mb moist static energy, $10^5 J$.

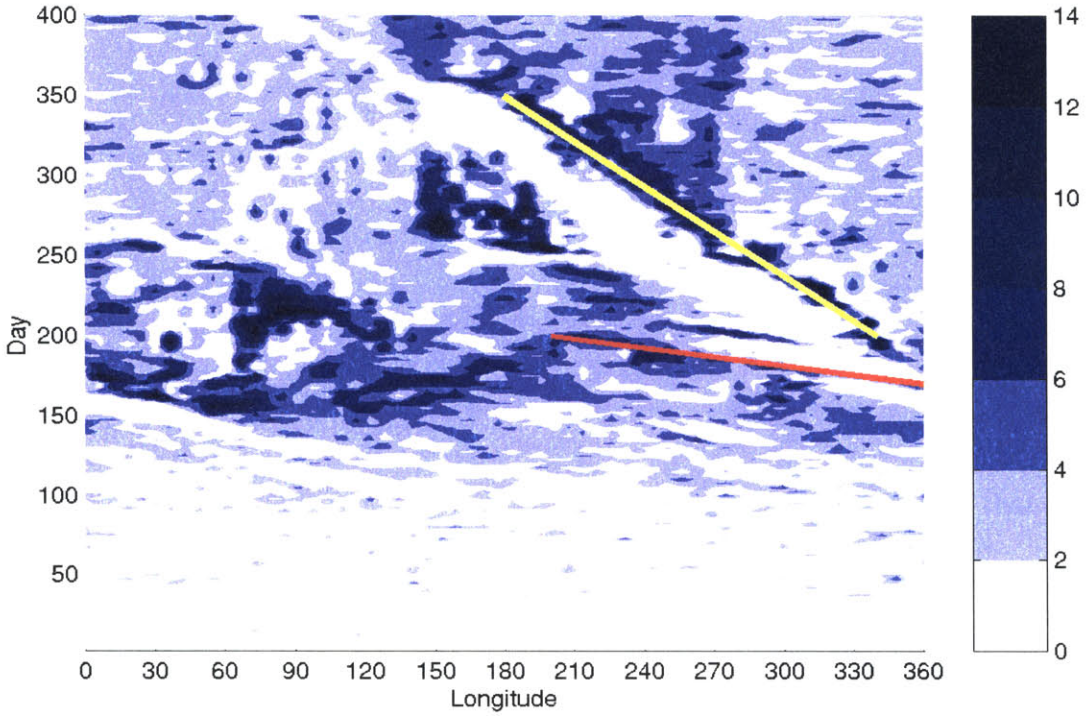

Figure 4-21: Zonally symmetric continent, coastline at ϕ_L = 8N, $THF_0 = 140\,W/m^2$, Hovmoeller diagram of precipitation at 18N, beginning at time of initial ramp-up of land forcing. Maximum land forcing reached at day 100. Red line indicates path of a fast eastward propagating wave; yellow line indicates path of a slow eastward propagating wave.

equatorward flow. The subcloud moist static energy field has a significant maximum over the continental interior.

The cases with $THF_0 = 130, 140\,W/m^2$ show little wave activity in the monsoon region, and have only relatively weak easterlies in the lower troposphere where a tongue extends from the upper level easterly jet towards the surface. However, the case with $THF_0 = 150\,W/m^2$ (not shown) has an easterly jet just poleward of the monsoon, centered near 650 mb, with core wind speeds greater than $5\,m/s$. The Eliassen Palm flux (not shown) shows a source of baroclinic waves associated with this jet, and the precipitation field over the subtropical continent develops a westward propagating wave signal approximately 200 days after onset of the monsoon (Figure 4-24). The waves move at approximately $2.5\,m/s$, and persist for at most a few tens of days. Precipitation and ascent occur on the eastern side of the waves, with subsidence and suppressed convection to the west; this is similar to the waves observed in the cases with $\phi_L = 8N, 16N$. The vertical structure of the wave (not shown) shows an eastward tilt of the ω and meridional wind fields with height throughout the entire depth of the troposphere; this is a result of the easterly shear which extends over

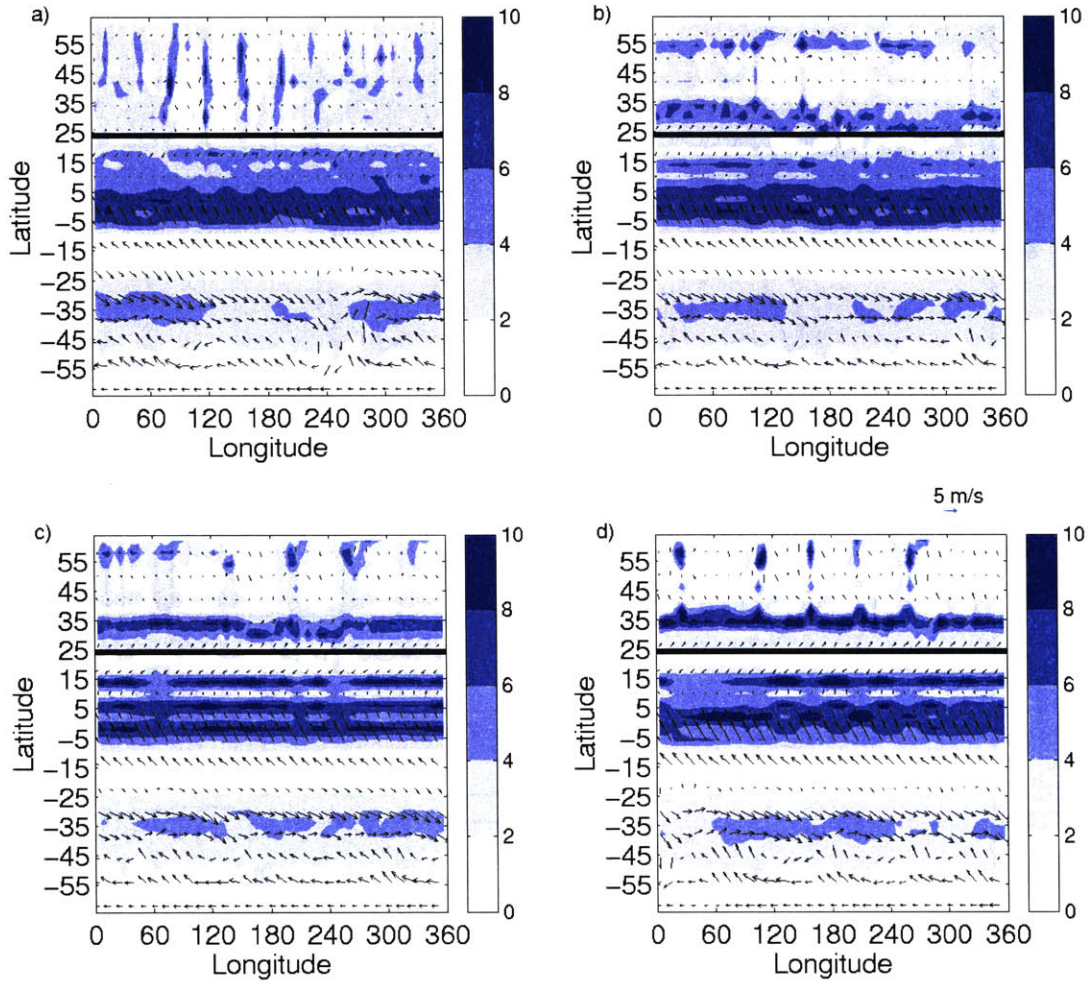

Figure 4-22: 1000 mb wind and precipitation, 360° continent, ϕ_L =24N, 100 day time mean. Contour interval 2 mm/day. a) $THF_0 = 125\,W/m^2$; b) $THF_0 = 130\,W/m^2$; c) $THF_0 = 140\,W/m^2$; d) $THF_0 = 150\,W/m^2$.

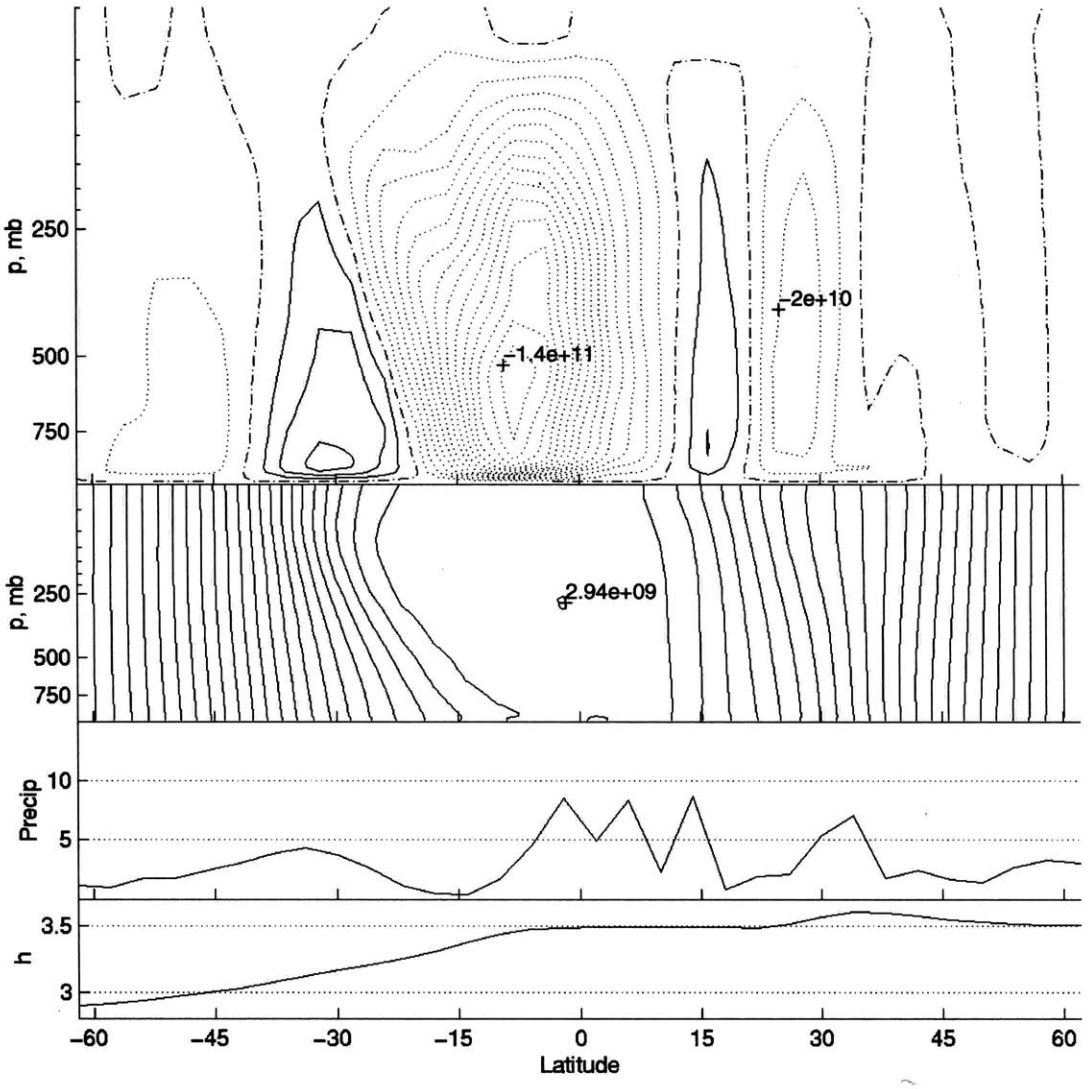

Figure 4-23: Zonally symmetric continent, coastline at ϕ_L =24N, $THF_0 = 140\,W/m^2$, summer-like SSTs; zonal mean fields, 100 day time mean. Top, streamfunction, contour interval 1.0e10 kg/s, dotted lines indicate counter-clockwise flow, solid lines indicate clockwise flow, dash-dot is zero contour. Upper center, absolute angular momentum, contour interval 1e8 $m62/s$. Lower center, precipitation, mm/day. Bottom, 1000 mb moist static energy, $10^5 J$.

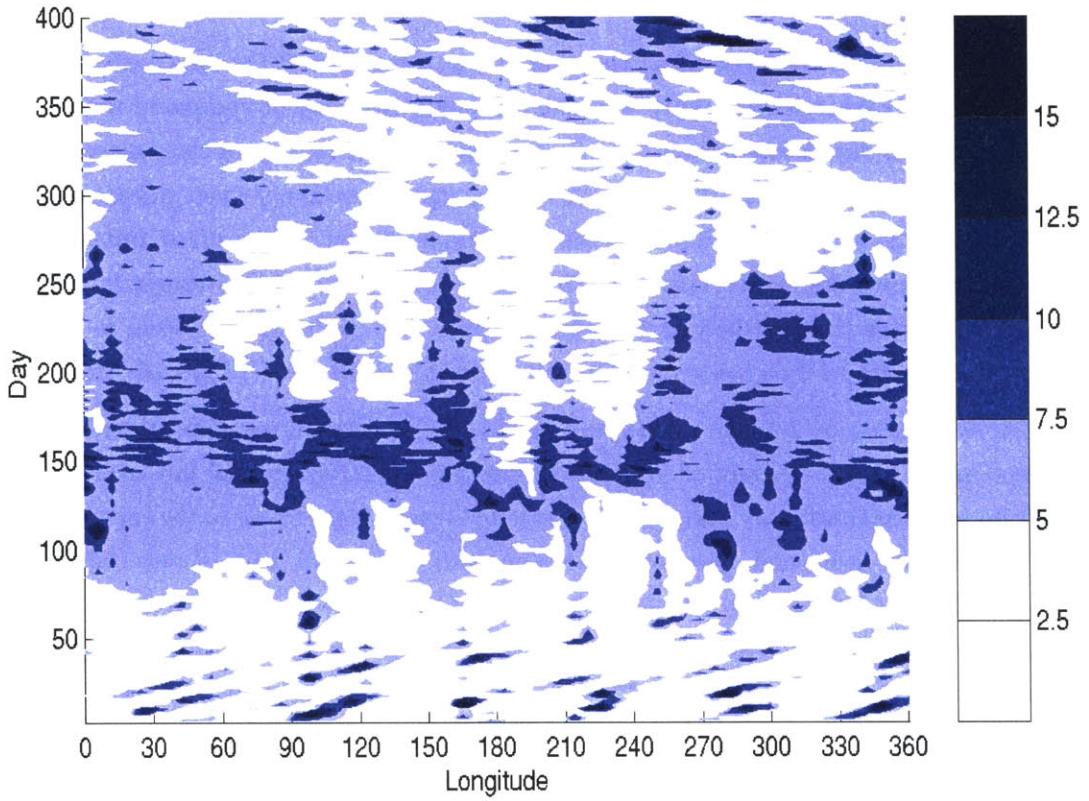

Figure 4-24: Zonally symmetric continent, coastline at ϕ_L = 24N, $THF_0 = 150\,W/m^2$, Hovmoeller diagram of precipitation at 26N, beginning at time of initial ramp-up of land forcing. Maximum land forcing reached at day 100.

the entire troposphere along the coastline.

4.1.5 Impact of Eddies

The use of a zonally symmetric continent with symmetric surface forcing and SSTs allows the resulting flow to be compared directly with the two dimensional model experiments from Chapter 3. In general, the zonal mean large-scale flow is reasonably similar to the two dimensional results. In comparison, the meridional circulation and monsoon precipitation are weaker in the three dimensional cases with eddies, with stronger land surface forcing required to induce a global mean monsoon than in the two dimensional cases.

How do eddies affect the meridional circulation associated with the monsoon? The angular momentum budget acquires a new term in the three dimensional cases to account for momentum transport by the eddies. The upper tropospheric westerly midlatitude jets and the tropical easterly jet are all weakened in the three dimensional cases. Eddies also act to decrease conservation of AAM; the result of this is an enhanced ability of the meridional

circulation to cross contours of absolute angular momentum in the upper troposphere.

Figure 4-8 shows the strength of the monsoon as a function of the land surface forcing for the various cases with zonally symmetric continent, and may be compared with Figure 3-22 for the two dimensional cases. The streamfunction maximum is of close magnitude to the two dimensional cases for $THF_0 \geq 135\,W/m^2$, when there is a strong, global monsoon. For $THF_0 \leq 125\,W/m^2$, the circulation over the land is shallow and localized, but may have a relatively strong, dry overturning cell. This dry circulation is slightly stronger in the three dimensional cases than in the two dimensional cases. The eddies do not seem to strongly affect the strength of the cross-equatorial cells associated with the SST distribution.

The weakening of angular momentum conservation in the three dimensional cases is evident in the center diagram of Figure 4-8, showing the minimum 150 mb level absolute vorticity over the continent. The absolute vorticity is much higher than in the corresponding two dimensional cases, and does not closely approach the critical value of zero even for the strongest land surface forcing. Threshold behavior of the circulation strength is not observed for the three dimensional cases with zonally symmetric continent, but neither was it found in the axisymmetric continental cases. The net precipitation over the continent is significantly greater in the three dimensional cases, especially for weak land surface forcing. This is a result of the presence of a midlatitude rain band caused by instability of the midlatitude westerly jet.

Why is a stronger land surface forcing needed to induce a monsoon in the three dimensional cases than in the two dimensional cases? For the cases which are monsoonal in two dimensions but non-monsoonal in three dimensions, the subcloud moist static energy maximum remains over the ocean or along the coastline in the three dimensional cases, but is located inland in the two dimensional cases. By the theory described in section §3.3, the three dimensional cases should not develop a monsoon with this distribution of h_b. The question then becomes: why is the h_b maximum further poleward in the two dimensional cases?

Figure 4-25 illustrates the expected changes in the subcloud moist static energy distribution due to eddies. The eddies tend to redistribute h_b, decreasing the moist static energy near the maximum, and increasing h_b near minimums. With the land forcing profile used here, h_b is increased far inland and decreased near the coastline near the h_b maximum. Because h_b is lower over the subtropical continent, less energy is needed to bring in-flowing air from the ocean to the inland subtropical h_b levels, and the inflow does not need to travel as far poleward as in the axisymmetric case. The h_b maximum is thus shifted slightly closer to the coastline than in the axisymmetric case, and the monsoon rains are located slightly closer to the equator.

4.2 Zonally Asymmetric Continent

Large-scale asymmetry of the forcing is introduced by limiting the longitudinal extent of the continent. Opposite the continent in the boreal hemisphere, the ocean is extended to the northern boundary of the model. The intent is to examine the role of asymmetrical forcing in the large-scale monsoon flow while maintaining a simple geometry. Several variations on continent shape are explored: a simple rectangular continent with subtropical coastline; an Asia-Africa conglomerate; and a continent which extends from the northern to southern boundary of the model. The total forcing over the continent is a function of latitude but does not vary in longitude, as in the previous cases with 360° continent, with the total prescribed forcing given by (4.1). Unless otherwise noted, the spin-up process is identical to that used in previous three dimensional cases.

4.2.1 Uniform Ocean SSTs

In this case, the ocean is assigned a warm surface temperature of 302 K at all latitudes. The continent is 180° in longitudinal expanse, and extends from the coastline at $\phi_L = 16$N poleward to the model boundary at 64N (Figure 4-26). The model is run for 300 days following the attainment of full summer strength surface forcing.

The circulation is non-monsoonal for land forcing of $THF \leq 125\,W/m^2$, with greatest precipitation over the tropical ocean. There is weak low-level inflow along the coastline, especially over the eastern half of the landmass (Figure 4-27). The horizontal lower tropospheric flow has a large anticyclone over the midlatitude ocean, with a weaker cyclone over the midlatitude continent; these features develop in response to the temperature difference between the relatively warm ocean and cooler landmass at high latitudes. Along the southern coastline, the poleward-increasing temperature gradient results in a low-level easterly

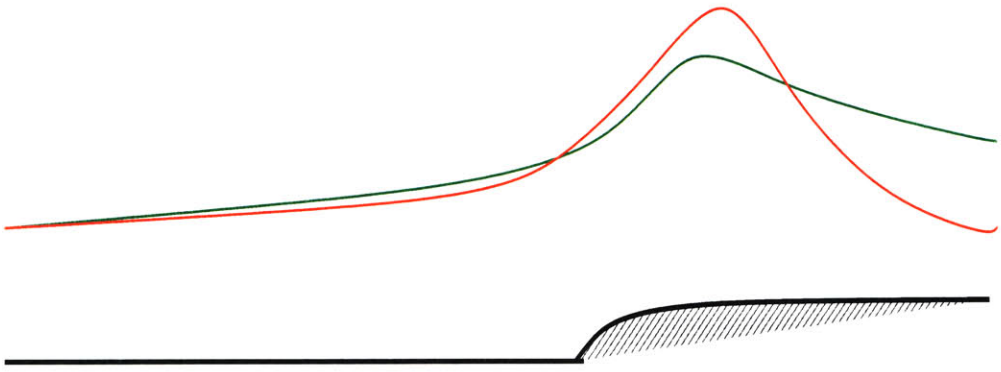

Figure 4-25: Schematic diagram of effects of eddies on subcloud moist static energy distribution. Red line indicates h_b without eddy effects, green line indicates h_b with eddies.

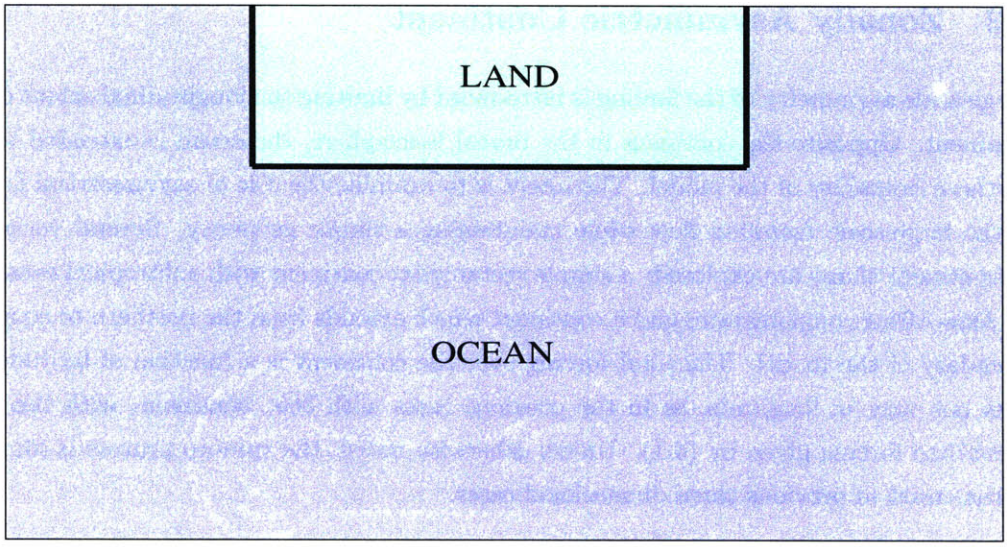

Figure 4-26: Schematic diagram of land configuration with 180° continent.

jet centered near 600 mb at 20N; this jet is stronger in the $THF_0 = 120\,W/m^2$ case (not shown) than in the $THF_0 = 125\,W/m^2$ case (Figure 4-28), as greater precipitation over the continent in the $THF_0 = 125\,W/m^2$ case increases surface latent heat flux at the expense of the sensible heat flux, reducing temperatures over the subtropical continent. There is no large-scale meridional overturning circulation either over the continent or over the oceans. In these cases, the boundary layer moist static energy does not have a maximum over the continent, and h_b decreases poleward from the coastline.

As in previous cases, this easterly jet develops baroclinic waves (Figure 4-29) which propagate westward along the continental coastline. These waves can be seen in the meridional wind field in the lower troposphere as well as in the precipitation field, both for the $THF_0 = 120$ and $125W/m^2$ cases, although the waves are stronger in the $THF_0 = 120W/m^2$ case. The easterly jet fluctuates in strength over time; the strongest wave signals are seen when the jet is robust, with fewer waves during periods of a weakened jet. The vertical structure of the waves is similar to that seen in Figure 4-14.

For forcing of $THF_0 \geq 130W/m^2$, a monsoonal regime develops, with intense precipitation over the subtropical continent (Figures 4-27, 4-31). Deep ascent and corresponding moist convection occurs in the subtropics across the entire longitudinal span of the continent, with much more arid conditions over the midlatitude continent. In the subtropics, the most intense precipitation favors the western half of the continent, while in the midlatitudes the eastern half of the continent receives greater precipitation. The greatest h_b is located over the western half of the continent; although the boundary layer temperature is slightly greater over the eastern edge of the subtropical continent, the specific humidity is much

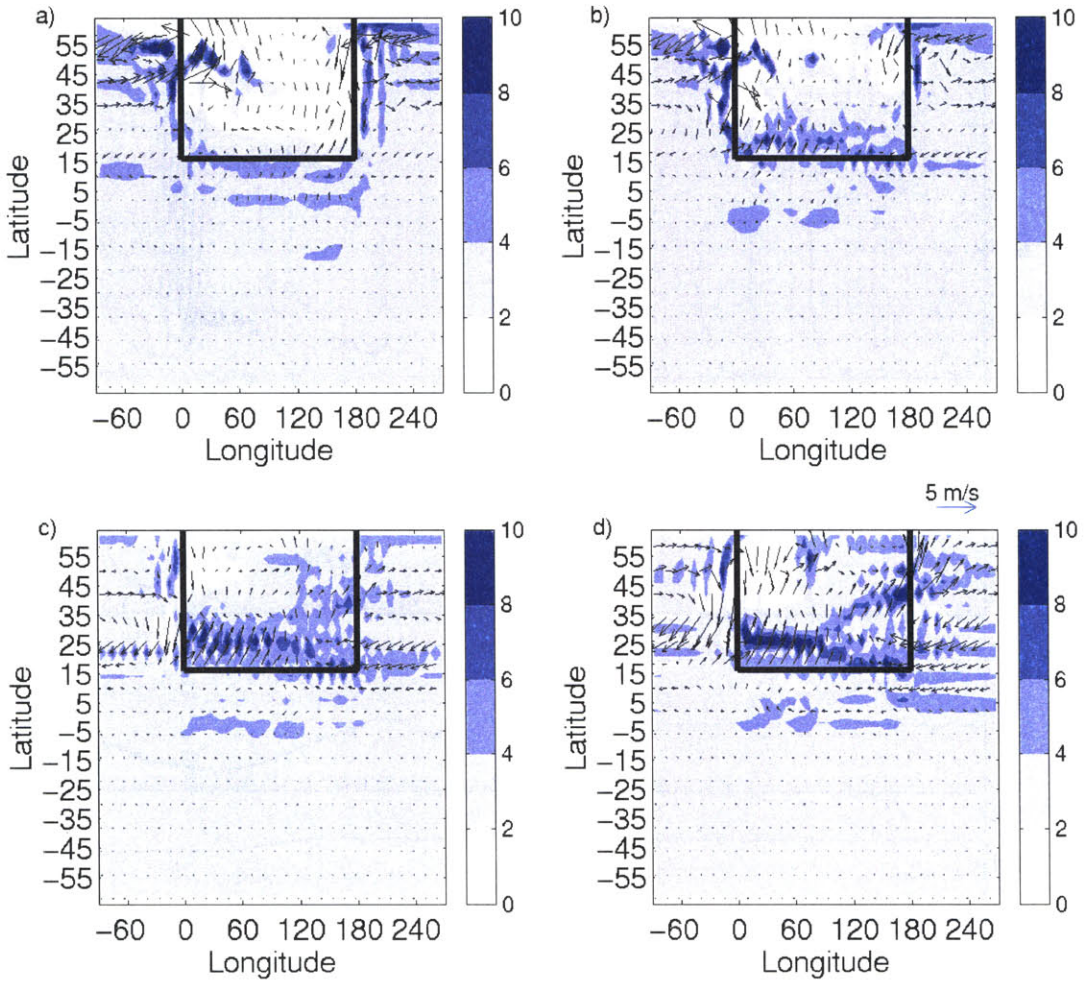

Figure 4-27: 1000 mb wind and precipitation, 180° continent and uniform SST distribution, 100 day time mean. Contour interval 2 mm/day. a) $THF_0 = 125\,W/m^2$; b) $THF_0 = 130\,W/m^2$; c) $THF_0 = 140\,W/m^2$; d) $THF_0 = 150\,W/m^2$.

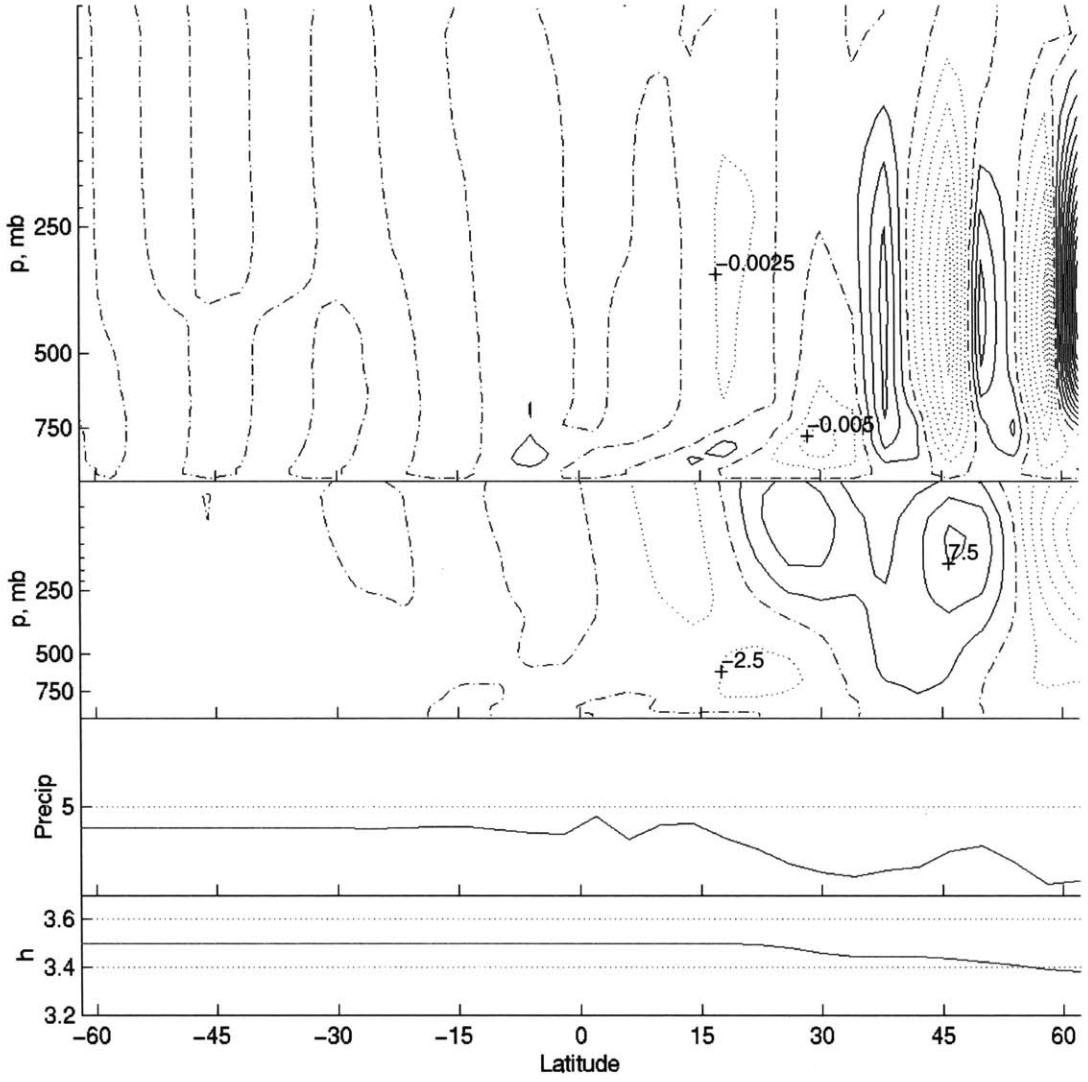

Figure 4-28: 180° continent, coastline at ϕ_L =16N, $THF_0 = 125\,W/m^2$, uniform SSTs; zonal mean over land only, 100 day time mean. Top, ω, contour interval 2.5E-3 Pa/s, dotted lines indicate ascent, solid lines indicate subsidence, dash-dot is zero contour. Upper center, zonal wind, contour interval 2.5 m/s, dotted line indicates easterlies, solid lines indicate westerlies. Lower center, precipitation, mm/day. Bottom, 1000 mb moist static energy, $10^5 J$.

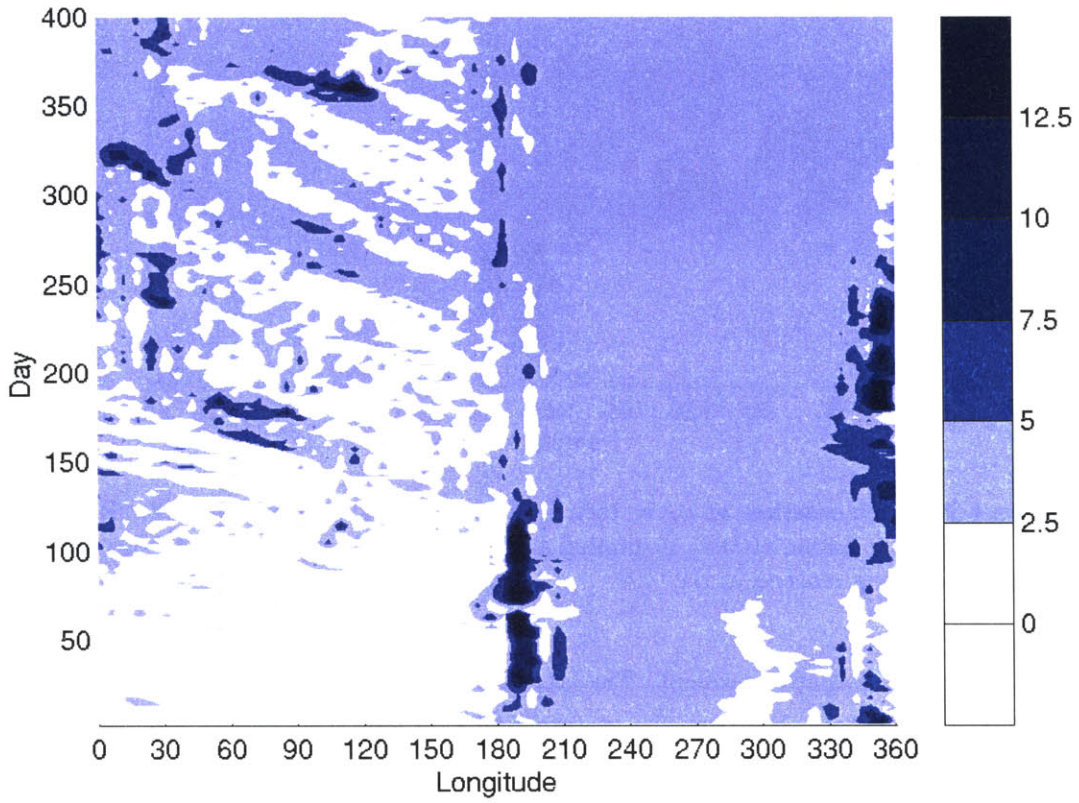

Figure 4-29: 180°, coastline at ϕ_L = 16N, $THF_0 = 125\,W/m^2$, uniform SSTs. Hovmoeller diagram of precipitation at 18N, beginning at time of initial ramp-up of land forcing. Maximum land forcing reached at day 100.

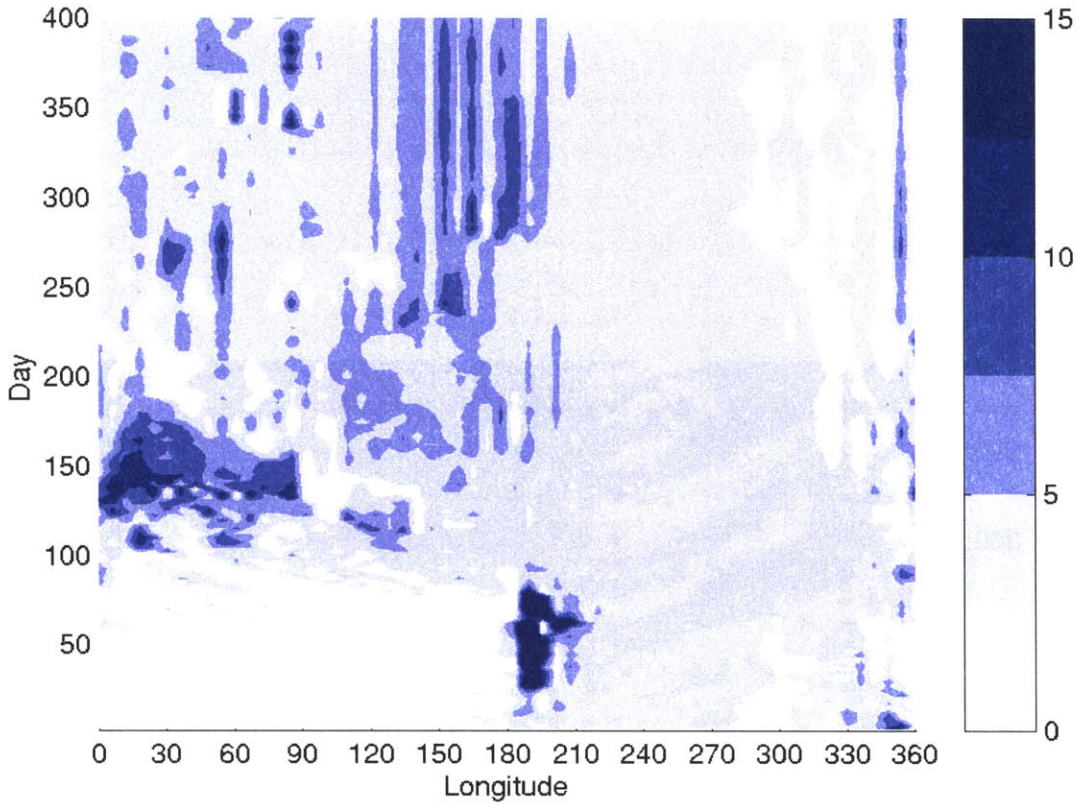

Figure 4-30: 180°, coastline at ϕ_L = 16N, $THF_0 = 140\,W/m^2$, uniform SSTs. Hovmoeller diagram of precipitation at 18N, beginning at time of initial ramp-up of land forcing. Maximum land forcing reached at day 100.

greater over the western continent. The large-scale flow pattern features convergence over the western continent, but over the eastern continent the flow turns southerly and then southeasterly, crossing back into the midlatitude oceans and exporting moisture from the eastern continent. As the land forcing is increased, the latitude of the maximum zonal mean precipitation over the continent moves poleward until reaching 26N, which appears to be the northernmost possible extent of the monsoon for this configuration. The monsoon is more widespread and is located further poleward in the case with 180° continent than with 360° continent.

The zonally averaged circulation calculated only over the continental longitudes includes a meridional cell with ascent over the subtropical land and subsidence over the northern hemisphere tropical ocean (Figure 4-31). There is little indication of cross-equatorial flow, even for the strongest land forcing case. Upper level easterlies (not shown) range across the northern hemisphere tropics, where there is equatorward flow, with a westerly jet in the midlatitudes. The meridional circulation is not closely angular momentum conserving,

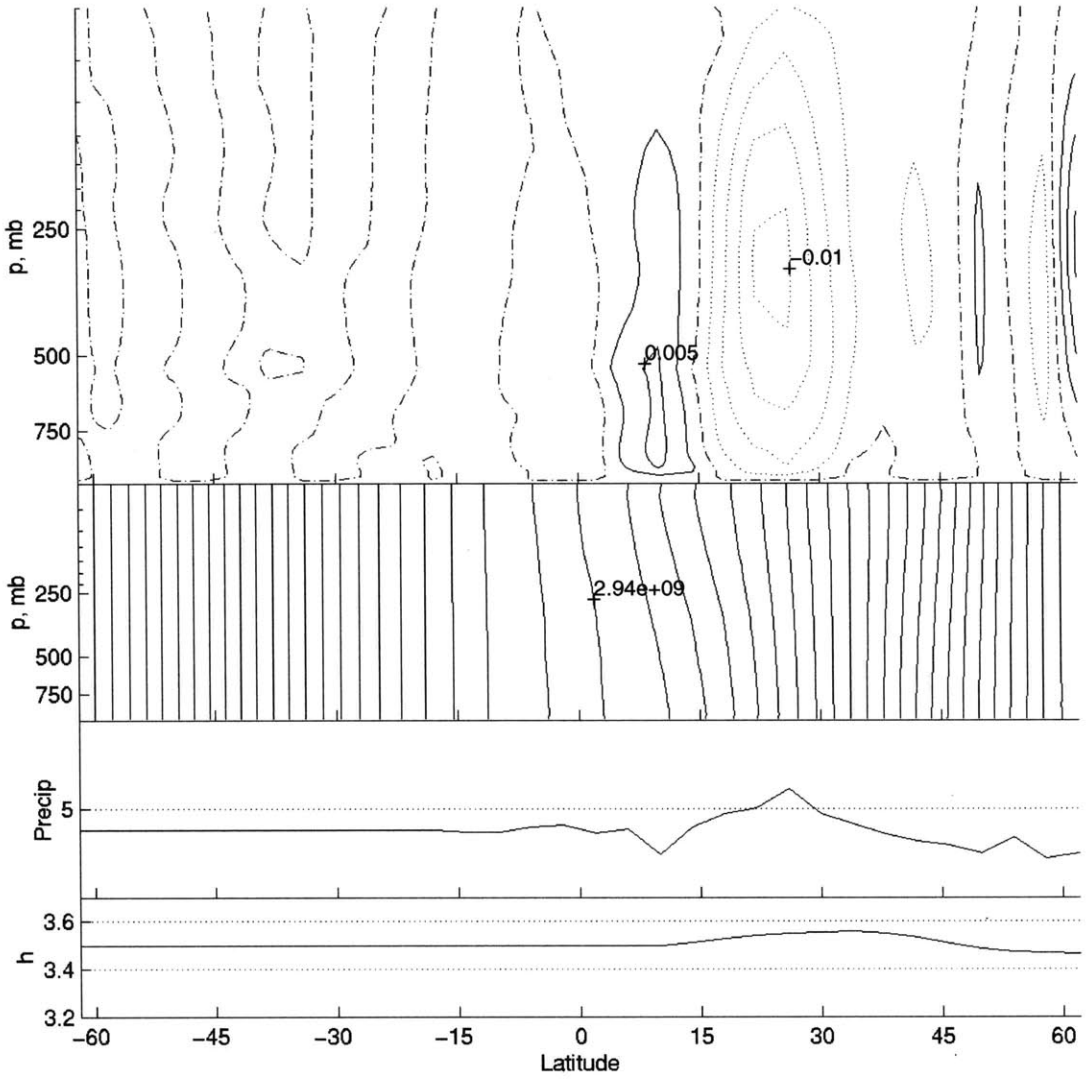

Figure 4-31: 180° continent, coastline at ϕ_L =16N, $THF_0 = 140\,W/m^2$, uniform SSTs; zonal mean over land only, 100 day time mean. Top, ω, contour interval 2.5E-3 Pa/s, dotted lines indicate ascent, solid lines indicate subsidence, dash-dot is zero contour. Upper center, absolute angular momentum, contour interval 1e8 m^2/s. Lower center, precipitation, mm/day. Bottom, 1000 mb moist static energy, $10^5 J$.

and the angular momentum field does not show significant distortion by the flow. There is little horizontal flow in the southern hemisphere, where the ocean has uniform SST. Prior to onset, there is a strong easterly jet along the coast (not shown), which develops westward propagating waves. These waves initiate precipitation over the landmass (Figure 4-30), which then becomes widespread. After the onset of precipitation, the low level temperature gradient weakens and the easterly jet dies off, as do the baroclinic waves. Regions of locally intense monsoon precipitation are nearly stationary in time, with few longitudinally propagating disturbances.

A region of strong subsidence is located over the ocean to the west and slightly to the north of the monsoon (Figure 4-32). The greatest subsidence occurs near the souther coastline, with a weaker tail extending into the central ocean. Although the subsidence region is adjacent to the monsoon ascent region, there is no indication of a direct circulation cell connecting the two areas. The subsidence is nearly in Sverdrup balance with the strong northerly winds which extend from the surface through the mid-troposphere, forming the eastern edge of the oceanic anticyclone. Rodwell and Hoskins (2001) investigated the link between monsoons and subtropical anticyclones, and found that Rossby and Kelvin waves generated by the monsoon region played a strong role in creating low level subtropical anticyclones. To the east of the monsoon, the Kelvin wave regime results in easterlies which form the branch of the anticyclone nearest the equator. To the west of the monsoon, the Rossby wave regime results in adiabatic subsidence, which induces equatorward flow in the lower troposphere due to Sverdrup balance. In their study, Newtonian cooling enhances the subsidence region, especially close to the western edge of the continent. The flow field in our model results follows that described by Rodwell and Hoskins, with easterlies over the tropical and subtropical ocean to the east of the continent, and an upper level cyclonic Rossby-type signal (not shown) to the northwest of the monsoon region.

A strong wavenumber one signal is observed in both dynamical and thermodynamic fields; it is desirable to determine whether this signal is fundamental to the monsoon or simply a result of the chosen land/sea distribution. To this end, a continent of only 60° longitudinal extent is introduced, with $THF_0 = 140W/m^2$ and uniform ocean SSTs as in the previous cases. The monsoon response is very similar to that seen with 180° continent, with intense precipitation over the subtropical continent. In the lower troposphere (not shown), the cyclonic flow associated with the heated continent is approximately the same longitudinal width as the continent, with the complimentary anticyclone spanning the entire ocean. There is strong southwesterly inflow along the southern boundary of the land, with only a small region along the southeastern corner dominated by easterlies; in the 180° continent case, the easterlies occur over a much greater area of the land. In the upper troposphere, an easterly jet spans the entire globe in the northern hemisphere tropics, with

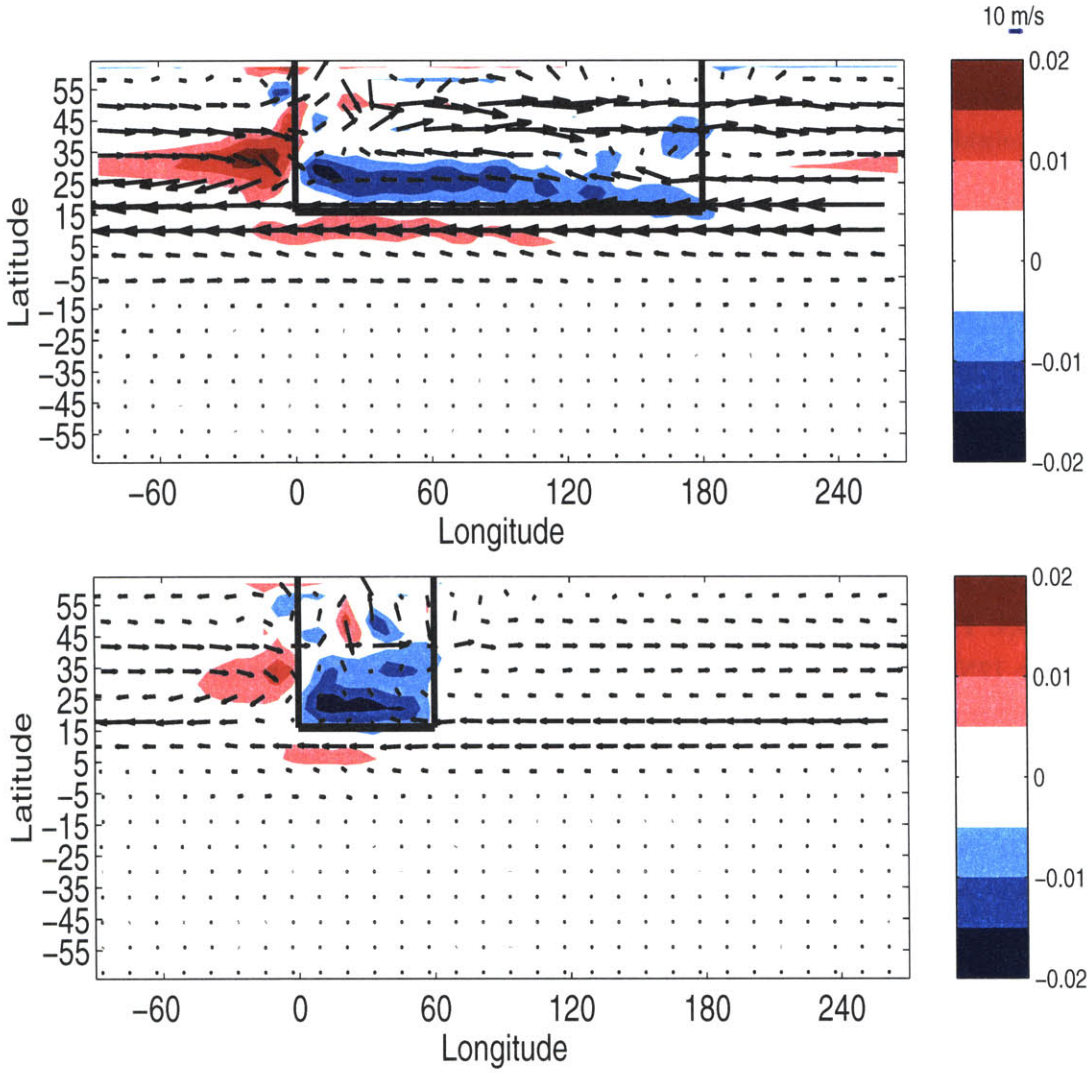

Figure 4-32: 500 mb ω and wind field, ϕ_L =16N, $THF_0 = 140\,W/m^2$, uniform SSTs; zonal mean taken over land only, 100 day time mean. Top, 180° continent; bottom, 60° continent.

a cyclone of approximately 90° longitudinal extent along the northwest edge of the monsoon region. The vertical velocity field (Figure 4-32) shows strong ascent over the monsoon area, with two main regions of subsidence: a narrow region over the tropical ocean just off the coast of the continent forming the descent branch of a meridional cell, and a larger region of subsidence to the northwest of the monsoon. This second region of subsidence is approximately 60° in longitudinal extent with a weak tail extending a further 90° over the central ocean, and is strongest just to the west of the coast. The size of the region of strong subsidence remains roughly the same when the continent size is decreased, indicating that the subsidence is not solely a response to the land/ocean asymmetry.

4.2.2 'Summer' SSTs

A more realistic ocean temperature distribution is introduced to the case with 180° landmass. The ocean SST distribution follows (3.8) both in the southern hemisphere and in the ocean portion of the northern hemisphere. The presence of cool midlatitude oceans in the northern hemisphere substantially impacts the large-scale behavior of the monsoon.

For $THF \leq 130\,W/m^2$, there is only weak rainfall over the subtropical continent in the long term mean (Figure 4-33). The vast majority of precipitation falls poleward of 40N over the continent in the midlatitude rain belt, with very arid conditions from the coastline to 40N. There is a broad band of strong tropical precipitation over the ocean ranging from 6S to 12N, with maximum rainfall near the equator. With strong sensible heat fluxes over the subtropical continent, there is a poleward-increasing temperature gradient (not shown) between the tropical ocean and desert-like land in the lower troposphere, but a decreasing-poleward gradient in the upper troposphere. A low-level easterly jet centered near 15N at 700 mb results (Figure 4-34):, with maximum wind speeds near $10\,m/s$ in the core of the jet. A heat low forms over the subtropical continent, with southerly inflow along the coastline. A shallow overturning cell features ascent over the continent, and subsidence over the coastal ocean which suppresses moist convection near the coast. The boundary layer moist static energy maximum remains over the tropical ocean, with lower h_b over the continent.

The meridional circulation over the ocean (not shown) is similar to that seen in the aquaplanet case with SST maximum at 8N (Figure 2-7). Strong tropical precipitation occurs from 6S to 20N, with greatest precipitation near the equator and a secondary maximum near 16N (Figure 4-33). The equatorial precipitation maximum is associated with the cross-equatorial Hadley circulation, while the local summer Hadley cell is associated with the subtropical precipitation maximum, and the strong low-level northeasterly winds between 14N and 30N are associated with the lower branch of this circulation. There is a vigorous

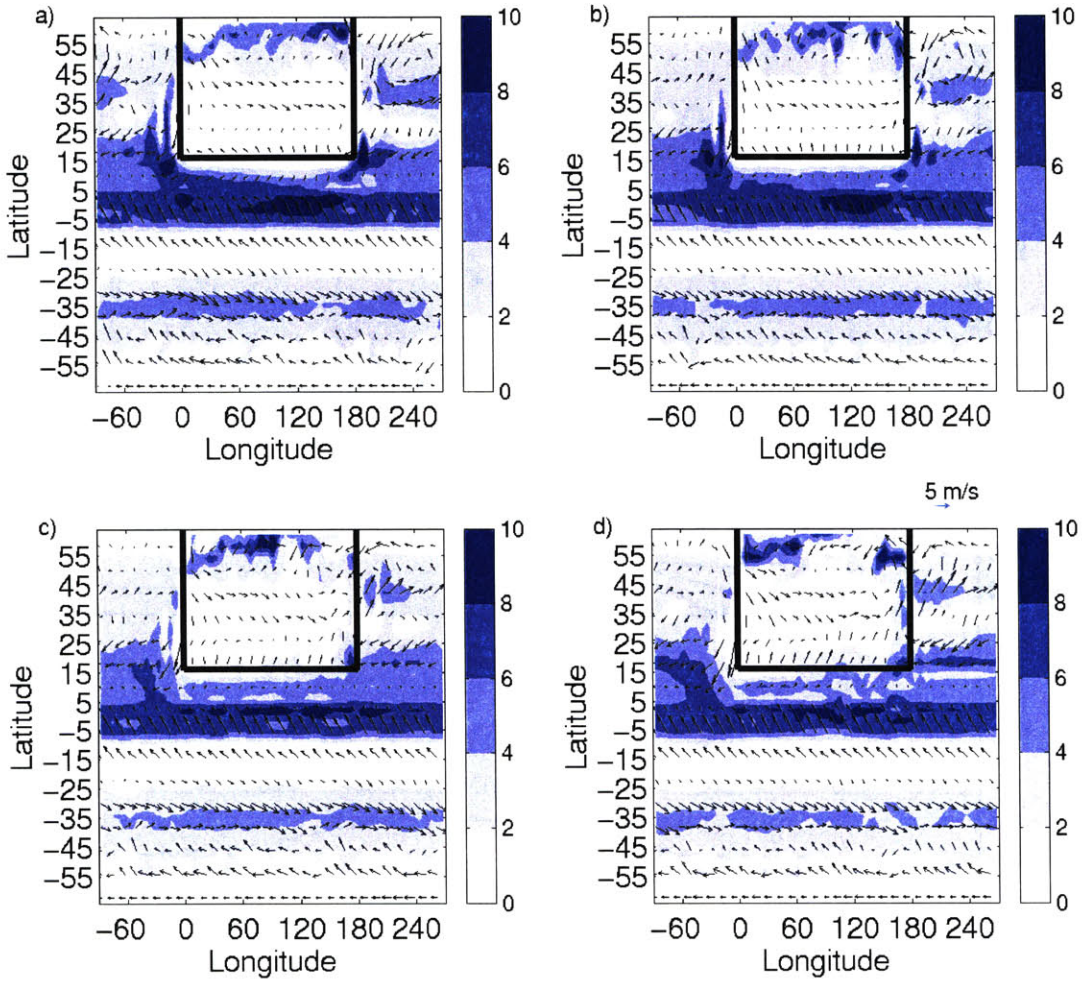

Figure 4-33: 1000 mb wind and precipitation, 180° continent and summer SST distribution, 100 day time mean. Contour interval 2 mm/day. a) $THF_0 = 125\,W/m^2$; b) $THF_0 = 130\,W/m^2$; c) $THF_0 = 140\,W/m^2$; d) $THF_0 = 150\,W/m^2$.

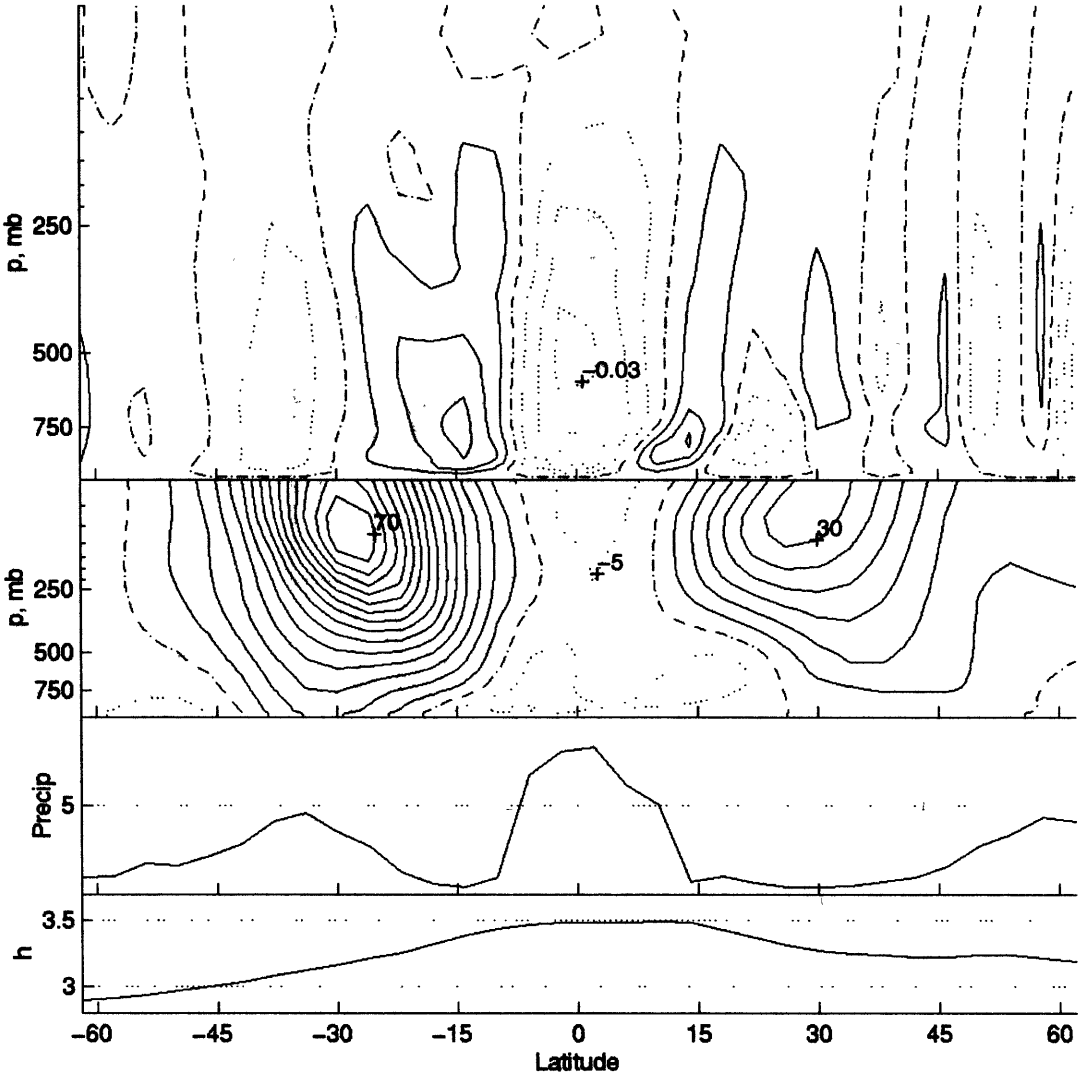

Figure 4-34: 180° continent, coastline at ϕ_L =16N, $THF_0 = 125\,W/m^2$, summer SSTs; zonal mean over land only, 100 day time mean. Top, ω, contour interval 1E-2 Pa/s, dotted lines indicate ascent, solid lines indicate subsidence, dash-dot is zero contour. Upper center, zonal wind, contour interval 5 m/s, dotted line indicates easterlies, solid lines indicate westerlies. Lower center, precipitation, mm/day. Bottom, 1000 mb moist static energy, $10^5 J$.

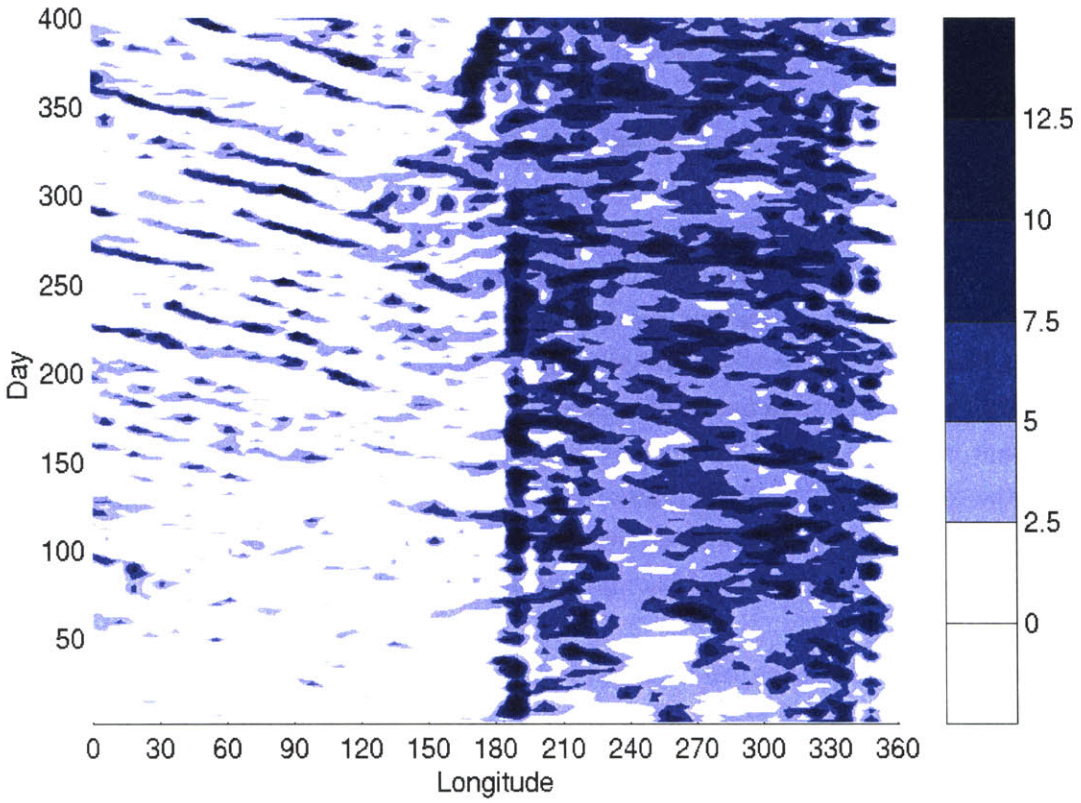

Figure 4-35: 180°, coastline at $\phi_L = 16$N, $THF_0 = 140\,W/m^2$, summer SSTs. Hovmoeller diagram of precipitation at 18N, beginning at time of initial ramp-up of land forcing. Maximum land forcing reached at day 100.

low-level anticyclone over the boreal hemisphere ocean, with easterlies from 16N to 20N, strong northerly flow near the western coast of the continent, and strong southerlies at the eastern coastline.

An intense low-level easterly jet along the coastline develops baroclinic waves, which travel westward at speeds from 2 to 4 m/s. These disturbances generate precipitation where southerly flow brings moist oceanic air across the coastline in conjunction with deep ascent; most of the precipitation over the coastal landmass is associated with these waves (eg. Figure 4-35 for $THF_0 = 140W/m^2$). The waves are similar to that seen in the $THF_0 = 130W/m^2$ case with 360° landmass, but these waves only traverse the continent (Figure 4-14) where the easterly jet exists, and quickly dissipate over the ocean. The disturbances are approximately 60° in longitudinal extent. The composite vertical structure of the waves shows an eastward tilt with height of the eddy fields of meridional wind, temperature, and vertical velocity up to 700 mb, with a westward tilt above 700 mb (not shown); this structure is indicative of a baroclinic wave associated with an easterly jet (Thorncroft and Hoskins, 1994). The

Eliassen-Palm flux (not shown) indicates wave generation between 10N and 25N, centered at 700 mb and extending up to 550 mb. The waves are warm-core, with large-scale ascent in the warm sector and subsidence in the cold sector. The humidity field is strongly correlated with the meridional velocity, with high moisture content in regions of southerly flow and dry conditions in regions of northerly flow.

As the land forcing is increased to $THF_0 \geq 140 W/m^2$, a local maximum in precipitation develops over the southeastern corner of the continent (Figure 4-33), intensifying and growing in extent as the forcing increases. In the southeast corner, easterly flow from the ocean meets with southwesterly flow along the southern coastline, diagonally traversing the corner of the continent before reaching the midlatitude ocean. The precipitation is nearly constant in time, and the boundary layer moist static energy develops a local maximum over the corner of the continent (Figure 4-36). Over the central and western continent, the land remains relatively arid, with an easterly jet and associated waves along the coast which bring westward propagating bands of precipitation (Figure 4-35).

8N Coastline The coastline is shifted equatorward to ϕ_L =8N while retaining the 180° landmass and the summer-like SSTs given by (3.8). The time mean flow is similar to that seen in the case with ϕ_L =16N coastline: precipitation over the continent is largely confined to the coastal region, with strongest steady precipitation in the southeast corner, and westward propagating disturbances over the central and western region of the continent (Figure 4-37). For $THF_0 \leq 130\, W/m^2$, a low level thermally balanced easterly jet occurs along the coastline. For $THF_0 \geq 140\, W/m^2$, there is sufficient rainfall along the coastal landmass to reduce the sensible heat flux considerably, resulting in a temperature maximum which is approximately 15° inland, so that the easterly jet is centered over the subtropical continent rather than over the ocean (Figure 4-38).

The time mean precipitation over the subtropical continent is significantly greater than in the corresponding cases with $\phi_L = 16N$ coastline. For $THF_0 \leq 140 W/m^2$, the precipitation maximum is located over the tropical ocean, with weaker rainfall over the continent dominated by baroclinic eddies. The precipitation associated with individual wave disturbances is clearly greater than in the 16N case. The $THF_0 = 120\, W/m^2$ case has the fastest westward propagating waves, which have a speed of approximately $2.5\, m/s$, while wave speeds of about $1.5\, m/s$ are seen for $THF_0 \geq 130\, W/m^2$. The boundary layer moist static energy maximum remains offshore for $THF_0 \leq 130\, W/m^2$, and all of the precipitation over the subtropical continent is associated with the baroclinic waves in these cases. For $THF_0 = 140\, W/m^2$, there is a weak maximum in h_b over the central and eastern continent near 14N, but not over the western edge of the continent. In this case, the eastern half of the continent develops areas of constant rainfall, while the western half of the continent only

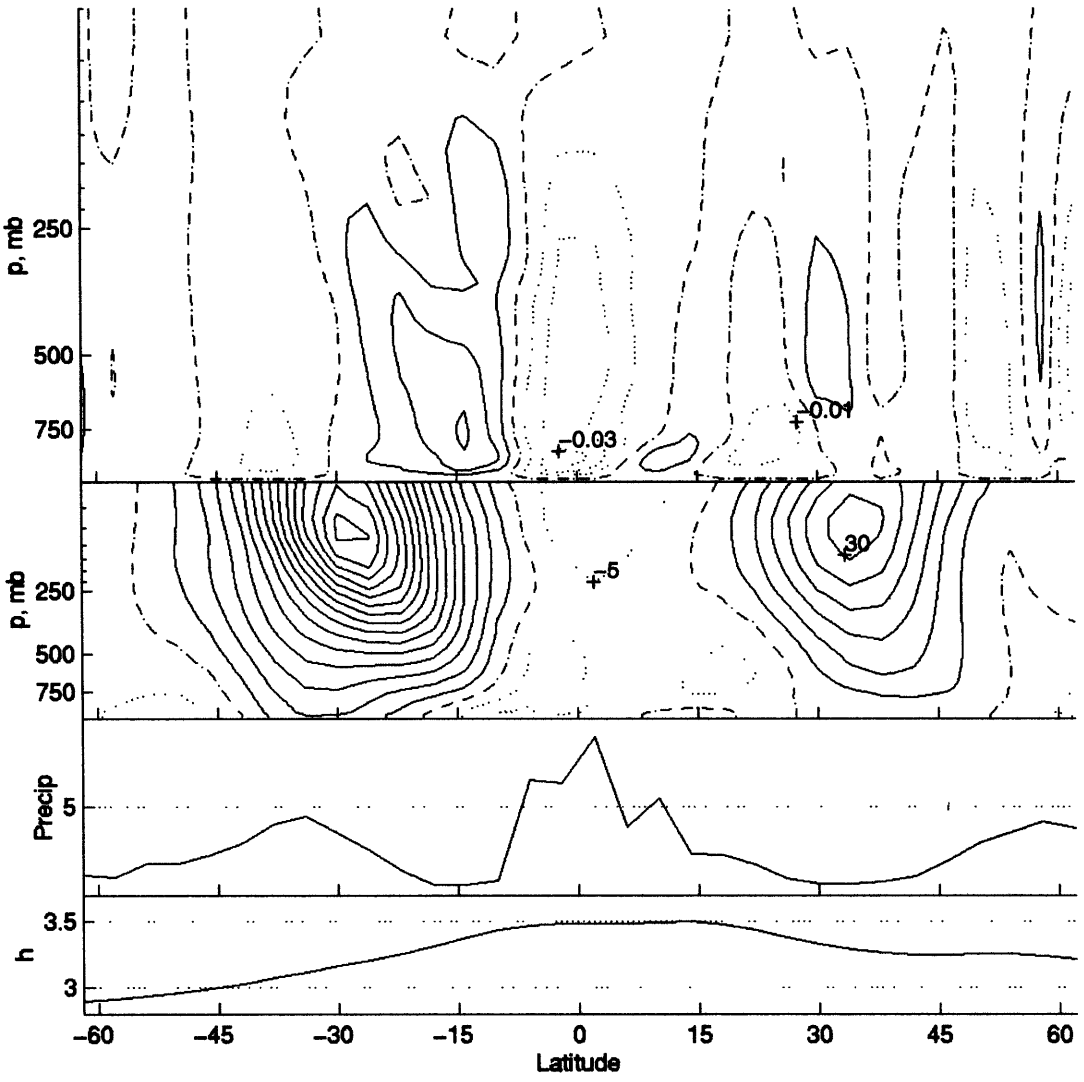

Figure 4-36: 180° continent, coastline at ϕ_L =16N, $THF_0 = 140\,W/m^2$, summer SSTs; zonal mean taken over land only, 100 day time mean. Top, ω, contour interval 1E-2 Pa/s, dotted lines indicate ascent, solid lines indicate subsidence, dash-dot is zero contour. Upper center, zonal wind, contour interval 5 m/s, dotted line indicates easterlies, solid lines indicate westerlies. Lower center, precipitation, mm/day. Bottom, 1000 mb moist static energy, $10^5 J$.

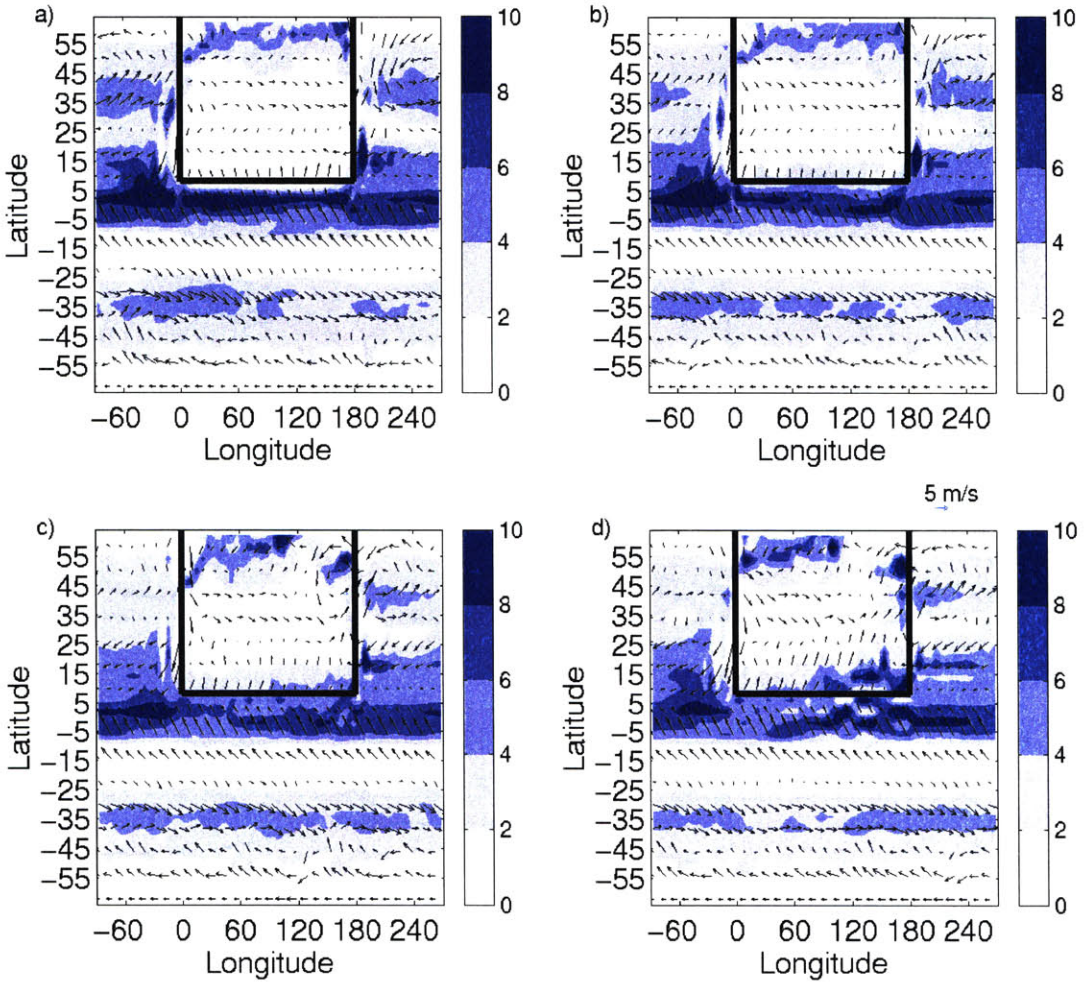

Figure 4-37: 1000 mb wind and precipitation, 180° continent, ϕ_l = 8N with summer SST distribution. Contour interval 2 mm/day. a) $THF_0 = 120\,W/m^2$; b) $THF_0 = 130\,W/m^2$; c) $THF_0 = 140\,W/m^2$; d) $THF_0 = 150\,W/m^2$.

sees precipitation associated with westward propagating waves. With greater surface forcing ($THF_0 = 150\,W/m^2$), there is a distinct maximum in h_b over the continent, which has a southwest-northeast tilt, reaching further inland on the eastern side of the landmass but remaining close to the coastline on the western edge. In this case, widespread precipitation develops over the central and eastern continent, with wave-induced precipitation dominant only over the western third of the coastline.

24N Coastline The coastline is shifted poleward to ϕ_L =24N, with land surface forcing also shifted so that $\phi_T = 16N$ in (3.7). The summer-type SST distribution is retained (3.8). In this case, the south coast of the continent remains very arid, except for along the eastern boundary of the landmass (Figure 4-39). South of the continent, precipitation occurs over the ocean between 6S and 16N, with two intense peaks at 6N and 14N. The 14N precipitation peak is associated with the local summer Hadley circulation, whose subsidence branch is located over the coastal regions, suppressing deep moist convection there. The southern edge of the continent is much more arid than in the corresponding cases with coastline at 8N or 16N (Figures 4-33, 4-37). An easterly jet in thermal balance with poleward-increasing temperatures in the lower troposphere along the coastline is centered near 850 mb, lower than in the 16N coastline case. There is little sign of baroclinic wave activity in the flow field or Eliassen-Palm flux, especially for $THF_0 \leq 140\,W/m^2$. In the $THF_0 = 130\,W/m^2$ case, there are only weak, sporadic, and short-lived precipitation events over the coastal continent; some of these events propagate eastward (not shown) and appear to be associated with disturbances of the midlatitude westerly jet. In the $THF_0 = 140\,W/m^2$ case, a few localized intense precipitation events occur over the eastern region of the continent; these disturbances remain nearly stationary and persist for up to 100 days. A few westward-propagating waves are observed in the $THF_0 = 150\,W/m^2$ case, but these are weak and short lived, with little associated precipitation. In all of the cases with 24N coastline, there is an area of moderate, persistent rainfall along the eastern coast of the continent where westerly flow over the continent meets easterly flow over the subtropical ocean (Figure 4-39).

Applying Axisymmetric Theory to Asymmetric Cases

For the cases with uniform, warm ocean SSTs, the monsoon circulation is similar in many ways to that found with symmetric continent. The precipitation and deep ascent over land occurs over the entire longitudinal extent of the continent, and does not show the east-west tilt found in observations; in fact, the rainfall is greater over the western continent than over the east. The maximum subcloud moist static energy occurs inland, with precipitation slightly equatorward of this maximum. The flow over the central and western continent is southwesterly at low levels, similar to that seen in the case with zonally symmetric continent.

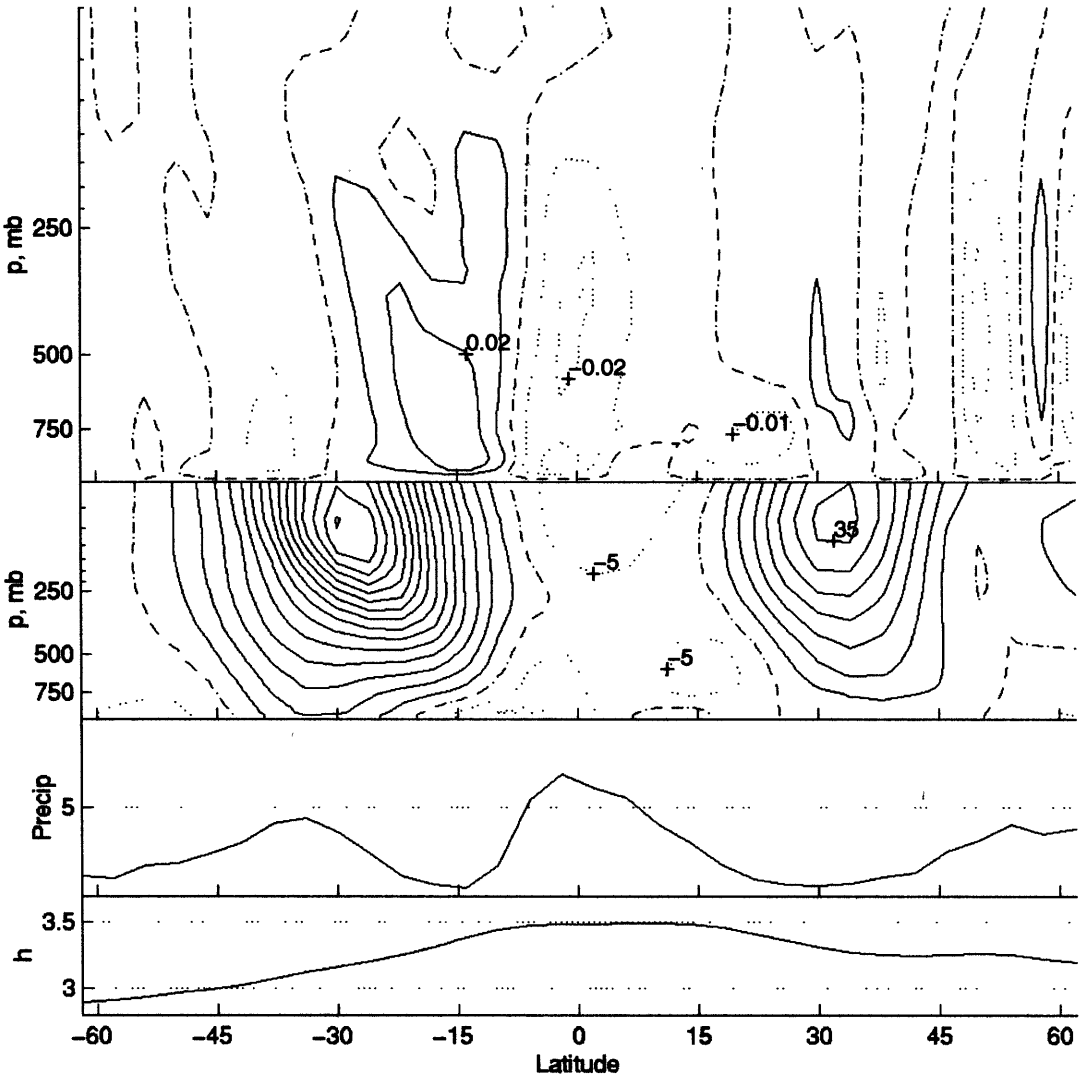

Figure 4-38: 180° continent, coastline at ϕ_L =8N, $THF_0 = 140\,W/m^2$, summer SSTs; zonal mean over land only, 100 day time mean. Top, ω, contour interval 1E-2 Pa/s, dotted lines indicate ascent, solid lines indicate subsidence, dash-dot is zero contour. Upper center, zonal wind, contour interval 5 m/s, dotted line indicates easterlies, solid lines indicate westerlies. Lower center, precipitation, mm/day. Bottom, 1000 mb moist static energy, $10^5 J$.

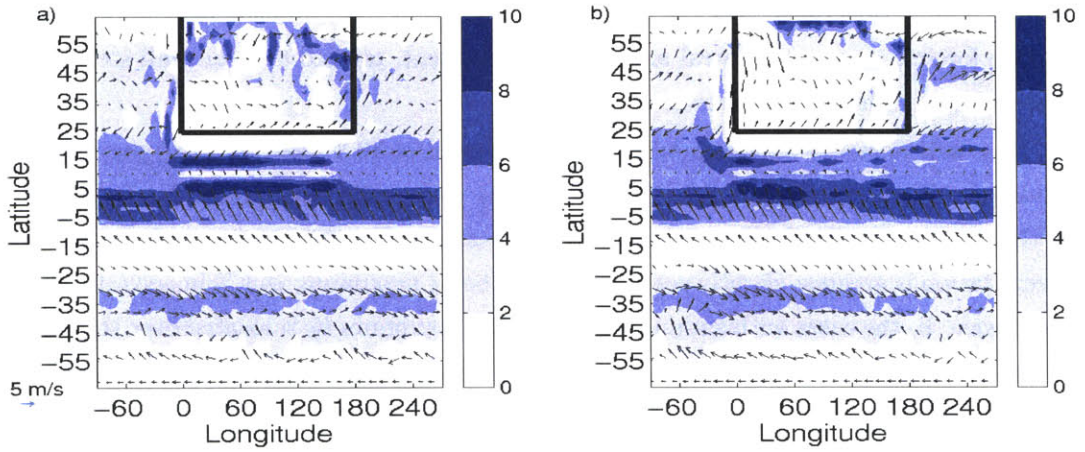

Figure 4-39: 1000 mb wind and precipitation, 180° continent, $\phi_l = 24$N with summer SST distribution, 100 day time mean. Contour interval 2 mm/day. a) $THF_0 = 130\,W/m^2$; b) $THF_0 = 150\,W/m^2$.

The monsoon has more widespread precipitation over the subtropical continent than in the zonally symmetric continent case, where there is a sharp latitudinal peak in rainfall.

There are several important differences between the uniform SST cases with symmetric and asymmetric continents. In the asymmetric continent cases, the meridional circulation does not become cross-equatorial, even for the strongest surface forcing. There are multiple factors which may account for the localized nature of the overturning cell. First, the monsoon occurs quite far inland, more so than in the zonally symmetric continent case. As shown in the two dimensional aquaplanet setup, the meridional circulation may become localized and confined to a single hemisphere when the ascent region is shifted poleward. Second, the asymmetry of the large-scale flow, with ascent over the continent and subsidence over the subtropical ocean to the west, may dominate the flow in such a way as to prevent a cross-equatorial circulation. Because a region of strong subsidence exists to the west of the monsoon, the total subsidence needed to balance the monsoon ascent is decreased. Thus, the limited region between the equator and the continent supports sufficient subsidence in the asymmetric continent case, but in the zonally symmetric continent case, a greater region of subsidence may be required, necessitating cross-equatorial flow.

With a summer-like ocean SST distribution and asymmetric continent, the behavior of the large-scale monsoon is drastically different with zonally symmetric continent. Even for very strong land surface forcing, there is no recognizable meridional overturning monsoon circulation in the asymmetric continent case. The monsoon shows a pronounced southwest-northeast tilt, with strongest precipitation in the southeastern corner of the continent, and much weaker precipitation over the central and western continent. Widespread steady

rainfall is only observed only in the southeastern corner of the landmass for cases with strong surface forcing. Over the central and western continent, rainfall does not fall steadily, but is associated with transient waves.

How well does the axisymmetric theory discussed in §3.3 describe the behavior of the monsoon with asymmetric forcing? In the cases with uniform ocean SST, the boundary of the meridional circulation occurs near the latitude of maximum h_b, and the monsoon precipitation is greatest slightly equatorward of the h_b maximum; this is in accordance with the theory. In the cases with summer-like SST, the maximum h_b is located over the tropical ocean for weak to moderate land surface forcing, and for strong forcing, the h_b maximum is located over the land only over the eastern continent. Where the h_b maximum is located near or equatorward of the coastline, precipitation over the continent is associated with baroclinic waves only; where the h_b maximum is located over the land, steady precipitation occurs over the landmass slightly equatorward of this maximum. This indicates two different dynamical regimes, depending on the location of the h_b maximum. In fact, these results are similar to those found in cases with zonally symmetric continent: westward propagating baroclinic waves dominate the precipitation field over the continent when there is no h_b maximum over land (eg. $THF_0 = 130 W/m^2$ case, §4-12), and widespread steady precipitation with strong deep ascent occurs when the h_b maximum is located inland.

The ocean SST distribution clearly has a strong impact on the monsoon. We hypothesize that the advection of low moist static energy air from the cool midlatitude oceans into the continental interior acts to change the distribution of continental h_b, thus affecting the strength and location of the monsoon. Chou et al. (2001) have shown that changes in the meridional flux of heat in the ocean from the tropics into the midlatitudes can strongly affect the geometry of the monsoon by altering the advection of moist entropy from the oceans. This theory will be explored further in §4.3.1, where low-level flow from the oceans into the continent will be blocked.

4.2.3 Africa

An Africa-like extension is added to the 180° continent in order to examine the monsoon flow with a slightly more realistic continental geometry. The extension is 60° in longitudinal width, and extends from 30S to the coastline; it is attached to the western side of the continent (Figure 4-40). Surface forcing is given by (3.7) over the land, with a summer-like SST distribution (3.8). In one case, the coastline of the eastern continent is situated at 16N; in a second case, the coastline is located at 24N. A strong land surface forcing of $THF_0 = 150\, W/m^2$ is tested for both cases, and a weaker forcing of $THF_0 = 130\, W/m^2$ is tested for the 16N coastline case.

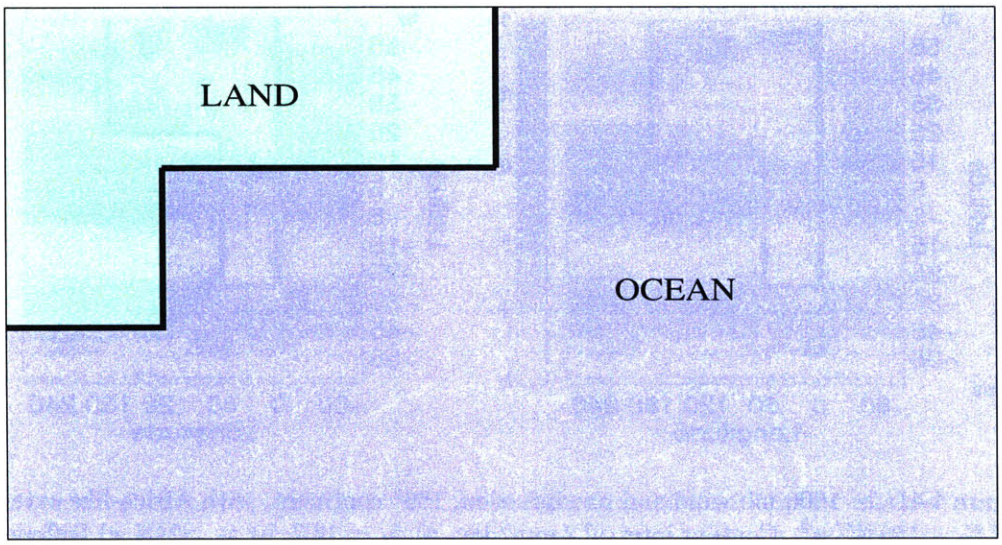

Figure 4-40: Schematic diagram of land configuration with Africa-like extension.

The greatest differences between these cases and the previous experiments occurs over the Africa-like extension. The ITCZ is much narrower and weaker over the extension than over the tropical ocean, occurring near the equator (Figure 4-41a,b). In the northern hemisphere tropics, the boundary layer moist static energy is decreased near and equatorward of the coastline, where the land is more arid than the adjacent tropical ocean (Figure 4-41c,d). In the southern hemisphere, the subtropical low level anticyclone is much weaker over the continental extension than over the ocean regions. A strong anticyclone is located over the ocean, with northerly flow near the eastern coastline of the extension, and southerlies near the western coastline of the extension.

The case with 16N coastline and $THF_0 = 130\,W/m^2$ (not shown) does not differ significantly over the subtropical continent from the corresponding case without land extension (Figure 4-33). There is very little difference in the flow or precipitation over the southeastern corner of the continent, but there is a slight increase in precipitation over the central continent, and a decrease in precipitation over the western subtropical continent. The central subtropical continent shows a region of increased h_b, where westerly flow advecting air from the midlatitudes is weaker. Most of the precipitation along the coastal continent is associated with westward propagating waves, but rainfall associated with these disturbances dies out after reaching the continental extension.

For the $THF_0 = 150\,W/m^2$ case with 16N coastline (Figure 4-41a,b), precipitation increases along the central region of the subtropical continent, where the h_b is significantly greater than in the case without the continental extension. The westward propagating disturbances are seen to traverse the entire width of the continent, although they do begin

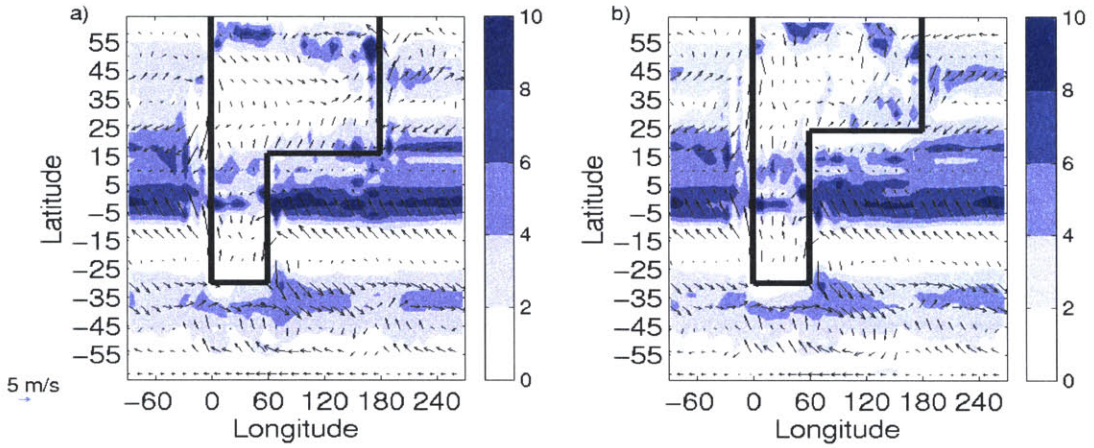

Figure 4-41a,b: 1000 mb wind and precipitation, 180° continent, with Africa-like extension, $THF_0 = 150\,W/m^2$. Contour interval 2 mm/day. a) $\phi_L = 16$N; b) ϕ_L =24N. c) Difference in 1000 mb winds and precipitation between Africa case and case without extension, ϕ_L =24N, contour interval 2 mm/day. d) Difference in 1000 mb winds and h between Africa case and case without extension, ϕ_L =24N, contour interval 1.1E4 J.

to weaken over the extension. The subcloud moist static energy (Figure 4-41c,d) is also greater over the interior of the continent along the western edge.

For $\phi_L = 24$N and land forcing of $THF_0 = 150W/m^2$, the boundary layer moist static energy is greatly increased over the subtropical and midlatitude continent, especially over the western half of the landmass (Figure 4-41c,d). The northwesterly inflow of air from the oceans into the continental interior is again weaker than in the case without continental extension. There is considerably greater precipitation over the subtropical continent (Figure 4-41a,b), associated with persistent, nearly stationary disturbances. There is little sign of westward propagating waves, as in the case without the continental extension and coastline at 24N.

There are two features of these results which are particularly notable. First, there is no dry region over the continental extension, equivalent to the Saharan desert. This may be due to the relative weakness of the monsoon in these cases, especially in light of the work of Rodwell and Hoskins (1996), who found that Rossby waves generated by forcing in the monsoon region cause subsidence to the west; this type of subsidence is seen in the uniform ocean cases of §4.2.1, but not in the summer ocean cases with weaker monsoon. Also, there is no albedo feedback in our model, which is a strong factor in the Saharan desert (Charney, 1975). The second feature is that the westward propagating waves travel across the continental extension, and that the precipitation associated with these waves is enhanced in areas of increased h_b. Changes in flow over the continental extension impact precipitation over the subtropical continent by decreasing the advection of low h_b air from

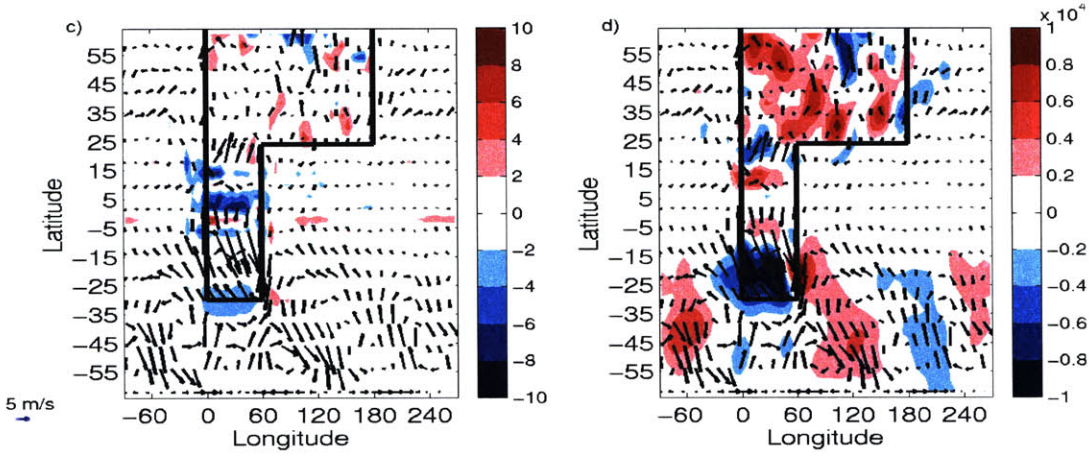

Figure 4-41c,d: Continued from Figure 4-41a,b.

the ocean into the continental interior.

4.2.4 Pole-to-pole continent

Baroclinic waves along the equatorward coastline of the continent have been shown to strongly affect monsoon precipitation with an asymmetric continent. These waves are caused by instability of a low level easterly jet which forms along the coastline where there is a temperature contrast between the relatively cool ocean and the strongly heated continent. A popular continental configuration amongst simple models of the monsoon is that of a landmass centered on the equator, with coastlines that run north-south, but no east-west coastline in the tropics or subtropics (Figure 4-42). This configuration lacks the meridional temperature contrast which would generate baroclinic waves - several published studies with this configuration of continent have found that the continent remains very arid, with precipitation confined to a local region along the eastern coast of the continent (ex. Cook and Gnanadesikan (1991), Chou et al. (2001)). Given the popularity of this choice of continental geometry in modeling studies, the impact on the monsoon flow is of particular interest. To investigate, a continent 180° in longitudinal width which extends from 64N to 64S (the model boundaries) is used with a boreal summer meridional distribution of SST (3.8). A diagram of the continental configuration is shown in Figure 4-42.

First, a range of land forcing strength is tested with forcing given by (3.7) with maximum land forcing at $\phi_T = 16N$. For weak land forcing of $THF_0 = 130\,W/m^2$, the continent is very arid, with precipitation occurring over the land only near the northern and southern boundaries of the model, and along the immediate coast in the tropics (Figure 4-43a,d). This distribution of precipitation with arid continental interior is close to that found by Cook and Gnanadesikan (1991). The boundary layer moist static energy is greater over the tropical

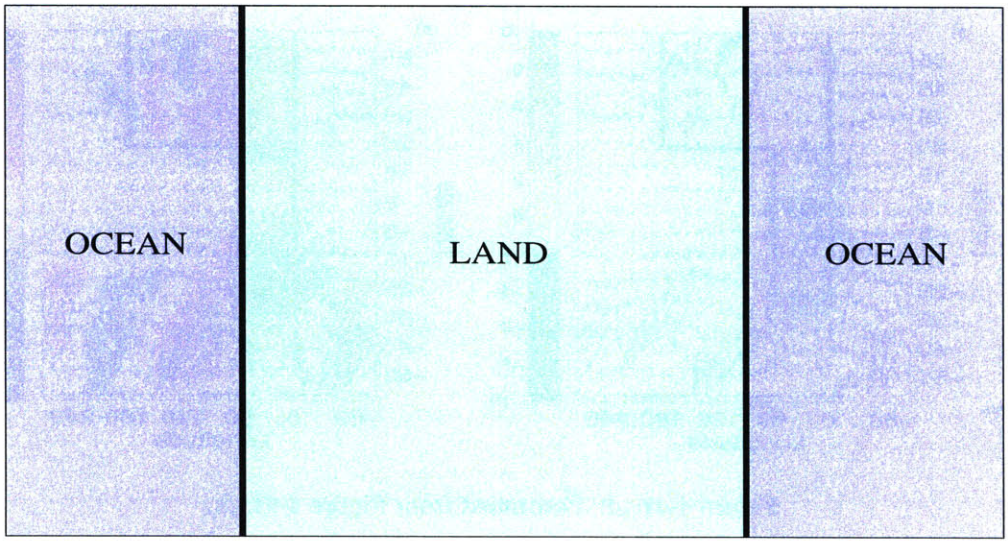

Figure 4-42: Schematic diagram of land configuration with pole-to-pole continent.

ocean than over the landmass. The zonal mean h_b over the land has a sharp peak between 5N-10N, with much lower h_b in the nearby subtropics, which are under areas of subsidence and experience little rainfall. The air temperature maximum in the lower troposphere occurs near the greatest surface forcing at 16N; dry adiabatic convection distributes this heating up above 600 mb. An easterly jet in balance with this temperature gradient is centered near 500 mb at 10N. Westward propagating waves are observed in the meridional velocity field which are associated with baroclinic instability of the easterly jet; however, there is little precipitation associated with the disturbances. The large-scale flow is strongly asymmetric, especially over the eastern third of the continent. Deep ascent (not shown) occurs primarily over the tropical ocean near the SST maximum at 8N, with subsidence over the western equatorial ocean and southern hemisphere continent. Meridional flow over the landmass features two sloppy Hadley cells with subsidence in the subtropics and two centers of ascent near 8S and 12N (not shown).

As the land forcing is increased to $THF_0 = 140W/m^2$, light precipitation occurs over the continental interior in the tropics; rainfall amounts remain much less than over the tropical and subtropical oceans (Figure 4-43a,d). The boundary layer moist static energy (not shown) is less over land than over the tropical oceans. There is a double-peaked broad precipitation maximum in the tropics, with greatest continental precipitation near 14N and a secondary maximum near 2S. Rainfall near 14N was primarily associated with westward propagating baroclinic disturbances, while rainfall near 2S was associated with eastward propagating tropical waves. The zonal mean zonal wind field over land has two low level easterly jets, a stronger jet centered near 6S at 600 mb, and a slightly weaker jet centered

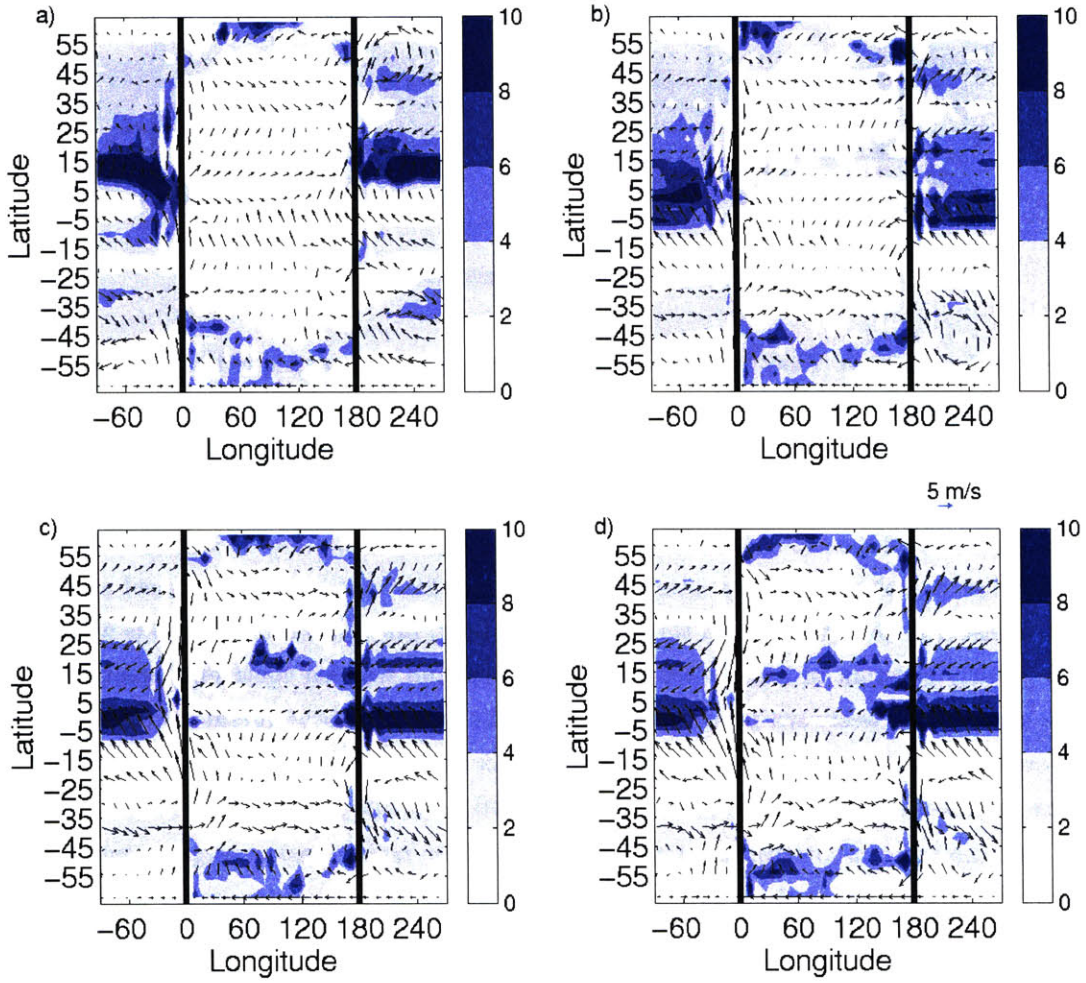

Figure 4-43a,d: 1000 mb wind and precipitation, pole-to-pole continent, SST maximum at 8N, 100 day time mean. Contour interval 2 mm/day. a) ϕ_T = 16N, $THF_0 = 130\,W/m^2$; b) ϕ_T =16N, $THF_0 = 140\,W/m^2$; c) ϕ_T =16N, $THF_0 = 150\,W/m^2$; d) ϕ_T =8N, $THF_0 = 150\,W/m^2$; e) ϕ_T =24N, $THF_0 = 150\,W/m^2$; f)ϕ_T =16N, SST maximum at 0N, $THF_0 = 150\,W/m^2$

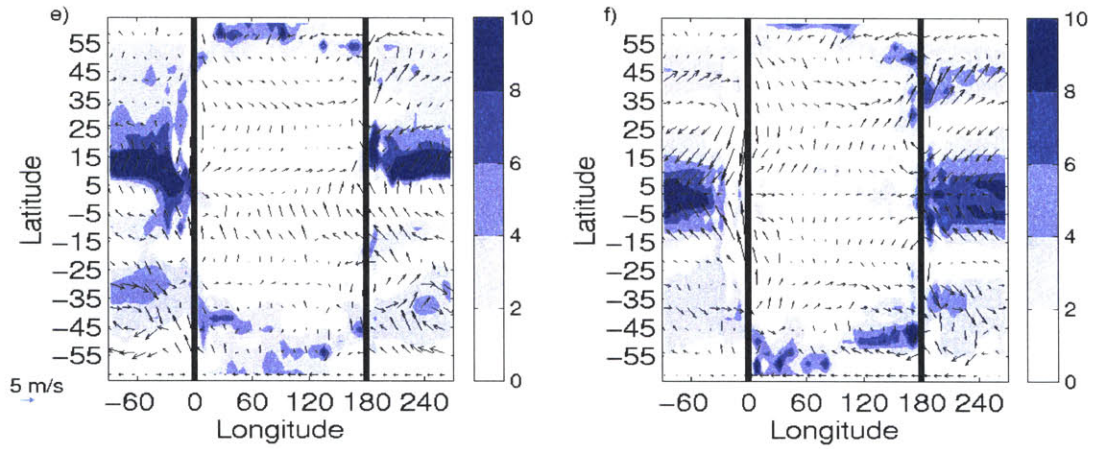

Figure 4-43e,f: Continued from 4-43a,d

near 18N at 550 mb. Flow over the continent is strongly asymmetric in longitude, especially in the tropics.

When a strong land forcing is applied ($THF_0 = 150W/m^2$), a band of precipitation develops over the interior of the continent near 18N, with strongest rainfall over the central and eastern continent (Figure 4-43a,d). The boundary layer moist static energy field (Figure 4-44) has a global maximum over the central continent, with a pronounced southwest-northeast tilt. Over the eastern third of the continent, precipitation near 18N is widespread and nearly constant in time, while over the central and western continent, precipitation is associated with westward propagating waves. The zonal mean temperature field over land shows a low level maximum near 28N, with a weak easterly jet near 22N. The Eliassen-Palm flux indicates strong baroclinic activity associated with this jet below 500 mb.

As the greatest precipitation and boundary layer moist static energy occur near the latitude of greatest land surface forcing in the $\phi_T = 16N$ case, two other choices of ϕ_T are tested with a range of forcing magnitudes. The SST maximum remains at 8N for all of these cases. As the land forcing maximum is shifted equatorward to $\phi_T = 8$N (Figures 4-43a,d), the resulting flow and precipitation fields are very similar to that found with the $\phi_T = 16$N cases. When the land surface forcing maximum is shifted poleward to 24N, there is very little change in the location of precipitation or in the geometry of the flow field from the 16N case (Figure 4-43e,f). This indicates an insensitivity of the large-scale flow to the land surface forcing. The distribution of moist static energy helps to explain this behavior: as shown in Figure 4-44, the h_b profile over the continent is not significantly altered by the relocation of the surface forcing. As in the previous cases with asymmetric continent, advection of air from the oceans strongly influences the distribution of h_b over the continent.

In order to test this hypothesis, the ocean SST distribution is shifted equatorward, so

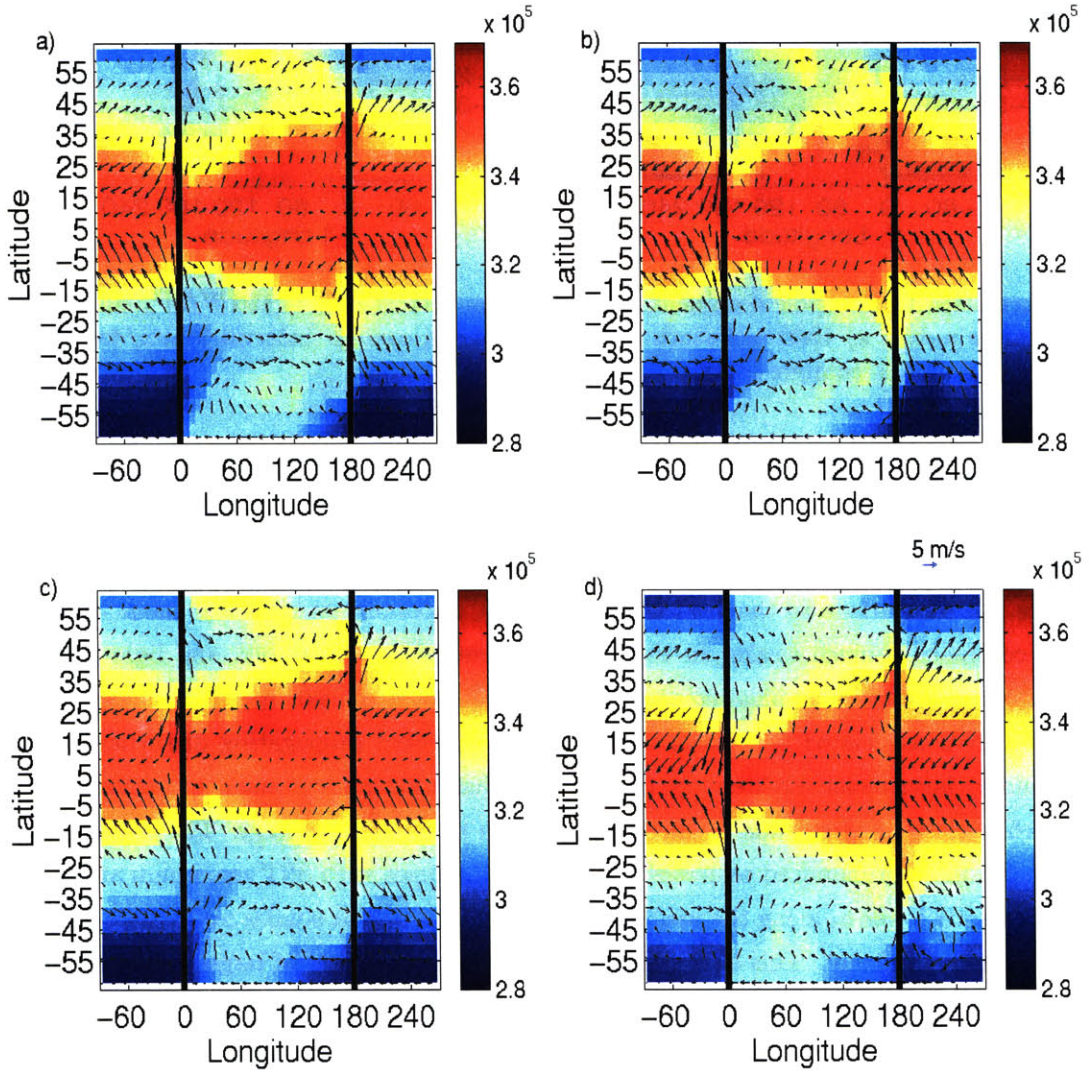

Figure 4-44: 1000 mb wind and h, pole-to-pole continent, SST maximum at 8N, 100 day time mean. Contour interval 2 mm/day. a) ϕ_T =16N, $THF_0 = 150\,W/m^2$; b) ϕ_T =8N, $THF_0 = 150\,W/m^2$; c) ϕ_T =24N, $THF_0 = 150\,W/m^2$; d)ϕ_T =16N, SST maximum at 0N, $THF_0 = 150\,W/m^2$

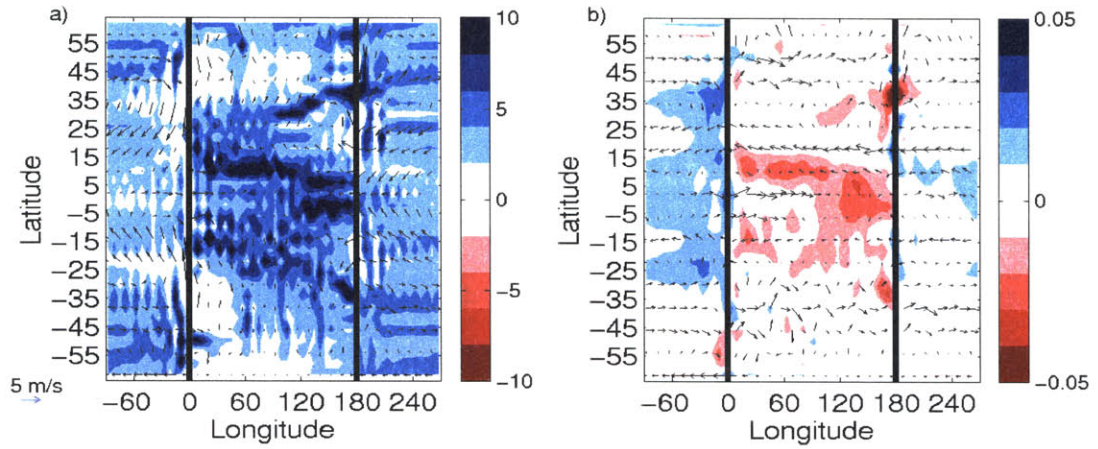

Figure 4-45: Pole-to-pole continent, uniform warm SST, $THF_0 = 150\,W/m^2$, ϕ_0 =8N, 100 day time mean. a) 1000 mb winds and precipitation, contour interval 2 mm/day. b) 500 mb winds and ω, contour interval 0.01 Pa/s.

that $\phi_0 = 0N$ in (3.8). A strong land forcing of $THF_0 = 150\,W/m^2$ is then compared with land surface forcing maximum at ϕ_T = 8N, 16N, and 24N (Figure 4-43e,f). The resulting precipitation and circulation is again insensitive to the land forcing latitude for all three cases. In comparison to the case with ocean SST maximum at 8N, the precipitation over the continent is much weaker in the northern hemisphere subtropics, and light precipitation occurs over the tropical continent. Precipitation in the northern hemisphere tropics near 10N is associated both with westward and eastward propagating disturbances. The boundary layer moist static energy (Figure 4-44) has a local maximum over the land surface which is close in magnitude to the tropical ocean moist static energy. The distribution of h_b has a more pronounced east-west tilt than in the cases with SST maximum at 8N, with significantly lower h_b along the western coastal subtropics, but similar magnitude of h_b over the eastern continent. This example emphasizes the importance of large-scale advection of h_b in controlling the strength and geometry of the monsoon.

An extreme example is found by replacing the summer-like SST distribution with a uniformly warm ocean (Figure 4-45). In a case with warm ocean, greatest land surface forcing at $\phi_0 = 8N$, and $THF_0 = 150\,W/m^2$, the large scale flow becomes extremely asymmetric. In this case, h_b is greater over the continent than over the ocean, with maximum h_b near 30N, and a secondary maximum near 20S. Strong ascent accompanied by precipitation is widespread over much of the continent from 40S to 35N. Subsidence occurs over the tropical and subtropical oceans, especially near the western coastline. There is little sign of Hadley circulation either over the continent or over the oceans, with the dominant circulation occurring from east to west.

The theory (§3.3) linking monsoon location to the boundary layer moist static energy distribution does not hold up well for these cases where the meridional circulation is weak and the flow highly asymmetric. However, the relative magnitude of the h_b over the continent versus the ocean does give insight into the nature of the monsoon. In those cases with summer-like ocean temperatures and weak land forcing where the global maximum h_b occurs over the ocean, precipitation over the interior of the continent is associated only with baroclinic waves. When h_b develops a global maximum over the continental interior, deep ascent and widespread precipitation develops over the landmass near the location of maximum h_b.

4.3 Thin Wall

One feature of the MITGCM is the ability to prevent flow and advection between adjacent gridpoints; the 'wall' is infinitely thin but impermeable. This feature may be used to reshape the large scale flow, and as a crude representation of orography.

4.3.1 Blocking Advection

Advection of low moist static energy from the oceans and cooler midlatitudes appears to significantly affect the scale and intensity of the monsoon, especially in the case with 180° continent and summer-like SSTs (§4.2.2). Westerly flow in the midlatitudes carries this low h_b air into the interior of the continent, suppressing convection and causing a pronounced east-west tilt of the monsoon. The impact of the advection of moist static energy is examined in two further cases which use thin walls to block flow in the lower troposphere.

In the first case, a 180° wide continent is used, with coastline at ϕ_L =16N, and $THF_0 = 140\,W/m^2$. Two thin walls are included, one along the western boundary of the continent from 16N to 64N, and the second along the eastern boundary of the continent, also from 16N to 64N. These walls extend from the surface to 700 mb, and are intended to prevent the advection of low subcloud moist static energy air from the oceans into the continental interior. The upper tropospheric flow (not shown) is relatively unimpeded by the presence of these walls. In the lower troposphere, the oceanic anticyclone does not extend over the continent in this case, so that the northerly flow along the western boundary of the continent is weak (Figure 4-46). The resulting boundary layer moist static energy field (Figure 4-47) is much greater across the entire continent, especially in the subtropics near 30N, and along the eastern edge of the continent where the flow impinges upon one of the thin walls. The zonal mean h_b maximum over the continent is located slightly inland near 20N. The time mean precipitation field (Figure 4-46) shows greater precipitation along the entire southern coastline of the continent, and also over the eastern third of the continental interior than

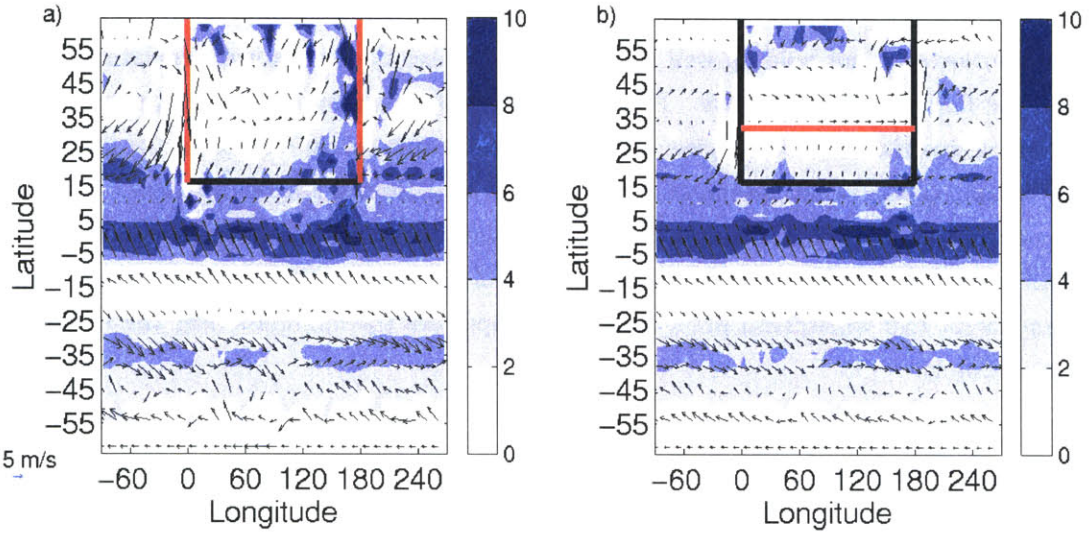

Figure 4-46: 1000 mb winds and precipitation, $THF_0 = 140\,W/m^2$, cases with thin walls, 100 day time mean. Red lines indicate wall locations. a) Thin walls along east and west coasts. b) Thin wall at 32N over continent.

the corresponding case without a wall (Figure 4-33). Over the eastern continent, rainfall is widespread and persistent, and appears to be associated with large scale ascent induced by the thin wall. Along the western coastal continent, precipitation is dominated by westward propagating disturbances.

In the second case, only one thin wall is applied to a 180° continent with coastline at 16N, and $THF_0 = 140\,W/m^2$. The wall is located at 32N, and extends from the west to the east coast of the continent, and from the surface to 700 mb. This configuration is intended to block the advection of midlatitude air into the subtropical continent. The resulting state features much greater boundary layer moist static energy (Figure 4-47) between the coastline and the wall, especially over the western region of the continent. Rainfall (Figure 4-46) is increased along the coastline, with the greatest difference just south of the coast along the western half of the land. The zonal mean h_b has a weak maximum at 18N, with local peak in precipitation at 14N. Precipitation over the subtropical continent is generally widespread, but does show some westward propagating wave activity.

In both of these experiments with blocking walls, the zonally averaged subcloud moist static energy over the subtropical continent increases in comparison to the cases without walls. The zonal mean ascent over the landmass also strengthens, with a local maximum of ω occurring near the coastline. The zonal mean meridional circulation over the continent features a single cross-equatorial cell (Figure 4-48), with deep ascent from the southern hemisphere tropics to the subtropical continent. The circulation is not closely angular

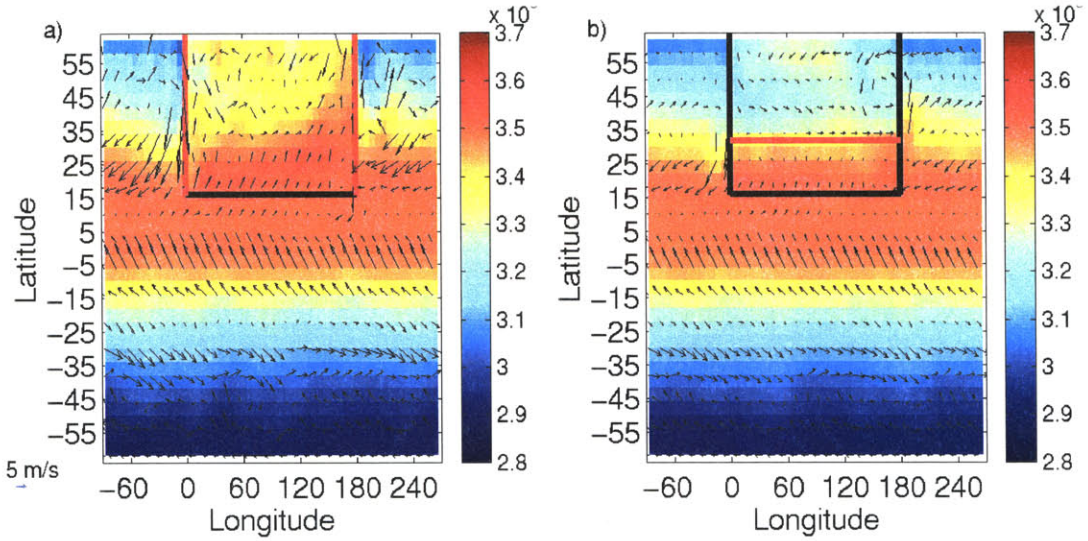

Figure 4-47: 1000 mb winds and h, $THF_0 = 140\,W/m^2$, cases with thin walls, 100 day time mean. Red lines indicate wall locations. a) Thin walls along east and west coasts. b) Thin wall at 32N over continent.

momentum conserving over the continent. The poleward limit of this ascent region is near the maximum in subcloud moist static energy.

These results illustrate the very strong impact of advection of low-level flow on the distribution of subcloud h_b and correspondingly on the monsoon. This implies that factors which affect the advection of h_b may also have a strong effect on the monsoon; these include both factors which influence the form of the large scale flow and those which influence the moist static energy content of the upstream atmosphere.

4.3.2 Cross Equatorial Wall

Observational studies (eg. Ninomiya and Kobayashi (1999), Kishtawal et al. (1994)) have shown that low level cross-equatorial flow can provide a significant fraction of the moisture which falls as monsoon rains. In the cases shown so far using the MITGCM, the flow has a strong aversion to crossing the equator in the boundary layer. To evaluate the impact of this jumping behavior on the monsoon precipitation, a thin wall which spans the equator is used to induce a local region of strong cross-equatorial flow. The thin wall extends from the surface to 700 mb, and runs from 30S to the coastline at 16N. The thin wall is tested in this configuration both with 360° and 180° continents (Figure 4-49). The presence of the thin wall is anticipated to have the greatest effect on cases which have land forcing near the threshold for incurring a monsoon; correspondingly, a range of forcings near this threshold are tested.

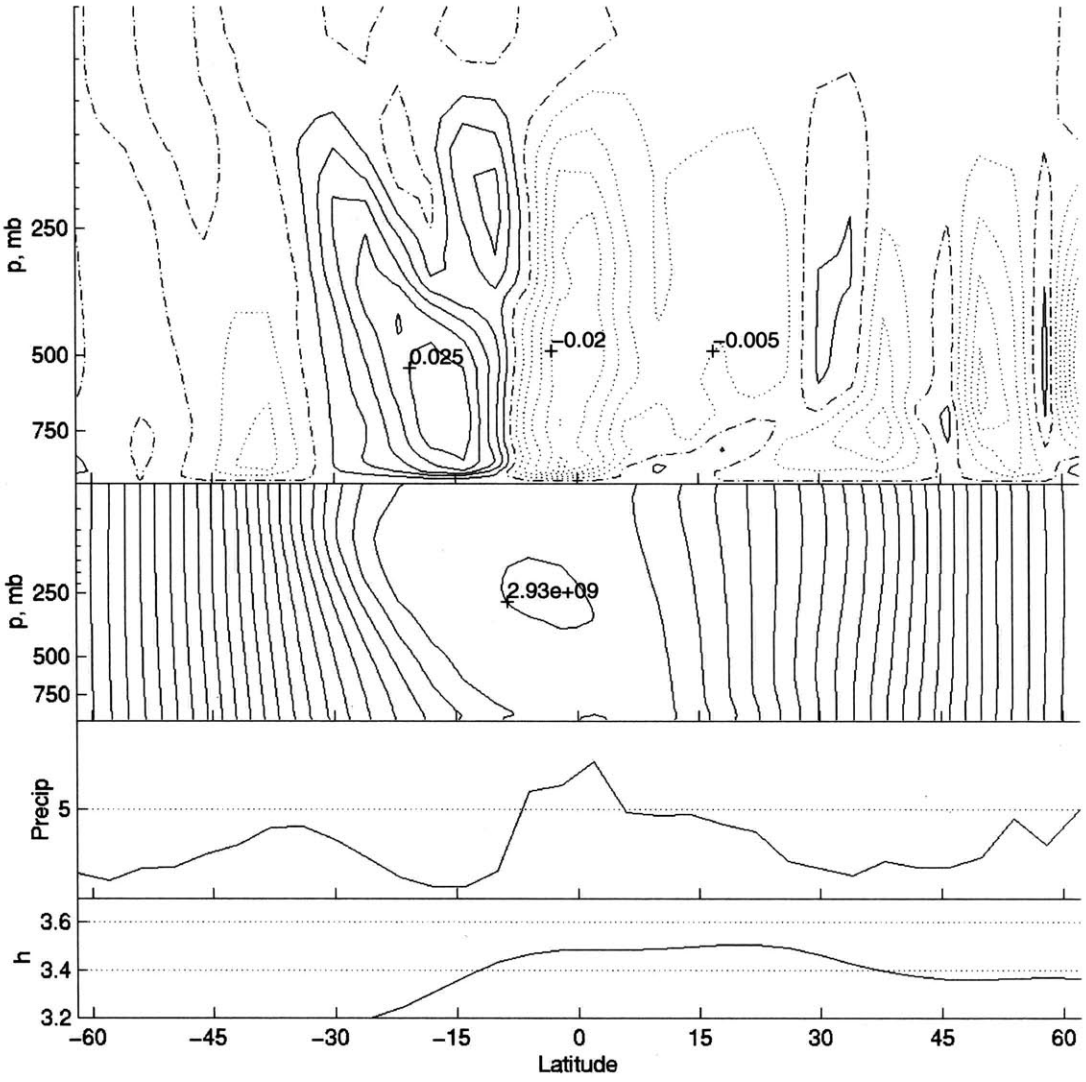

Figure 4-48: Zonal mean fields over land only, case with walls along east and west coastlines, 100 day time mean. Top, ω, contour interval 5E-3 Pa/s, dotted lines indicate ascent, solid lines indicate subsidence, dash-dot is zero contour. Upper center, absolute angular momentum, contour interval 1e8 m^2/s. Lower center, precipitation, mm/day. Bottom, 1000 mb moist static energy, $10^5 J$.

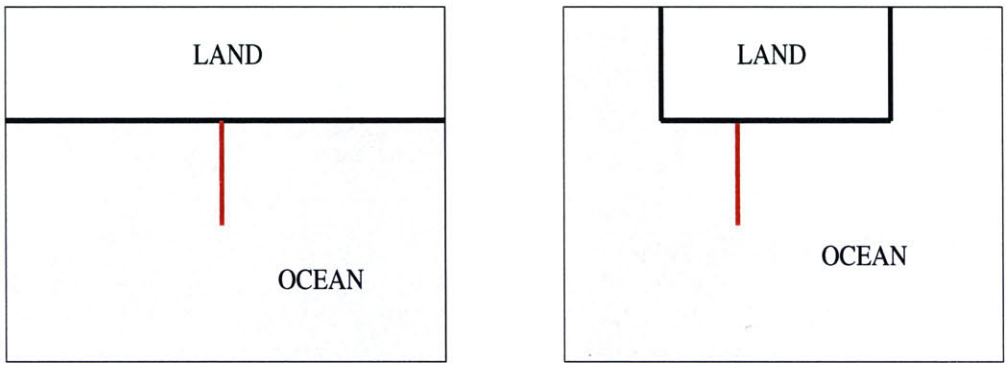

Figure 4-49: Schematic diagram of land configuration with thin wall across the equator (Red line). a) 360° continent; b) 180° continent.

360° **continent** In all cases examined, a narrow southerly jet forms just to the east of the thin wall, where tropical easterlies are deflected (Figure 4-51). This jet has a maximum near 950 mb with wind speeds at the equator of $5 - 10 m/s$, and extends from the surface to approximately 650 mb. The jet has longitudinal extent of 10°, and turns southwesterly when approaching the coastline. In two non-monsoonal cases ($THF_0 = 125, 130\, W/m^2$), the cross-equatorial jet leads to greater moisture content of the air over the tropical ocean within 60° to the east of the wall (not shown). This increase in humidity is the result of both increased moisture transport across the equator and increased surface latent heat flux due to faster wind speeds. The precipitation field (Figure 4-50a,d) shows an increase in precipitation over the tropical ocean near 14N within 60° to the east of the thin wall, but there is little effect on moisture or precipitation over the continent. In a monsoonal case ($THF_0 = 140\, W/m^2$, not shown), the thin wall leads to an increase in atmospheric moisture content along the coastline across the entire globe. However, there is little difference in the precipitation field either locally or on a worldwide scale.

180° **continent** For the cases with 180° continent, the thin wall is located 60° from the western boundary of the landmass. Again, a range of surface land forcings are tested with this configuration, from $THF_0 = 120$ to $140\, W/m^2$. The impact of the thin wall on the monsoon flow was similar for the entire range of land forcing. In addition to the creation of a southerly cross-equatorial low level jet to the east of the wall, the wall deflects southwesterly flow near the coastline on the western side of the wall, forming a local cyclonic circulation over the land (Figure 4-50a,d). In the immediate vicinity of this cyclone, where moist oceanic air is drawn inland, there is an increase in the atmospheric moisture content and the boundary layer moist static energy (Figure 4-50e,f). The westward propagating baroclinic disturbances have increased associated rainfall in this area in comparison to the

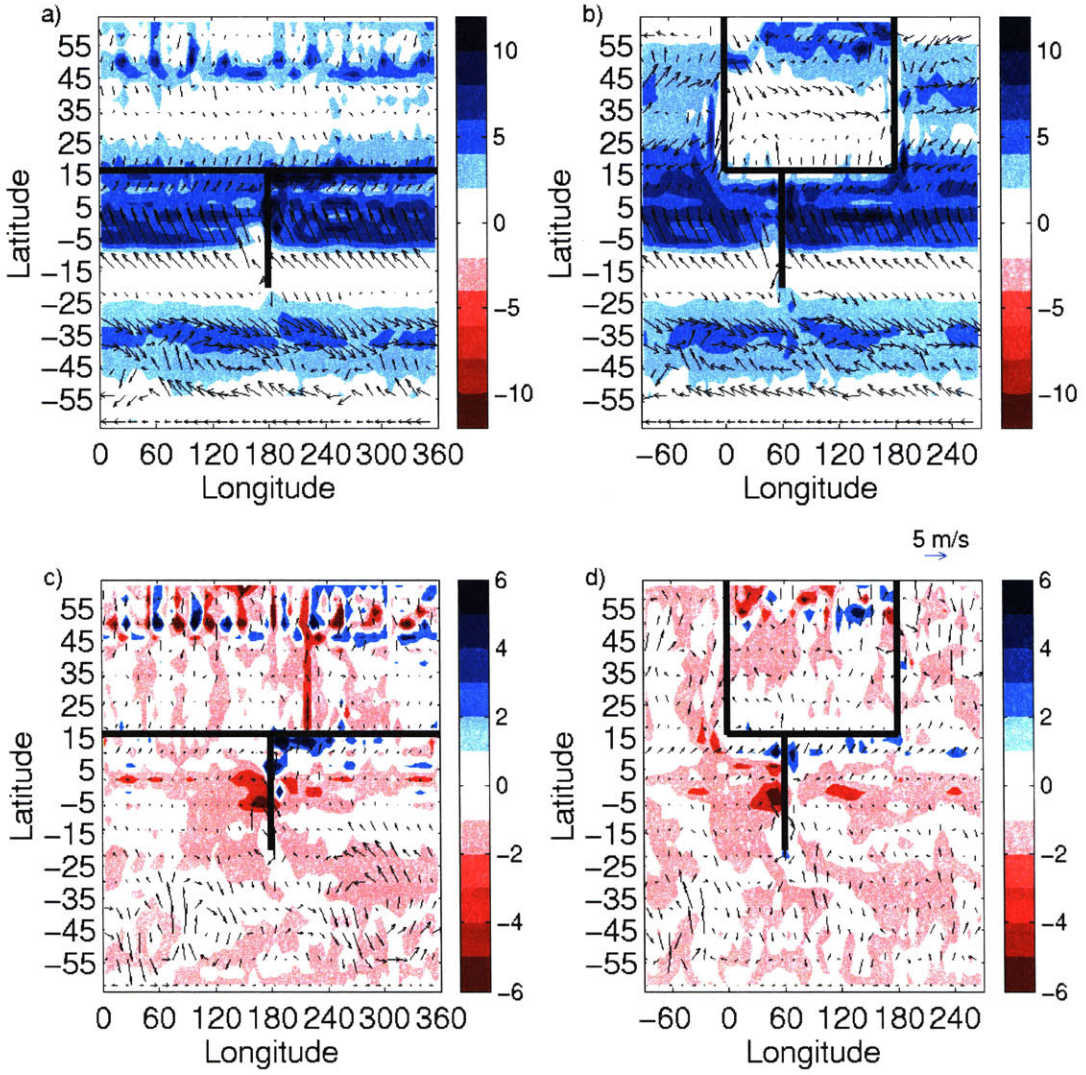

Figure 4-50a,d: Cross-equatorial thin wall cases, 100 day time mean. a), c), e) 360° continent; b), d), f) 180° continent. $THF_0 = 130\,W/m^2$. a), b) 1000 mb winds and precipitation, mm/day. c), d) Difference in 1000 mb winds and precipitation between thin wall cases and cases with no wall, mm/day. e) f) Difference in 1000 mb winds and moist static energy between thin wall cases and cases with no wall, J.

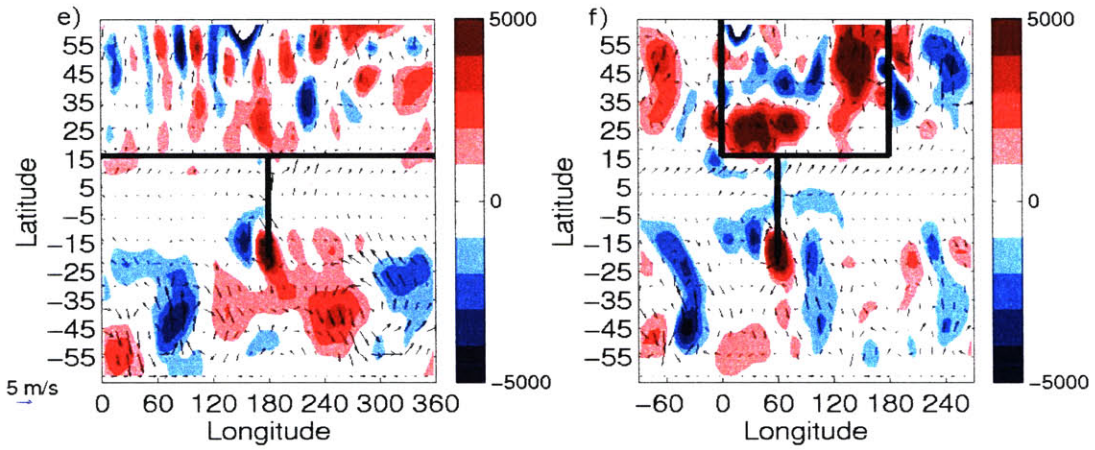

Figure 4-50e,f: Continued from 4-50a,d

cases without a thin wall; the strength of this impact varies between individual cases. The presence of the thin wall does not block propagation of the westward propagating waves. However, there is no sign of an area of persistent local precipitation, only a strengthening of rainfall associated with the waves (Figure 4-50a,d.

Although the inclusion of a thin wall at the equator results in an intense (but narrow) cross-equatorial jet, the presence of the jet does not have a significant impact upon the monsoon. The jet acts to moisten the lower troposphere near the coastline, but increased precipitation is not observed. The implication of this is that the availability of moisture is not a limiting factor for the monsoon, even when the meridional circulation shows jumping behavior. After the circulation jumps at the equator, depleting the moisture content of the air, the strong surface fluxes over the boreal tropical ocean supply enough moisture to support the monsoon.

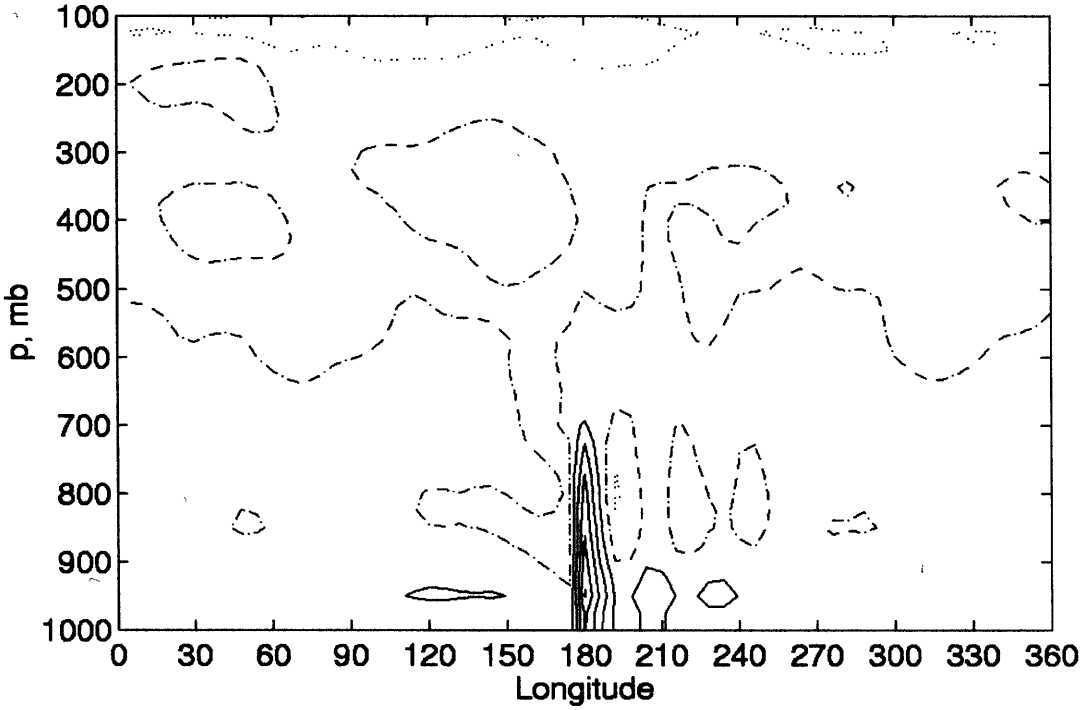

Figure 4-51: Cross-section of 100 day time-mean meridional velocity at the equator, case with 360° continent and $THF_0 = 130\,W/m^2$. Contour interval 2 m/s, solid lines southerly wind, dotted lines northerly wind, zero line in dash-dot.

Chapter 5

Observations

Both the axisymmetric theory and the model setup used in these experiments are highly idealized, which raises the question of how relevant the findings are to the real world. Observed data is examined to determine how well the model results relate to reality. Reanalysis data is chosen as a basis for study due to the good spatial and temporal coverage of the data; however, in the data-sparse tropics, reanalyses are particularly reliant on numerical models, so that error in the reanalysis data may be large. The ERA40 data set from the European Centre for Medium-range Weather Forecasting is used.

5.1 Comparing Model Results to Observed Monsoons

How similar are the observed monsoons to the monsoon circulations which are achieved in the highly idealized model? The long term mean data averaged over 45 years of ECMWF data is used here to explore the observed monsoons over Asia, West Africa, Australia, and South America.

5.1.1 West Africa

The West African monsoon is arguably the closest to a zonally symmetric monsoon: the coastline of Africa is nearly parallel to the equator at 5N; there are no significant orographic features in the local monsoon region; and the observed flow is quite symmetric. The long term mean July monsoon features a band of intense precipitation (Figure 5-1) centered near 8N which stretches from the eastern Atlantic to east central Africa; this band is nearly parallel to the equator. The low level flow over the tropical African coast is highly symmetric, with southeasterly flow near the equator shifting to southwesterly flow near the coast. The flow averaged between 10W and 10E includes a cross equatorial circulation with a narrow region of deep ascent from 5N to 12N and subsidence in the southern hemisphere

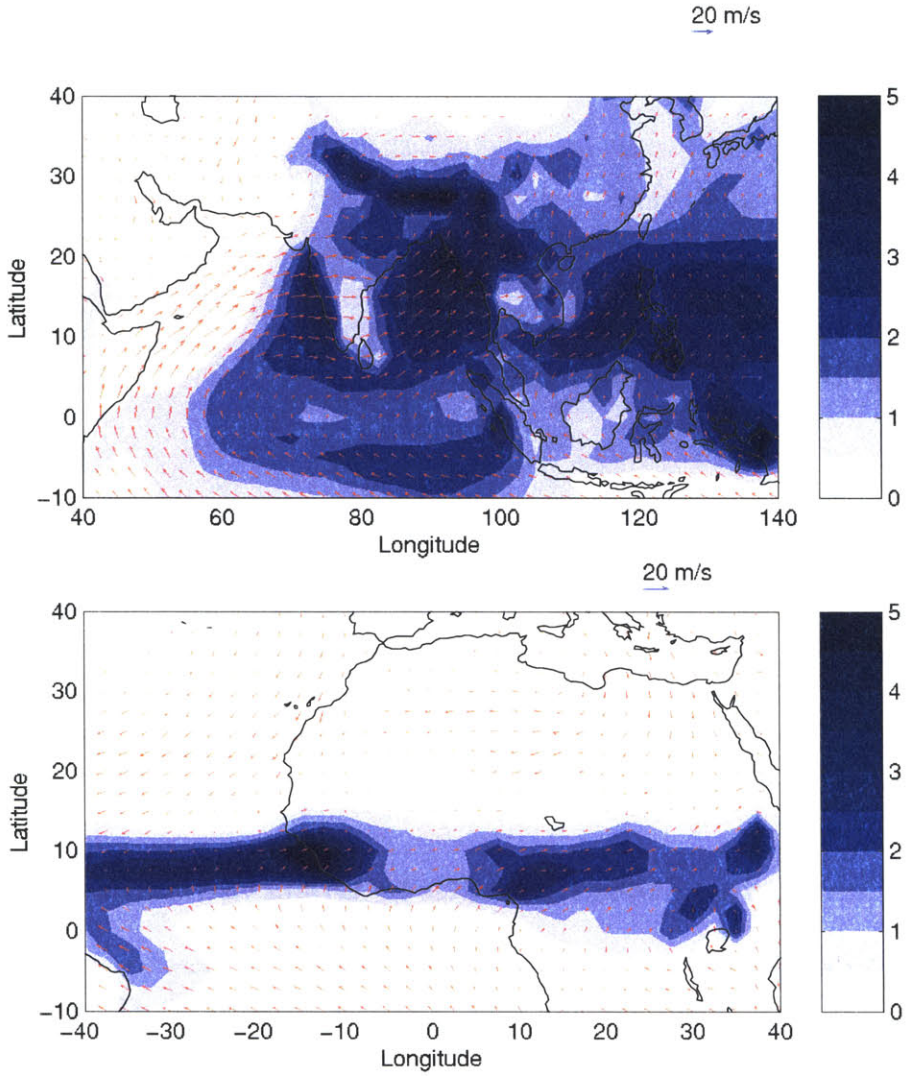

Figure 5-1: Long term mean precipitation for July, mm/day, from ECMWF reanalysis. Arrows indicate boundary layer winds. Top, Asian monsoon; bottom, West African monsoon

(Figure 5-3). There is an area of shallow, dry ascent over the desert regions from 15N to 22N, which is not considered to be part of the cross-equatorial circulation. The pattern of low level flow turning from southeasterly to southwesterly, the narrow band of precipitation located inland, and the character of the meridional circulation are similar to the GCM results with zonally symmetric continent §4.1.2, Figure 4-9.

The sum of the sensible and latent surface heat flux is estimated to be approximately $130 W/m^2$ over the West African coast in July by the ERA-40 reanalysis (Figure 5-2); this forcing level was adequate to induce a monsoon in the model with zonally symmetric continent case with 8N coastline (§4.1.3, Figure 4-18). However, surface heat fluxes are

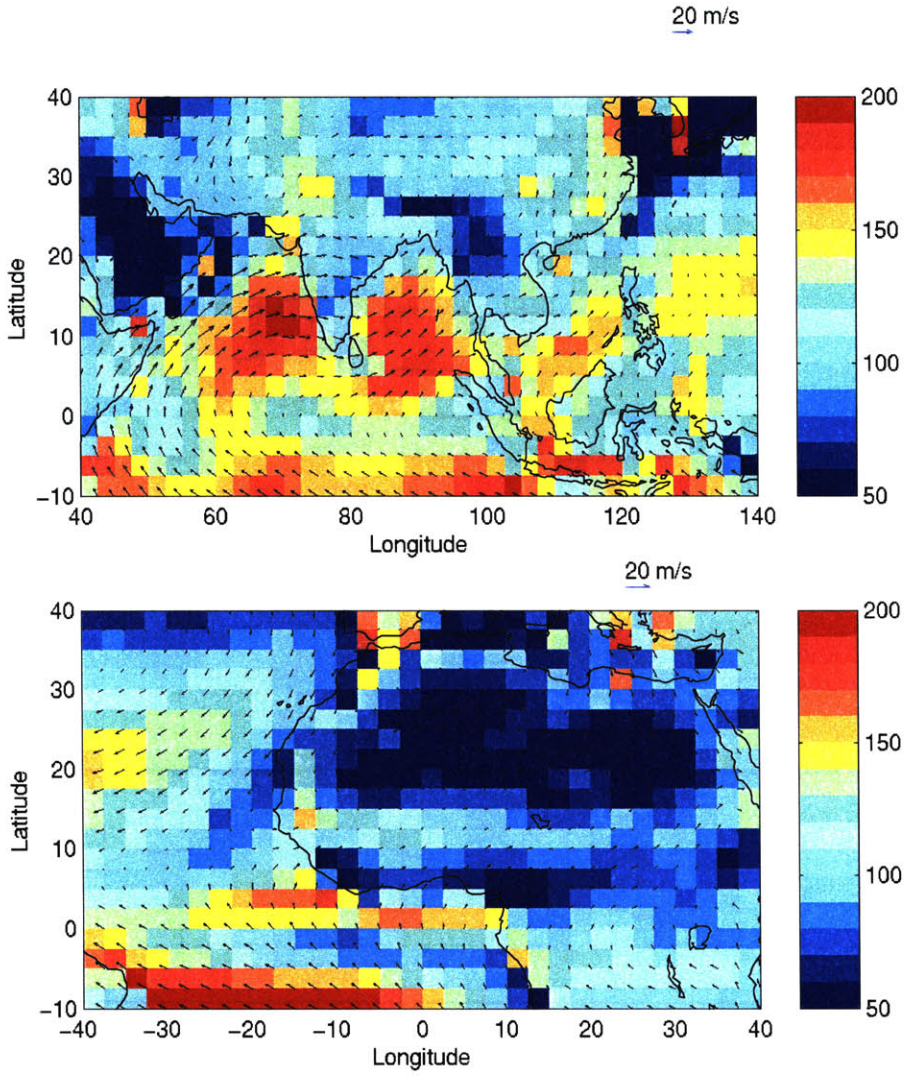

Figure 5-2: Long term mean net upward sum of sensible and latent surface heat fluxes for July, W/m^2, from ECMWF reanalysis. Arrows indicate boundary layer winds. Top, Asian monsoon; bottom, West African monsoon

notoriously difficult to observe and model accurately; the corresponding net surface fluxes in the NCEP reanalysis (not shown) differ significantly from the ERA-40 reanalysis fields over the continents. The large-scale maximum net flux field over West Africa is relatively consistent between the ERA and NCEP data sets, with greatest fluxes over the western coast, although the maximum fluxes in the NCEP data are higher, near $140W/m^2$.

The West African monsoon experiences westward traveling monsoon depressions which are associated with barotropic-baroclinic instability of the African easterly jet (Burpee (1972), Pedgley and Krishnamurti (1976), Thorncroft and Hoskins (1994)). The dynamics

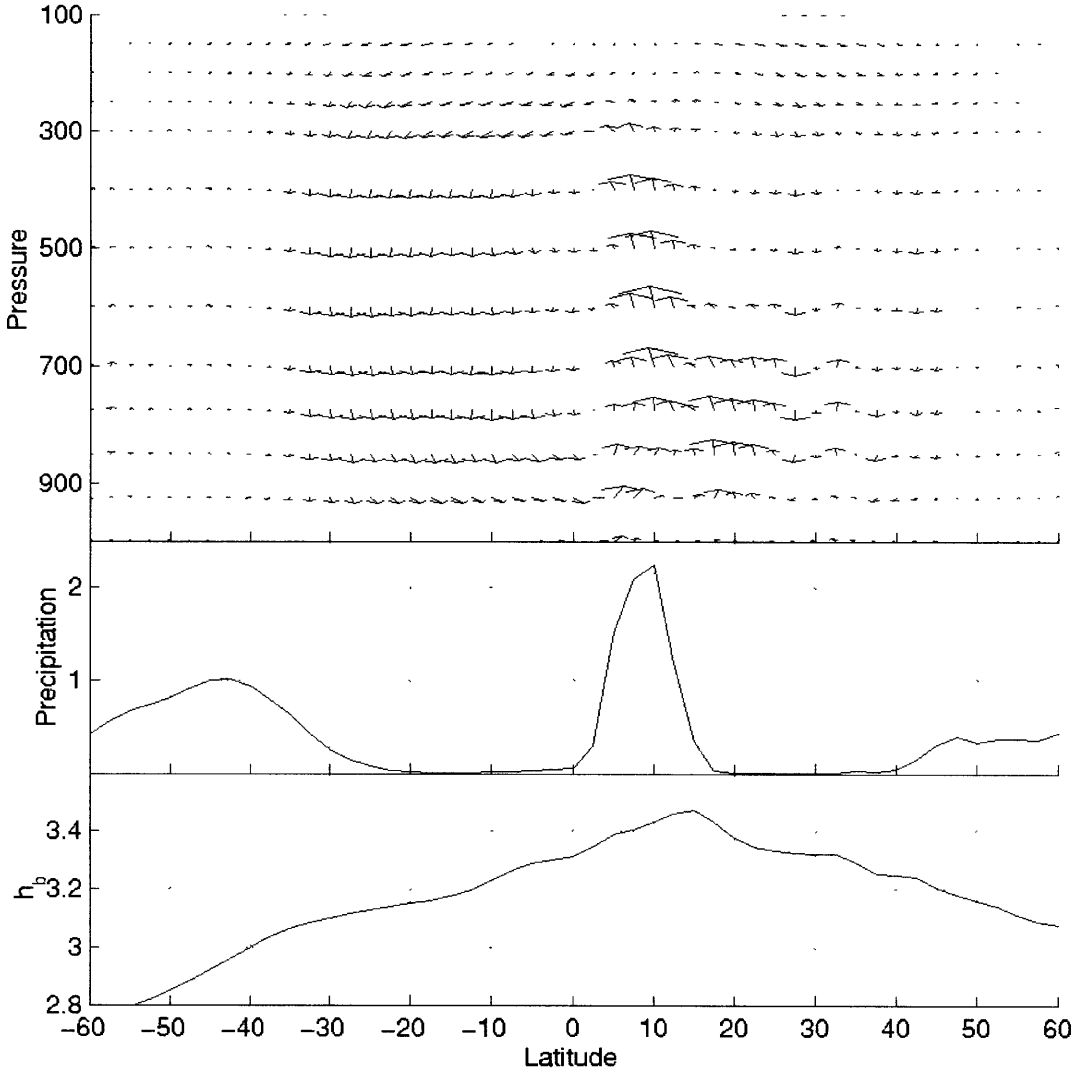

Figure 5-3: Long term mean July circulation, 10W-10E, from ECMWF reanalysis. Top, meridional circulation. Center, subcloud moist static energy, 10E5 J; bottom, precipitation, mm/day.

of the observed waves is complex and not fully understood at present. Burpee (1972) found that the energy conversion due to baroclinic processes were greater than that due to barotropic processes while the easterly waves traveled over land. In a linear study of the growth of African easterly waves, Thorncroft and Hoskins (1994) found that barotropic instability was the dominant growth mode of dry easterly waves, but that the inclusion of moist convection lead to an increase in baroclinic wave growth. The easterly waves found in the MITGCM experiments have an EP flux signature which is solely baroclinic.

The observed waves are cold-core, which contrasts with the warm-core baroclinic waves

seen in the three dimensional model results. Whereas the precipitation associated with the westward propagating waves was strongest to the southeast of the wave trough in the GCM, this region had the least rain in observations of African easterly waves. (Pedgley and Krishnamurti, 1976) found that very little convective precipitation was associated with the composite observed waves, with most of the rain in the monsoon region originating in lower tropospheric stratiform clouds.

5.1.2 Asia

As discussed in §1.5, the Asian monsoon exhibits a southwest-northeast tilt, with rainfall extending furthest poleward along the eastern coast of Asia. The long term mean precipitation field features a line of strong rainfall (Figure 5-1) which slants along the Tibetan plateau, another maximum of precipitation along the western coast of India, and a swath of moderate rainfall over the interior of India. Widespread rainfall is also observed over the entire Bay of Bengal. The monsoon over southeast Asia includes a broad region of precipitation from the equator to 35N, with a broad peak from 10N to 20N (Figure 5-5). The greatest rainfall over the eastern continent occurs over southern China near 20N.

The distribution of precipitation associated with the Asian monsoon is closest to the model results with zonally asymmetric continent and summer-like SSTs (§4.2.2, Figure 4-33), where rainfall is confined to the southeast corner of the continent. The observed precipitation extends further inland in observations than in the model, however. The low-level flow observed with the Asian monsoon (Figure 5-1) includes cross-equatorial flow, with southeasterlies in the Southern Hemisphere shifting to southwesterlies near the coastline. Over the west Pacific, tropical easterly flow converges with the monsoon southwesterlies, resulting in southerly flow along the east coast of China. This overall wind pattern is similar to that seen in the model with zonally asymmetric continent, although low-level cross-equatorial flow is stronger in observations, particularly across the Maritime continent and in the Findlater jet, which are subject to orographic effects.

The meridional circulation associated with the monsoon (Figures 5-4 and 5-5 for India and Southeast Asia, respectively) includes a cross-equatorial cell with deep ascent over the continent and subsidence in the southern hemisphere subtropics. The long term mean SSTs in the central Indian Ocean during July (not shown) are maximum near the equator, and nearly uniformly warm in the Northern Hemisphere Indian Ocean, but the SST decreases quickly south of the equator. In contrast, the zonal mean meridional circulation in the model results with zonally asymmetric continent and summer SSTs (Figure 4-36) has deep ascent associated with the oceanic SST maximum, but with little meridional circulation associated with the precipitation over the subtropical continent. The circulation in observations is

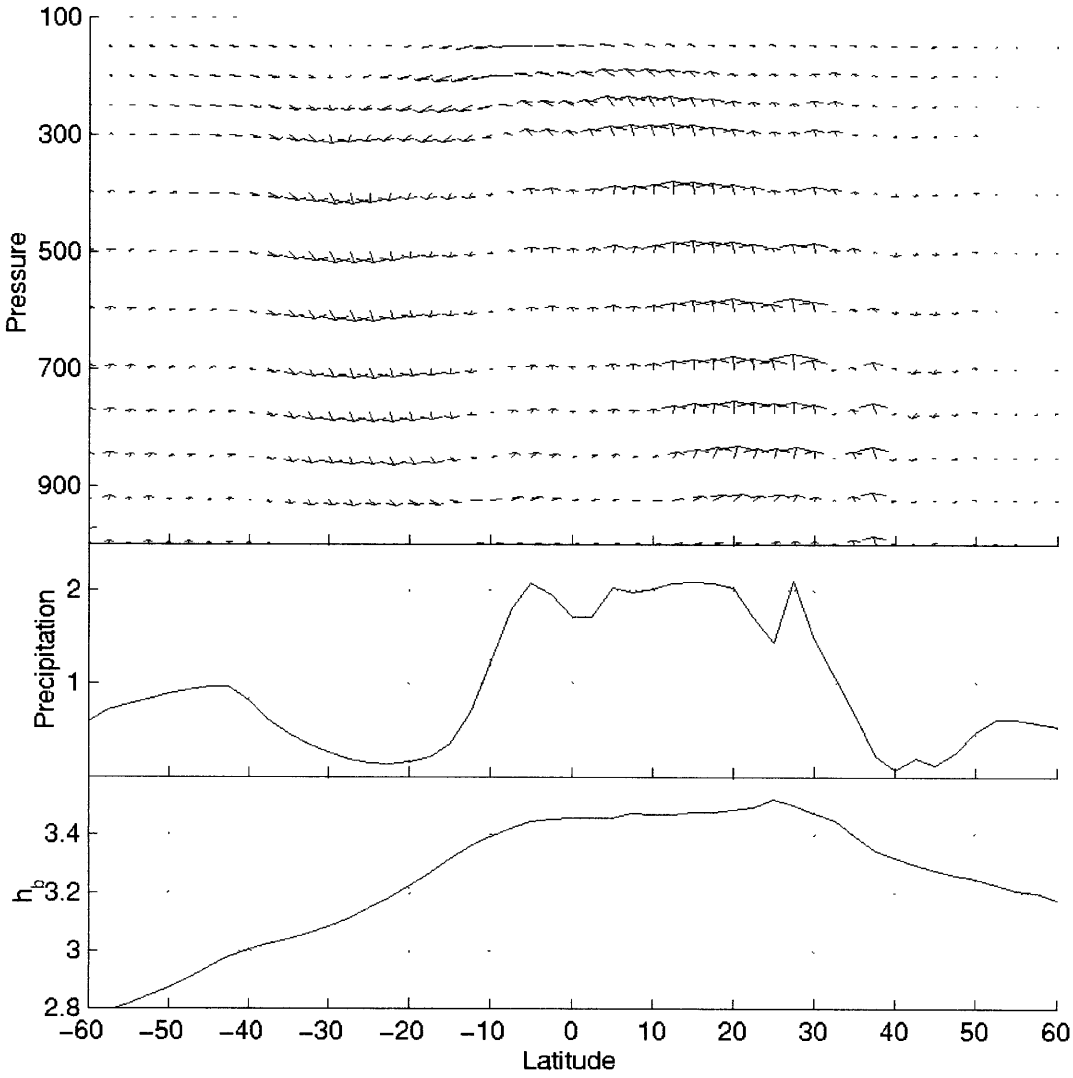

Figure 5-4: Long term mean July circulation, 60E-100E, from ECMWF reanalysis. Top, meridional circulation. Center, subcloud moist static energy, 10E5 J; bottom, precipitation, mm/day.

closer to that seen in the model with zonally symmetric continent (§4.1.2, Figure 4-16). The estimated net latent and sensible heat flux over the Asian region (Figure 5-2) has a maximum of near $140W/m^2$ over the continent in the vicinity of the Himalayas in the ERA data, which is in the stronger forcing range used in the model. The NCEP data set also has the greatest surface fluxes over the Himalayan region during July (not shown), with maximum fluxes of greater than $150W/m^2$.

Much of the monsoon rainfall over the Indian peninsula is associated with westward propagating low pressure systems, termed 'monsoon depressions'. These depressions develop

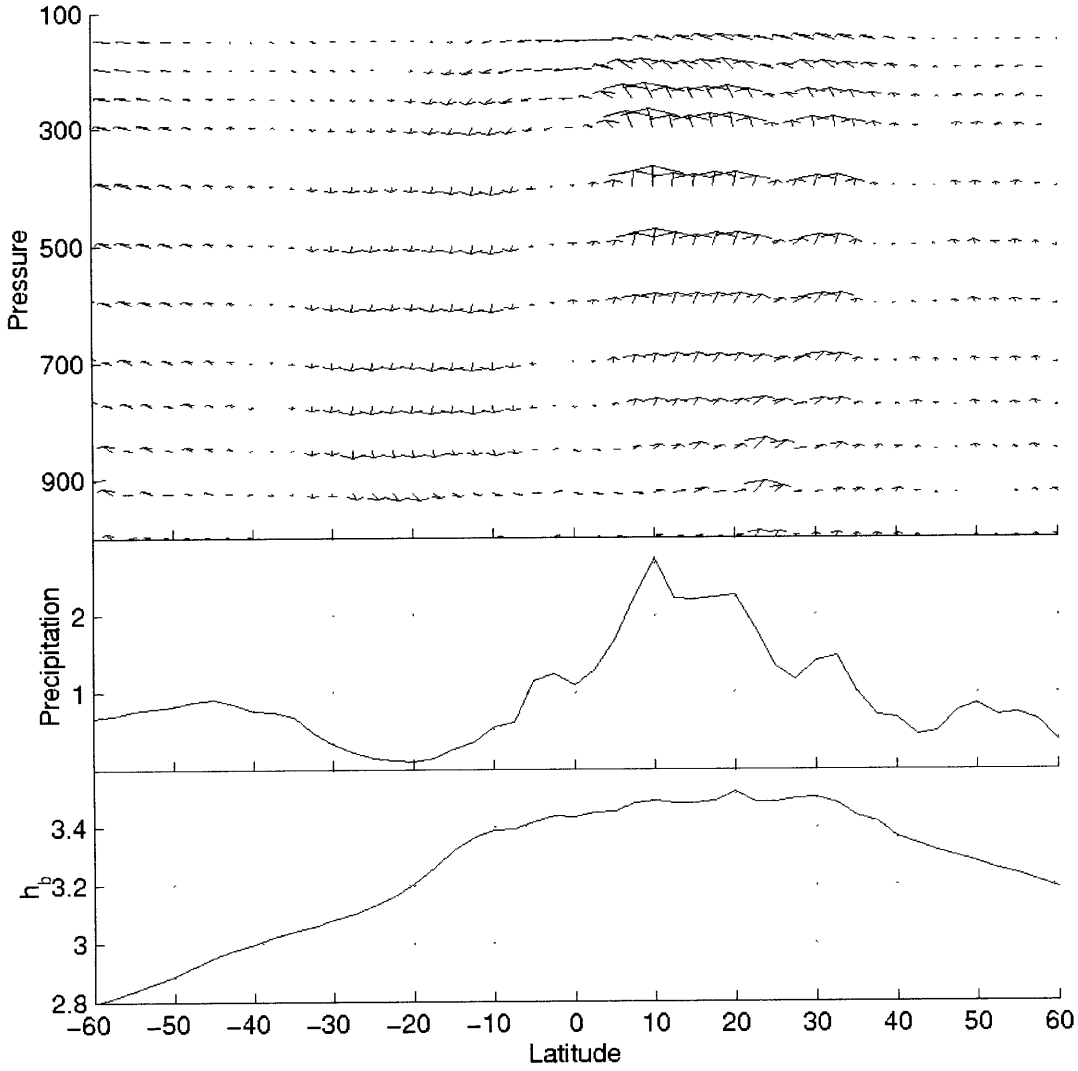

Figure 5-5: Long term mean July circulation, 100E-120E, from ECMWF reanalysis. Top, meridional circulation. Center, subcloud moist static energy, 10E5 J; bottom, precipitation, mm/day.

over the Bay of Bengal and travel west-northwest over India, with a life span of 3 to 5 days (Godbole, 1977). The depressions are cold-core in the lower troposphere, but warm-core in the upper troposphere, and may exhibit either westward, eastward, or near zero tilt with height. The greatest precipitation occurs in the southwest sector of the depression (Godbole, 1977). A large body of literature exists examining the nature of these depressions, and baroclinic (eg. Saha and Chang (1983), Mishra and Salvekar (1980)), barotropic (eg. Lindzen et al. (1983)), and mixed barotropic-baroclinic (eg. Shukla (1978)) mechanisms have been prescribed, as well as others such as short Rossby waves (Sobel and Horinouchi,

2000).

The structure of these monsoon depressions differs from the warm-core waves which are found over the subtropical continent in the GCM results. Although the modeled waves travel westward, they propagate at speeds of 2 to 5 m/s, while the observed waves travel at near 7 m/s (Krishnamurti et al., 1975). The modeled waves have purely baroclinic EP flux signature, and feature the greatest precipitation in the southeast sector of the wave, which differs from observed monsoon depressions.

5.1.3 Australia

The Australian monsoon is confined to the far northern coast of Australia; the greatest precipitation occurs over the nearby oceans and over the Maritime Continent, and the monsoon does not shift inland as in the Asian and West African monsoons (Figure 5-6). The immediate coast receives the greatest rainfall, and precipitation drops off rapidly inland, where the continental interior is host to deserts. The Australian monsoon does not exhibit a significant east-west tilt. The meridional circulation over the Australian region (120E-145E) features a cross-equatorial circulation with deep ascent from 15S to 5N, and subsidence in the northern hemisphere subtropics (Figure 5-8). Low-level ascent occurs between 25S and 15S, over the desert regions, but is not considered part of the cross-equatorial circulation cell.

The most similar model results are from the zonally symmetric land case with $THF_0 = 130W/m^2$ (Figure 4-11), with a meridional circulation whose boundary is just inland from the coast, and with maximum precipitation over the coastal oceans and weaker precipitation along the immediate coast. The greatest estimated net surface heat flux from the ERA data set is close to $120W/m^2$ along the northern coast (Figure 5-7), but the western and interior continent have much weaker net flux of less than $100W/m^2$. The NCEP flux data is very different over the Australian region, with much stronger fluxes over the land, especially along the eastern coast (not shown). The maximum heat flux over the northern coast of Australia is near $170W/m^2$ in the July mean NCEP data.

5.1.4 South America

The existence of a South American monsoon has been disputed because there is no seasonal reversal of the large-scale circulation which is commonly considered a definition of the monsoon. However, if the mean tropical easterly flow over South America is subtracted out, the resulting anomalous flow does show reversal of wind direction (Zhou and Lau, 1998). The South American monsoon also has common features with other monsoons, such as low-level cross-equatorial flow, northwesterly flow into the monsoon area, and an

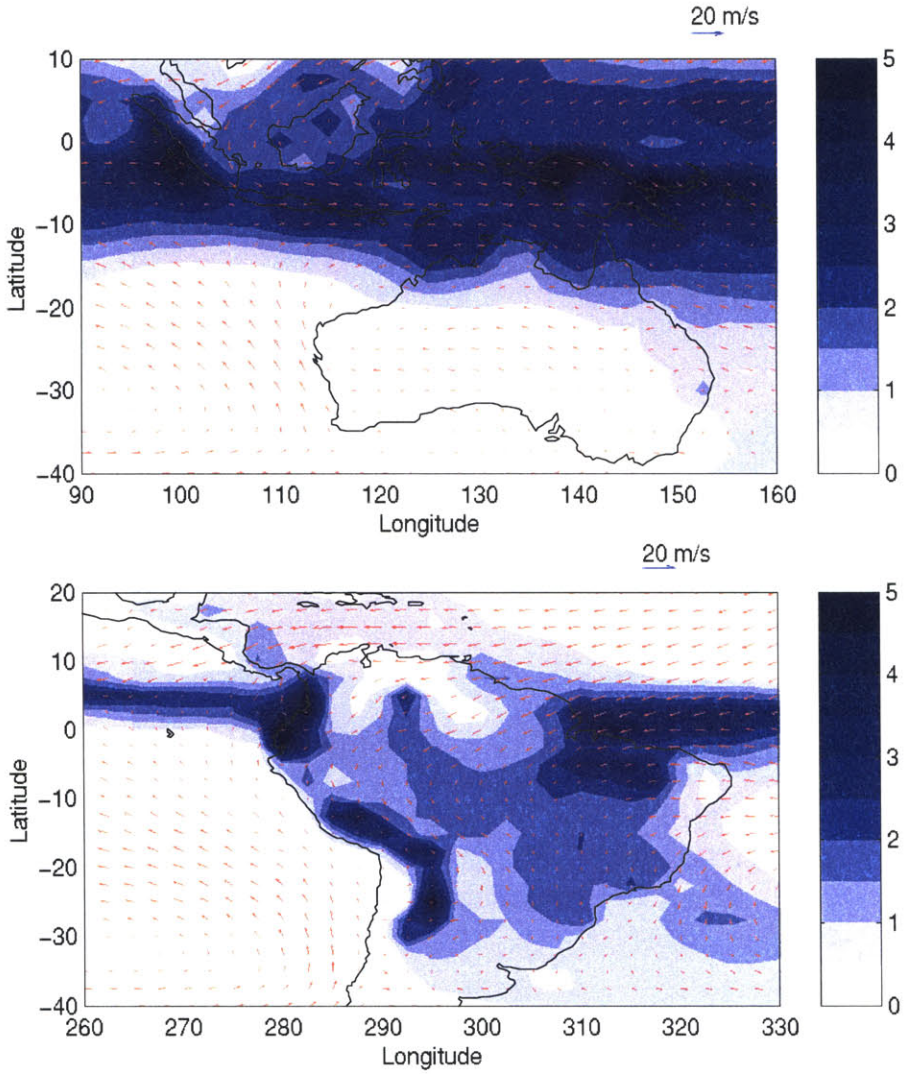

Figure 5-6: Long term mean precipitation for January, mm/day, from ECMWF reanalysis. Arrows indicate boundary layer winds. Top, Australian monsoon; bottom, South American monsoon

overturning meridional cross-equatorial circulation. Because of the Andes mountains and the complicated coastline which crosses the equator, flow over South America is complex and highly asymmetric (Figure 5-6).

There is widespread precipitation over much of central South America from 30S to the equator (Figure 5-6). There are two strong precipitation peaks at the equator and 5-10S, with a third, weaker maximum at 20S (Figure 5-9). A region of intense rainfall is located along the western flank of the Andes mountains. with reduced rainfall on the eastern flank. The precipitation is located in regions of deep ascent; there is a very broad area of large

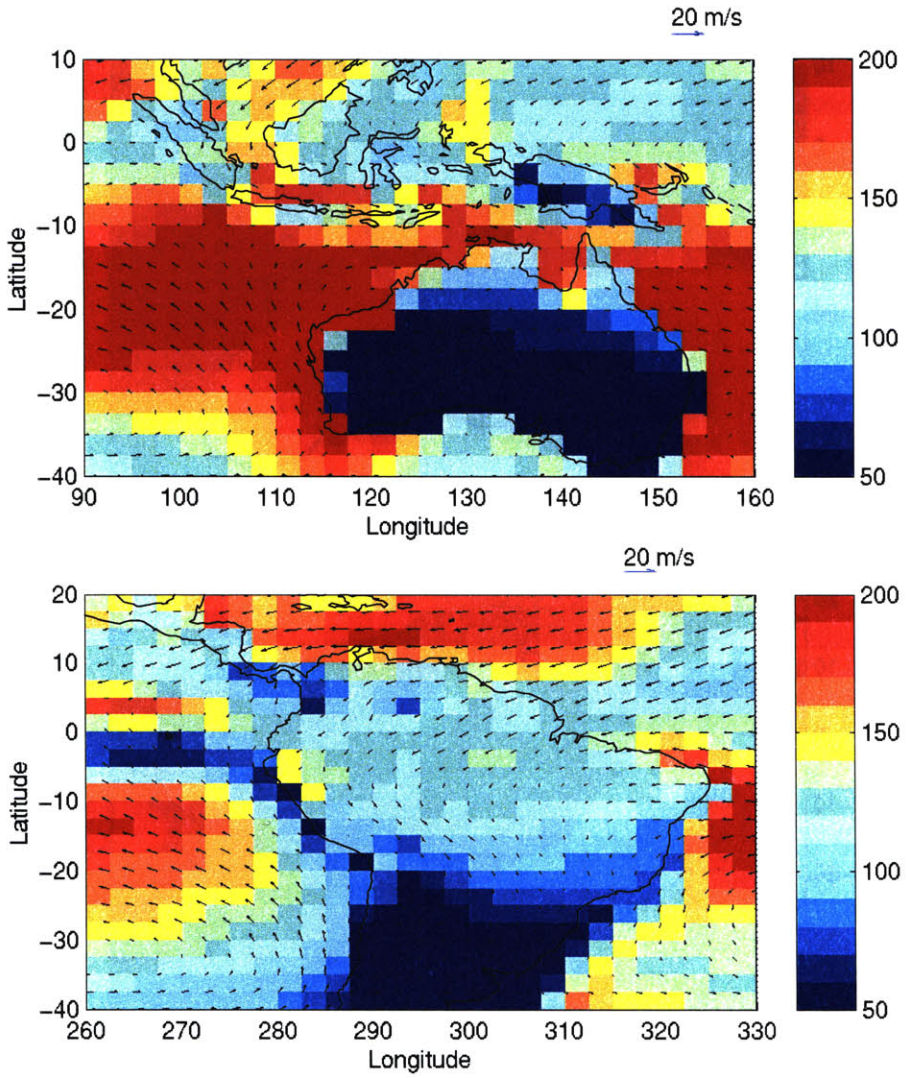

Figure 5-7: Long term mean net sum of sensible and latent surface heat fluxes, W/m^2 , from ECMWF reanalysis. Arrows indicate boundary layer winds. Top, Australian monsoon; bottom, South American monsoon

scale deep ascent from 30S to the equator, with subsidence in the northern hemisphere tropics. The South American monsoon does not have a close analog in any of the modeled cases, which is not surprising given the equatorial location of the coastline and the very asymmetric flow associated with the monsoon.

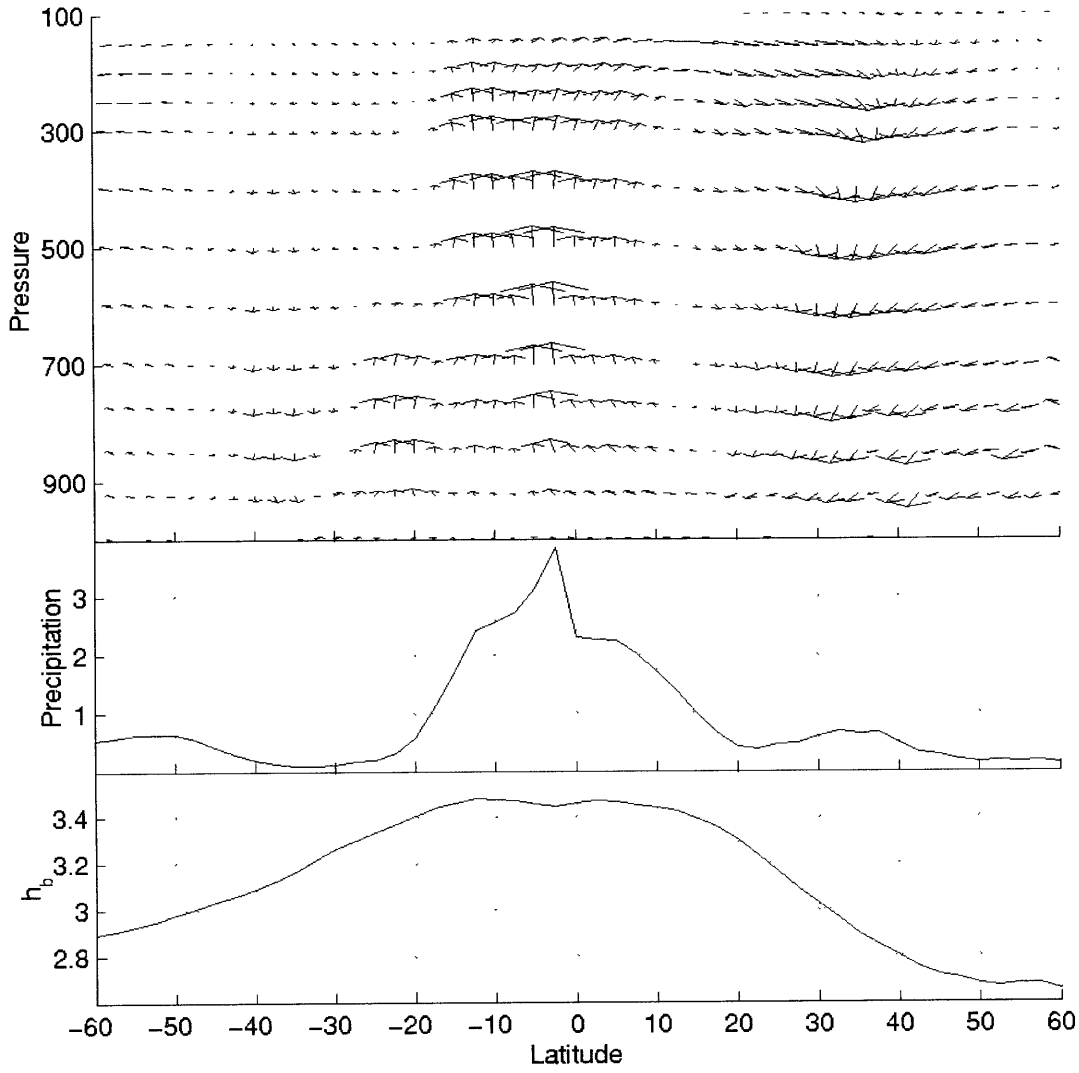

Figure 5-8: Long term mean January circulation, 120E-145E, from ECMWF reanalysis. Top, meridional circulation. Center, subcloud moist static energy, 10E5 J; bottom, precipitation, mm/day.

5.2 Monsoon Circulation vs. Theory

While the analytic theory (§3.3) linking the location of the monsoon to the subcloud moist static energy distribution works well in the simplified GCM used here, the validity of the theory should also be assessed in observations, as the real world features much more complex flow and more feedbacks than are accounted for in the idealized model. Circulation and thermodynamical quantities are diagnosed for different monsoon regions using ECMWF data in order to investigate how closely observations follow the analytic theory. The long-

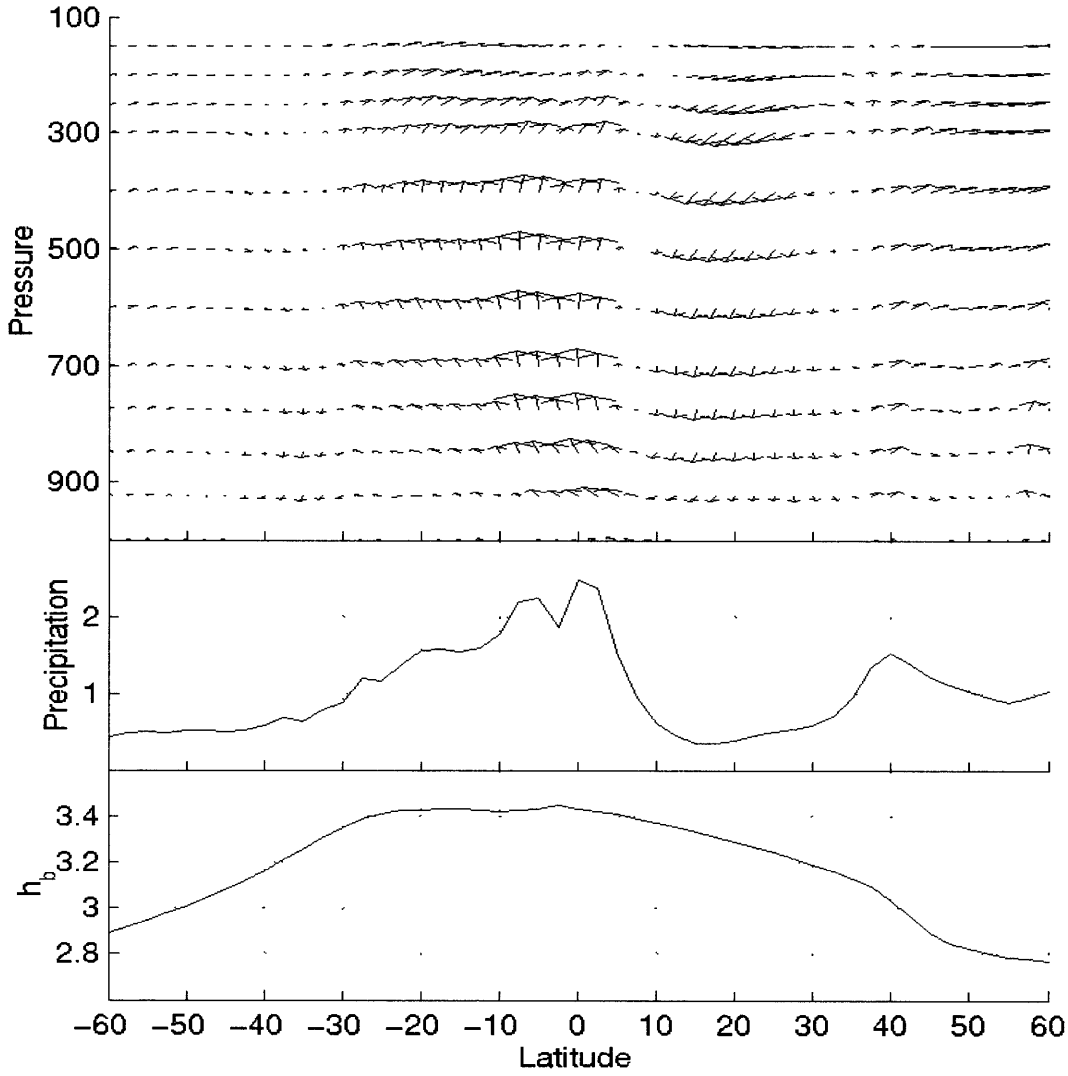

Figure 5-9: Long term mean January circulation, 50W-70W, from ECMWF reanalysis. Top, meridional circulation. Center, subcloud moist static energy, 10E5 J; bottom, precipitation, mm/day.

term summer mean fields (averaged from 1957 to 2002) are examined; also, data from 1976 (year arbitrarily chosen) is compared to give an example of the behavior during an individual season.

In order to calculate subcloud moist static energy, the gridpoint two levels above the surface is chosen as the 'subcloud' level, and h_b is calculated from the fields of geopotential, temperature, and specific humidity. Because the saturation moist entropy is assumed to be near constant in the vertical in monsoon regions (and thus equal to the subcloud moist entropy), the meridional gradient of moist entropy may be taken in the subcloud layer

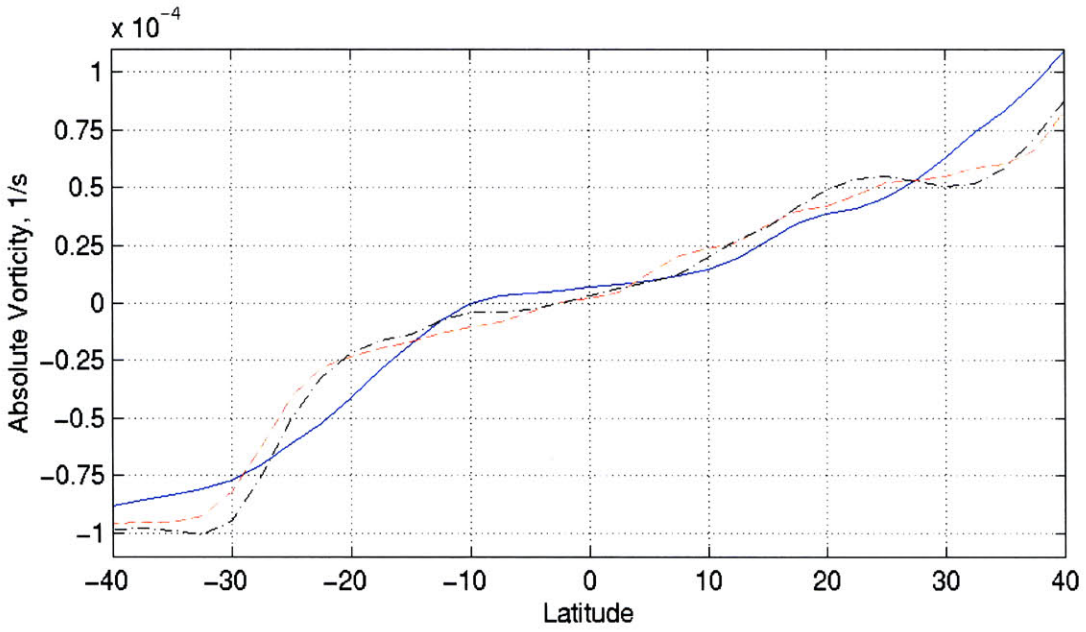

Figure 5-10: 250 mb absolute vorticity, 1/s, summer 1976 from ECMWF reanalysis. Solid blue line, June 1 - August 31 mean 10W-10E; dashed red line, July 1- August 31 mean, 60E-100E; dash-dot black line, July 1 - August 31 mean, 100E-120E.

although the height of the layer may vary considerably in latitude.

5.2.1 West African Monsoon

The long term mean July flow averaged between 10W and 10E includes a cross equatorial circulation with a narrow region of deep ascent from 5N to 12N and subsidence in the southern hemisphere (Figure 5-3). The absolute vorticity in the upper troposphere (Figure 5-10) includes a region of flat, near-zero vorticity from 10S to 10N, which is consistent with an angular momentum conserving circulation.

The long term subcloud moist static energy has a maximum well inland near 15N (Figure 5-11), with greatest h_b over west Africa. The presence of a large desert over the continental interior maintains low moist static energy far inland, so that there is a pronounced maximum in h_b over the subtropical continent. The zonal mean subcloud h (Figure 5-3) has a marked peak at 12N-15N, with sharp gradients of h_b on either side of the maximum. The bulk of the monsoon precipitation occurs approximately 5° equatorward of the h_b maximum, and the poleward limit of the large-scale meridional circulation is close to the h_b maximum, in accordance with the analytic theory.

Eltahir and Gong (1996) compared the circulation and subcloud moist static energy distribution for two different summers: one with a strong monsoon, and the other with a

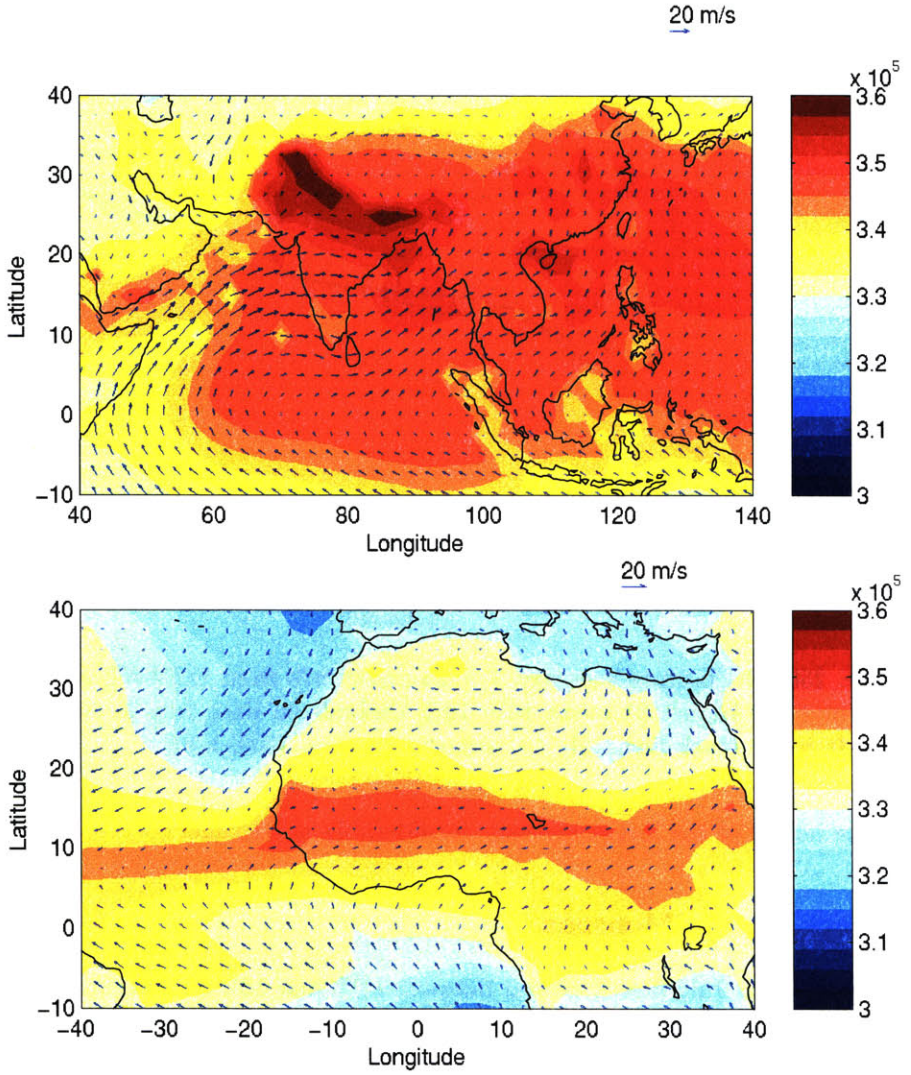

Figure 5-11: Long term mean subcloud moist static energy for July, J, from ECMWF reanalysis. Arrows indicate boundary layer wind from the same level as h_b. Top, Asian monsoon; bottom, West African monsoon

weak monsoon. They found that the gradient of subcloud h over the West African region was much weaker in the summer with a failed monsoon and that the gradient was not strong enough to meet the critical threshold for initiation of an AMC cross-equatorial circulation (as described by Emanuel (1995)). In the summer with a strong monsoon, the subcloud h distribution was supercritical, and the meridional circulation was vigorous.

Although 1976 was during the middle of the extended severe drought over West Africa caused by weakening of the monsoon, that particular summer monsoon saw close to average rainfall over most of West Africa, with moderate drought over the Sahel and the Guinea

Coast (Nicholson, 1993). The July 1976 circulation, precipitation, and h_b fields (not shown) are very similar to the long term July mean (Figure 5-3). In the early summer, precipitation was concentrated just inland of the coast; the precipitation band slowly shifted inland to near 10N (not shown), then abruptly moved several degrees equatorward in mid August 1976. The subcloud moist static energy maximum (not shown) shifted northward from 5N at the beginning of May to near 19N by the beginning of August; during the second half of August, the maximum h_b location began to move equatorward. More study is needed to determine the whether there is a true causal relationship between the precipitation and subcloud moist static energy distribution on the transient timescale.

5.2.2 Indian Monsoon

The Indian region is considered separately from the rest of southeast Asia in hope of finding a cleaner circulation by excluding some of the longitudinal variation in orography, coastal location, ocean conditions, and large-scale flow. The thermodynamic and dynamic fields are zonally averaged between 60E and 100E, which excludes the Findlater jet, but captures the subcontinent of India and the Bay of Bengal.

The long-term mean July conditions include a strong subcloud h maximum over the southern flank of the Tibetan plateau which slants from approximately 33N at 70E to near 25N at 90E (Figure 5-11. A local maximum of h_b is located over the central and northern Bay of Bengal. The zonally averaged subcloud h over the Indian region (Figure 5-4) has high moist static energy over the tropics from 5S to 35N, with a distinct maximum at 25N. The zonally averaged precipitation field has a complex triple-peaked structure with widespread strong precipitation from 6S to 28N. One local peak in rainfall is located at 6S, and is associated with jumping behavior; this will be discussed in section §5.3. A second, broad peak, is located from 12N to 20N; the third, very sharp peak is located at 28N.

The zonal mean meridional circulation over the Indian region is shown in Figure 5-4. The absolute vorticity in the upper troposphere (Figure 5-10) is relatively flat from 20S to 5N, and the vorticity is reasonably close to zero from 20S to the monsoon region, especially given the long time mean and large longitudinal region used to calculate the vorticity. A broad area of large-scale ascent throughout the depth of the troposphere occurs from 12N to 20N; this corresponds well with the second precipitation maximum. There is a weaker region of deep large-scale ascent from 5S to 2S, which corresponds to the southern hemisphere precipitation maximum. The third, sharp peak in rainfall occurs over the Himalayas, so that the zonal mean wind field output in reanalysis data is compromised at low altitudes; in this region, there is only very weak ascent in the upper troposphere, and the precipitation may be due to orographic effects. Despite the strong zonal asymmetry of the large-scale flow

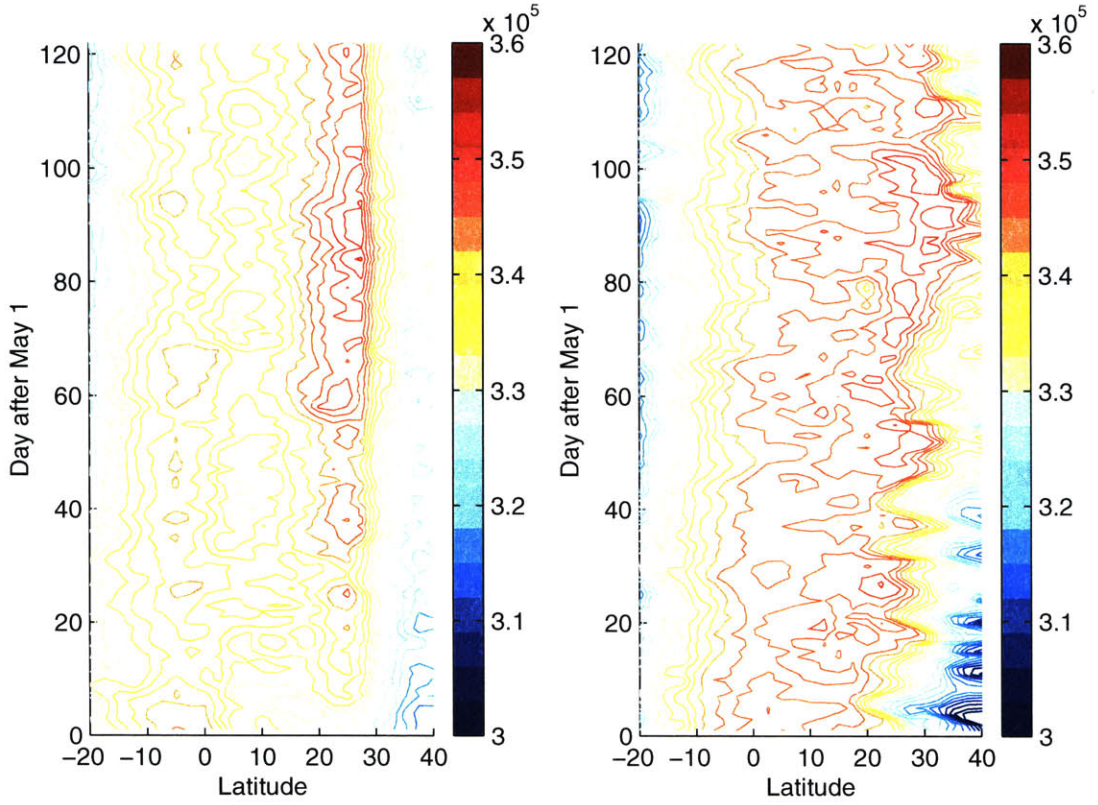

Figure 5-12: Zonal mean subcloud h over Asia, May 1 through August 31 1976, J, from ECMWF reanalysis. Left, 60E-100E; right, 100E-122E.

in the Indian region and the presence of an impressive mountain range, the analytic theory is in agreement with the observed monsoon circulation: the large-scale ascent and monsoon precipitation occurs slightly equatorward of the maximum in subcloud moist static energy.

The evolution of the mean rainfall and subcloud h during the summer of 1976 is shown in Figure 5-12 and Figure 5-13. Precipitation over the Himalayan range is persistent throughout the summer, with greatest rainfall during the mid and later summer. Over central India, the monsoon onsets at the end of May, with a break monsoon occurring at the end of June. The monsoon recovers at the end of June, and remains strong for the remainder of the summer. During the middle of May, a maximum in subcloud moist energy develops over the Himalayas; onset of the monsoon occurs when this h_b maxima becomes greater than the equatorial oceanic h_b. The h_b maximum continues to increase until the end of July, although there is a period of relative weakness which is concurrent with the break monsoon during June. The analytic theory appears to hold up well to the transient behavior of the Indian monsoon, and the potential link between the break monsoon and the distribution of h_b is worthy of future study, although no conclusions may be drawn at this time.

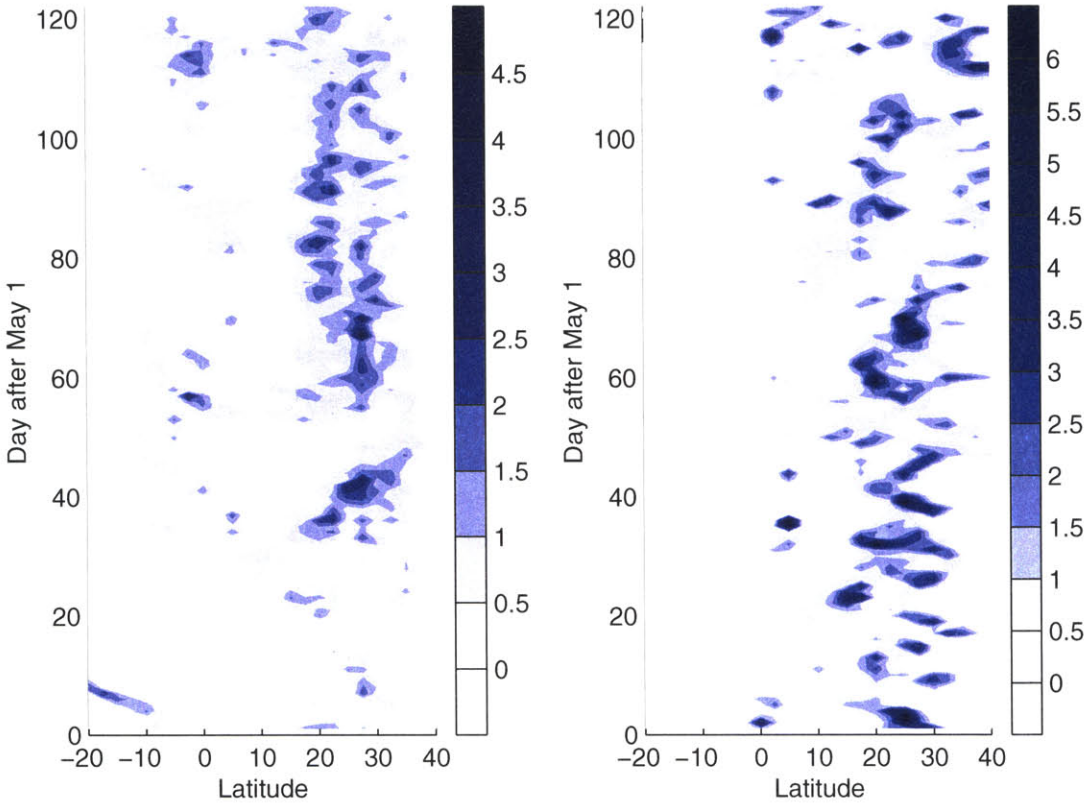

Figure 5-13: Zonal mean precipitation over Asia, May 1 through August 31 1976, mm/day, from ECMWF reanalysis. Left, 60E-100E; right, 100E-122E.

5.2.3 Southeast Asian Monsoon

The southeast Asian monsoon is separated from the Indian monsoon to achieve a clean analysis as previously discussed; zonal means for this region are taken from 100E to 120E. The subcloud moist static energy is generally high across much of southeast Asia and the neighboring oceans, with a continental maximum over central and eastern China near 30N. The zonal mean h_b between 100E and 122E has a broad maximum from 10N to 30N, with three slight local peaks at 10N, 20N, and 30N (Figure 5-5). Poleward of 30N, the subcloud moist static energy falls off rapidly with latitude. The zonal mean precipitation field (Figure 5-5) also has a broad maximum from 2S to 32N, with strongest rainfall at 10N and a secondary maximum at 20N. The meridional circulation has strong deep ascent from 10N to 32N. The absolute vorticity in the upper troposphere (Figure 5-10) is similar to that seen over India, and indicates a nearly AMC circulation, especially from 15S to 10N.

In the long term mean July data, the subcloud moist static energy has near zero meridional slope from 10N to 30N; according to the analytic theory, the boundary of the monsoon circulation may occur anywhere within that range. The actual boundary is coincident with

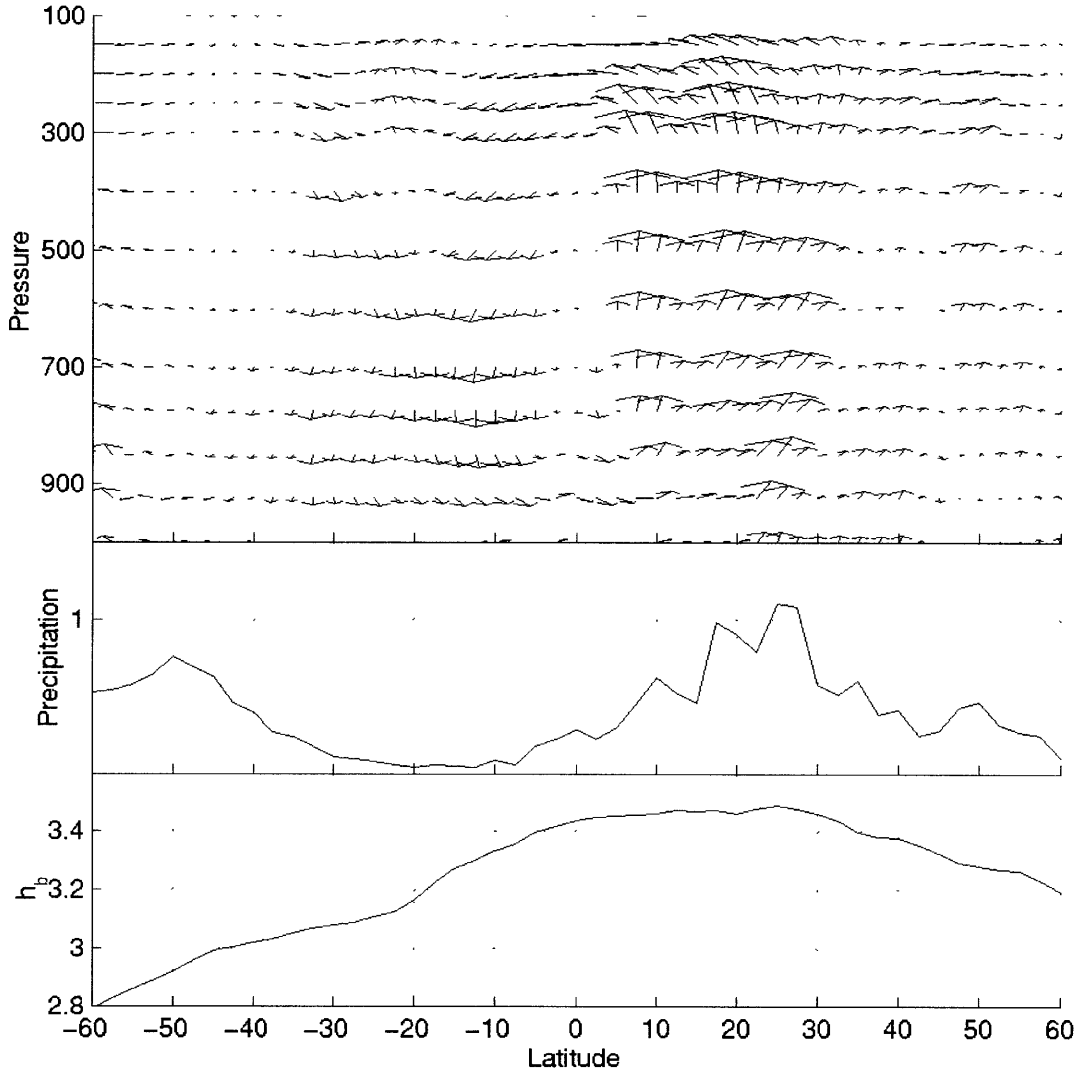

Figure 5-14: Time mean July 1976 circulation, 100E-120E, from ECMWF reanalysis. Top, meridional circulation. Center, subcloud moist static energy, 10E5 J; bottom, precipitation, mm/day.

the poleward limit of this region near 30N, which is in agreement with the theory. The mean fields for July 1976 (Figure 5-14) do not follow the theory as closely: the poleward boundary of the meridional circulation and a considerable portion of the monsoon rainfall occurs slightly northward of the h_b maximum.

The time evolution of the subcloud moist energy (Figure 5-12) and precipitation (Figure 5-13) shows that during most of the summer, the theory holds up well, with monsoon precipitation generally occurring slightly equatorward of the h_b maximum. However, during mid July, a region of heavy rainfall develops slightly poleward of the h_b maximum, persist-

ing for approximately two weeks. At the beginning of August, the monsoon precipitation abruptly jumps 10° south to the equatorward side of the h_b maximum. This demonstrates that the steady state theory does not always apply to the transient monsoon.

5.2.4 Australian Monsoon

The Australian monsoon occurs over the northern coast of Australia, and does not progress far inland. For the calculations made here, the circulation and thermodynamic fields are zonally averaged from 120E to 145E. During January, there is a wide swath of precipitation across the southern hemisphere tropics, from 20S to 5N (Figure 5-6). Near the date line, the precipitation field splits into two maxima: a narrow precipitation band near the equator which stretches into the ITCZ in the east Pacific, and the South Pacific Convergence Zone (SPCZ) which ranges from Australia to the central Pacific near 20S. The subcloud moist static energy field has a broad region of very high h_b from 20S to 5N, with a double-peaked structure over the west Pacific (Figure 5-15).

The zonal mean subcloud moist static energy (Figure 5-8) has a maximum at 12S, just equatorward of the northern coast of Australia, with a weaker local maximum at 3N. The meridional circulation features deep ascent from 19N to 15S, with a region of shallow low-level ascent over the desert from 25S to 15S. The long term mean circulation appears to be in good agreement with the analytic theory. The boundary of the circulation is colocated with the maximum subcloud moist energy near 13S, and the precipitation region occurs near and equatorward of the h_b maximum.

The low level circulation over Australia is highly asymmetric (Figure 5-6), which is unsurprising given the small size of the continent. Some low-level cross-equatorial flow is observed over Indonesia, with flow turning from northeasterly in the northern hemisphere to northwesterly along the northern coast of Australia. A strong low level cyclone forms over western Australia, with southerly flow along the western coast and easterly flow across the continental interior. In northern Australia, three different low-level flows converge: easterly flow from the south Pacific, northerly flow from southern Australia, and northwesterly flow from the equatorial Pacific. These flow patterns strongly impact the advection of moist static energy over the continental interior: h_b over the central continent, where northerly flow carries air inland from the cool midlatitudes, is lower than along the eastern and western coasts (Figure 5-15).

The monsoon during January 1976 (not shown) was similar to the long term mean January monsoon state, with a wide swath of precipitation from 15S to 15N, near constant h_b from 15S to 10N, and a cross-equatorial circulation with deep ascent from 15S to 10N. The transient monsoon behavior also follows the analytic theory: the poleward limit of the

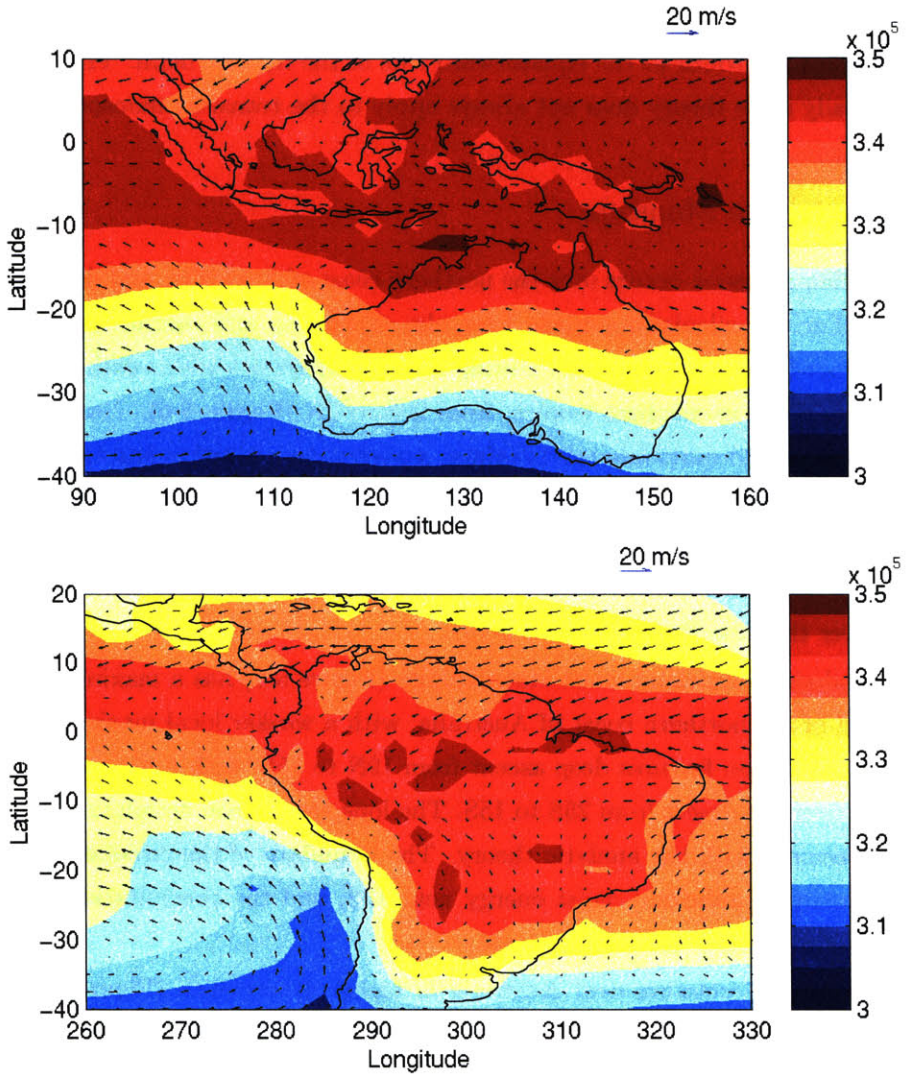

Figure 5-15: Long term mean subcloud moist static energy for January, J, from ECMWF reanalysis. Arrows indicate boundary layer winds from the same level as h_b. Top, Australian monsoon; bottom, South American monsoon

monsoon rains is colocated with the poleward limit of the region of maximum h_b. This limit ranges from near 10S to 25S over the course of the summer (Figures 5-16, 5-17).

5.2.5 South American Monsoon

A zonal average from 50W to 70W is used to investigate the meridional circulation. The subcloud h field has a broad region of high values from 30S to 5N, with a weak maximum at 2S (Figure 5-9). The meridional flow features deep ascent from 30S to 2S. There is no significant maximum in h_b associated with the South American monsoon; instead, the

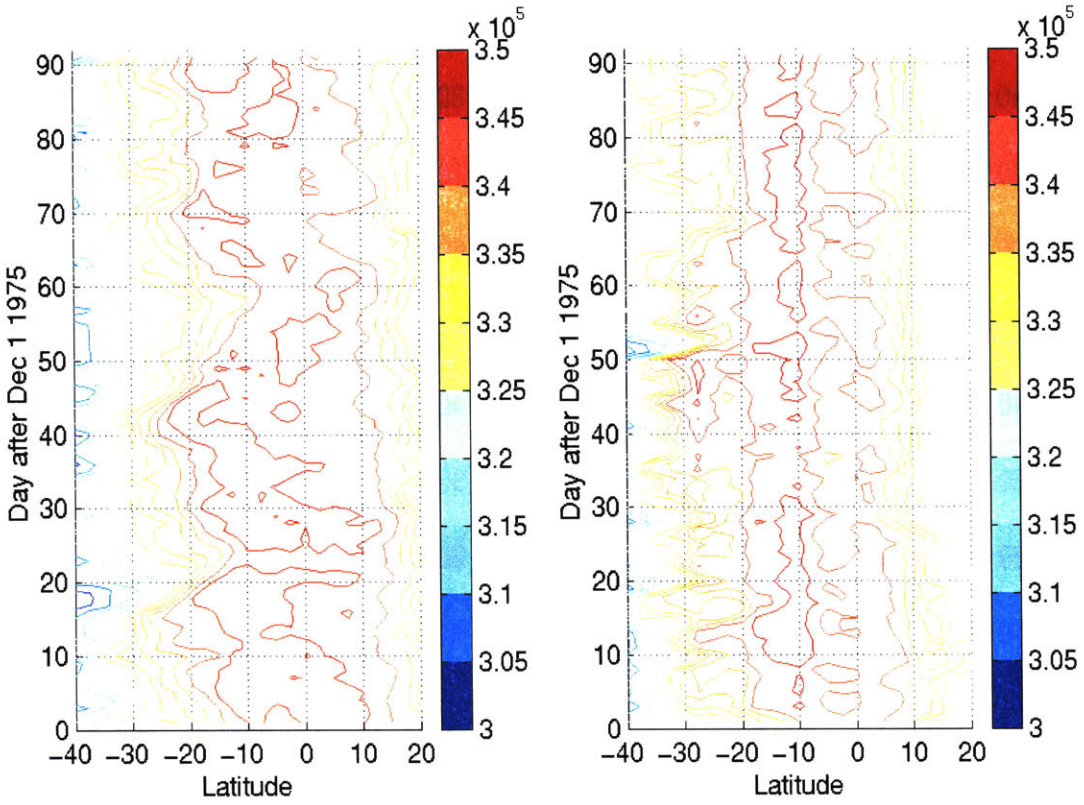

Figure 5-16: Zonal mean subcloud h, Dec 1 1975 through February 29 1976, J, from ECMWF reanalysis. Left, 120E-145E; right, 70W-50W.

distribution of subcloud moist static energy is nearly flat across the southern hemisphere tropics. According to the analytic theory, the poleward boundary of the monsoon circulation must be located in a region where the meridional slope of h_b is zero, so that in this case, the boundary could occur anywhere in the region of flat h_b. In fact, the boundary occurs at the poleward-most limit of near-constant h_b, where the moist static energy begins to decrease. Large-scale ascent occurs between this boundary and the equator, over the entire region of high h_b. Thus, the analytic theory is in agreement with the large-scale flow.

The South American monsoon during austral summer of 1976 (not shown) was similar to the long term mean monsoon. The subcloud moist static energy over South America has a broad maximum from 27S to 2N, with widespread monsoon precipitation over this entire region (not shown). The meridional circulation had a poleward boundary at 27S, with deep ascent from 27S to 10N, in agreement with the analytic theory. The transient fields of precipitation (Figure 5-17) and h_b (Figure 5-16) show that the monsoon did not vary greatly in location during the course of the summer. The rainfall was generally colocated with the region of high h_b, with only a few transient convecting disturbances developing slightly

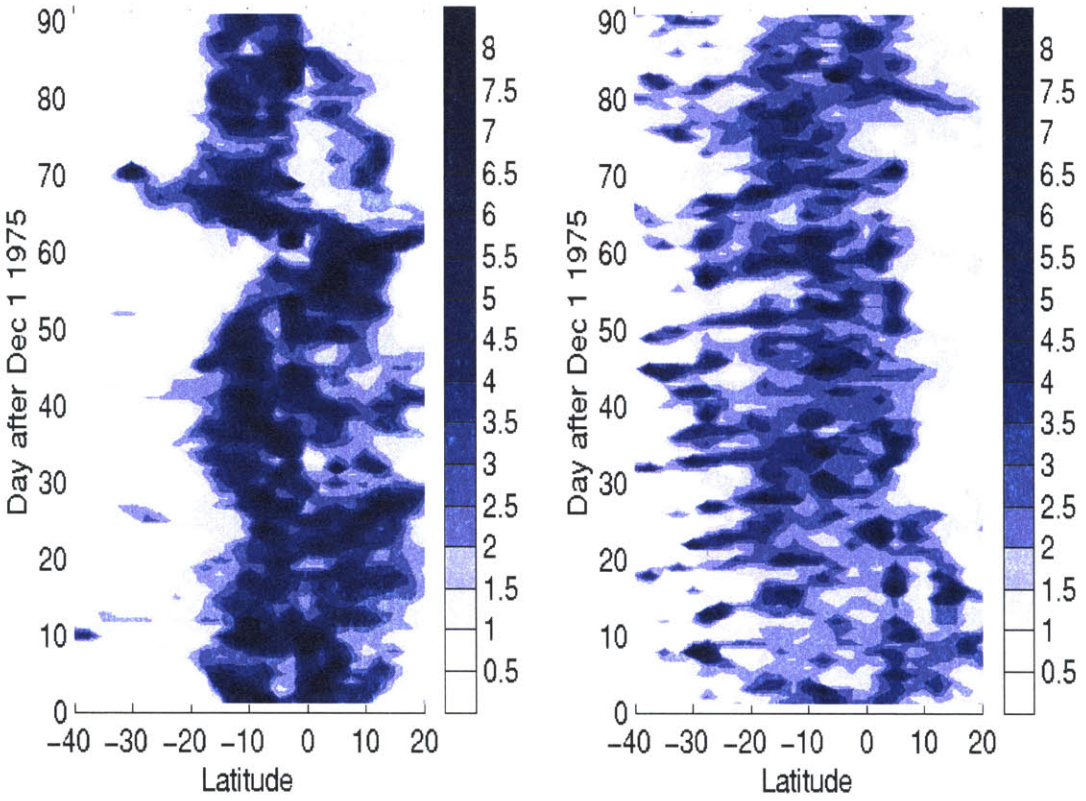

Figure 5-17: Zonal mean precipitation, Dec 1 1975 through February 29 1976, mm/day, from ECMWF reanalysis. Left, 120E-145E; right, 70W-50W.

poleward of the h_b maximum; these disturbances moved equatorward into the monsoon region.

5.3 Jumping Behavior

The model results from cases without a strong SST gradient at the equator show a pronounced tendency for the lower tropospheric branch of the cross-equatorial circulation to jump at the equator, crossing into the summer hemisphere in the free troposphere rather than in the mixed layer. This behavior results in a precipitation maximum near the equator, where the flow undergoes large scale ascent. Jumping of the circulation is not simply an artifact of the model numerics, but is related to the constraints on meridional mass fluxes in the mixed layer as discussed by Pauluis (2001) and in §3.1.2. Therefore, jumping of the large-scale circulation should be observed in the real world in locations where a particular set of conditions are met: 1) a strong cross-equatorial circulation exists; 2) pressure gradients across the equator are weak.

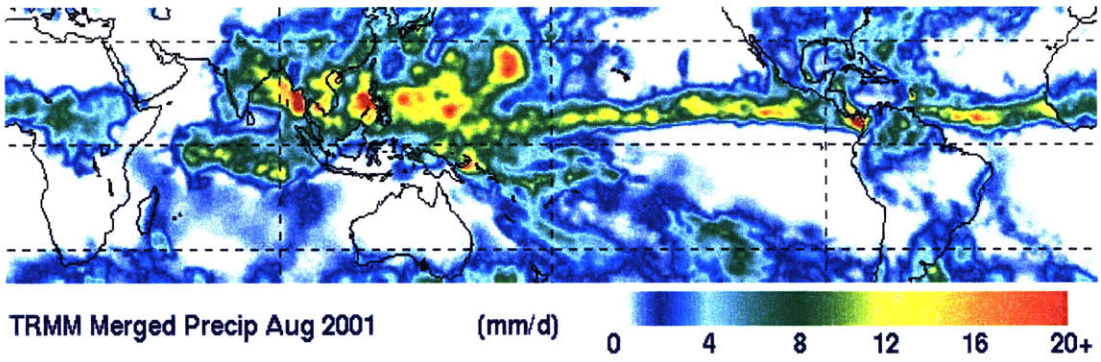

Figure 5-18: Rainfall estimates from TRMM satellite for the month of August 2001.

Vertical velocities are difficult to observe over the tropical oceans; the reanalysis data for ω are particularly suspect. Instead, moist convection and precipitation are chosen to identify regions which are likely to feature large-scale ascent near the equator. The region determined to be most likely to be affected by jumping behavior is the Indian Ocean during boreal summer, for several reasons. First, the Indian Ocean has weak meridional gradients of SST near the equator, and the Indian monsoon is located more than 10° distant from the equator. Observed rainfall from the Tropical Rainfall Measurement Mission (Figure 5-18) shows a distinct maximum in rainfall south of the equator in the Indian Ocean during boreal summer, which is an indicator of likely vertical motions.

The circulation over the Indian Ocean during boreal summer is examined in the reanalysis data. The low level flow over the Indian Ocean is highly asymmetric, with the majority of the cross-equatorial flow occurring within the Findlater jet over the western edge of the Ocean; this jet is believed to be strongly influenced by the presence of the East African mountain range (Rodwell and Hoskins, 1995). Over the central and eastern Indian Ocean, low-level cross equatorial flow is weak, and the predominant flow is easterly in the southern hemisphere (Figure 5-1). The long-term mean summer precipitation field shows a strong maximum over India and southeast Asia associated with the monsoon, but also a band of precipitation just south of the equator which stretches from 60E to 100E. This secondary precipitation maximum is suggestive of the precipitation observed in the model due to jumping behavior.

Figure 5-19 shows the progression of rainfall in the vicinity of India over two different summers; the summer of 1994 features unusually intense precipitation over the entire ocean basin throughout the summer, while the summer of 1999 has a more typical rainfall pattern. Near-equatorial precipitation is a persistent presence during the monsoon season.

The meridional circulation over the central and eastern Indian Ocean (excluding the Findlater jet) often includes a region of ascent in the southern hemisphere eg. (Figure 5-

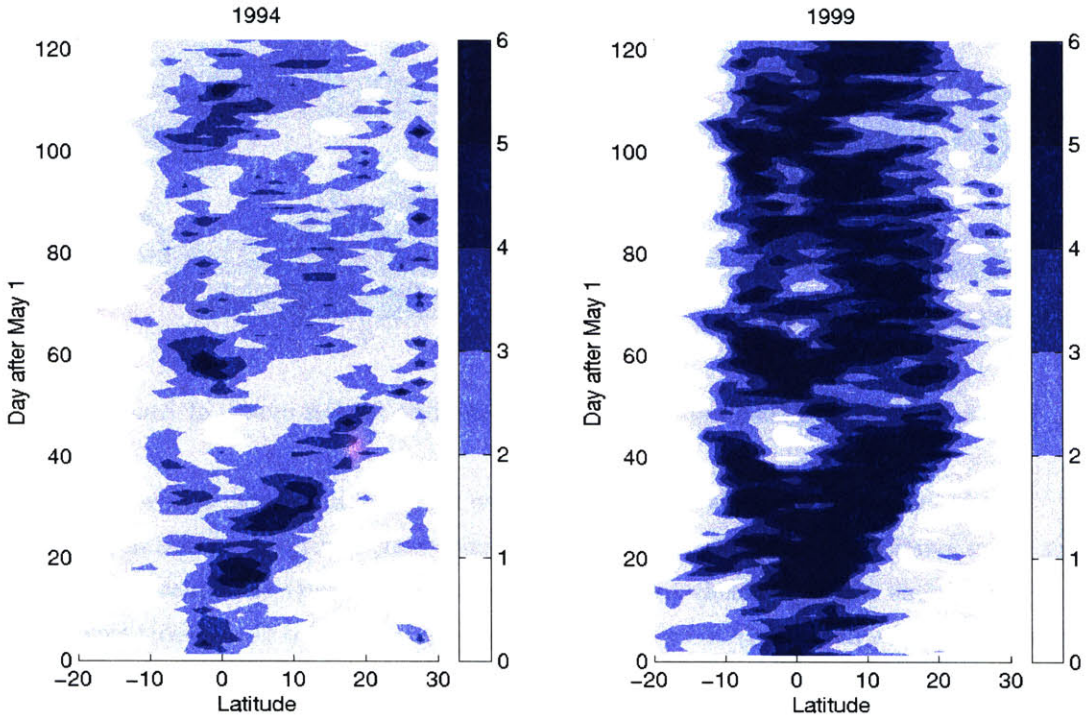

Figure 5-19: Zonal mean precipitation between 60E and 100E, May 1 through August 31, mm/day, from ECMWF reanalysis. Left, 1994; right, 1999.

20); this ascent region varies in strength and location, and is not always discernible. This ascent region is present both when low-level cross equatorial flow is weak, and when the flow is relatively strong. The position of the ascent region varies from approximately 10S to slightly north of the equator. After ascending, the flow joins the southward flow in the upper troposphere, and does not appear to cross the equator and continue into the monsoon region; instead, ascent in the monsoon region is fed by convergence from the Findlater jet and westerly flow over the Arabian Sea.

Figure 5-20 compares the circulation from ECMWF and NCEP reanalyses for the same time period; ascent near the equator occurs in both reanalyses, but the location of deep ascent is displaced approximately 5° between the two data sets. Because the equatorial Indian Ocean is a very observationally data poor region, the vertical velocity in the reanalyses is strongly dependent upon the numerical models rather than on actual observations. However, the TRMM data (Figure 5-18) lends credence to the existence of deep vertical motions near the equator in the Indian Ocean.

According to the theory of Pauluis (2001), cross-equatorial flow in the mixed layer is reduced when the pressure gradient across the equator is weakened. The mean meridional velocity at the equator from the surface to 925 mb and averaged between 60E and 100E is

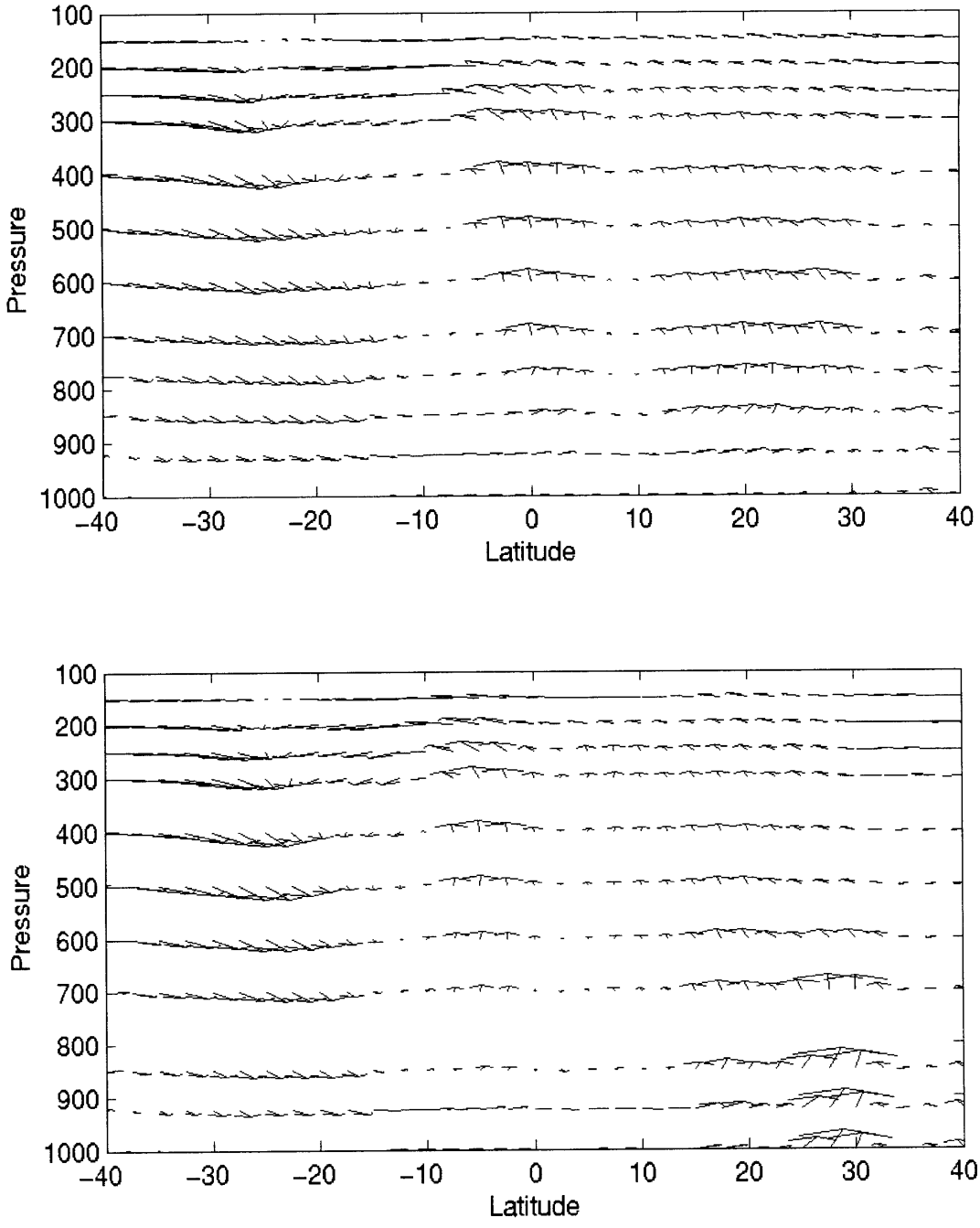

Figure 5-20: Zonal mean meridional circulation between 60E and 100E, mean June 20 through June 30 1994. Top from ECMWF reanalysis; bottom, from NCEP reanalysis.

compared to the meridional sea level pressure gradient over this longitudinal range (calculated as the difference between the mean sea level pressure from 0N-10N and the pressure between 10S-0N); during the summer of 1999, the correlation coefficient between these two fields is -0.5 at the 95% confidence level. The negative correlation is expected: weaker pressure gradients are associated with reduced southerly flow at the equator.

The circulation over the central and eastern Indian Ocean shows definite signs of inhibited cross-equatorial flow at low levels: frequent convergence and ascent near the equator, and a significant correlation between meridional flow at the equator and the large-scale pressure gradient. In the model with zonally symmetric setup (either in 2D or 3D), the inhibition to cross-equatorial flow manifests as jumping of the flow, as the only way for flow to cross the equator is for this to occur in the free troposphere. In the highly asymmetric flow over the Indian Ocean, flow may cross easily over the western Indian Ocean in the Findlater jet, so that the air which ascends near the equator is not required to cross the equator aloft for mass conservation.

Chapter 6

Discussion

The dynamics of the steady Hadley circulation has been described by a series of analytic studies by Held and Hou (1980), Lindzen and Hou (1988), Plumb and Hou (1992), and Emanuel (1995). Plumb and Hou speculated that this theory of angular momentum conserving circulations might explain the behavior of the monsoon. However, there are several limitations of the simple analytic theory: it does not consider the effects of a subtropical landmass, which forces the atmosphere differently from an aquaplanet or simple applied forcing; it does not account for the presence of eddies, or for asymmetry of the flow or the forcing; and it applies only to the steady state and does not account for onset or transient behavior. In light of these limitations, this thesis addresses two scientific questions:

1. How well does axisymmetric theory represent the fully three dimensional interactive monsoon?

2. What determines the strength and location of the monsoon?

Most previous studies of monsoon dynamics have taken one of two forms: either a highly idealized, axisymmetric framework, often with simplified dynamics; or a full GCM with realistic representations of continents, moist convection, radiation, and the accompanying host of intertwined feedbacks. This work attempts to take a middle ground between these two extremes, to capture the basic dynamics of the monsoon while reducing complexity sufficiently that the physical processes behind the model results may be understood. An idealized general circulation model was used to examine these two questions. The complexity of the model is gradually increased from a zonally asymmetric aquaplanet setup to a configuration with an asymmetric subtropical continent. By incrementally increasing the complexity of the model, the individual roles played by eddies, by the presence of a subtropical continent, and by asymmetry of forcing may be explored.

6.1 What determines the location of the monsoon?

The axisymmetric theory is extended in this thesis to predict the extent of the meridional circulation and the location of the monsoon. The work of Plumb and Hou (1992) and Emanuel (1995) focused on the viability of a subtropical angular momentum conserving meridional circulation, but did not address the location of the circulation. Although Lindzen and Hou (1988) calculated the extent and position of a cross-equatorial circulation in a dry model with forcing near the equator, they did not consider circulations driven by subtropical forcing or the effects of moist convection upon the dynamics of the circulation.

As described in detail in §3.3, the location of the deep ascent branch of an AMC circulation is strongly tied to the distribution of subcloud moist entropy. If a localized region of subtropical forcing is strong enough to induce an AMC meridional circulation, the ascent branch of the circulation, where there is no horizontal advection in the free troposphere, should occur in a region of zero vertical shear of zonal wind. Assuming quasi-equilibrium in regions of deep moist convection, the vertical temperature distribution in the vicinity of the monsoon is determined by the distribution of subcloud moist entropy. Although the moist convection may itself transport angular momentum, it redistributes momentum only within a vertical column, and does not change the requirement for zero vertical wind shear. In thermal wind balance with temperatures following a moist adiabat in the vertical, the only regions which have no vertical shear of zonal wind are those with no meridional gradient of subcloud moist entropy. Therefore, given a local maximum of subcloud moist entropy, the poleward boundary of the circulation will be colocated with the maximum s_b, and the large-scale ascent and precipitation will occur near and slightly equatorward of the maximum. The boundary of the circulation may not occur on the poleward side of the s_b maximum, as the poleward-decreasing s_b gradient would result in westerly shear and would require a source of angular momentum to supply the ascending air.

6.2 Does axisymmetric theory apply to the interactive monsoon?

Is the monsoon fundamentally a relocation of the ITCZ in a manifestation of a nonlinear, cross-equatorial Hadley circulation? The applicability of the nonlinear theory of Held and Hou (1980), Plumb and Hou (1992), and Emanuel (1995) to the monsoon has been explored in this work. According to Plumb and Hou (1992), the atmospheric response to a localized subtropical forcing may take one of two forms, depending upon the strength and distribution of the forcing: for weak forcing, the atmosphere will remain close to radiative convective equilibrium, with only weak, viscously driven meridional circulation; for sufficiently strong

forcing, a vigorous angular momentum conserving meridional circulation must result. The threshold between these two possible states is existence of an extremum of absolute angular momentum in the free troposphere in the thermal equilibrium solution. Emanuel (1995) expanded this theory to a moist atmosphere, and found that the threshold could be expressed in terms of the subcloud moist entropy distribution.

The atmosphere feels the difference between land and ocean surface through differing surface fluxes of heat and momentum. The ocean tends to store much of the incoming radiative energy internally, whereas the land surface has a much lower heat capacity and may be represented as having a balance of incoming and outgoing heat flux. The ocean has a virtually unlimited supply of moisture which may be evaporated from the surface, but the land surface evaporation is strongly constrained by availability of water, so that much of the flux into the atmosphere may take the form of sensible heating. Prior to onset of the monsoon, the continental airmass may be very arid, with the vertical temperature profile closer to a dry adiabat than a saturated adiabat; as a result, upper tropospheric temperatures may be lower than over the ocean, even though the lower troposphere is very warm over the land (§3.2.1). Without deep moist convection over the land to communicate surface heating into the upper troposphere, can the analytic theory still apply?

The initial aridity of the continent is not found to be an unscalable barrier to the onset of the monsoon. Although the model setup was not designed to emulate realistic onset conditions, the initiation of the monsoon is of some interest. In the two dimensional cases, an intense shallow, dry circulation forms over the coastline prior to onset of the monsoon. This circulation carries moisture from the tropical ocean over the hot landmass, gradually increasing the humidity until moist convection is possible. After precipitation begins, the land surface becomes wetted, allowing latent heat fluxes to increase over the continent. The subcloud moist entropy increases over the land as the humidity increases (although the temperature decreases after onset of rain), and a maximum of s_b develops over the continent. As this maximum strengthens, the meridional circulation rapidly intensifies, becoming global in extent. In the three dimensional cases, the general behavior of the circulation is similar, although eddies also help to carry moisture inland during the onset phase of the monsoon.

Two hallmarks of the cross-equatorial meridional circulation are examined to determine the nature of the flow induced by a local, subtropical forcing. One is the presence of threshold behavior, the other is the vanishing of absolute vorticity in the upper troposphere. In an aquaplanet setup with localized SST perturbation at 16N (§3.1.2), the meridional circulation clearly exhibits threshold behavior, with a pronounced increase in the strength of the circulation for forcing above a certain magnitude. These strong circulations are nearly AMC, with upper tropospheric absolute vorticity close to zero; the degree of conservation

is highly dependent upon the strength of the applied vertical viscosity. When the SST perturbation is replaced with a subtropical continent, as in §3.2, threshold behavior is not clearly seen when the land forcing strength is varied. However, the meridional circulations which develop for strong land forcing appear to be angular momentum conserving, with near zero absolute vorticity in the upper troposphere. The transition between a local (single-hemispheric) circulation and a global (cross-equatorial) circulation is coincident with the near-vanishing of absolute vorticity, which is a sign of threshold behavior.

The lack of threshold behavior in the two dimensional cases with a subtropical continent in comparison to the prominence of the behavior in the aquaplanet situation is ascribed to a combination of factors. One, in the aquaplanet cases, there is a WISHE feedback between the circulation strength and the surface fluxes through the surface wind speed. When the circulation is weak, the winds are weak and the surface fluxes are also weak; when the circulation is strong, the winds can dramatically increase the surface fluxes, particularly the latent heat flux, which in turn increases the strength of the circulation. This feedback tends to accentuate threshold behavior of the circulation strength in the aquaplanet case. In the continental cases, the net surface flux is prescribed, so that WISHE-type feedback will not occur, and the circulation strength is not expected to show as strong an increase above the threshold as in the aquaplanet cases.

A second, more subtle, factor is the poleward progression of the monsoon with increased forcing in the continental cases. A series of aquaplanet cases with varied location of the SST perturbation (§3.1.2) has shown that as the circulation extends further poleward, and it is presumed that the strength diminishes due to increased viscous forces on the rapidly intensifying equatorial easterly jet. Thus as the monsoon moves poleward in the continental cases, broadening the circulation, the circulation strength is expected to weaken somewhat, obscuring threshold behavior. In the aquaplanet cases, the surface fluxes are greatest near the SST maximum, and the monsoon does not stray far from the SST perturbation, so that this effect is not observed.

Why does the monsoon move inland when the strongest forcing is along the coast? The monsoon is expected to exist just equatorward of the maximum in subcloud moist entropy, as previously discussed. In radiative convective equilibrium, the greatest subcloud moist entropy occurs where the net surface fluxes are greatest, over the coastal continent (§3.2.1). Once the meridional circulation develops, the low-level flow carries air from the oceans, which has lower subcloud moist entropy, over the coastal regions, locally reducing the moist entropy so that the maximum entropy is located inland. As the forcing is increased, the circulation also intensifies, with a greater flux of low entropy air being carried onto the continent which must be heated by the surface forcing to bring it to the RCE entropy state (§3.3). The inflowing air must travel further over the landmass while being heated from the

surface to reach the maximum subcloud moist entropy.

How well do the modeled circulations hold to the location of the monsoon predicted by theory (§3.3)? The two dimensional cases with subtropical continent uphold the theory quite well: the poleward boundary of the meridional circulation is colocated with the maximum subcloud moist entropy, and the monsoon precipitation occurs slightly equatorward of this maximum. The theory holds reasonably well for the aquaplanet cases, but there are a few examples in which the boundary of the circulation occurs poleward of the subcloud moist entropy maximum, and the ascending branch of the circulation has westerly shear with height. In these cases, the numerical filters break down angular momentum conservation in the ascent branch of the circulation, and the theory does not apply.

According to the theory laid out by Plumb and Hou (1992), the forcing strength required to induce an AMC circulation is dependent upon both the shape and location of the forcing: the closer to the equator, the less forcing is required. This is borne out by the modeled cases with the coastline located at 8N. In these cases, a global AMC circulation occurs at a weaker forcing level than in the cases with coastline at 16N, and the circulation is more vigorous. When the coastline is moved to 24N, an AMC circulation may still result for sufficiently strong forcing, but the cell is local and not global, following the theory of Schneider (1983).

6.3 Does the theory apply to the asymmetric monsoon?

The analytic theory was developed in an axisymmetric framework, with no allowance for eddies or asymmetry of the large-scale flow of forcing. The model is expanded from axisymmetry to fully three dimensional dynamics, first with a zonally symmetric continent to examine the impact of eddies, and then with asymmetric continent and forcing.

The existence of eddies in the midlatitudes and equatorial regions has relatively little impact on the zonal mean steady monsoon in the cases with zonally symmetric continent. The eddies do act to redistribute moist entropy in the subcloud layer, bringing the maximum s_b closer to the equator, and weakening the magnitude of the maximum. This results in a monsoon which is slightly weaker and closer to the equator than in the axisymmetric cases (with no eddies). These eddies also act to weaken the upper tropospheric jets, and they decrease the angular momentum conservation of the zonal mean meridional circulation. Even through the meridional circulation does not conserve angular momentum as closely as the axisymmetric cases, the axisymmetric theory appears to be upheld reasonably well.

Localized wave disturbances form within the monsoon, and also in some cases with submonsoonal forcing. These warm-core waves feature cyclonic flow associated with a lower tropospheric heat low, with strong precipitation in the southeastern quadrant where there

is poleward flow. The waves exist along the coast and slightly inland, where they propagate westward. The waves have a baroclinic signature, and form from instability of the lower-tropospheric easterlies which exist in thermal wind balance with the transition from cool tropical ocean to heated subtropical landmass. In the monsoonal cases, the easterlies form on the poleward edge of the monsoon, where the cooler rainy region abuts the arid, hot interior. The speed of the waves depends on the strength and depth of the easterly jet. These waves do not have a significant impact on the zonal mean monsoon; the overall behavior of the monsoon is quite similar to the axisymmetric cases.

The axisymmetric theory does not fare as well with an asymmetric continent and forcing. When the longitudinal extent of the continent is limited to 180° with uniform ocean temperatures (§4.2.1), the meridional monsoon circulation remains confined to the summer hemisphere for even the strongest land surface forcing. These overturning cells are not closely angular momentum conserving; the absolute vorticity in the upper troposphere does not approach the critical value at zero, and the contours of AAM are not folded over by the flow. Although the monsoon moves quite far inland for the stronger forcing cases, the circulation does not appear to be the localized AMC type described by Schneider (1983) and seen in the axisymmetric cases with coastline at 24N (§3.2.3). Although the meridional circulation is relatively weak, there is strong deep ascent and considerable precipitation over the continent at the same forcing levels which produce a monsoon in the cases with zonally symmetric continent. Much of the compensating subsidence occurs not in the descent branch of the meridional circulation, but in a region to the northwest of the monsoon. This subsidence region is similar to the descent induced by Rossby waves found by Rodwell and Hoskins (1996, 2001). When the asymmetry is increased to a configuration with pole-to-pole continent (§4.2.4), the large scale circulation becomes very asymmetric, with little evidence of a meridional circulation.

Although the meridional circulation does not closely follow the axisymmetric theory of AMC circulations when an asymmetric landmass is used, the subcloud moist entropy distribution remains a good indicator of deep moist convection over the continent. In the cases with uniform ocean temperatures and asymmetric continent (§4.2.1), deep ascent and moist convection occurs over the landmass only when the subcloud moist entropy has a global maximum over the continent. The ascent and precipitation occur on the equatorward side of the s_b maximum, which is the location predicted by theory. Although the upper tropospheric, equatorward branch of the meridional circulation is not closely AMC, if the ascent region is nearly AMC and is not influenced by advection of angular momentum from other regions, the relationship between the subcloud moist entropy distribution and the location of ascent and precipitation described by the theory should hold.

The impact of advection of moist entropy is revealed in the cases with zonally asymmetric

continent and summer SSTs (§4.2.2). In these cases, the cool midlatitude oceans are a source of low moist entropy air, which is advected into the continental interior by the prevailing westerly winds and by cyclonic flow over the landmass. This advection drastically reduces the subcloud moist entropy over the continental interior and along the western subtropical continent, so that s_b is greater over the ocean than over the continent in these areas. No meridional monsoonal circulation forms over the land, and the only precipitation along the central and western continent is weak even for the strongest forcing levels. Over the eastern continent, the low level flow carries tropical ocean air inland, and a maximum in s_b forms over the subtropical continent for strong forcing, allowing deep ascent and steady precipitation only in the southeastern corner of the continent. Over the central and western continent, where the land is relatively dry, a low level easterly jet forms in thermal wind balance with the poleward-increasing temperature gradient; baroclinic disturbances form in this jet and propagate westward along the coastline and are the only source of precipitation over the central and western continent. This result supports the work of Chou et al. (2001) and Chou and Neelin (2003), who found that 'ventilation' of the monsoon region by advection of low moist entropy air limits the poleward and westward extent of the monsoon. The analytic theory linking the monsoon location to the subcloud moist entropy distribution gives a framework to explain why the advection of s_b is so influential. It is doubtful that the Rodwell-Hoskins effect of subsidence due to Rossby waves is responsible for the strong asymmetry of the monsoon in the cases with summer SSTs: if it was, the cases with uniform SSTs, which have a much stronger monsoon, should also show significant east-west asymmetry, but they do not.

When a thin wall is used to block advection of midlatitude air into the monsoon region (§4.3.1), a cross-equatorial meridional circulation with deep ascent over the subtropical asymmetric continent. When low s_b air is blocked, a maximum in subcloud moist entropy forms over the subtropical continent, with precipitation and deep ascent over the continent. This ascent region is joined to the cross-equatorial Hadley cell, although stronger ascent occurs over the equatorial ocean. Subsidence occurs both in the southern hemisphere subtropics, and in a region to the northwest of the monsoon, as in the cases with uniform SSTs and asymmetric continent (§4.3.1). Although the monsoon is not as large or strong as in the uniform SST cases with asymmetric continent, the SST gradient at the equator ensures the formation of a cross-equatorial circulation.

6.4 Comparison with existing literature

In this section, the model results from the MITGCM are compared with other modeling studies to characterize the behavior of the model and to place the results in context with

existing research.

Few axisymmetric studies use models which are similar in complexity to a GCM; fewer still focus on meridional circulations which occur in response to subtropical forcing. Zheng (1998) used an axisymmetric aquaplanet model with the convective scheme of Emanuel (1991) to test the threshold theory of Emanuel (1995). A localized subtropical SST maximum was employed to induce a steady cross-equatorial meridional circulation, and the magnitude of the SST maximum was varied to test a range of behaviors. This setup is similar to that used in §3.1.2, although the form of the SST maximum was different, and located further poleward; additionally, Zheng fixed the surface wind speed used in the surface flux calculations, removing WISHE feedbacks. The meridional circulations which formed for supercritical forcing were similar in form to those seen in the aquaplanet cases with the GCM (§3.1.2), with pronounced jumping of the flow at the equator. The threshold behavior of the circulation strength found by Zheng was not as pronounced as that seen in the MITGCM (§3-5), presumably due to the lack of WISHE feedback in Zheng's model.

The linear, two layer, β-plane Gill model (Gill, 1980) which describes the response to a local tropical heat source in terms of Kelvin and Rossby waves has been used to explain the large-scale monsoon circulation (Hoskins and Rodwell, 1995). The response to an off-equatorial local forcing consists of low-level easterlies to the east of the forcing due to Kelvin waves, and two cyclones to the west of the forcing due to Rossby waves. With off-equatorial forcing, the cyclone in the same hemisphere as the forcing is stronger, with a weak cyclone in the opposite hemisphere, with westerlies between these cyclones and with some cross-equatorial flow at the equator. A meridional cell features ascent in the vicinity of the forcing and subsidence in the opposite hemisphere. Rodwell and Hoskins (1996) found subsidence to occur in the Rossby-wave regime poleward and to the west of the forcing region. This Gill-type response was observed only for the model cases with zonally asymmetric continent and uniform, warm SSTs (§4.2.1). The forcing in these cases was further poleward than in Gill's off-equatorial forcing case, and the response in the opposing hemisphere is much weaker, with no cross-equatorial flow.

A handful of studies have investigated monsoons using general circulation models with highly idealized representations of continents. Cook and Gnanadesikan (1991) used a rectangular continent centered on the equator in the Geophysical Fluid Dynamics Laboratory GCM with a simple bucket hydrology and fixed SST slab ocean with maximum temperatures 7° from the equator in the summer hemisphere. An interactive radiative scheme was used with a perpetual summer setup, and with net downward radiative forcing in the summer hemisphere near $150\,W/m^2$ with an interactive hydrology. The resulting precipitation field was similar to that seen in §4.2.4 with pole-to-pole continent and weak surface forcing: the landmass is quite arid except for along the tropical eastern coast. The low-level flow

over the continent and oceans is also similar to the weak forcing case in §4.2.4, although the continent used by Cook and Gnanadesikan is only 60° in width in comparison to the 180° wide continent used with the MITGCM.

The pole-to-pole continent was also investigated by Chou et al. (2001) using a quasi-equilibrium tropical circulation model (QTCM) of intermediate complexity with a mixed-layer ocean with prescribed meridional ocean heat flux. The model uses radiation with a seasonal cycle; the summer state with interactive land hydrology and no meridional ocean heat flux is quite similar to that found in the perpetual solstice case of Cook and Gnanadesikan (1991). The flow and precipitation are again similar to that seen in the MITGCM with weak land forcing (§4.2.4), although the low-level winds over the subtropical continent are northeasterly in the MITGCM but northwesterly in the QTCM. It is noteworthy that a much narrower continent is used in the QTCM, one which is only 45° wide. When the meridional ocean heat flux is increased so that the ocean becomes nearly uniformly warm from the tropics to the midlatitudes (their Figure 6), the precipitation and flow fields in the summer hemisphere are reminiscent of the flow in the MITGCM case with pole-to-pole continent and uniform SSTs (§4.2.4), although the winter hemisphere has a very different, more arid circulation in the QTCM. The summer hemisphere state is also similar to the MITGCM cases with asymmetric subtropical continent (§4.2.1), with strongest precipitation over the western continent and weak east-west tilt.

Perhaps the most similar model setup used with a different GCM is that by Xie and Saiki (1999), who used a simple Africa/Asian continent with the University of Tokyo's GCM, with a bucket hydrology, Arawaka-Schubert convection scheme, and prescribed SSTs. The summer circulation and precipitation over their 180° wide continent in the seasonal cases is quite similar to that seen in the MITGCM cases with strongly forced zonally asymmetric continent and summer SSTs (§4.2.2): steady precipitation occurs over the southeastern corner of the continent, but remains offshore of the western continent, where there is equatorward low-level flow. However, in a perpetual summer case (their Figure 7), the precipitation and flow over the continent is closest to the MITGCM cases with uniform SSTs (§4.2.1), with widespread precipitation over the continental interior across the entire width of the continent. This difference could be due to the differences in the convection schemes used in the two models, or the different land flux balance; Xie and Saiki used interactive radiation rather than prescribed radiative fluxes to calculate the surface flux balance.

Westward-propagating waves which travel along the coastline are found to occur prior to onset of the monsoon by Xie and Saiki (1999). Their waves are baroclinic in origin, forming from a low-level easterly jet which exists along the coastline in thermal wind balance prior to monsoon onset. The waves show eastward tilt with height, and have the greatest precipitation to the east of the wave depression, where poleward winds carry moist oceanic

air inland. The waves act to moisten the land surface, after which precipitation becomes widespread across the continent, and the waves are less prominent. These waves are very close in nature to the westward propagating waves seen in the three dimensional cases in the MITGCM, although these waves do not initiate onset of the monsoon. In fact, the wetting of the continent by the waves in the MITGCM is very short-lived, and the land dries out quickly after passage of each wave.

Chou (2003) investigated the monsoon over a single Asia/Africa conglomerate continent using the QTCM with mixed-layer ocean and a seasonal cycle. The summer monsoon was confined to only the southeast corner of the continent, as in Xie and Saiki (1999)'s seasonal case and in the MITGCM cases with asymmetric continent and summer-like SSTs (§4.2.2). For a control case with no meridional ocean heat flux, the monsoon in the QTCM was similar to the MITGCM case with very weak land forcing - the subtropical precipitation remains over the ocean with very little precipitation over the continent. As the land forcing is increased in the QTCM, precipitation and low-level inflow over the southeastern corner increases, but does not spread across the central or western continent. This is similar to the results seen in the MITGCM with asymmetric continent and summer-like SSTs.

The only study to examine both a zonally symmetric and an asymmetric subtropical continent is that of Dirmeyer (1998), who used the Center for Ocean-Land-Atmosphere Studies GCM with a simple rectangular continent but complex physical parameterizations. A seasonal cycle was used, with seasonally varying prescribed SSTs and a simple biosphere parameterization over the land surface. In the case with zonally symmetric continent with coastline at 13.3N, the ITCZ remains in the southern hemisphere throughout the entire year, with only weak precipitation along the immediate coastline; this is similar to the non-monsoonal MITGCM cases with zonally symmetric continent and weak land forcing. When the longitudinal extent of the continent is limited to 120° or less, precipitation over the subtropical continent remains weak, although it strengthens slightly in the southeastern corner, where easterlies carry moisture inland from the nearby ocean; the ITCZ remains south of the equator. However, if the zonally asymmetric continent is moved equatorward, so that that coastline is at 8.8N, the ITCZ does move over the subtropical continent during the summer months, and shifts to the northern hemisphere tropical ocean during boreal winter. The results for the continent with coastline at 13.3N are similar to the model results with weak land forcing in the MITGCM and a submonsoonal circulation.

6.5 Comparison with observations

The analytic theory and the model simulations are both highly idealized, and it is not obvious that the real world should bear a strong resemblance to either. Monsoons are

found in Asia, West Africa, Australia, South America, each with unique characteristics. How well does the theory explain the circulation of each of these monsoons? Do the model results at all resemble observations?

The analytic theory of angular momentum conserving meridional circulation appears to be reasonably closely held by the global monsoons, as discussed in §5.2. All of the observed monsoons feature a large-scale cross-equatorial meridional circulation, with ascent in the monsoon region and subsidence in the opposite hemisphere. The upper tropospheric absolute vorticity is close to zero in the upper branch of these circulations, which indicates that the circulations are nearly angular momentum conserving, of the type predicted by Plumb and Hou (1992) to occur in response to strong subtropical forcing.

The location of the observed monsoons is in agreement with the predictions of the analytic theory; that is, the poleward limit of the monsoon is close to the maximum in subcloud moist entropy, or in a region where the meridional gradient of s_b is zero. In cases where the subcloud moist entropy has a broad, flat maximum rather than a localized maximum, the boundary of the monsoon circulation is colocated with the poleward-most edge of this s_b maximum. The location of the monsoon is in agreement with the theory not only in the long term mean, but also (usually) for the transient monsoon.

The modeled monsoon circulations have many features in common with the observed monsoons. The southwest-northeast tilt of the Asian monsoon is captured in the modeled cases with zonally asymmetric continent and summer-like SSTs. The narrow band of inland precipitation seen in the West African monsoon is captured in the modeled cases with zonally symmetric continent. The greatest rainfall remains offshore in the Australian monsoon, which is similar to the modeled cases with forcing just below the level needed to induce a full monsoon.

The observed meridional circulation is captured in the model when a zonally symmetric continent is used, but not with an asymmetric continent. In the zonally asymmetric continent cases with uniform SSTs (§4.2.1), which have deep ascent and strong precipitation over the continent, the ocean temperatures are so unrealistic that it is not surprising that the meridional circulation bears little resemblance to observations. In the cases with more realistic, summer-like SSTs (§4.2.2), the monsoon is so weak over the land that a meridional circulation is again not unreasonably absent. When the more realistic ocean SSTs are used, the subcloud moist entropy over the land does not have the strong, inland maximum that is seen in observations for the African, Asian, and South American monsoons, and which induces an inland monsoon with a vigorous meridional circulation. This difference in the moist entropy distribution is likely due to features which are absent from the highly idealized model, such as orography, and spatial variations in albedo and other radiative feedbacks. The only cases with asymmetric continent which have a cross-equatorial merid-

ional circulation with deep ascent over the continent are the cases with thin walls that block flow from the midlatitudes into the monsoon area (§4.3.1), allowing a maximum in s_b to form over the subtropical continent with realistic ocean temperatures in the tropics.

The jumping behavior which is so prominent in the model is also seen over the Indian Ocean in association with the Asia monsoon; the jumping behavior is not expected to occur strongly near West Africa or South America because of the proximity of the coastline to the equator. The myriad mountainous islands and complex flow over the West Pacific obscure any jumping behavior near the Australian monsoon.

Although the modeled results prominently feature westward propagating baroclinic waves, the modeled waves have fundamental dynamical differences from the observed monsoon depressions which propagate westward across India and West Africa. The modeled waves are warm-core waves which develop from baroclinic instability of the low-level easterly jet in thermal wind balance along the coastline; the observed monsoon depressions are cold-core, and have a mixed barotropic-baroclinic signature. While the precipitation associated with the waves in the model occurs to the east of the depression, the observed waves have the strongest precipitation on the west side of the depressions. The types of waves which are dominant in the GCM are dependent upon the resolution, the numerical filtering, the convection scheme, and other factors; it is difficult to determine why the modeled waves differ from the observed monsoon waves. For example, if the numerical Shapiro filter is changed from eighth order to fourth order, the westward propagating waves are entirely damped out.

6.6 Implications

The analytic theory suggests that the location and extent of the monsoon is controlled by the distribution of subcloud moist entropy. Thus, the question of the effect of various mechanisms upon the location of the steady monsoon may be reduced to a determination of the impact upon the subcloud moist entropy.

For example, orography can affect the subcloud moist entropy in multiple ways. Molnar and Emanuel (1999) have shown that the radiative-convective equilibrium surface air temperature decreases at a rate of approximately $2\,K/km$ as the surface is raised, which is less steep of a decline than the moist adiabatic lapse rate. Assuming a moist adiabatic lapse rate, the saturation entropy will be greater over an elevated surface than over a lower surface receiving the same incoming radiation, and the subcloud moist entropy will also be greater. In addition, mountains can act to block the large-scale low-level flow, perhaps preventing the influx of low moist entropy air from other regions, as demonstrated in §4.3.1.

Why is the Asian monsoon the largest and strongest of the observed monsoon regions?

Over Asia, the Tibetan Plateau blocks the advection of low moist entropy from the continental interior, and the elevation effects simultaneously increase the local subcloud moist entropy, especially where moist tropical air encounters the southern flank of the mountains. Molnar and Emanuel (1999) have shown that entropy at a given pressure level is greater over an elevated surface than over a surface at sea level; this helps to explain the strong maximum in moist entropy over the Himalayas. In the summer months, the upper tropospheric temperature field features a strong maximum over the Tibetan Plateau, which has long been presumed to be major factor in causing the Asian monsoon to be the most intense of the global monsoons. The results of this study suggest that the blocking effect by the Tibetan Plateau may have a very significant impact on the moist entropy distribution, by shielding India and southeast Asia from inflow from the Asian midlatitudes.

In contrast to Asia, the Australian monsoon is confined only to the coastal region, with the strongest moist convection occurring over the tropical ocean. Australia has a maximum in s_b at the coastline, with moist entropy decreasing rapidly inland over the interior desert. Advection of low moist entropy air from the nearby oceans keeps s_b levels low over the interior, banishing the monsoon to the immediate coastal region.

A pool of high subcloud moist entropy forms over Amazonia during the summer months; this region is sheltered from influx of low entropy air by the Andes mountains to the west, and the Brazilian Highlands to the southeast. Although the Brazilian highlands are not exceptionally tall mountains, the western Atlantic ocean is relatively warm in the tropics during austral summer, so that the moist entropy levels over the nearby ocean are relatively high. In contrast, the eastern Pacific has quite low moist entropy, but the lofty Andes almost completely block flow from the Pacific. Along the eastern flank of the Andes, where the moist monsoon flow meets the elevated surface, the subcloud moist entropy is particularly high. This has implications for paleoclimate, especially as the Andes are a relatively young mountain range; without a tall mountain range along the west coast, the subcloud moist entropy over South America would be much lower, and the monsoon would be both weaker and more limited in extent.

The West African region is devoid of mountains of significant height, although the Atlas mountains along the northwest coast may deflect some of the northerly flow from the cool Atlantic ocean. The main feature over the interior of West Africa is the Sahara desert, which has a high albedo, resulting in weaker net radiative forcing at the surface. The existence of this large desert keeps the moist entropy low over the interior of the continent. Along the southern coast, strong inflow from the oceans maintains low moist entropy along the coastline; thus, the entropy maximum is limited to a narrow region between the coast and the desert.

6.7 Limitations

The idealized physics used in this study neglects many important processes which may have substantial impacts upon the monsoon. The version of the MITGCM used here does not support orography, which may strongly influence the monsoon, as previously discussed. The model has only the simplest representation of boundary layer physics, consisting of a momentum mixed layer of fixed depth and dry adiabatic adjustment of variable depth. The land surface hydrology is very primitive, and there is no allowance for vegetation or other surface biosphere components. Given the importance of boundary layer thermodynamics to the large scale monsoon which has been emphasized in this study, the simplicity of the boundary layer representation in the model is a serious limitation.

One important process which was omitted from the model is radiation. Although the use of Newtonian cooling makes the dynamics much more straightforward, the prescribed net radiative flux used to calculate the surface energy balance is not very realistic. The model neglects feedbacks from clouds, the radiative influence of water vapor, longwave feedbacks from the surface temperature, albedo and vegetative effects on radiation, all of which may impact the monsoon. A diurnal cycle is also not included in the model, which may impact the steady state.

This study has focused almost solely on the steady state monsoon, but the real monsoon is very transient. The timescales needed to reach a steady state in the model are quite long, especially in the two dimensional cases. In the seasonal-like experiments with an axisymmetric setup (§3.4), the transient monsoon circulation only bore a resemblance to the steady state during the late summer period. Intraseasonal variability, such as break-monsoon and onset, is an important aspect of the monsoon circulation which is not addressed by this study.

6.8 Conclusions

The goals of this thesis were to determine the applicability of the analytic, axisymmetric theory of angular momentum conserving meridional circulations (Plumb and Hou (1992), Emanuel (1995)) to the asymmetric, interactive monsoon; and to explain controlling factors which determine the location and strength of the monsoon. The existing literature had only explored the analytic theory in a purely axisymmetric framework with prescribed forcing, and no attempts were made to account for the presence of a subtropical continent, although the land-sea contrast is generally deemed to be intrinsic to the development of the monsoon.

Starting in an axisymmetric setup, the analytic theory is found to hold well in an aqua-planet framework with local subtropical SST perturbation: with small SST perturbation,

only a weak local meridional circulation cell forms, while a strong, cross-equatorial angular momentum conserving cell occurs above a certain forcing threshold. When a subtropical continent is introduced in place of the SST perturbation, the theory still holds well, with a cross-equatorial meridional circulation forming with ascent over the continent when the land forcing was sufficient to create a significant maximum in subcloud moist entropy over the landmass. The circulation with a continent differs from the aquaplanet circulation in that the strong feedback between the wind and the surface flux in the aquaplanet mode is not seen over the continent; also, the circulation interacts with the subcloud moist entropy over the land to determine the location of the monsoon. When eddies and asymmetry of the flow are introduced while retaining zonal symmetry of the continent and forcing, there is little change to the zonal mean monsoon circulation; the net effect of the eddies is to slightly weaken the monsoon, but the overall steady flow remains nearly zonally symmetric.

When zonal asymmetry of the continent and forcing is introduced, the axisymmetric theory does not hold as closely, and the large-scale flow becomes very asymmetric. An angular momentum conserving, cross-equatorial circulation does not attain in response to only an asymmetric subtropical forcing; only a local, weak meridional circulation occurs. Subsidence which compensates for deep ascent in the monsoon region occurs poleward and to the west of the monsoon, similar to Rossby-wave subsidence found in a linear model by Rodwell and Hoskins (1996).

The analytic theory is expanded to explain the location and extent of the monsoon. The poleward boundary of the monsoon circulation is found to be colocated with the maximum in subcloud moist entropy, with the bulk of the monsoon precipitation occurring slightly equatorward of this boundary. This theory is found to hold in the modeled cases both with axisymmetric and asymmetric continent; it also appears to apply to observed monsoon circulations around the globe. The advection of subcloud moist entropy by the large-scale circulation is found to have a very strong impact on the entropy distribution, and thus on the location and strength of the monsoon. This is exemplified in the cases with zonally asymmetric continent and summer-like SSTs, in which advection of low moist entropy air from the midlatitude oceans into the continental interior greatly weakens the monsoon, and limits monsoonal precipitation to only the southeastern corner of the continent.

Future work is suggested to investigate how different physical processes impact the subcloud moist entropy and the large scale monsoon circulation. Important processes which were neglected from the idealized model used here include radiative feedbacks, orographic effects, and boundary layer physics. The theory linking the monsoon location to the subcloud moist entropy maximum may also be able to help explain transient monsoon features, such as onset and break monsoon.

Bibliography

2004, Initial monsoon floods assessment report 2004, draft. Bangladesh Disaster and Emergency Response DER Sub-group.

Anderson, D.: 1976, The low-level jet as a western boundary current. *Mon. Wea. Rev.*, **104**, 907–921.

Burpee, R.: 1972, The origin and structure of easterly waves in the lower troposphere of North Africa. *J. Atmos. Sci.*, **29**, 77–90.

Charney, J.: 1975, Dynamics of desert and drought in Sahel. *Quart. J. Roy. Meteor. Soc.*, **101**, 193 - 202.

Chou, C.: 2003, Land-sea heating contrast in an idealized Asian summer monsoon. *Climate Dynamics*, **21**, 11 - 25.

Chou, C. and J. D. Neelin: 2003, Mechanisms limiting the northward extent of the northern summer convection zones. *J. Climate*, 406–425.

Chou, C., J. D. Neelin, and H. Su: 2001, Ocean-atmosphere-land feedbacks in an idealized monsoon. *Quart. J. Roy. Meteor. Soc.*, 1869–1891.

Cook, K. and A. Gnanadesikan: 1991, Effects of saturated and dry land surfaces on the tropical circulation and precipitation in a general circulation model. *J. Climate*, 873–889.

Dirmeyer, P.: 1998, Land-sea geometry and its effect on monsoon circulations. *J. Geophys. Res.*, 11555–11572.

Eltahir, E. and C. Gong: 1996, Dynamics of wet and dry years in West Africa. *J. Climate*, **9**, 1030–1042.

Emanuel, K. A.: 1986, An air-sea interaction theory for tropical cyclones. Part I: steady state maintenance. *J. Atmos. Sci.*, **42**, 585–604.

— 1991, A scheme for representing cumulus convection in large-scale models. *J. Atmos. Sci.*, **48**, 2313–2335.

— 1995, On thermally direct circulations in moist atmospheres. *J. Atmos. Sci.*, **52**, 1529–1534.

Emanuel, K. A., J. D. Neelin, and C. S. Bretherton: 1994, On large-scale circulations in convecting atmospheres. *Quart. J. Roy. Meteor. Soc.*, **120**, 1111–1143.

Emanuel, K. A. and M. Živković Rothman: 1999, Development and evaluation of a convection scheme for use in climate models. *J. Atmos. Sci.*, **56**, 1766–1782.

Fang, M. and K. Tung: 1996, A simple model of nonlinear Hadley circulation with an ITCZ: analytic and numerical solutions. *J. Atmos. Sci.*, **53**, 1241–1261.

— 1997, The dependence of the Hadley circulation on the thermal relaxation time. *J. Atmos. Sci.*, **54**, 1379–1384.

Findlater, J.: 1969, A major low-level air current near the Indian Ocean during the northern summer. *Quart. J. Roy. Meteor. Soc.*, **95**, 362–380.

Gadgil, S.: 2003, The Indian monsoon and its variability. *Annual Review of Earth and Planetary Science*, **31**, 429–467.

Gill, A. E.: 1980, Some simple solutions for heat-induced tropical circulation. *Quart. J. Roy. Meteor. Soc.*, **106**, 447–462.

Godbole, R.: 1977, The composite structure of the monsoon depression. *Tellus*, **29**, 25–40.

Gregory, D., R. Kershaw, and P. M. Inness: 1997, Parametrization of momentum transport by convection. II: tests in single-column and general circulation models. *Quart. J. Roy. Meteor. Soc.*, **123**, 1153–1183.

Hadley, G.: 1735, Concerning the cause of the general trade-winds. *Phil. Trans. of the Royal Soc. of London*, **39**, 58–62.

Halley, E.: 1686, An historical account of the trade winds, and monsoons, observable in the seas between and near the Tropicks, with an attempt to assign the phisical cause of said winds. *Phil. Trans. of the Royal Soc. of London*, **26**, 153–168.

Hayashi, Y.: 1971, A generalized method of resolving disturbances into progressive and retrogressive waves by space Fourier and time cross-spectral analyses. *J. Met. Soc. Japan*, **49**, 125–128.

Held, I. M. and A. Y. Hou: 1980, Nonlinear axially symmetric circulations in a nearly inviscid atmosphere. *J. Atmos. Sci.*, **37**, 515–533.

Held, I. M. and M. J. Suarez: 1994, A proposal for the intercomparison of the dynamical cores of atmospheric general circulation models. *Bull. Amer. Meteor. Soc.*, **75**, 1825–1830.

Hide, R.: 1969, Dynamics of the atmospheres of the major planets with an appendix on the viscous boundary layer at the rigid bounding surface fo an electrically-conducting rotating fluid in the presence of a magnetic field. *J. Atmos. Sci.*, **26**, 841–853.

Hoskins, B. and M. Rodwell: 1995, A model of the Asian summer monsoon. Part 1: the global scale. *J. Atmos. Sci.*, **52**, 1329–1340.

Kirkwood, E. and J. Derome: 1977, Some effects of the upper boundary condition and vertical resolution on modeling forced stationary planetary waves. *Mon. Wea. Rev.*, **105**, 1239–1251.

Kishtawal, C., N. Gautam, S. Jaggi, and P. Pandey: 1994, Surface-level moisture transport over the Indian Ocean during southwest monsoon months using NOAA/HIRS data. *Boundary-Layer Meterology*, **69**, 159–171.

Krishnamurti, T., M. Kanamitsu, R. Godbole, C.-B. Chang, F. Carr, and J. Chow: 1975, Study of a monsoon depression i: synoptic structure. *J. Met. Soc. Japan*, **53**, 227–239.

Lindzen, R. S., E. Batten, and J.-W. Kim: 1968, Oscillations in atmospheres with tops. *Mon. Wea. Rev.*, **96**, 133–140.

Lindzen, R. S., B. Farrell, and A. Rosenthal: 1983, Absolute barotropic instability and monsoon depressions. *J. Atmos. Sci.*, **40**, 1178–1184.

Lindzen, R. S. and A. Y. Hou: 1988, Hadley circulations for zonally averaged heating off the equator. *J. Atmos. Sci.*, **45**, 2416–2427.

Manabe, S.: 1969, Climate and the ocean circulation: the atmospheric circulation and the hydrology of the earth's surface. *Mon. Wea. Rev.*, **97**, 739–773.

Marshall, J., A. Adcroft, J.-M. Campin, and C. Hill: 2004, Atmosphere-ocean modeling exploiting fluid isomorphisms. *Mon. Wea. Rev.*, **132**, 2882–2894.

Mishra, S. and P. Salvekar: 1980, Role of baroclinic instability in the development of monsoon disturbances. *J. Atmos. Sci.*, **38**, 383–394.

Molnar, P. and K. Emanuel: 1999, Temperature profiles in radiative-convective equilibrium above surfaces at different heights. *J. Geophys. Res.*, **104**, 24265–24271.

Nicholson, S.: 1993, An overview of African rainfall fluctuations of the last decade. *J. Climate*, **6**, 1463–1466.

Ninomiya, K. and C. Kobayashi: 1999, Precipitation and moisture balance of the Asian summer monsoon in 1991.Part II: moisture transport and moisture balance. *J. Met. Soc. Japan*, **77**, 77–99.

Pauluis, O.: 2001, Axially symmetric circulations in a moist atmosphere. *Thirteenth Conference on Fluid Dynamics of the AMS*, American Meteorological Society.

Pedgley, D. and T. Krishnamurti: 1976, Structure and behavior of a monsoon cyclone over West Africa. *Mon. Wea. Rev.*, **104**, 149–167.

Plumb, R. and A. Hou: 1992, The response of a zonally symmetric atmosphere to subtropical forcing: threshold behavior. *J. Atmos. Sci.*, **49**, 1790–1799.

Qian, W., Y. Deng, Y. Zhu, and W. Dong: 2002, Demarcating the worldwide monsoon. *Theoretical and Appiled Climatology*, **71**, 1–16.

Randel, W. and I. Held: 1991, Phase speed spectra of transient eddy fluxes and critical layer absorption. *J. Atmos. Sci.*, **48**, 688–697.

Rodwell, M. and B. Hoskins: 1995, A model of the Asian summer monsoon. Part 2: cross-equatorial flow and PV behavior. *J. Atmos. Sci.*, **52**, 1341–1356.

— 1996, Monsoons and the dynamics of deserts. *Quart. J. Roy. Meteor. Soc.*, **122**, 1385–1404.

— 2001, Subtropical anticyclones and summer monsoons. *J. Climate*, **14**, 3192–3211.

Saha, K. and C.-P. Chang: 1983, The baroclinic processes of monsoon depressions. *Mon. Wea. Rev.*, **111**, 1506–1514.

Sashegyi, K. and J. E. Geisler: 1987, A linear model study of cross-equatorial flow forced by summer monsoon heat sources. *J. Atmos. Sci.*, **44**, 1706–1722.

Schneider, E.: 1977, Axially symmetric steady-state models of the basic state for instability and climate studies. Part II. Nonlinear calculations. *J. Atmos. Sci.*, **34**, 280–296.

— 1983, Martian great dust storms: axially symmetric models. *Icarus*, **55**, 302–331.

Shukla, J.: 1978, CISK-barotropic-baroclinic instability and the growth of monsoon depressions. *J. Atmos. Sci.*, **35**, 495–508.

Sobel, A. and T. Horinouchi: 2000, On the dynamics of easterly waves, monsoon depressions, and tropical depression type disturbances. *J. Met. Soc. Japan*, **78**, 167–173.

Thorncroft, C. and B. Hoskins: 1994, An idealized study of African easterly waves: I: a linear view. *Quart. J. Roy. Meteor. Soc.*, **120**, 953–982.

Xie, S.-P. and N. Saiki: 1999, Abrupt onset and slow seasonal evolution of summer monsoon in an idealized gcm simulation. *J. Met. Soc. Japan*, **77**, 949–968.

Yano, J.-I. and J. McBride: 1998, An aquaplanet monsoon. *J. Atmos. Sci.*, **55**, 1373 – 1399.

Zheng, X.: 1998, The response of a moist zonally symmetric atmosphere to subtropical surface temperature perturbation. *Quart. J. Roy. Meteor. Soc.*, **124**, 1209 – 1226.

Zhou, J. and K.-M. Lau: 1998, Does a monsoon climate exist over South America? *J. Climate*, **11**, 1020 – 1041.